Discrete Tire Model Application for Vehicle Dynamics Performance Enhancement

Yaswanth Siramdasu

Dissertation submitted to the Faculty of the
Virginia Polytechnic Institute and State University
in partial fulfillment of the requirements for the degree of

Doctor of Philosophy
in
Mechanical Engineering

Saied Taheri, Chair
Mehdi Ahmadian
Corina Sandu
Tomonari Furukawa
Muhammad Hajj

June 11, 2015
Blacksburg, Virginia

Keywords: Tire Modeling, ABS, Braking, Handling, Ride, Rigid Ring, Enveloping, Tire Vehicle interactions, Performance metrics, Lane change, Short wavelength road profiles

Discrete Tire Model Application for Vehicle Dynamics Performance Enhancement

Yaswanth Siramdasu

(Abstract)

Tires are the most influential component of the vehicle as they constitute the only contact between the vehicle and the road and have to generate and transmit forces necessary for the driver to control the vehicle. The demand for the tire models are increasing due to the need to study the variations of force generation mechanisms due to various variables such as load, pressure, speed, and road surface irregularities. Another need from the vehicle manufactures is the study of potential incompatibilities associated with safety systems such as Anti-lock Braking System (ABS) and Electronic Stability Control (ESC) and tires. For vehicle dynamic simulations pertaining to the design of safety systems such as ABS, ESC and ride controllers, an accurate and computationally efficient tire model is required. As these control algorithms become more advanced, they require accurate and extended validity in the range of frequencies required to cover dynamic response due to short wavelength road disturbances, braking and steering torque variations. Major thrust has been provided by the tire industry to develop simulation models that accurately predict the dynamic response of tires without the use of computationally intensive tools such as FEA.

The objectives of this research are

- To develop, implement and validate a rigid ring tire model and a simulation tool to assist both tire designers and the automotive industry in analyzing the effects of tire belt vibrations, road disturbances, and high frequency brake and steering torque variations on the handling, braking, and ride performances of the vehicle.
- To further enhance the tire model by considering dynamic stiffness changes and temperature dependent friction properties.

- To develop, and implement novel control algorithms for braking, stability, and ride performance improvements of the vehicle.

GRANT INFORMATION

This work was funded by the industry members of the Center for Tire Research (CenTiRe), a National Science Foundation Industry/University Cooperative Research Center (I/UCRC). CenTiRe operates with funds provided by the member universities, the National Science Foundation (NSF), the tire industry, the automotive industry, the heavy equipment/farm equipment industry, and the testing industry among other sources.

Dedication

To Nikola Tesla, who did cool things to produce 700 patents

Acknowledgements

My passion towards understanding of vehicle dynamics would not have been sparked without the help of Dr. Saied Taheri and I am indebted to him, for giving me an opportunity to explore the mysterious world of tires. Apart from sharing his fundamental knowledge of tires, the key take away are his guidance on how to summon these resources to come up with ideas or solve intricate problems.

I would also like to thank my committee members: Dr. Mehdi Ahmadian, Dr. Corina Sandu, Dr. Tomonari Furukawa and Dr. Muhammad Hajj, for their valuable comments and time, despite their busy schedule. I would also like to thank all the industry members/mentors of CenTiRe for their technical and financial support.

It was also a great pleasure working and interacting with lab mates at CenTire especially Srikanth and Hojong Lee for sharing their industrial expertise. It was very good learning experience working with undergraduate research assistants. I would also thank my friends Vineeth, Bharadwaj and Sai for their support and fun times.

Contents

List of Figures

List of Tables

Chapter 1

Introduction

This chapter provides a summary of research motivation, objectives and a brief outline of the dissertation.

To reduce the product development cycle time and cost, automotive companies rely heavily on computational simulation tools. Before designing a vehicle, most vehicle components are fixed with the exception of tires, suspension, and steering components [10]. These parts can be used to optimize and enhance the vehicle ride and handling performances. This forces the tire developers to utilize complex models to study tire components and properties effecting vehicle characteristics (such as driving behavior, performance, comfort, passive safety etc.,). Another major change in automobiles in the past few decades is the integration of more complex chassis control systems into vehicle development (Anti-locking Braking systems (ABS), Electronic Stability Controller (ESC), Active and Semi-active suspension, Active Front Steering (AFS), Rear Wheel Steering (RWS)). Apart from tires, vehicle manufactures rely on proprietary application softwares featuring advanced control algorithms to meet all vehicle performance and safety regulations without compromising the other requirements (Active or Semi-active suspension for comfort optimization and for improving the resolution of the classic design conflict between safety and comfort requirements). For development of control algorithms for these advanced chassis systems a good understanding of vehicle

dynamics under all operating conditions is needed. In this context, the tire is considered as one of the most challenging components to include in these developments.

With the advances in computational capabilities, computer simulations seems indispensable either for advanced chassis control system design and reliability or for understanding of complex tire and vehicle dynamic interactions. The availability of an advanced and accurate simulation tool is considered a competitive advantage as this enables engineers to analyze multiple test cases without experimentation and rapidly optimize their final product design. Using such tools allows for the decisions on the right system to choose and basic tuning questions to be moved forwards to early stages of vehicle development. This is only feasible when sufficiently reliable analytical methods are available for all vital components of the vehicle, so that preliminary designs and variant assurances can be performed on the basis of simulations [11].

1.1 Motivation

Tires are the most influential component of the vehicle as they constitute the only contact between the vehicle and the road which is why tires contribute to a wide change in vehicle performance characteristics like handling, braking, comfort (ride and noise generation), fun to drive, etc. To evaluate these characteristics, requires a practically-oriented tire model that can generate forces and moments that are closely related to real vehicle tires. The reliability of tire models under various operating conditions is still a big challenge. In addition, demand and requirements for tire models are increasing to study the incompatibilities associated with safety systems such as Anti-lock Braking System (ABS) and Electronic Stability Control (ESC), which are essential features in all modern automobiles. Another requirement from the vehicle manufactures is the study of the variations of force generation mechanisms of tire due to road irregularities.

Handling performance of a vehicle is dominated by tire forces, which are generated due to

viscoelastic deformation of the tire from leading edge to trailing edge of contact patch (slip angle at the ground). These forces play a crucial role in guiding, controlling and stabilizing the vehicle. The driver controls these forces indirectly by inducing steering or braking input. Crolla [12] lists different operating regimes of handling of the vehicle as follows:

1. linear, low lateral acceleration (< 0.3 g)
2. non-linear, up to limiting lateral acceleration ($\cong 0.8$ g)
3. non-linear, combined cornering and braking or acceleration maneuvers

For the first regime, vehicle operates in the linear region, tire parameters which effect mostly vehicle handling performance are tire cornering stiffness, tire size and tire pressure in front and rear. A simple 3 DOF vehicle model with body roll, yaw and lateral motion with suspension and steering kinematics and compliances is usually used for these studies. The tire model of choice is the well known Magic Formula Tire Model [12]. This tire model works for low-frequency and steady state vehicle motions and on large-wavelength road profiles but fails to meet realistic representation of tire road interaction under short wavelength road profiles and neglects tire inertial effects. The variations of tire stiffness and damping parameters due to these short wavelength road profiles has a strong effect on the vehicle handling performance. The second and third regime is limit handling region of vehicle, operating at lateral acceleration of around 0.8 g, where saturation of tire forces occurs due to the available friction, road undulation or surface conditions. The behavior of vehicle just before the saturation of forces is more responsive and deviates from normal behavior. This is because at higher slip angles of tire, yaw damping of vehicle and relaxation length of tire decreases and tire force variations are largely due to belt vibrations. The driver has indirect control of these forces either by steering or braking and can adapt slowly to varying road conditions. The normal drivers under these situations become nervous and over compensate by inducing sudden steering or braking inputs. van Zanten [13] developed optimal brake slip distribution control for best tuning of braking control while cornering which results

in reduced deviation of vehicle from target path and minimum stopping distance. This is achieved by using ABS integrated with Active slip controller (ASR). Understanding the dynamic response of the tire under these short wavelength road profiles at limit handling helps design vehicle controllers with good reliability, so that transition in vehicle behavior from linear to nonlinear regime is slow and predictable for the normal driver.

Ride comfort analysis of a vehicle consists of two domains: Primary ride concerns with acceptable control of the body attitude and adequate control of the dynamic tire loads within the constraint of suspension rattle space. This can be analyzed using a quarter car model and a simple point contact tire model. For relatively low-frequency, transient and vertical oscillatory vehicle motions on a large-wavelength road profiles, the effect of the finite length of the contact patch may be neglected. The Secondary ride involves higher frequency response ($>$ 15 Hz), harshness, response to longitudinal inputs from bumps, and potholes.The point contact tire model is not suitable for predicting these effects accurately due to perceived harshness rating of a suspension in response to a discrete input such as a pothole. This is due to the dynamic response of the tire as it deforms around the road inputs and the longitudinal and vertical (non-linear) dynamics of the tire and suspension [12]. A nonlinear tire model with dynamic contact patch variations and accurate prediction of dynamic force to discrete road short wavelength profiles will provide good understanding for development of suspension and evaluation of active suspension controllers.

The force and moment generation mechanisms of tires directly relate to the deflection of the tire as a result of contact with the road surface. As tire is a dynamic system with complex structure and different components, longitudinal, lateral and vertical forces change dramatically due to road irregularities. Apart from road irregularities, fluctuations in the wheel angular speed due to braking and driving torque generate longitudinal force variations. The cornering force acting in the lateral direction shows fluctuations due to steering oscillations. These input vibrations induced due to road irregularities, braking system and steering system can excite the natural frequencies of tire belt ($<$ 80 Hz) and have a large influence on the force generation of tire [4]. Simplified lump parameter models with 3-dimensional vehicle

simulations are not adequate for capturing these variations [12]. This is especially true for simulating crash avoidance maneuvers. The need for such evaluation tools employing dynamic tire models with the effect of tire belt vibrations have been validated through previous studies by [14], [15] and [16] which conclusively state that the tire belt vibrations on ABS braking and steering is significant and cannot be neglected. Accurate modeling of braking and panic steering maneuvers under short wavelength road profiles is one of motivation for this research. This requires high frequency tire models with included effects due to high frequency pulse inputs of ABS and steering systems [17]. Another motivation is using the developed tire model in development and implementation of novel active control systems under short wavelength road profiles.

The tire model that is developed in this research is partially based on the work of others found in the literature. In addition to developing this complex tire model, two enhancements have been developed and added which have made the model response match those of the experimental results much better. Besides the dynamic force and moment characterization of tires under braking and handling, including the temperature effects on the variation of friction potential available at ground is also considered. Rather than modeling the temperature effects using complex multiscale modeling of frictional heating in rubber-substrate contact region, a simple thermal energy based temperature increase at the contact patch is modeled with the thermal properties of tire determined from experiments. The effective modeling of dynamic stiffness variations while rolling over a cleat is another enhancement proposed for the dynamic tire model. The tire model is based on different modular subsystems with the flexibility to enhance force generation characteristics with temperature effects and dynamic stiffness variations.

1.2 Objective

The objectives of this study is:

1. To develop, implement and validate a rigid ring tire model and a simulation tool to assist both tire designers and the automotive industry in analyzing the effects of tire belt vibrations, road disturbances, and high frequency brake and steering torque variations on the handling, braking, and ride performances of the vehicle.

2. To further enhance the tire model by considering dynamic stiffness changes and temperature dependent friction properties.

3. To develop, and implement novel control algorithms for braking, stability, and ride performance improvements of the vehicle.

This tool would provide a common simulation platform for both tire designers and the automotive industry for optimized tuning of vehicle and tire characteristics. Once deployed into the industry, this tool could eventually be integrated into the development work flow of engineers.

1.3 Thesis Outline

Section 2.1 provides a comprehensive literature review of all the available modeling tools and existing technology which can be leveraged towards the development of the tool. This is followed by the discussion of the importance of tire inertial belt vibrations during ABS braking, limit handling and rolling over short-wavelength road profiles. Chapter 2, concludes with the reasons for selection of rigid ring based dynamic model. Chapter 3, explains the mathematical modeling of the tire, vehicle and the ABS models. Chapter 4, discusses the implementation of tire model in simulation environment and validation of the dynamic tire model and nonlinear vehicle model against the experimentally obtained data. Chapter 5 discusses the integration of the developed tire and ABS models with Carsim vehicle model to form a simulation tool. The simulation tool is used to perform various vehicle dynamic maneuvers. This chapter, introduces one of the main contribution of this research,

to understand the underlining physics in interaction of tire dynamics with road and vehicle components during on ABS braking and limit handling. This is accomplished with the identification of different independent maneuvers (split-μ, step steer, lane change etc). This chapter also, studies the interaction of longitudinal and lateral dynamics of the tire during combined braking and handling maneuver and development of a comprehensive tire dependent handling performance metrics which includes the effects of the road characteristics. Chapter 6 and 7 discuss the development of novel control algorithms integrated with the dynamic tire model. Chapter 6, introduces another main contribution of this research, a novel double damper semi active suspension which can further improve the performance of the semiactive suspension. Simulation results are presented which compare the performance of novel semi active suspension against active and passive suspensions. In Chapter 7, a four-wheel steering control algorithm is introduced to improve the stability and handling performance of the vehicle. Chapter 8, addresses the scope for further enhancement of the dynamic tire model. Two enhancements are proposed, one is the introduction of a separate module to compensate for dynamic stiffness variations due to road undulations and the other is a heat transfer based thermal model with temperature dependent friction properties. Finally, Chapter 9 concludes the study and proposes future tasks for further improving the work presented in this research.

1.4 Thesis Contributions

The primary contributions of this study are:

- Enhancement of the rigid ring dynamic tire model to compensate for dynamic stiffness changes and temperature dependent friction properties
- Development of different independent maneuvers and performance metrics to understand the effects of tire belt vibrations, road disturbances and high frequency brake and steering torque variations on the handling, braking and combined braking and

handling vehicle response.

- Introduction of novel double damper based semi-active suspension.

Chapter 2

Background

2.1 The Pneumatic Tire

Manufacturing of pneumatic tires for automobiles began in 1895, with an advantage over solid tires of vibration isolation and reduced moment of inertia. After the rampant growth of automobiles in 1930's, the importance of mechanics of grip generation of tires was recognized, with the need for safety under braking and stability under steering. The importance of the tire as the source of vehicle control forces was further strengthened with the study of visco-elastic properties of the rubber and complex interactions between the tire and the road. Today's tires are highly engineered structural composites whose performance is designed to meet the needs of the high performance vehicles [1].

- Carry Load
- Transmit Drive/Braking torque
- Produce Cornering Force
- Provide Steering response
- Cushion Road Inputs

- Dimensional Stability
- Consume Minimum Power
- Low Noise/Vibration
- Tolerate Poor Maintenance
- Durable and Safe Performance
- Long Wear Life

These multiple requirements are partially met using advanced visco-elastomeric polymers which are blended with 18 components, 12 compounds, 2 fabrics, 2 steels, and 60 raw materials. Figure 2.1 shows the construction of a modern radial-ply tire. The parallel cords

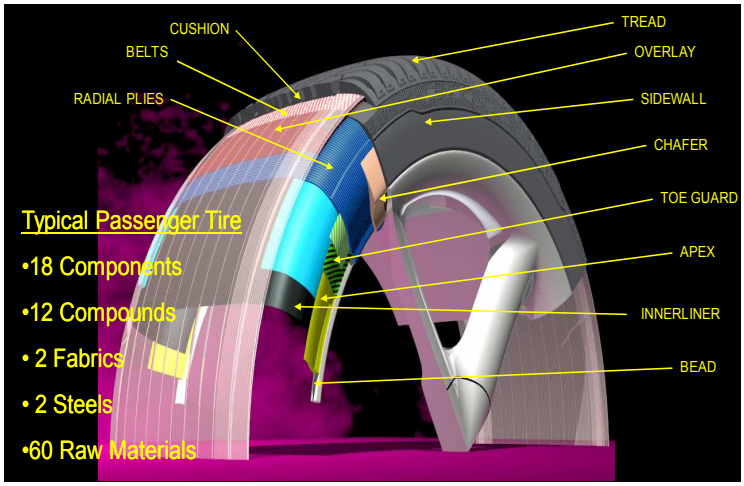

Figure 2.1: Construction of a radial pneumatic tire [1]

running across the tire from one bead to the other are called carcass plies which provide strength and stability. The two steel belts run at opposite angles to one another on top of the carcass plies, under the tread area. They restrict the expansion of the body ply cords, stabilize the tread area and provide impact resistance. Typical angle between belts is around

22 ° and varying the belt widths and belt angles affects the vehicle ride and handling characteristics. The Bead which is running on each side of the tire, serve to anchor the inflated tire to the rim. Apex provides the transition from rigid bead and rim to less stiffer sidewall. Apex reduces stress gradient and balances between high stiffness of lower part and softer upper part. It effects handling and ride performance. The tread compound is specially formulated to provide a balance between wear, traction and handling. The tread design balances between wear, hydroplaning, rolling resistance, noise generation, cornering response and snow traction. The thin innerliner improves air retention by lowering permeation outwards through the tire. From above it is clear that tire contains different elements when combined the behavior is highly complex. To appreciate the sheer complexity, for understanding the tire-to-ground traction involves a knowledge in various fields of physics, chemistry, metallurgy, dynamic, tribology, thermodynamics, heat transfer, elasticity, viscoelasticity, rheology, elastohydrodynamics, and lubrication technology [18]. Although developing a comprehensive model is highly unrealistic, but a simple and intuitive modeling methods valid under a particular domain can be adopted. In this research, dynamic force and moment response of tire are modeled.

2.2 Tire Modeling

The main purpose of a tire is to transmit forces between the road and the axle, so that the driver can control the vehicle. The tire also works as a low pass filter in the suspension system by reducing the high frequency vibrations from small irregularities in the road. For integrating a certain tire with the vehicle, tire has to meet stringent requirement of handling, ride and braking performances. Designing suspension, steering systems and chassis controllers (ABS, ESC, Ride Control) without consideration of tire behavior might lead to unfavorable results during the operation of the vehicle in terms of comfort and safety. The properties of tires change a lot by wear, temperature, road conditions, etc,. A lot of work has been done in the area of modeling of tires to characterize tire material behavior, thermal

response, strain mechanics and dynamics. In this research, modeling towards the characterization of dynamic force response of the tire is pursued. Over the last few decades, various tire models are proposed covering different applications of interest for understanding their behavior of force response under various operating conditions to ensure proper design of other components in the vehicle.

With the rapid advancement in detailed modeling of vehicle components, a more reliable tire model for understanding the behavior of vehicle under various operating conditions is required. For example, a tire model should accurately predict the vehicle, passing an obstacle in a sharp curve when braking at the same time, with an anti-lock braking system (ABS) controller being active. These growing demands from OE manufactures necessitate a more detailed tire model with wide range of application.

From Figure 2.2, H.B.Pacejka [2] classified tire models into four categories based on the modeling approach. The tire models span from simple models aiming for understanding the physics to advanced finite element models that can predict the behavior precisely. From Figure 2.2, models on left side are empirical based linear or non-linear mathematical relations which rely heavily on experimental data. Based on the frequency of force inputs acting on the tire, tire models are classified into steady state, transient and dynamic models.

2.2.1 Steady-State Response Models

A steady state condition arises when there are low variations in the input quantities of the tire (vertical load, slip). These models are valid within the frequency range of less than 10 Hz and consequently called handling tire models. Some of the scenarios that match this condition involve slow steering maneuvers such as cornering, on center steering and lane changing etc. These models can be used for calculations in simulations or for real time implementations due to its less modeling complexity.

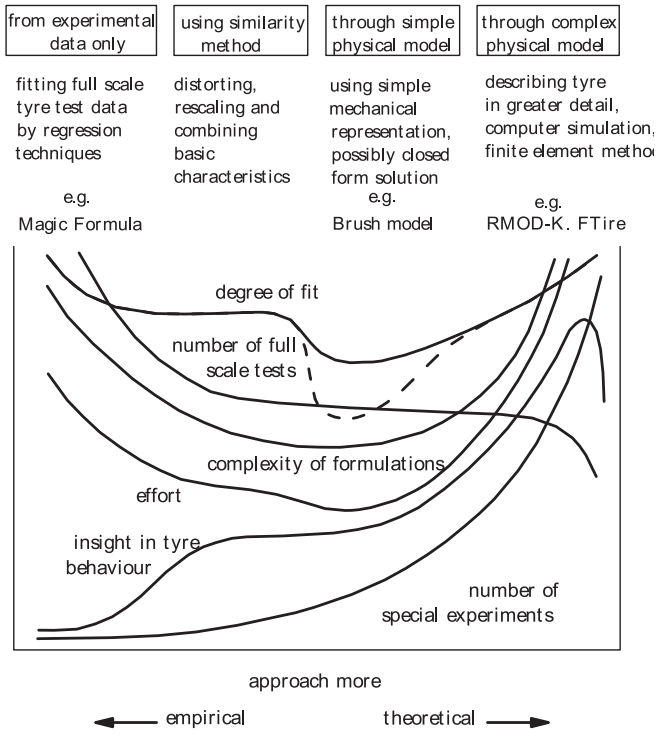

Figure 2.2: Classification of tire models according to H.B.Pacejka [2]

Magic Formula

The most popular example of an empirical tire models is the Magic Formula by Pacejka [19] which is considered a standard tire model in the industry for vehicle dynamic simulations. The general formulation of force response for the longitudinal or lateral slip, at a given values of vertical load and camber angle is given as

$$y = D \sin\left[C \arctan\left(Bx - E\left(Bx - \arctan Bx\right)\right)\right] \tag{2.1}$$

$$Y(X) = y(x) + S_v \tag{2.2}$$

$$x = X + S_H \tag{2.3}$$

where Y is the output variable representing longitudinal F_x or lateral force response F_y, X is the input variable of longitudinal κ or lateral slip α, B is stiffness factor, C is shape factor, D is peak value, E is curvature factor, S_H is horizontal shift and S_V is vertical shift. Although it is an empirical model, some of the parameters in the model capture the basic parameters

of tire like cornering stiffness, aligning stiffness, longitudinal stiffness, peak friction, load sensitivity of tire etc,.

TMeasy

TMeasy is a semi-physical tire model for low frequency handling maneuvers. The longitudinal and the lateral forces are described as functions of the slip ratio or slip angle [3]. The nonlinear force characteristics are defined using the initial inclination dF^0, the maximum magnitudes of tractive forces F^M with the corresponding slip ratio or slip angle s^M, and the magnitudes of tractive forces at the sliding F^S with the corresponding slip ratio or slip angle s^S as shown in Figure 2.3. The combined force characteristics are then directly generated via a generalized slip approach which does not need any additional fitting parameters. For a detailed modeling description refer to [3, 20].

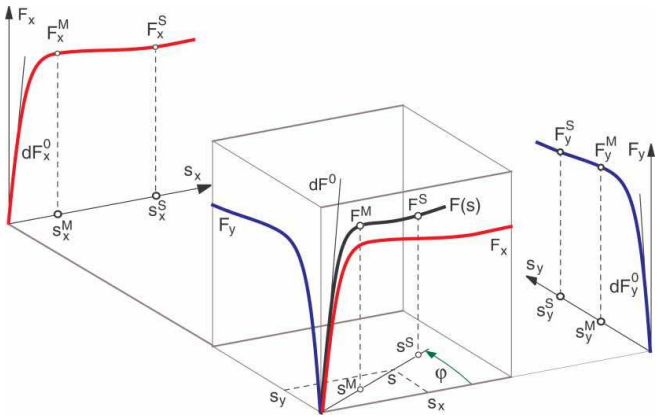

Figure 2.3: Tire force characteristics using TMeasy model [3]

2.2.2 Transient Response Models

Steady state tire models are not valid under transient events such as lane change maneuver on a uneven road surfaces or under the influence of oscillatory the cycling effects of ABS

brakingng and steering inputs. This is because the force generation in tire contact patch does not instantaneously follow slip variations. The compliance of the tire carcass with respect to the rim causes a lag in the longitudinal and lateral response of the tire. The time constant of this response is described using the concept of relaxation length which is defined as the distance traveled before the force generated in response to a step variation in longitudinal or lateral slip. These effects are called transient response of the tire. Transient tire models take into account the effect of relaxation length using various differential equations and can predict the force response more accurately.

Brush model

For analytical modeling of transient behavior of the tire, a brush model can be used. Brush model was developed by Dugoff, Francher and Segel [21] which was later improved by Bernard, Segel and Wild [22]. A brush model is a simple physical model with a possible closed form solution. A brush model contains a finite number of elastic bristles connecting the belt of the tire to the road surface. These bristles may be called tread elements. Their compliance represents the elasticity of the combination of carcass, belt, and actual tread elements of the real tire. These tread elements can deflect in a direction parallel to the road surface, the forces and moments are calculated based on the deformation of these elements and based on the position of tread element, where the transition from the adhesion to the sliding region occurs.

Lugre Tire Model

Lugre tire model is a physics based dynamic friction model and is used to represent contact patch model for a tire model. This model provides a physical interpretation of the friction forces as a result of elastic deformation on the surfaces in contact. Its dynamic nature allows the study of the transient behavior of tire friction while the singularities associated at lower slip velocities are avoided. The LuGre model [23, 24, 25] was based on the friction

model developed by Dahl [26]. The Dahl model describes the hysteresis behavior of ball bearings under the influence of very small amplitude oscillations. Similar to brush model, bristle elements are attached from belt to road interface. The contact friction model of each bristle adopts a stress-strain curve from solid mechanics and describes using a differential equation. In case of a Lugre model, the contact friction model is augmented with a decreasing coefficient of sliding friction ($\mu(v_r)$) by incorporating the Stribeck effects. The friction forces are calculated using the deformation, longitudinal lumped stiffness, the lumped internal damping, the viscous relative damping normal force.

Semi - Empirical Transient Models

In these models, low carcass dynamics are modeled using the relaxation length approach. The contact forces are calculated by integration of first order kinectic/dynamic models (using contact mass) with magic formula or other steady-state contact model. Zegelaar [4] introduced a semi - empirical contact model in combination with the carcass stiffness, as shown in Figure 2.4. Comparing the analytical discrete brush model's frequency response to small variations in slip ratios with semi - empirical model, which approximates the exact transient response of brush model. The transient response of the discrete brush model is represented by first order system with a time constant as relaxation length of the tire. The relaxation length is calculated by using actual local slip stiffness divided by the total longitudinal tire stiffness. The first order approximate of this contact model in series with the longitudinal carcass spring, is valid for small variations of slip ratio. However, this approximation is not valid for the nonlinear response of contact model at very higher frequencies variations of slip ratios and modeling this using a discrete brush model is computationally expensive. From the literature, authors proposed various methods of approximation of relaxation behavior of tire either using first order delay in force response [27] or slip response [28] or deformation response of tire [29] or using a mass in contact patch [30]. These models are termed as pragmatic models because they use differential equations rather than physical tire. This

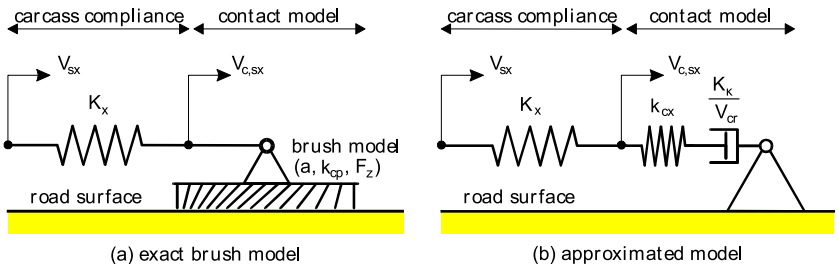

Figure 2.4: Approximation of brush contact model with tread element stiffness k_{cx} and local slip stiffness K_κ [4]

approach of using first order delay equations, increases the range of validly to these models to 25 Hz. In [15, 31] authors used these pragmatic models for vehicle simulations and to study the shimmy phenomena. Here in this work, a first-order approximation of relaxation length based on delayed slip response of the contact patch is considered.

2.2.3 Dynamic Tire Models

The transient model has its limitations because it is valid at only lower frequency inputs. For the higher-frequency range, the tire modeling should consider structural or the vibration modes [32] of the tire. The dynamic response of the tire structure that is relevant to vehicle dynamics has to be modeled accurately. It is understood from [33, 2] that, for fast lane change and braking maneuvers under the influence of higher frequencies road inputs, the inertial effects of the tire cannot be neglected. Also, the dynamic properties of the tire play a very important role in the design of Anti-lock Braking Systems (ABS) as rapid variations in brake pressure can lead to oscillations in the tire and the wheel. There have been efforts to understand these effects and to model the response [34, 35]. Tire models to the right of Figure 2.2 are dynamic models with inertial effects of the tire included. Due to the detailed modeling of tire physical structure, the range of validly of these models is up to 250 Hz. The outputs from these models tend to have a higher level of scope in terms of analysis and can correlate outputs to specific tire design parameters. Hence, they are extensively utilized

during the design stage of the tire. Based on the modeling approach, Schmeitz [5] classified dynamic tire models into three categories, as shown in Figure 2.5.In this research as the dynamic tire model has to simulate dynamics while rolling over uneven surfaces,addition, a general classification of dynamic tire models given in literature for uneven road surfaces are also shown in Figure 2.5. A detailed literature survey of all transient dynamic tire models has been done by Chang et al [36].

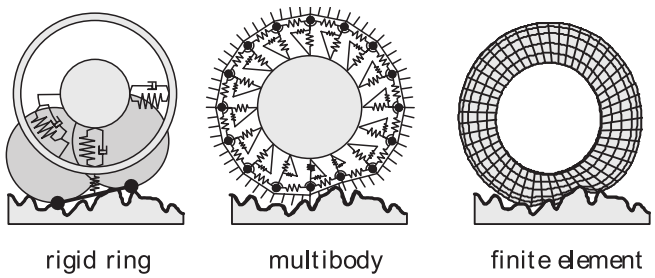

Figure 2.5: General classification of dynamic tire models [5]

Ring Based Tire Models

This modeling approach assumes the belt of the tire as a ring which is connected with the rim. This ring is connected to the axle through a set of springs and dampers which represent the pressurized sidewall. The dynamic response of the tire structure due to belt inertial and carcass compliance are effectively captured using this ring based approach. The main objective of these models is to understand the frequency response of the tire structure rather than the detailed modeling of contact forces due to tread-road interactions. These contact forces are modeled either using elastic springs and dampers or using empirical transient models. The ring is modeled either as flexible or rigid element. Earlier models developed using ring based approach, are primarily used to study tire belt vibrations and standing wave phenomena. Clark [37] modeled the rotating ring model supported on radial springs to study the dynamic stiffness of the tire, free vibrations of tire and rolling contact mechanics. Bohm [38] also used same techniques to study the tire inertial vibrations and compared

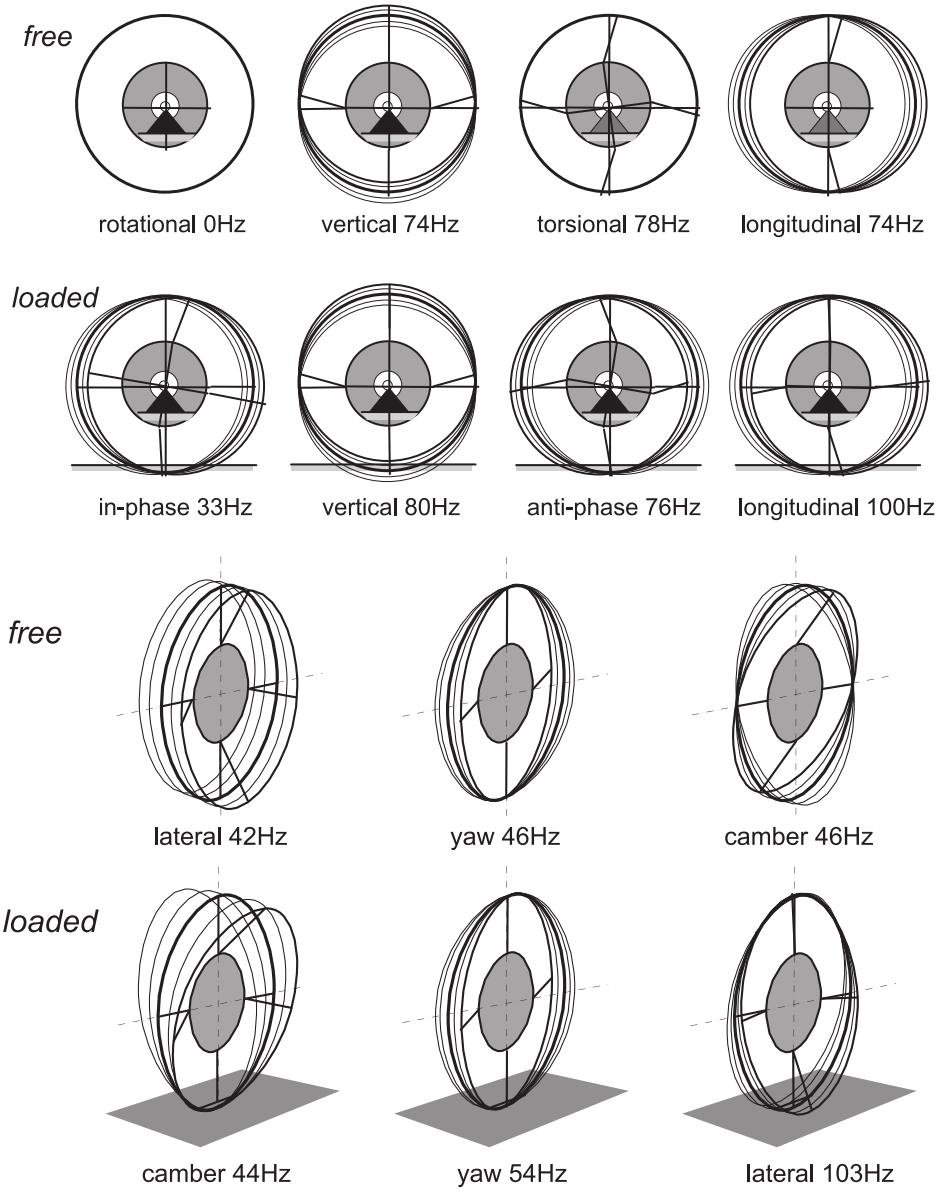

Figure 2.6: Rigid modes of vibration of tire under unloaded and loaded (F_z = 4000 N) condition at zero speed [2]

it with experimental results. Pacejka [39] added tangential spring to the contact model to study the effects of inflation pressure and centrifugal effects. Padovan [40] added contact and sidewall damping, to study the shift in resonant peaks. Potts [41] using the similar model developed by Pacejka [39], studied the importance of first vibrational mode on vibration transmission of the tire. Yamagishi and Jenkins [42, 43] improved the tire-contact model with second set of distributed radial springs to include the compliance of the tread elements also. With the potential of ring based model in predicting the dynamic effects of the tire, several authors used different modeling techniques like thin shell structure, green functions etc,. to quantify the dynamic force response of tire acted upon by higher frequency inputs.

If the road surface is considered to be not perfectly rigid, tire forces in the contact patch are difficult to model due to complexity of deformable soil characteristics. Using ring based tire modeling techniques, the team at the Advanced Vehicle Dynamics Laboratory (AVDL) in Virginia Tech, has developed interaction of tire with various terrains like uneven rigid terrain [44], switchable on-road and off-road [45], and off-road soft soil [46]. The contact model will require contact forces as input and react with ground geometry as output. For detailed literature review on tire-terrain interactions models refer to [47]. Recently, using flexible ring based model, Gong [48] performed a comprehensive study of in-plane dynamics of tire and analyzed tire inertial vibrations, tire-road contact mechanics and vibration transmissibility of tires from analytical persecutive. The flexible ring model is used to obtain more insight into the differences between the modes of a free tire and the modes of a standing tire. This model is also used to identify modes which were hard to measure accurately.

For frequencies less than 100 Hz, the tire modes of vibrations show only rigid modes, with no deformations in the tire belt. From Figure 2.6,it can be seen that tthe modes of vibration of the tire under unloaded and loaded conditions are rigid and below 100 Hz. Under the loaded condition, due to a finite contact patch at the ground, two additional in-phase and anti-phase rational modes are seen. Longitudinal and lateral modes are moved above 100 Hz which can be excited with relatively large deformations in the contact patch. The camber and yaw modes which are identical in the unloaded condition, exhibit a difference, with the camber

mode frequency becoming smaller and the yaw mode frequency larger. Considering using only rigid modes of tire, modeling using rigid ring based approach, Zegelaar [49] analyzed in-plane force response of tires due to short wavelength road irregularities. Later Maurice [14, 50] extended the model to account for out-of-plane dynamics. Other implementations of this model include the work done by Allison and Sharp [51] and Bruni et al [52]. The rigid ring model has been used for various commercial simulation tools for tires including MF-SWIFT by TNO Automotive [53] and more recently, the UniTire model [54]. A very similar approach of Rigid-ring tire model is developed by Mancosu [55]. Since these ring models are based on a single point of contact, they are generally used in conjunction with an enveloping model which can be chosen by the availability of parameters and modeling requirements.

Multi-body Models

In these models, flexible belt modes of vibrations are effectively modeled using a discrete lumped mass approach. As these models consider flexible modes also, the frequency range of these models is effectively increased (200 Hz) as compared to rigid-ring based model. From Figure 2.5, in a multi-body simulation model, the tire belt is constructed as an elaborate discrete point mass network which are interconnected through tension and rotational springs. Multiple elastic belts with a similar discrete mass arrangement are assumed to simulate lateral behavior which are again connected to each other in a similar fashion. The elastic belts are connected to the axle through radial and tangential springs. Typically, some 50 - 2000 point masses make up such a system. The tread elements are assumed to be brushes that can slide over or stick to the road surface. Earlier model developed based on this approach is Dynamical Non-Linear Spatial Tire Model (DNS-Tire [56]), it is a coarse non-linear time-domain FE model used to study the influence of tire design details on dynamic tire forces. An improved version of DNS-Tire is commercially available as FETire [57]. Taheri [47], modeled the dynamic behavior of tires on soft soil, using a hybrid (lumped mass- brush model) discretized model (HSSTM), and studied the transient and dynamic response of tire

and validated using modal analysis and fixed axle cleat experiments. Gipser introduced a computational simplifier version of FETire model as FTire [57, 9]. Dorfi [58, 59] using FTire, extensively studied dynamic response of tire rolling over cleats, to accurately predicted the tire force response at different rolling speeds, cleat shapes, tire constructions and loading parameters.

Finite Element Models

Finite element models are constructed using detailed geometry and descriptions of the tire. They are generally the most accurate in terms of simulation output and can be directly used for simulating dynamic tire response. Although multi-body and finite element based models can predict the response to frequency excitations of up to 250 Hz, they tend to be computationally heavy and difficult to parameterize. For vehicle dynamic simulations pertaining to the design of safety systems such as Anti-lock Braking System (ABS) and Electronic Stability Control (ESC), a computationally fast tire model is required. From the research interests set forward in Chapter 1, for understanding tire dynamic effects under various vehicle operating conditions, the most suitable model seems to be a rigid ring based model.

2.2.4 Enveloping Model

The behavior of a tire while rolling over obstacles is a complex phenomenon as the tire is in contact with the ground at multiple points. This effect is clearly evident when the road disturbances have short wavelengths as the tire contact creates a filtering effect by smoothening out sharp obstacles. This is known as the enveloping property of the tire, which is illustrated by Zegelaar [4] and shown in Figure 2.7. As a result of the enveloping effect, the effective road disturbance which acts on the tire is different from the actual road surface. To represent the force response of tire over cleat or other local structural deformations within the

length of the contact patch properly, enveloping features have to be integrated with dynamic tire models. When the tire rolls over uneven roads, the assumption of a single point of contact

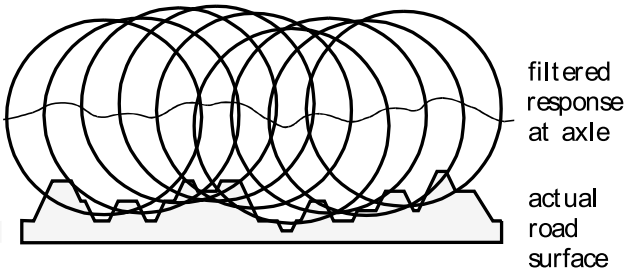

Figure 2.7: Tire enveloping property

might not hold true. Hence, various enveloping models, both physical and semi-empirical have been proposed to simulate this effect. The overview provided here is based on the

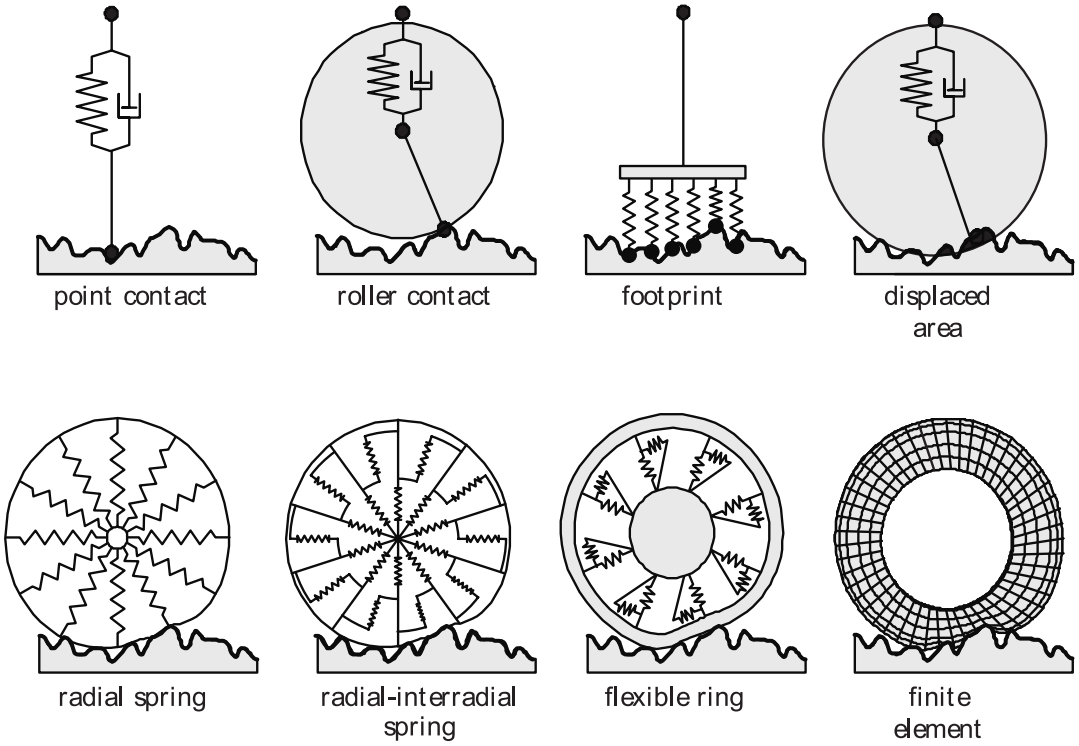

Figure 2.8: Tire enveloping models

work previously done by Schmeitz [5]. A broad list of various methods used for enveloping models found in literature are shown in Figure 2.8, covers from simple point contact model

to detailed flexible ring model. Point contact model represents tire-road interface with single spring and damper. This model is valid for very large wavelength road profile (> 3m). Roller contact model was proposed by Guo [60], it considers radius of tire but fails to account for the deformation of the tire. Footprint model considers a linearly distributed spring and dampers across the contact patch but fails to account for tire geometry. For displaced area models, resultant force acts along the centroid of the total displaced area. Although accuracy has improved as compared to the roller contact model, but it loses its validity under sharp obstacles. Radial Spring and flexible ring models contain a radially deformable body instead of a rigid wheel. Although these models have good accuracy, it is achieved at the cost of high computational load due to detailed modeling of tire deformation around the obstacles.

Based on the analysis conducted by Lippmann [61], various attempts have been made to develop empirical models that can be used for computing enveloping characteristics. Based on the findings of Bandel [62], a basic function approach, was developed by Zegelaar [4], which involved summing elementary curves to obtain the effective road profile. These basic curve parameters change with respect to the obstacle type. A semi-empirical approach was adopted by Schmeitz [63, 5] using two tandem rigid elliptical cams which roll over the uneven road surface. The tire curvature effects are taken into account using the curvature of the cams. The effect of tire deformation in the contact are accounted by changing the distance between the cams. The average height of the cams is considered to be the effective road surface or excitation to the tire. This model has the advantage of being suitable for arbitrary road profiles and can be extended to three dimensions. A variation of this model has been proposed by Allen [64] to reduce the experiments required for parametrization. In this research, the semi-empirical enveloping model is used in conjunction with point contact rigid ring model.

2.3 Anti-lock Braking Systems

The two primary functions of a braking system are to retain control of the vehicle at a steep inclination or a declination and to bring the vehicle to a complete stop in the shortest distance possible. Conventionally, braking is accomplished in automobiles using a hydraulic circuit. When the driver presses the brake pedal, it pushes fluid through the master cylinder into the hydraulic circuit. This eventually translates into a pressure which pushes the brake shoes against the disk and generates braking torque through friction.

Initial systems were based on drum brakes on all four wheels where the drum is mounted on the wheel with brake shoes positioned inside the drum. The hydraulic actuators press the brake shoes against the drum and this would cause braking due to frictional force. Currently, vehicles are equipped with disc brakes since they were more efficient during braking and had a better heat dissipating mechanism. In these systems, a caliper is mounted on a solid disc which is attached to the wheel. The calipers are actuated through hydraulics and generate braking force by clamping the disc through brake pads. A detailed diagram of a vehicle braking system with disc brakes on the front and drum brakes on the rear is shown in Figure 2.9 Improvements in electronics led to the development of reliable control systems

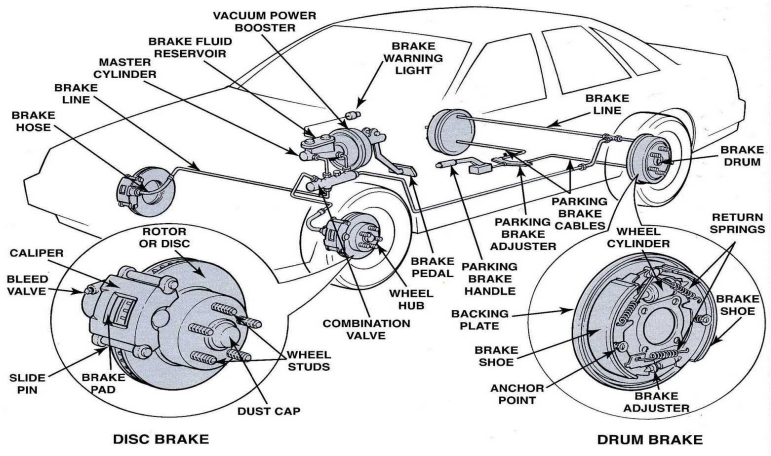

Figure 2.9: Conventional vehicle braking system

which could be used for the improvement of safety systems. This led to the development of

the Anti-lock Braking System (ABS). This was a revolutionary concept in which the ABS controller cycles the braking action such that the wheel is always at a desired optimum slip ratio and wheel lock up is also prevented. As a result, this system retains directional control to the driver even during severe braking events and prevents the vehicle from going unstable due to the wheel lockup. Earlier versions of ABS began to appear in aircrafts as early as 1929 and they remained exclusive due to their high costs. Modern ABS systems for use in automobiles were introduced in 1971. The automotive industry was interested in utilizing this technology for incorporating it as a safety system in their vehicles and began to adapt them for vehicle applications. Following their introduction in vehicles, ABS systems came to be widely adopted as they drastically reduced the number of automotive-related accidents. Currently, ABS in a vehicle is considered a critical safety system and is mandated in many countries. Figure 2.10 shows a detailed overview of an ABS braking system. A time-line of the development of ABS systems is described as an SAE Standard [65].

2.3.1 Principle of Operation

The operation of an ABS system is centered around the longitudinal force versus slip characteristic of a tire. From Section 7.3 we know that the force generated at the contact patch is dependent on the slip ratio. This is the braking force that is generated in the direction opposite to the motion of the vehicle. Figure 2.11 shows the variation of longitudinal force with slip ratio for a generic tire. From this, we can notice that the braking force peaks at a particular slip ratio and then reduces. The braking force available when the tire is fully sliding (unstable region) is also comparatively less than the peak value. Hence one would expect to see a reduction in braking distance if the wheel slip ratio is maintained around this peak.

The ABS system achieves this through a Hydraulic Control Unit (HCU) which is essentially a complex circuit of control valves which are actuated through solenoids. Based on the current wheel slip ratio, the ABS control algorithm, which is generally implemented through

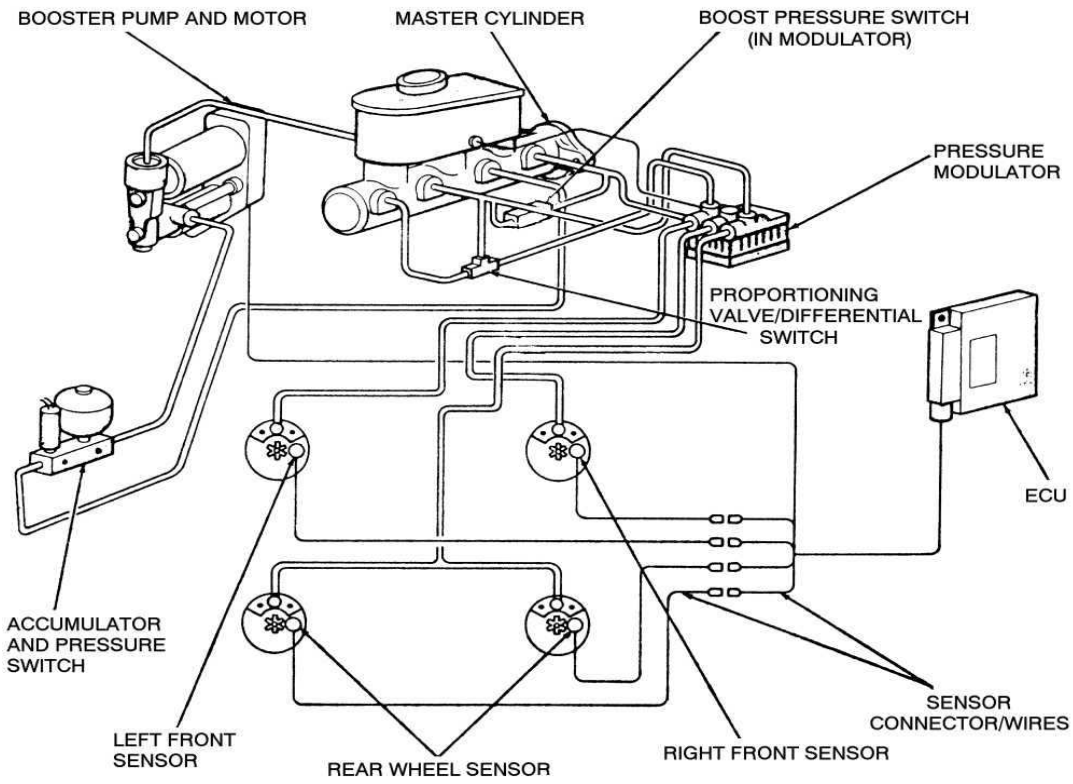

Figure 2.10: Bendix ABS system schematic

a micro-controller, calculates the optimum braking torque based on wheel speed information from sensors and correspondingly chooses whether to increase, hold or reduce the pressure in the brake line by actuating the solenoid valves. This way, the ABS controller achieves its objective of maintaining wheel slip in the desired range and in the stable region for all four tires. Typically, an ABS controller executes control signals at the rate of 10-20 Hz.

2.3.2 ABS Control Algorithms

The ABS control algorithm mainly performs two tasks: prediction and re-selection. Prediction involves the judgment of the controller on whether the wheel is going towards lock-up and re-selection is when the controller decides to re-apply brakes based on its assessment of whether has sufficiently accelerated.

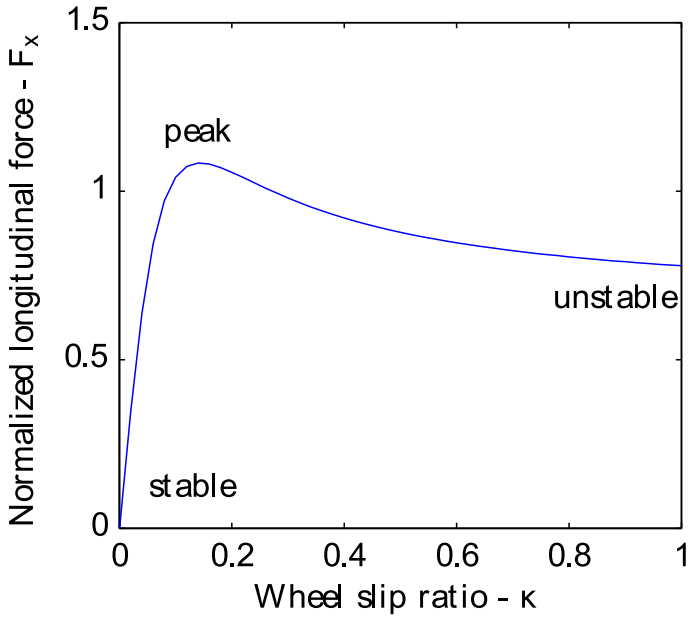

Figure 2.11: General variation of tire longitudinal force with slip

The performance of an ABS is decided to a large extent by the controller algorithm being used in the micro-controller that sends signals to the solenoids in the modulator circuit. Unlike regular controllers, ABS control algorithms have multiple layers of redundancies written into them to ensure failsafe operation. The type of control algorithm used depends on the state variable being controlled. Most of the algorithms on production ABS today are based on a combination of the control of two states which are described below.

Wheel Slip Control In this method, the wheel slip is continuously calculated through wheel speed and vehicle speed sensors and is sent as a state to the ABS controller which, based on various control methodologies drives the wheel slip to the desired value. For wheel slip control, a model based law is adapted and currently this is the most widely used method for advanced ABS systems used in modern automobiles. As new control methodologies are formulated, various ABS algorithms have been proposed and evaluated over the years towards creating a more robust system that would operate under varying surface conditions. Slip control systems are known to work well for non-

decreasing force conditions.

Wheel Acceleration Control The concept of an ABS system based on the measurement of peripheral angular acceleration of the wheel is implemented using a rule-based approach. In this system, the braking cycle is designed to operate in three states: 1. Apply 2. Hold 3. Release. The ABS controller is supplied with an exhaustive look-up table that would account for different braking scenario. This table is essentially a set of threshold values for wheel deceleration and slip ratios that would decide the brake state during the prediction and re-selection stage. In a typical system, the ABS would activate when the wheel deceleration drops below a specific value. The brake states are continuously regulated such that the wheel deceleration and slip are within the provided thresholds. This method is considered to be an indirect way of controlling wheel slip because it requires careful adjustment of wheel acceleration thresholds to achieve optimum performance.

Some of the earliest work done in this area includes the work done by Guntur [66, 67] who proposed an adaptive brake control system. Taheri [68] investigated the use of non-linear control laws for ABS systems and proposed a sliding mode based control algorithm [69], a variation of which was also proposed by Drakunov et al [70]. Some authors including Mauer [71] have proposed intelligent controllers based on fuzzy logic. Robust adaptive control based on the Lyapunov method was suggested by Yu [72]. Due to the complex nature of the hydraulic actuators which cause the pressure change in the brake line, PID controllers are considered to be very robust and are popularly implemented at the lower level, such as the ones proposed by Taheri and Law [73]. Recent advances in sensor-based estimation techniques have led to the development of ABS control methods based on intelligent tires as explained by Singh et al [74]. A comprehensive review of various ABS wheel slip control algorithms has been explained by Aly [75]. Although more advanced controllers have been developed since their introduction, wheel acceleration based ABS controllers are still popularly implemented in multiple vehicle simulation models which require the wheel acceleration

signals. One of the most widely used algorithms in this regard is the Bosch® HVE version 1 algorithm which has been explained in detail by Roberts et al [17] and in their automotive handbook [76]. For the exploitation of maximum friction available at the ground, ABS control algorithms contains multiple stages of: initialing, holding, increasing, fast increasing, decreasing, fast decreasing, step increasing and step decreasing of braking pressure.

2.4 Importance of Tire Inertial Effects on ABS Braking Performance

Due to cost effectiveness, in case of wheel acceleration based ABS controllers, vehicle velocity is not measured. As mentioned, these controllers indirectly control the wheel slip based on preset wheel acceleration thresholds. The main assumption in the selection of acceleration thresholds is that, if acceleration of the wheel has reached the preset threshold, then the longitudinal slip is assumed to have reached the peak friction force and the control logic reduces the brake pressure. The vehicle reference velocity is estimated from the wheel velocity at which the wheel acceleration threshold is maximal, which is used for calculation of longitudinal slip. The advantage of this controller is its adaptability to road frictional conditions. On low frictional surfaces, the peak value of longitudinal friction is reached at lower slip ratio, as the tendency of wheel to slip is more, the wheel acceleration thresholds are reached at lower slip values. Using these methods, although the ABS is preventing wheel from locking, but the coefficient of friction available at the ground is not completely utilized. The preset wheel acceleration thresholds does not really correspond to the tire operating at peak value of friction. From the studies by Rangelov [77], it is concluded that the wheel deceleration values at the peak frictional force are dependent on initial velocity of the vehicle and the rate of application of braking torque. With the increase in initial velocity, corresponding wheel deceleration at 20% of longitudinal slip also increases. With the increase in the rate of application of braking torque, corresponding wheel deceleration at 20% of longitudinal slip

also increases. Due to fixed preset thresholds, this causes control algorithm to operate at a slightly less peak slip ratio, thus reducing the braking performance. On rough roads, this effect is aggravated where the variation in wheel acceleration signals is large. As the wheel acceleration threshold is used for the reduction in brake pressure, these disturbances cause ABS to intervene more than necessary. These frequency of fluctuations in wheel acceleration due to uneven road profiles (3 - 40 Hz) overlaps with frequency of wheel acceleration due to brake pressure cycling frequency (0 - 20 Hz), so using a low pass filter could cause ABS to respond slowly thus reduce the effective performance of the ABS. Watanabe [78] developed a control algorithm which shifts the wheel acceleration thresholds based on the level of road disturbances. He estimated wheel acceleration disturbances due to continuous road disturbance and sudden road shocks using multiple low-pass filters. Using a control logic, the acceleration thresholds are adjusted accordingly. For development and tuning of advanced ABS controllers, a high frequency dynamic tire model is needed.

When the wheel lock-up is incipient, pressure in the brake cylinder reduces rapidly and to reach the peak tractive force again, the pressure is increased in an stepwise fashion. The side effect of this rapid pressure increasing pulse is possible excitation of the torsional modes of the tire (mainly in-phase mode at 33 Hz) as shown in Figure 2.6. From early experimental studies conducted by Zanten [79], it was observed that after each pressure step input, wheel speed signals seen to contains oscillatory response. It is confirmed that these oscillations are due to transient dynamics of the tire. The Force vs Slip curve shown in Figure 2.11 is measured under steady state condition of the tire and road interface $i.e$ the forces acting between tire and road is equal to forces acting between the rim and suspension. Under dynamic conditions of ABS braking, inertial effects associated with tire-wheel assembly has to be taken into account for realistic simulation of ABS braking. The dynamic force response at the axle shows the influence of tire inertial dynamics causing limit cycles around the steady state values as illustrated in Figure 2.12, for the stepwise increase (from number 1 to number 3) and decrease (number 4) of braking torques. Under the stable region, for slip values less than 20%, a step increase in braking torque causes relatively larger braking force values than

the steady state values and after a few oscillations, a new stable point on steady curve is reached, which is seen for cases 1 and 2. In case of number 3, a step increase of brake torque drives the slip ratio to unstable equilibrium point, with a large overshoot of peak friction force than the steady state and causes slip ratio to increase rapidly. With step decrease in brake torque, the force response seems to follow the typical steady state curve. It is

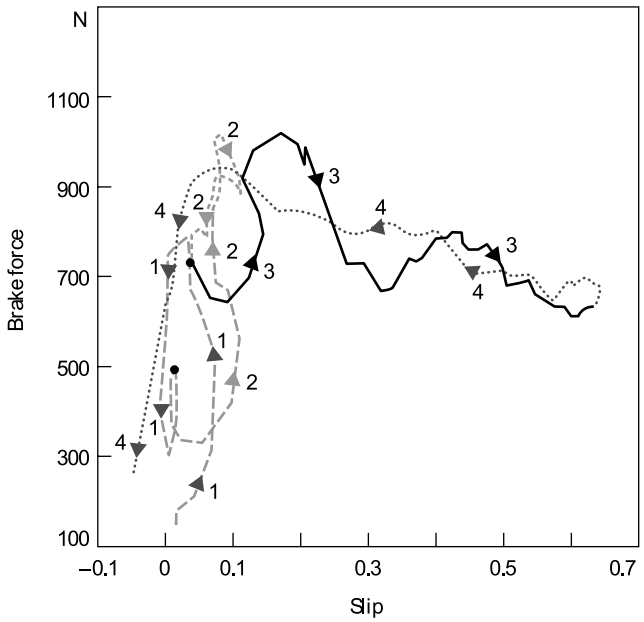

Figure 2.12: Dynamic force response for stepwise increase (from number 1 to number 3) and decrease (number 4) of brake torque [6]

clear that the nonlinear nature of the tire is causing these loops around steady state values. The nonlinearities associated with the tire are its relaxation behavior, belt inertial effects, materials etc,. As mentioned earlier, due to viscoelastic properties of tire tread components, after the slippage of the tire, it takes some finite rolling distance for the tire to generate tractive forces. This causes an initial increase in slip ratio and followed by a delayed sudden increase in tractive force as seen for cases 1 and 2 in Figure [6]. Second nonlinear effects are due to inertial vibrations of tire belt. Under the assumption of a rigid tire, angular speed at the circumference of tire belt is equal to angular speed at the rim. Due to flexible sidewalls under non steady state conditions, the slip values at the ground and at the rim are different.

The angular speed of the belt determines actual forces at the ground but the slip values are determined based on the angular speed at the rim. This causes a dynamic interaction between axle and ground contact, thus causing loops around the stationary values. For a large pressure step inputs, these inertial effects are much more predominant and cause large limit cycles or loops. The tire dynamic force response also depends on operating velocity of wheel and on surface conditions. It is clear that for accurate simulation of ABS braking maneuvers, a simple steady state model is not sufficient. For evaluation and tuning of ABS control algorithm, tire model should contains inertial and transient effects. The developed tire model should contain some physical tire parameters which have an effect on tire dynamic behavior.

Zegelaar [80] conducted various experimental studies on dynamic response of tire for various initial loads on the tire, successive step increasing of braking torque and step braking at different velocities. He developed a high frequency rigid ring tire model and analyzed the frequency and damping associated with in-phase and anti-phase torsional rigid modes of the tire under these conditions. Increase in vertical load on the tire and increase in velocity of wheel causes a change in boundary condition at the contact patch. This eventually increases the relative damping associated with in-phase mode thus decreasing the loops in the dynamic force response curves. In case of high brake torque inputs, the slip stiffness at the contact patch is decreased which decreases the damping in the in-phase mode, thus generating larger loops. Following this, Jansen et al [16] have focused on demonstrating the potential of dynamic tire models such as the rigid ring model and their comparison with steady-state and transient tire models for the analysis of the performance of ABS systems. Following this, Paulwelussen et all [15] implemented the MF-SWIFT model in a full vehicle with an ABS model and analyzed the braking response of their model at different velocities under varying road conditions. Rangelov [77] constructed a simulink model of a quarter car with MF-SWIFT and Bosch® ABS algorithm and analyzed the performance of different control methodologies.

For this research, an improved version of wheel acceleration algorithm developed at the Cen-

ter for Tire Research (CenTiRe) at Virginia Tech is used. This controller utilizes wheel peripheral angular acceleration and wheel slip ratio for the control of fast pressure cycles. Detailed modeling of ABS in explained in Chapter 3. This algorithm was originally implemented on a 2002 Volkswagen® Jetta with additional braking states and self-adjusting thresholds and reference speeds. The Hardware-In-the-Loop (HIL) validation [81] of this algorithm has also been explained in detail to demonstrate its performance when in comparison to commercial ABS systems.

2.5 Importance of Tire Inertial Effects on Ride and Comfort Performance

Another important requirement in vehicle development process is achieving a reasonably good ride and comfort performance while driving across cleats. Driving over vertical cleats excites the tire belt vibrations in longitudinal, vertical and lateral directions. Figure 2.13 shows the passenger car tire rolling over a vertical step at 80 kmph under a constant slip angle. The generated tire belt vibrations are in between a frequency of 35 - 350 Hz, these vibrations have significant effects on the ride performance of the vehicle. These effects have to be considered in the design of suspension and other chassis components. This requires a dynamic tire model to be valid at least up to 80 Hz, for the analysis and design of suspension ride controllers [82] on short wavelength road profiles. Using a quarter car model, Schmeitz [5] used a rigid ring based tire model combined with tandem based enveloping model to evaluate dynamic tire response on uneven surfaces. He concluded that tire enveloping behavior must be considered in ride comfort simulations. Recently, Frey [83] used several tire models and concluded that point contact and the roller contact models do not emulate contact patch envelopment and therefore overestimate both vertical and horizontal accelerations. In this research, not only the dynamic effects of tire on vehicle ride performance is studied but also the dynamic tire model is integrated in the development of a novel double damper based

semi-active suspension.

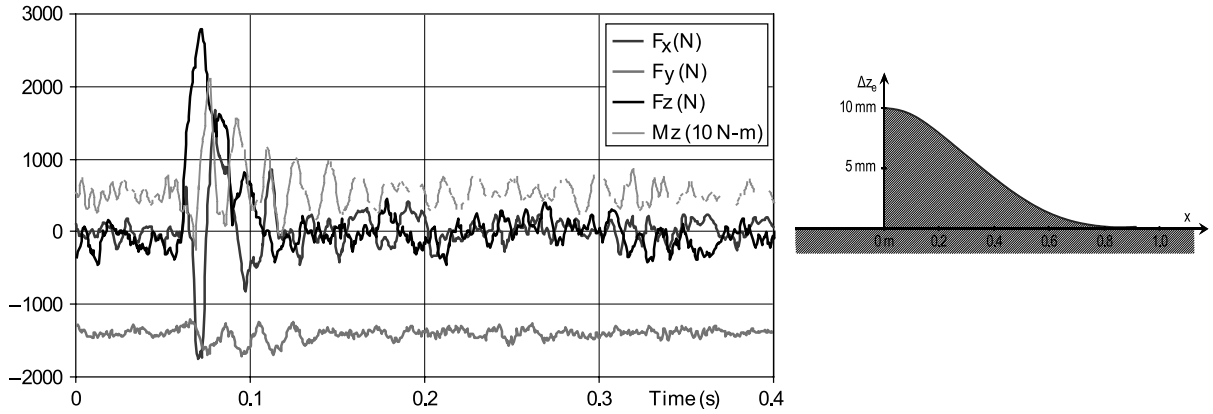

Figure 2.13: Dynamic force response of tire driving across 1 cm vertical step at 80 kmph [7]

2.6 Importance of Tire Inertial Effects on Limit Handling

Lateral forces are adversely effected due to load variations on uneven roads which eventually changes cornering stiffness and relaxation length [2] of the tire. To analyze the effects of tire belt vibrations, road disturbances and high frequency steering torque variations on the handling performance of a vehicle, a dynamic tire model should be at least valid up to 75 Hz and able to rollover uneven and relatively sharp roads [2]. In the past, handling performance of the tire-vehicle combination has been evaluated using magic formula in the tire and automotive industries for steady state handling which fails to meet realistic representation of tire road interaction. Transient tire models, based on relaxation property of tire are valid up to 20 Hz [14], because at higher slip angles of tire, relaxation length decreases and tire inertial forces due to belt vibrations are significant. These models usually lack realistic representation of tire road interaction and are not suitable for combined steering and braking maneuvers which may activate the anti-lock braking system (ABS). Maurice [84] studied lateral transient dynamics using step road wheel steer angle. Experimental studies

by Wei [85], have concluded that the tire lateral transient dynamic effects on vehicle behavior without the road effects is minimal. In this study, behavior of tire lateral transient dynamics under hard steering and also fast lane change maneuvers under the influence of uneven road is studied. Electronic stability control activates only when the physical limits of the tire is reached. Understanding the lateral tire inertial effects on uneven roads paves the way for design of ABS based advanced ESC controllers.

2.7 Literature Review of Dynamic Tire Models used for Vehicle Dynamic Simulations

First Author	Approach	Braking	Handling	Ride	Uneven Roads
van Zanten [86]	Preliminary experimental studies on ABS induced tire inertial vibrations. Developed a simple 3DOF rigid ring model with a tread and friction model to predict these effects and used for evaluating ABS control performance	✓			
Taheri Sh [47]	Developed a Hybrid Soft Soil Tire Model (HSSTM) using a brush model based on a discretized lumped mass approach				✓
van Zanten [79]	Extended the model to 6DOF and studied interactions of in-plane and out-of-plane modes of vibration on ABS control performance	✓	✓		

Jaiswal [87]	Studied and compared the ABS braking performance of stretched-string and contact mass based transient tire models. While the inertial effects of tire belt are approximated using a simple carcass compliance element	✓			
Braghin [31]	Developed an Enhanced Nonlinear Transient Tire model (ENLTT) with addition of slip dependent relaxation length effects and also shown incompetency of steady state Magic formula model	✓			
Yamashita [88]	Developed flexible ring model using absolute nodal coordinate formulation technique and LuGre model as a contact model. Studied structural deformation of tires under severe braking maneuvering and influence on force distribution in contact patch	✓			
Adcox [89]	Used only torsional DOF of rigid ring and LuGre contact model to studied errors introduced by torsional dynamics on ABS control performance	✓			
Persson [90]	In this study temperature effects during ABS braking are studied with less emphasizes on torsional belt vibrations. Developed a 2 DOF tread model using discrete masses connected with viscoelastic springs and integrated with a comprehensive velocity and temperature depended rubber friction model.	✓			
Rangelov [77]	Used MF-SWIFT tire model and integrated with quarter car and Bosch ABS algorithm to analyzed the braking performance of different control methodologies	✓			✓

Pauwelussen [15]	Used MF-SWIFT model in a full vehicle with an ABS model and analyzed the braking response at different velocities	✓			
Takahashi [91]	Used a simple first order relaxation based transient model, for wavelengths $>$ 0.2 m and small slip angle (1 deg) and studies static and dynamic cornering force losses due to vertical load variations		✓		✓
Schmeitz [5]	Developed a complete MF - SWIFT model, and used for ride comfort and durability simulations			✓	✓
Frey [83]	Compared and analyzed ride comfort simulations using different enveloping models like point contact, rigid contact follower, constant footprint model, adaptive footprint model, two point follower with rigid ring model, five point follower with rigid ring model. Ranked these models based on maximum chassis accelerations over different obstacles at different velocities			✓	✓
Hofstad [92]	Improved MF-SWIFT model to accurately model vertical load variations at high camber angle and slip angle for roll over simulations			✓	
Gim [93]	The tire dynamic properties and contact force characteristics are explicitly formulated using analytically derived functions of the tire deformations, slip ratio, slip angle, camber angle	✓	✓		
Lee [94]	The dynamic behavior of tire contact patch under severe crash avoidance maneuvers is modeled. A discrete brush model and a methodology for relating dynamic effects of contact patch on dynamic force generation is developed	✓	✓		

Table 2.1: Literature review of dynamic tire models used for vehicle dynamic simulations

From Table 2.1, only [77] simulated ABS braking maneuvers on uneven road profiles. Rangelov [77] studies emphasized the importance of various control logics on ABS braking performance. In this research work, a comprehensive study of tire dynamic effects during ABS braking on uneven roads, and under spilt-μ condition are performed. The influence of high frequency inertial vibrations induced due to the presence of cleats, and high pressure pulse inputs from ABS, on braking performance are studied. Regarding the study of handling performance on uneven road profiles, Takahashi [91] studied the loss of cornering stiffness due to vertical load variations. As the vertical load variations are bound to low frequency and inertial effects of tire are not considered, this approach is not valid under short wavelength road profiles and at higher slip angles. In the research presented here, tire lateral inertial effects under limit handling condition is studied using different independent maneuvers. In addition, a more tire dependent objective performance metrics was developed. From literature, a very few models [93, 94] are developed for high frequency combined braking and handling studies. As the models developed by Gim [93] and Lee [94] are preliminary studies, more emphasis is placed on ability of the tire model to predict the vehicle response. van Zanten [79] studied the effects of excitation of lateral belt vibrations on ABS controller performance without road effects, and concluded it is minimal. In this research, behavior of tire lateral transient dynamics under the influence of road undulations, hard steering, braking, combined braking and steering and accelerating and steering are studied comprehensively. For detailed technical survey of tire models used for tireterrain interactions refer to [95].

2.8 Handling Performance Metrics

The handling performance are expressed in terms of steerability, controllability, and stability [96]. The steerability is the ability of vehicle to follow a turn without taking much steering effort and it is categorized into on-center and transient handling response of the vehicle. Norman [97] developed the testing procedure and the metrics to characterize on-center handling. Mimuro [98] developed a methodology to characterize the transient response of the vehicle by using four independent parameters, extracted from impulse steering test. Recently, Crolla performed and developed a comprehensive objective handling performance metrics, for correlating to subjective feel of the driver. In collaboration with MIRA automotive testing company, performed various experimental constant radius, step steer, impulse steer and lane change maneuvers and derived performance metrics using both time and frequency response of various vehicle variables [12, 99]. For more information on handling objective tests refer to ISO standard procedures [100, 101, 102, 103, 104]. In this research work, derogation in handling performance of the vehicle on uneven roads in terms of controllability and and stability is studied. From literature [2], it is known that when a vehicle goes around a turn on uneven roads, the slip angles are increased than on smooth roads, due to continuous vertical load variations and the reduced cornering stiffness. Performance metrics are developed from constant radius maneuvers on smooth and uneven roads, to quantify uneven road effects on handling.

2.9 Electronic Controllers

The study of two types of electronic controller system is pursued in this research; active suspension control and active four wheel steering control. In real world, vehicles are subjected to a vast range of surface roughnesses, road input events, speeds, braking/accelerating forces, etc. The control laws developed based on linear vehicle models, should be robust enough to work under various conditions. This requires advanced control theory in the development

of vehicle dynamics controllers, which has a capability to adapt to the operating conditions. In this study, a Lyapunov based adaptive control algorithm was utilized in the development of active and semi-active damper control and a four wheel steering control. The advantage of Lyapunov based controller is its computational simplicity due to effective exploitation of system dynamics. In [105], a similar methodology is used for control of robot manipulators and later modified to apply to vehicle applications [106].

2.9.1 Active and semi-active Suspension Controller

The active and semi-active suspension controllers can improve the ride comfort for driver and passengers with the acceptable control of body attitude and adequate control of the dynamic tire loads within the constraint of suspension working space available [12]. Although the potential improvements of ride comfort with active suspension is much more than passive suspension, several major disadvantages like high power consumption, unreliability, more complex and much costly system, placed the active suspension on the shelf. Semi-active suspension system, on the other hand, seems to be the best compromise in terms of cost, reliability and power consumption. In this case, as the damper can only draw energy from the vehicle system by opposing the motion of the mass, the ride performance when compared with active systems are decreased.

In this study, a novel double damper suspension is introduced to show that a simple design modification of suspension can further improve the performance of the semi-active suspension. In [107], the concept of two controllable dampers was applied to one DOF base excitation case. It was observed that addition of controllable damper in parallel with passive spring changes the equivalent stiffness of spring thus controls the stiffness of the system without physically varying the spring stiffness. With this background, two controllable semi-active dampers were used to improve the vibration characteristics of the vehicle. A suspension system with two dampers attached in series is introduced in this study and its scope of potential improvements of ride control, without bottoming of suspension and deterioration of

road holding properties is discussed. The outcome of this study is a novel semi-active suspension system emulating an active suspension, thus the primary hurdle of power consumption and unreliability in implementation of active suspension control is overcame. Therefore, the objective of this study is to achieve the ride performance equivalent to a full active suspension system using a semi-active suspension and integrating dynamic tire model in development of active suspension controllers.

2.9.2 Four Wheel Steering Controller

The primary advantages of four wheel steering (4WS) systems are [12]:

1. improved transient response
2. improved yaw damping following a transient
3. reduced peak yaw rates
4. reduced lateral acceleration phase lag and
5. reduced body sideslip angles

Using a 4WS controller can improve the handling performance of the vehicle. This is due to the ability of rear tire forces to be controlled independently from the front tires. Typically, in a turn after the driver induces handwheel angle, side forces at front tire are generated, but the forces in the rear tire are only generated after the vehicle yaw moment is induced (rotates about its vertical axis). With the help of a 4WS control, the delay is generation of rear slip angles is reduced significantly, thus improving the transient response of the vehicle. Due to the greater potential of 4WS control in improvement of handling performance, the behavior of vehicle under the influence of 4WS control is studied extensively at higher speeds and lower speeds [108, 109]. From the mid-1980s, a large number of theoretical studies aimed at deriving control strategies [110, 111, 112] for 4WS were published and a number

of commercial systems have appeared, particularly on Japanese cars [113, 114]. For detailed literature review of 4WS controllers refer to [115]. In this study, a Lyapunov based 4WS controller is developed based on a linear bicycle model. The performance of controller is evaluated for a double lane change maneuver against a normal front wheel steering vehicle.

2.10 Enhancements to Rigid Ring Dynamic Model

2.10.1 Dynamic Stiffness Variations

From Figure 2.6, during the unloaded condition, the inplane rigid modes of vibrations of the tire are only vertical and torsional modes, where as in case of a loaded condition there were four modes. The other two extra modes are due to the presence of contact patch under a loaded condition. It is evident that different boundary conditions acting on the tire can change the natural frequencies of the tire, Richards [116] used finite element and modal test techniques and demonstrated the dependence of dynamic stiffness on the boundary conditions of the contact patch and the spindle. These natural frequencies also changes with respect to the rolling velocity of the tire, tire construction, and road unevenness. From the experimental studies [117, 118, 119], it is found that the frequencies of the vertical mode, the in-phase rotational mode, and the anti-phase rotational mode decrease with velocity. Rigid ring model proposed by Zegelaar [4], effectively captures these effects by considering the sidewall stiffness parameters to be velocity dependent. From the experimental and simulation studies using FTire model, Dorfi [120] studies the dynamic stiffness variations due to tire construction (belt angle and belt filler), and inflation pressure. The variations in in-phase rotational mode, and the anti-phase rotational mode frequencies are observed due to the footprint boundary condition. From the literature, it is found that when rolling over uneven road profiles, longitudinal stiffness of the tire changes due to high frequency inputs [121], thus effecting the in-phase and the anti-phase rotational modes. This is caused due to the rapid variations in the length of contact patch. Wei [121] using the FE model,

analyzed the variations of contact patch while rolling over the cleat of different heights. He concluded that the tire cannot envelop the obstacles completely with the increasing height of the cleat. Due to decrease in contact area, this tends to lower the longitudinal natural frequency, particularly inplane mode. Present rigid ring model is unable to capture these dynamic longitudinal stiffness variations effectively, although rigid ring model takes velocity effects into account. As, rigid ring model is a single point contact model integrated with multiple cam based enveloping model which uses a finite contact length. The multiple contact patches due to the obstacle shape are not represented by this model. In this research, these dynamic longitudinal stiffness variations are taken into account by considering the sidewall stiffness parameters to be dependent upon variations of vertical force acting in the contact patch.

2.10.2 Thermal Modeling

Usually, the force and moment characteristics of the tire are modeled taking into account tire mechanical properties, normal load and inflation pressure. Due to the visco-elastic nature of tire, especially tread component is sensitive to the ambient temperature changes [18]. From the previous studies, it is common knowledge that tire/road friction coefficient is heavily affected by the temperature level of the tire component [122, 123]. The variation in tire thermal properties when the tire is subjected to different stress types (high slip and camber angles, normal load, inflation pressure, vehicle speed) has to be considered in the tire modeling. Especially for transient vehicle maneuvers like sudden steering input and heavy ABS braking, due to the continuous operation of tire at peak friction and induced stress from road roughness, the temperature of tire surface grow exponentially [90, 124]. Recently, experimental measurement of force response of tire on a rear-wheel driven vehicle during a power-on cornering maneuver, showed a decreased grip than estimated [125] on rear wheels, thus causing an oversteer. The objective of this study is to model the thermal effects of the tire. To see how surface temperature varies depending upon various conditions and how

these variations influence the tire behavior will be of prior concern.

From literature, various approaches are used to estimate the surface temperature of the tire. Sorniotti [122], Masahiko [123] estimated surface temperature using a heat transfer based approach. Using these temperature rise values, the empirically developed peak frictional model is used. These thermal tire models are developed based on indoor testing where tire measurement input conditions do not correspond to the actual road surface conditions. Michelin developed physics based thermal model called TameTire [124]. It consist of three models: one for the tire mechanics to estimate structure deformations, one for the compound characteristics (shear modulus and friction) and one for the tire surface temperature estimation. Recently, Farroni [126] proposed a new model which can predict dynamic response of a tire and its frictional and thermodynamic behavior by means of specific track sessions and a few laboratory measurements of tire material properties. This model contains four modules which are modeled using empirical and physical modeling techniques. In this research, for modeling the temperature depended force characteristics, two different modules are developed. A heat transfer based module to estimate the rise in temperature according to the energy loss due to the slippage of tire. The other module uses a magic formula based model whose parameters are shifted accordingly with the increase in temperature.

2.11 Model Requirements

From the above literature review on tire models and also for understanding the importance of tire dynamic effects under ABS braking, handling and rolling over short wavelength road profiles. The key tire and vehicle model requirements for high frequency vehicle dynamic simulations are as follows:

- The model should contain physical tire parameters for parametric sensitivity studies and their relative importance on performance of the vehicle.

- The simulation tool should be capable of modeling the dynamic response of the tire for excitations up to 75 Hz.
- The model should be capable to enveloping any type of uneven road surfaces with relatively sharp unevenness including short wavelength disturbances at least 10 cm in wavelength.
- The tire model should be integrated with thermal model to characterize frictional variations due to rise in temperature at the contact patch.
- The simulation results should be accurate within the operating limitations of the models and verifiable through experiments.
- The tire model should be integratable in development and implementation of novel active control systems under short wavelength road profiles.
- The developed tire model should be fast enough for vehicle dynamic simulation as this tire model will be used in Hardware-In-the-Loop (HIL) simulation for the development and tuning of electronic controllers.
- The vehicle model used should be accurate enough with multi degree of freedom nonlinear model valid within the range of tire model, this is achieved with the interface of commercial vehicle dynamic software such as CarSim®.
- Steering system model of vehicle should contains some compliance and nonlinear effects associated with power steering.
- The ABS algorithm should be based on a commercial ABS system on a production vehicle with comparable performance and response.
- The parameters required for the simulation model should be kept to a minimum with low experimental effort required for parameter estimation.

- Standard formats should be adopted for the exchange of experimental data and tire parameters for model parametrization and validation to avoid ambiguity and improve integration into the existing design work-flow.
- Implementation of the model should be done on a commonly used simulation platform and should be capable of being adopted to other platforms or run as a standalone application.

The biggest challenge for the selection of a model is parameterization. Usually, some of the models [93, 94] contain many model parameters which requires a large number of experimental data and some of the testing procedure are still not yet standardized. These parameters cannot be easily determined or measured directly. Although, recently developed MF-SWIFT model [127] is also difficult to parameterize but efforts are made to improve the parameter identification process using industry common test facilities (for a detailed procedure for parameterization refer to [128]).

2.12 Conclusions

A comprehensive literature review of all the available modeling tools and existing technology which can be leveraged towards the development of the simulation tool has been conducted. Based on this, the following conclusions have been drawn which have been listed below:

- The reaction forces generated by a tire are influenced by the belt vibrations induced due to road unevenness, variations in brake and steering torque and the oscillations in axle height. The direct resultant of this is their effect on braking, handling and ride performance of the vehicle.
- Simple transient models are not sufficient for modeling all the above influencing factors. Various tire models are available to account for such factors. Multi-body and FE based models are computationally expensive for vehicle dynamic simulations.

- Dynamic tire models show considerable difference in response to braking in comparison to steady-state and transient tire models which validate their necessity.
- The enveloping property of the tire should be included in conjunction with the tire model to account for the filtering effect of the tire and the influence of road unevenness on force response.
- ABS controller indirectly controls the slip based on preset wheel acceleration thresholds. These thresholds change with respect to operating conditions (velocity, braking torque, tire, etc).
- For evaluation and tuning of ABS control algorithm, tire inertial and transient effects are very important.
- Lateral and vertical forces are adversely effected due to load variations on uneven roads, which are inturn excited due to tire belt vibrations.

Chapter 3

Mathematical Modeling

Following the detailed literature review and the consequent selection of available models from literature, this chapter presents mathematical modeling of all components needed to be undertaken for vehicle dynamic simulations which is discussed in the next chapter. This chapter explains the assumptions for each model and respective equations, constitutive relations and curves that govern their behavior. Detailed knowledge of the mathematical aspects and range of validity of the rigid ring model, enveloping model, contact model, slip model and vehicle model in CarSim are explained. ABS, steering model and suspension models form the basis for vehicle dynamic simulations pursued in this study (braking, handling and ride) and are explained in detail. For the dynamic tire model, most of the equations were based on the work by Schmeitz [5], which were later improved by TNO Automotive during its commercial implementation as MF-SWIFT and described in their equation manual [127] and in latest version of the book [2].

3.1 Dynamic Tire Model

The mathematical modeling of tire consists primarily of:

1. Enveloping Model - models the enveloping behavior of tire using multiple elliptical cams model

2. Rigid Ring Tire Model - models the tire inertia properties using rigid ring connected with springs and dampers to the rim

3. Contact Model - models slippage of tire contact patch using lumped mass with 3 DOF model connected to rigid ring.

4. Slip Model - models longitudinal and lateral relaxation behavior of tire with first order ODE's

3.1.1 Coordinate System

The axis system used in this chapter are right-handed, orthogonal with ISO-definitions of z-axis pointing upwards. As shown in Figure 3.1 the wheel axle system is defined by the location of the wheel center (x^a, y^a, z^a) with orientation angles of (γ_a, θ_a, ϕ_a) with respect to ground axis system (G). The wheel angular rotation is given by Ω. The origin of the belt axis system (b) is located at the belt center and the belt plane is spanned by the x^b- and z^b-axis. The effective road surface axis system (e) is defined to be in such a way that the effective road plane is spanned by the x^e- and y^e-axis with z^e -axis normal to the effective road plane. The origin of the effective road axis system lies at a distance h vertically above the ground axis system (G). A contact axis system (x^C, y^C, z^C) is defined with x-axis pointing forward and runs along the line of intersection of the wheel plane and the effective road plane (e). The axis lies in the plane normal to the road plane and passes through the wheel spin axis. The z axis forms the normal to the road surface.

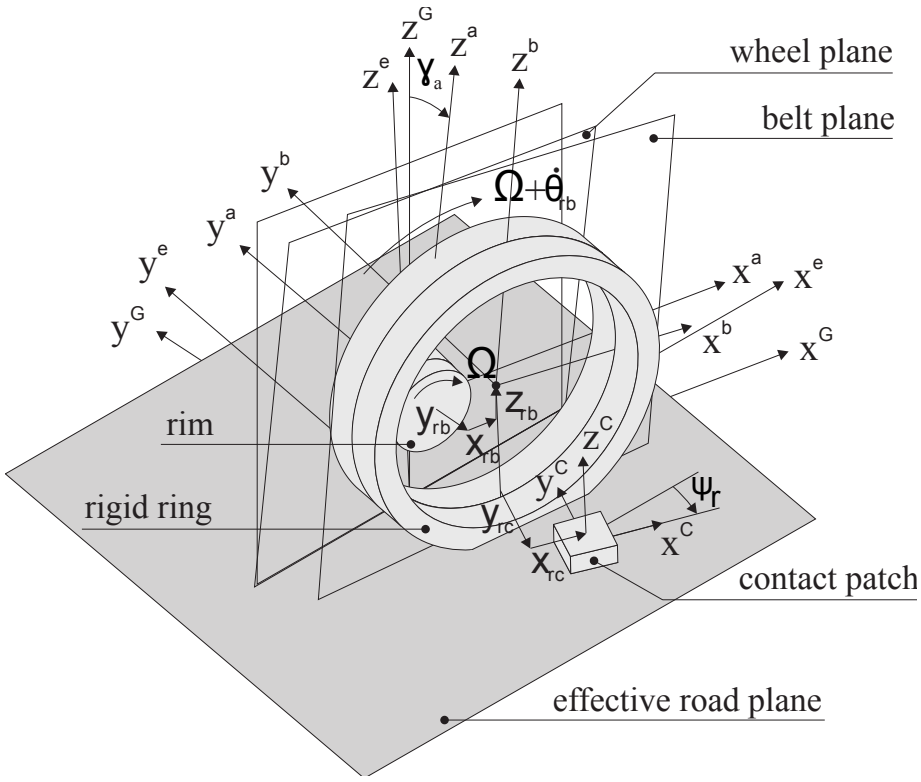

Figure 3.1: Axis system of rigid ring model corresponding to different components: ring, axle, contact model, effective road surface [5]

3.1.2 Enveloping Model

The enveloping property of the tire is modeled using the tandem elliptical cam model developed by Schmeitz [5]. This model can be used for any short wavelength road profile and can adapt to load variations. This model is used for calculation of the effective road surface over which point contact rigid ring model rolls. Each elliptical cam is of a shape of standing egg with radius of curvature smaller than free tire and height approximately equal to the tire. As explained in the literature, this semi-empirical model assumes multiple elliptical cams in a tandem (connected by rods) rolling over the uneven road surface, constrained to move only in the vertical direction. Figure 3.2 shows a two cam tandem model rolling over an obstacle, as illustrated by Schmeitz [5]. Figure 3.3 shows extension of the two-dimensional tandem model with two parallel tandems in lateral direction, characterizing effective height

w, effective slope β_y and effective camber β_x of road surface. The elliptical cam has a width

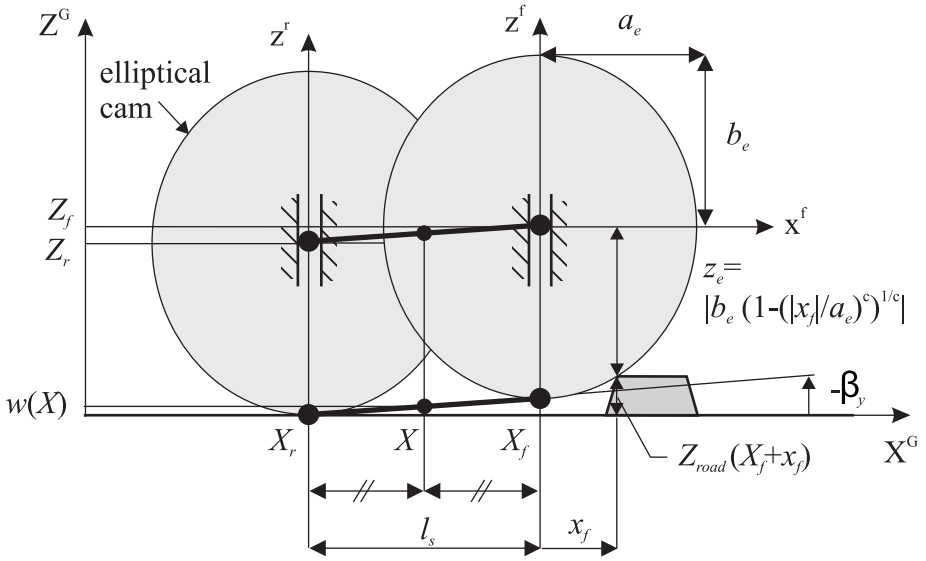

Figure 3.2: Two-dimensional tandem elliptical cam model [5]

a_e and height b_e. The subscripts 'G','f' and 'r' are used to denote the coordinate systems for the global road, front and rear elliptical cam respectively. The cams are separated by a distance l_s in longitudinal direction. This parameter is a function of the vertical load on the tire and is calculated based on the contact length $2a$:

$$l_s = p_{ls} \cdot 2a \tag{3.1}$$

where p_{ls} is a model parameter estimated through experiments. In lateral direction distance between the cams equal to contact width $2b$. The distance (shift) between the cams increases as the load increases.

The inputs to this model are the wheel center position X and the cam center height Z coordinates in the global frame of reference, where Z_f and Z_r are the global heights of the front and rear cams respectively as shown in Figure 3.2. For the front ellipse, we know its equation in the local coordinate system as:

$$\left(\frac{x_f}{a_e}\right)^{c_e} + \left(\frac{z_f}{b_e}\right)^{c_e} = 1 \tag{3.2}$$

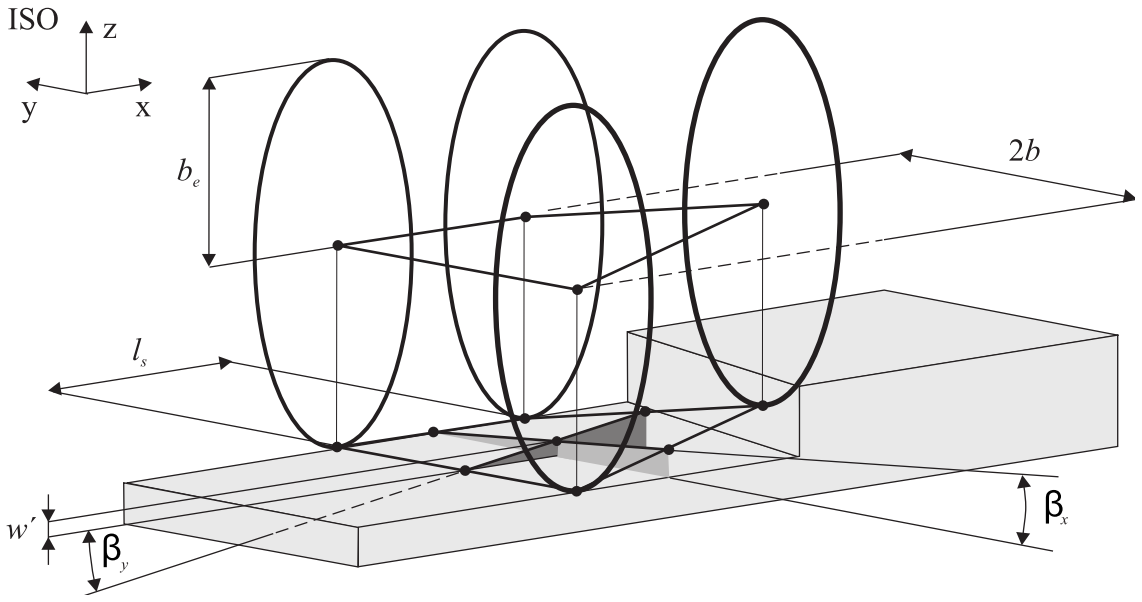

Figure 3.3: Three-dimensional tandem elliptical cam model [5]

where x_f and z_f are the local position coordinates for the front ellipse. The vertical distance (z_e) between the local X-axis and the ellipse for any local position x_f is calculated based on Equation (3.2) as:

$$z_e(x_f) = \left| b_e \cdot \left(1 - \left(\frac{|x_f|}{a_e}\right)^{c_e}\right)^{\frac{1}{c_e}} \right| \tag{3.3}$$

From Figure 3.2, we can observe the front ellipse rolling over an obstacle of height Z_{road}. Thus the global height of the front ellipse(Z_f) is calculated using a maximal relation as the sum of the road height and the vertical distance between the ellipse contact point and the center:

$$Z_f = \max\left[Z_{road}(X_f + x_f) + z_e(x_f)\right] \quad \forall\, x_f \in [-a_e, a_e] \tag{3.4}$$

Equation (3.4) is a maximal relation because to calculate Z_f it is necessary to find out where the ellipse actually makes contact with the road profile. This is done using an iterative procedure where the road profile is sampled at specific intervals around the global position of the front ellipse X_f with a maximum limit of the ellipse width a_e where the global height of the front ellipse is calculated at each interval using Equation (3.4) and the maximum

obtained value at the end of the iteration is taken as the final global height. The same procedure is also repeated for the rear ellipse.

Special care must be given to the selection of the sample interval and the total scan width because the number of points to scan at each road position would play a major role in determining the speed and accuracy of the algorithm. Scan intervals which are too big might lead to inaccurate results. Also, scanning the entire width of $[-a_e, a_e]$ might severely slow down the calculation speed as this step is repeated at each simulation time step. Generally, the resolution of the road profile is taken as the sample interval and the scan width is adjusted accordingly to achieve the right balance between accuracy and speed. The maximum allowable sampling interval is 2 cm to achieve acceptable results.

Following the scan of respective road profile at the contact of all four cams, the global heights of all four: front left, front right, rear left and rear right cams are calculated. The effective height w is calculated by averaging the effective heights of all four tandem at the wheel center X.

$$w(X) = \frac{Z_{f,left} + Z_{f,right} + Z_{r,left} + Z_{r,right}}{4} - b_e \tag{3.5}$$

The effective forward slope angle β_y is calculated by averaging the effective slope of left and right cams

$$\tan \beta_y(X) = \frac{Z_{r,left} - Z_{f,left} + Z_{r,right} - Z_{f,right}}{2l_s} \tag{3.6}$$

The effective forward slope angle β_y is calculated by averaging the effective slope of front and rear cams

$$\tan \beta_x(X) = \frac{Z_{f,left} - Z_{f,right} + Z_{r,left} - Z_{r,right}}{2(2b)} \tag{3.7}$$

Usually a simple four tandem cam model is not sufficient to characterize camber and slope changes in sharp road profiles, Schmeitz [5] suggests that a minimum of 10 cams in each longitudinal and lateral directions in total of 36 cams around the contact patch area are needed to characterize any short wavelength road profiles. The modeling parameter of enveloping cam p_{ls}, a_e, b_e and c_e are obtained by quasistatic rolling of tire over various obstacles and optimizing measured and simulated responses. Three dimensional cam requires same parameters as

two dimensional cams and it was validated in previous studies by Sivaramakrishnan [129].

3.1.3 Rigid Ring Model

The rigid ring tire model consists of a circular rigid body with mass m_b and moment of inertia I_{bx}, I_{by} and I_{bz}. The axle is assumed to be a rigid body with moment of inertia I_{ay}. The inertia quantities of belt are calculated based on the corresponding parts which move around the belt of tire (tread, bead and outer sidewall) and inertia quantities of axle are those corresponding to the parts which move around the axle (inner sidewall and ABS brake disc and callipers). The Rigid ring model is based on the assumption that the belt remains rigid and inextensible below 75 Hz. As shown in Figure 2.6, this is a valid assumption as the tire modes of vibration below 100 Hz are rigid modes of vibration of belt. The flexible tire sidewall is represented by connecting the rigid ring with the axle in longitudinal, lateral, vertical, camber, torsional and yaw directions using nonlinear spring (k_{bx}, k_{by}, k_{bz}, $k_{b\gamma}$, $k_{b\theta}$, $k_{b\phi}$) and dampers (c_{bx}, c_{by}, c_{bz}, $c_{b\gamma}$, $c_{b\theta}$, $c_{b\phi}$), as shown in Figure 3.4, To describe the small relative angular displacements of the tire belt with respect to the rim in the non-rotating axle axis system, three rotations γ_{rb}, θ_{rb} and ϕ_{rb} and relative displacements x_{rb}, y_{rb} and z_{rb} are introduced as shown in Figure 3.1. The contact model with a small mass m_c and moment of inertia I_c is connected to the outer circumference of rigid ring using residual stiffness and damping elements as shown in Figure 3.4.

Inputs and Outputs

The rigid ring model requires inputs from other models to compute forces at the axle, namely:

Axle Motion Axle deflections represented by x_a, y_a and z_a and velocities of axle with respect to axle axis are V^a_{ax}, V^a_{ay} and V^a_{az} and angular velocities are ω^a_{ax}, ω^a_{ay} and ω^a_{az}, where ω^a_{ay} equal to rotational velocity of wheel Ω. These deflections are generated due to external forces acting from axle and reaction forces from the vehicle. When the

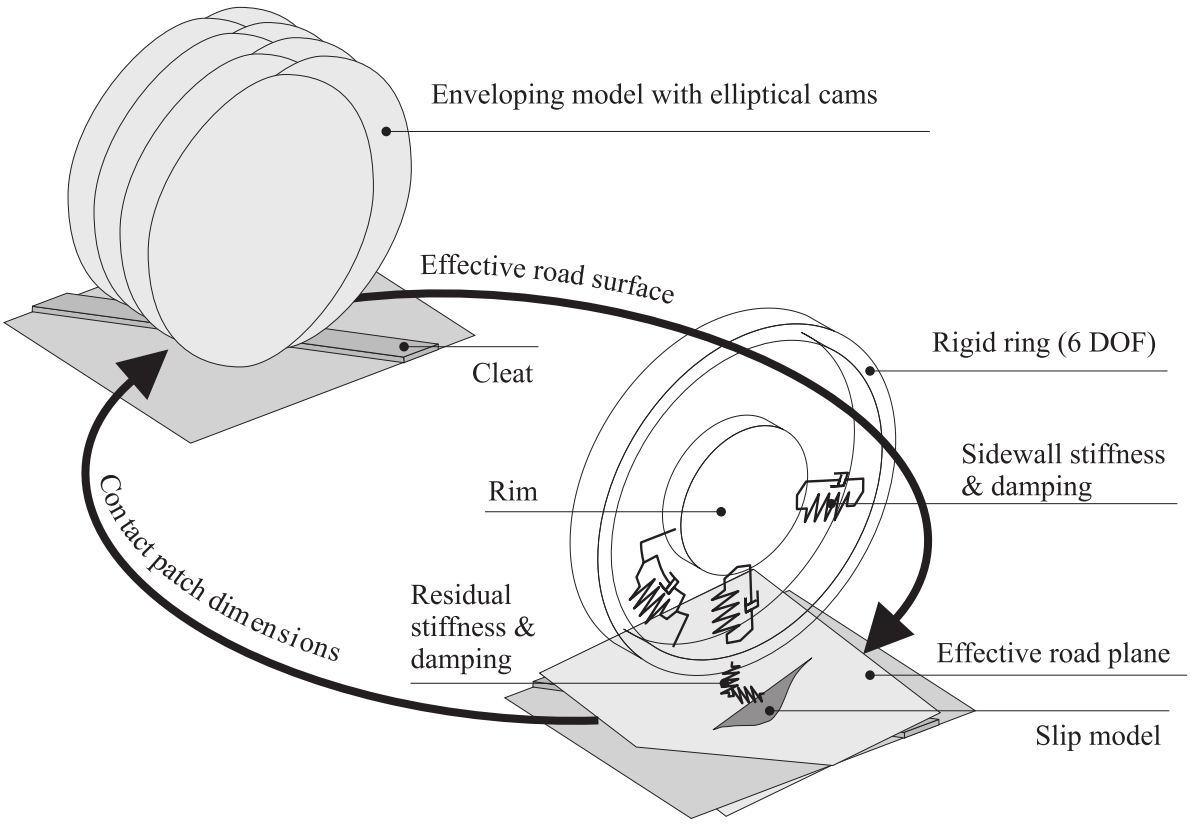

Figure 3.4: Structure of rigid ring model with integrated enveloping model [5]

tire is loaded, the axle is given an initial vertical displacement (which is negative) to represent the deflection in the tire. In the case of experiments with a fixed axle, z_a is kept constant and $V_{az} = 0$.

Effective Road Surface This is filtered road surface generated from road undulations using enveloping model, as shown in Figure 3.4. This consists of the effective road height w, road slope β_y and road camber β_x. These values are calculated for each time step. This surface acts as input to point contact rigid ring model with contact model.

Camber of Wheel This is initial camber angle of the wheel axis γ_a with respect to vehicle.

External Forces on belt These are external forces F_{bx}^b, F_{by}^b and F_{bz}^b acting on belt from contact model. These forces generated from the deflection of residual spring in contact

model which are transformed into effective surface plane.

Braking Moment This is denoted by M^a_{ay} and this input is provided by the braking module which calculates the applied torque at the axle during a braking event. This can either be due to ABS or manual braking.

Steering Torque at Kingpin Along with rotational deflections due to suspension and axle motion, in case of handling studies inputs from steering also induces additional deflections at the axle due to steering wheel input.

Based on the above inputs, the rigid ring model calculates the following outputs which serve as inputs to the vehicle, ABS model, Active Slip Controller (ASC) and ESC models:

Reaction Forces and Moments at axle These are the forces and moments acting on the vehicle from the tire, denoted by F^a_{bx}, F^a_{by}, F^a_{bz}, M^a_{bx}, M^a_{by} and M^a_{bz} due to internal deflection of spring and dampers representing sidewall, given in equation (3.9).

Wheel Slip Ratio The dynamics of the tire rolling over uneven surfaces causes fluctuations in the angular velocity of the wheel due to the deformation of the belt in the rotational direction. The practical slip ratio κ is calculated from the slip model.

Wheel Slip Angle The dynamics of the tire rolling over uneven surfaces and steering inputs causes fluctuations in the lateral deformations at wheel due to the deformation of the belt in the lateral direction. The slip angle α, which acts an input to active slip controller is calculated from the slip model.

Contact Patch Area This is effective contact patch area, calculated either based on the net load acting on the contact patch or the vertical deflection of the tire due to road undulations. The length of the contact patch is denoted by $2a$ and width by $2b$. These serves as an input to the enveloping model to calculate the shift between the tandem elliptical cams in longitudinal and lateral directions.

Equations of Motion of Belt

The equation of motion of 6 DOF ring using Newton-Euler transformations in a non-rotating belt ISO axis system are given by

$$m_b\left(\dot{V}^a_{ax} - \omega^a_{az}V^a_{ay} + \ddot{x}_{rb}\right) + c_{bx}\dot{x}_{rb} + k_{bx}x_{rb} - c_{bz}\Omega z_{rb} = F^b_{bx} \tag{3.8a}$$

$$m_b\left(\dot{V}^a_{ay} + \omega^a_{az}V^a_{ax} - \omega^a_{ax}V^a_{az} + \ddot{y}_{rb}\right) + c_{by}\dot{y}_{rb} + k_{by}y_{rb} = F^b_{by} \tag{3.8b}$$

$$m_b\left(\dot{V}^a_{az} - \omega^a_{ax}V^a_{ay} + \ddot{z}_{rb}\right) + c_{bz}\dot{z}_{rb} + k_{bz}z_{rb} + c_{bx}\Omega x_{rb} = F^b_{bz} \tag{3.8c}$$

$$I_{bx}\left(\dot{\omega}^a_{ax} + \ddot{\gamma}_{rb}\right) - I_{by}\left(\Omega + \dot{\theta}_{rb}\right)\left(\omega^a_{az} + \dot{\psi}_{rb}\right) + c_{b\gamma}\dot{\gamma}_{rb} + k_{b\gamma}\gamma_{rb} - c_{b\psi}\Omega\psi_{rb} = M^b_{bx} \tag{3.8d}$$

$$I_{by}\left(\ddot{\theta}_{rb} + \dot{\Omega}\right) + c_{b\theta}\dot{\theta}_{rb} + k_{b\theta}\theta_{rb} = M^b_{by} \tag{3.8e}$$

$$I_{bz}\left(\dot{\omega}^a_{az} + \ddot{\psi}_{rb}\right) + I_{by}\left(\Omega + \dot{\theta}_{rb}\right)\left(\omega^a_{ax} + \dot{\gamma}_{rb}\right) + c_{b\psi}\dot{\psi}_{rb} + k_{b\psi}\psi_{rb} - c_{b\gamma}\Omega\gamma_{rb} = M^b_{bz} \tag{3.8f}$$

where internal forces acting on axle are give by

$$F^a_{bx} = c_{bx}\dot{x}_{rb} + k_{bx}x_{rb} - c_{bz}\Omega z_{rb} \tag{3.9a}$$

$$F^a_{by} = c_{by}\dot{y}_{rb} + k_{by}y_{rb} \tag{3.9b}$$

$$F^a_{bz} = c_{bz}\dot{z}_{rb} + k_{bz}z_{rb} + c_{bx}\Omega x_{rb} \tag{3.9c}$$

$$M^a_{bx} = c_{b\gamma}\dot{\gamma}_{rb} + k_{b\gamma}\gamma_{rb} - c_{b\psi}\Omega\psi_{rb} \tag{3.9d}$$

$$M^a_{by} = c_{b\theta}\dot{\theta}_{rb} + k_{b\theta}\theta_{rb} \tag{3.9e}$$

$$M^a_{bz} = c_{b\psi}\dot{\psi}_{rb} + k_{b\psi}\psi_{rb} - c_{b\gamma}\Omega\gamma_{rb} \tag{3.9f}$$

Equations of Motion of Axle

The rigid axle with moment of inertia I_{ay} has one rotational DOF and with external braking torque M^a_{ay} acting on it. The equation of motion is given by

$$I_{ay}\ddot{\theta}_a + c_{b\theta}\left(\dot{\theta}_a - \dot{\theta}_b\right) + k_{b\theta}\left(\theta_a - \theta_b\right) = M^a_{ay} \tag{3.10}$$

For detailed derivation of equation of motion refer to [5]

3.1.4 Contact Model

The contact model consists of a 3 DOFs contact mass (m_c, I_c) moving over effective road surface as shown in Figure 3.1. Contact mass is attached to the outer circumference point contact of the belt through residual springs (k_{rx}, k_{ry} and $k_{r\psi}$) and dampers (c_{rx}, c_{ry} and $c_{r\psi}$). The residual springs and dampers compensate for over all stiffness and unmodeled higher modes of the tire. The inputs to the model are the external forces and moments (F_{sx}, F_{sy} and M_{sz}) generated due to slippage of contact patch given in equation (3.22) and internal forces (F_{cx}, F_{cy}, M_{cz}) due to deflections of the residual springs and dampers as shown in Figure 3.5. The outputs from the model are slip velocities in contact patch $V_{c,sx}$ and $V_{c,sy}$ which acts as input to slip model in equation (3.15) and (3.18).

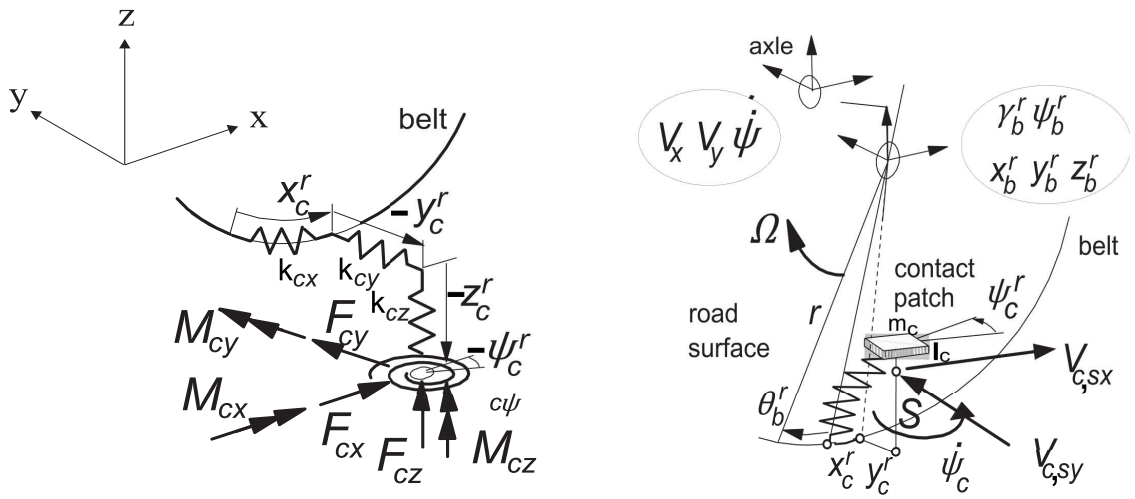

Figure 3.5: External forces acting on contact mass causing slip velocities in contact patch [2]

$$m_c\left(\dot{V}_{c,sx} - \dot{\psi}_c\dot{V}_{c,sy}\right) + F_{cx} = F_{sx} \tag{3.11a}$$

$$m_c\left(\dot{V}_{c,sy} + \dot{\psi}_c\dot{V}_{c,sx}\right) + F_{cy} = F_{sy} - F_{y,NL} \tag{3.11b}$$

$$I_c\ddot{\psi}_c + M_{cz} = M_{sz} \tag{3.11c}$$

where $F_{y,NL}$ is non-lagging lateral force due the camber of wheel or road. The internal forces in residual spring and dampers are given by

$$F_{cx} = c_{rx}\dot{x}_{rc} + k_{rx}x_{rx} \tag{3.12a}$$

$$F_{cy} = c_{ry}\dot{y}_{rc} + k_{ry}y_{rc} \tag{3.12b}$$

$$M_{cz} = c_{r\psi}\dot{\psi}_{rc} + k_{r\psi}\psi_{rc} \tag{3.12c}$$

The residual deflections x_{rc}, y_{rc} and ψ_{rc} are calculated based on deflections of the belt, slippage in contact model and additional slip velocity due to effective rolling radius (curvature of road surface). The equations are given as

$$\dot{x}_{rc} = V_{c,sx} + V_{b,cx} - (\psi_{rb} + \psi_{rc})\, V_{b,cy} + r_e\dot{\theta}_b - \rho_z\frac{d\beta_y}{dt} \tag{3.13a}$$

$$\dot{y}_{rc} = V_{c,sy} - V_{b,cy} + (\psi_{rb} + \psi_{rc})\, V_{b,cx} \tag{3.13b}$$

$$\dot{\psi}_{rc} = \dot{\psi}_c - \dot{\psi}_{rb} - \dot{\omega}^a_{az} \tag{3.13c}$$

where $V_{b,cx}$ and $V_{b,cy}$ are the velocity of point contact of belt to which the contact model is connected and transforming into effective road axis system, are given by

$$V_{b,cx} = \cos\beta_y\,(V^a_{ax} + \dot{x}_{rb}) - \sin\beta_y\,(V^a_{az} + \dot{z}_{rb}) \tag{3.14a}$$

$$V_{b,cy} = \cos\beta_x\left(V^a_{ay} + \dot{y}_{rb} + r_{lb}\,(\omega^a_{ax} + \dot{\gamma}_{rb})\cos\beta_y - r_{lb}\left(\omega^a_{az} + \dot{\psi}_{rb}\right)\sin\beta_y\right) \tag{3.14b}$$

where r_e is effective rolling radius given in equation (3.48) and ρ_z is vertical deflection of tire given in equation (3.33).

3.1.5 Slip Model

The forces and moments acting in the contact patch (F_{sx}, F_{sy}, M_{sy}) are generated due to slippage in the contact model ($V_{c,sx}$ and $V_{c,sy}$). The dynamic interactions between the tread elements of the rolling tire and the ground leads to variations in the slippage of the tire. Both the longitudinal slip ratio and lateral slip angle are also influenced by the deformation of the belt. The longitudinal slip is also influenced due to variations in the effective rolling radius

as seen in Equation (3.13). Accurate modeling of this process of force and slip generations plays a crucial role in the analysis of extreme braking and cornering maneuvers. Due to viscoelastic nature of tire, the force generation in the contact patch occurs after rolling a finite distance which is called relaxation behavior of tire. Hence, a slip model is required for the tread elements to simulate the transient slippage. The overall relaxation behavior of tire changes due to loading conditions and operating slip of the tire. This behavior is modeled using an analytical transient slip model with a delayed longitudinal slip κ, slip angle α and camber γ values. It consists of first order approximations of respective relaxation behavior of tire with a relaxation length constant for slip σ_c, relaxation length for self-aligning moment with trail slip σ_2 and relaxation behavior of camber force with σ_3. The inputs to the model are slip velocities calculated from contact model (3.11).

The longitudinal (κ) and lateral transient (α) slip quantities are calculated using a contact patch relaxation length constant σ_c,

$$\sigma_c \cdot \dot{\kappa} + |V_{cx}|\kappa = -V_{c,sx} \tag{3.15a}$$

$$\sigma_c \cdot \dot{\alpha} + |V_{cx}|\alpha = V_{c,sy} + |V_{cx}|\psi_{rst} \tag{3.15b}$$

To obtain the correct steady-state forces, the static yaw deflection angle of the contact patch ψ_{rst} with respect to the wheel plane is used to compensate for the correct contact patch slip angle which is smaller from that of the wheel plane.

$$\psi_{rst} = M_{sz}\left(\frac{1}{k_{b\psi}} + \frac{1}{k_{r\psi}}\right) \tag{3.16}$$

where V_{cx} is longitudinal velocity of the contact patch with respect to axle. It is calculated with the addition of slippage of contact patch $V_{c,sx}$ and rotational velocity of contact patch V_{cr}.

$$V_{cx} = V_{c,sx} + V_{cr} \tag{3.17}$$

where $V_{cr} = r_e\dot{\theta}_b$.

For characterizing the relaxation behavior of self-aligning moment generation, Maurice [84] found that this mechanism is more complex and the transient response of the pneumatic trail

should also be included. He suggested that a first-order system, as given in equation (3.15), and addition of phase-leading network in series can approximate the analytically assessed response function of the pneumatic trail to slip angle variations. The transient lateral slip quantity from equation (3.15) is used as input to a first-order differential equation for calculation of transient trail slip α_t, which increases the order of system to two.

$$\sigma_t \cdot \dot{\alpha}_t + |V_{cx}|\alpha_t = |V_{c,sx}|\alpha \tag{3.18}$$

where σ_t is given as

$$\sigma_t = \sigma_c \frac{t_0}{a} \tag{3.19}$$

t_0 is the pneumatic trail value at vanishing slip ($\kappa = 0$) and a is half of contact patch length given in equation (3.40).

Higuchi [130] found that due to the torsional deformation of the tire carcass and tread, the aligning torque response to a step change in camber has relatively short relaxation length. To model this, a transient camber angle γ is calculated with a first order approximation of relaxation length constant σ_3 equal to quarter of contact pacta length $2a$.

$$\sigma_3 \cdot \dot{\gamma} + |V_{cx}|\gamma = |V_{cx}|\gamma_a^e \tag{3.20}$$

where γ_e^a is the camber angle with respect to the effective road surface plane given as

$$\gamma_e^a = \gamma^a - \beta_x \tag{3.21}$$

From the delayed longitudinal slip κ, lateral slip angle α and camber angle γ quantities, the steady state forces and moment characteristics of tire are calculated using empirical magic formula.

$$F_{sx} = F_{x,MF}\left(\kappa, \alpha, F_{cN}\right) \tag{3.22a}$$

$$F_{sy} = F_{y,MF}\left(\kappa, \alpha, F_{cN}, \gamma_a^e\right) \tag{3.22b}$$

$$t = F_{t,MF}\left(\kappa, \alpha_t, F_{cN}, \gamma_a^e\right) \tag{3.22c}$$

$$M_{zr} = M_{zr,MF}\left(\kappa, \alpha, F_{cN}, \gamma\right) \tag{3.22d}$$

where M_{zr} is residual aligning moment calculated based on the delayed transient camber angle γ.

The total self-aligning moment ($M_{z,MF}$) is generated due to the pneumatic trail, the residual aligning moment and the product of the longitudinal slip force and its arm s

$$M_{z,MF} = -t \cdot F_{y,MF} + M_{zr,MF} + s \cdot F_{x,MF} \tag{3.23}$$

As the steady-state magic formula characteristics are determined with respect to wheel plane, moments about the contact patch are obtained by correcting the moments due to the contribution of the lateral static deflection y_{rst} at ground level.

$$M_{cx} = M_{sx} = M_{x,MF} - y_{rst}F_{cN} \tag{3.24a}$$

$$M_{sz} = M_{z,MF} + y_{rst}F_{x,MF} \tag{3.24b}$$

where the lateral static deflection is given as

$$y_{rst} = F_{y,MF}\left(\frac{1}{k_{by}} + \frac{1}{k_{ry}} + \frac{r_l^2}{k_{b\gamma}}\right) \tag{3.25}$$

3.1.6 Constitutive Relations

In this section, relaxation length, dynamic stiffness and damping, contact patch dimensions, rolling resistance, effective rolling radius, vertical deflection, and the vertical force in the contact patch are formulated.

Sidewall Stiffness and Damping

The stiffness and damping of the sidewall are calculated from the natural frequencies of the rigid body modes of the unloaded, inflated tire which is mounted on a fixed spindle without touching the ground. Under unloaded condition, vertical rigid mode is equivalent to longitudinal mode and camber rigid mode is equivalent to yaw mode, as shown in Figure 2.6. Comparison with the results of experimental modal analysis showed that with the accurate

modeling of the contact model and integration with rigid ring model, which is based on the modes of the free tire, can accurately represent the modes of vibration of the tire under loaded conditions.

Sidewall stiffness and damping values are calculated as:

$$k_{bx0} = k_{bz0} = 4\pi^2 \cdot m_b \cdot f_{long}^2 \tag{3.26a}$$

$$k_{by0} = 4\pi^2 \cdot m_b \cdot f_{lat}^2 \tag{3.26b}$$

$$k_{b\theta 0} = 4\pi^2 \cdot I_{by} \cdot f_{windup}^2 \tag{3.26c}$$

$$k_{b\gamma 0} = k_{b\psi 0} = 4\pi^2 \cdot I_{bx} \cdot f_{yaw}^2 \tag{3.26d}$$

$$c_{bx0} = c_{bz0} = 4\pi \cdot \zeta_{long} \cdot m_b \cdot f_{long} \tag{3.26e}$$

$$c_{by0} = 4\pi \cdot \zeta_{lat} \cdot m_b \cdot f_{lat} \tag{3.26f}$$

$$c_{b\theta 0} = 4\pi \cdot \zeta_{windup} \cdot I_{by} \cdot f_{windup} \tag{3.26g}$$

$$c_{b\gamma 0} = c_{b\psi 0} = 4\pi \cdot \zeta_{yaw} \cdot I_{by} \cdot f_{yaw} \tag{3.26h}$$

where f_{long} is the primary eigen-frequency (in Hz) and ζ_{long} is the dimensionless damping factor of the vertical/longitudinal motion of the belt, also known as the in-plane vertical mode, f_{lat} and ζ_{lat} are the eigen-frequency and damping factor of the lateral motion of the belt, also known as the out-of-plane lateral mode, f_{windup} and ζ_{windup} are the eigen-frequency and damping factor of the rotational motion of the belt, also known as the in-plane torsional mode, f_{yaw} and ζ_{yaw} are the eigen-frequency and damping factor of the yaw/camber motion of the belt, also known as the out-of-plane yaw/camber mode. The subscript '0' denotes stiffness and damping values of the tire at non-rolling conditions. Equation (3.26) is valid only for rigid body modes because under such situations, the belt moves as a rigid body and can be approximated to have the same behavior as a single degree of freedom mass, spring and damper system. During the modal analysis, the spindle is clamped to ensure the belt mass is the primary inertial component.

Based on previous studies by Vinesse [131] and Zegelaar [80], it is understood that the in-plane natural frequencies of the rolling tire change with velocity. Hence, the actual sidewall

stiffness is much lower than the values obtained from the natural frequencies at stationary condition using Equation (3.26). In order to account for this effect, the in-plane sidewall stiffness is made dependent on the rolling velocity. The velocity depedence of out-of-plane modes is not observed. The sidewall stiffness variations with respect to velocity, load and pressure are taken into account through correction factors:

$$k_{bx} = k_{bx0}\left(1 + 0.65 \cdot dp_i\right)\left(1 - q_{bVx}\sqrt{Q_V}\right) \tag{3.27a}$$

$$k_{bz} = k_{bz0}\left(1 + 0.65 \cdot dp_i\right)\left(1 - q_{bVz}\sqrt{Q_V}\right) \tag{3.27b}$$

$$k_{by} = k_{by0}\left(1 + 0.74 \cdot dp_i\right) \tag{3.27c}$$

$$k_{b\theta} = k_{b\theta 0}\left(1 + 0.49 \cdot dp_i\right)\left(1 - q_{bV\theta}\sqrt{Q_V}\right) \tag{3.27d}$$

$$k_{b\gamma} = k_{b\psi} = k_{b\gamma 0}\left(1 + 0.69 \cdot dp_i\right) \tag{3.27e}$$

where the variable Q_V is a non-dimensional quantity which represents the rate of deformation of the tire due to rolling, calculated using the relation:

$$Q_V = \frac{|\Omega|}{V_0}\sqrt{x_{rb}^2 + z_{rb}^2} \tag{3.28}$$

where V_0 is the nominal rolling velocity in m/s. The pressure dependency of sidewall stiffness is included using empirical factors. The variable dp_i measures the change in inflation pressure:

$$dp_i = \frac{P - P_0}{P_0} \tag{3.29}$$

where P_0 is the nominal inflation pressure and P is the current inflation pressure, measured either in bar or kPa.

Vertical Deflection

The vertical deflection of tire is given by

$$\rho_z = r_0 + \Delta r - r_l \tag{3.30}$$

where r_0 is unloaded radius, Δr is increase in radius of tire due to centrifugal forces

$$\Delta r = r_0\left(q_{V1}\left(\frac{\Omega r_0}{V_0}\right)^2\right) \tag{3.31}$$

r_l is loaded radius of tire which is calculated by addition of unloaded radius of tire and deflection of contact patch due to vertical road input in effective road plane

$$r_l = r_0 + (z_a - w)\cos\beta_y \tag{3.32}$$

The vertical deflection of tire is given as

$$\rho_z = (w - z_a)\cos\beta_y + \Delta r \tag{3.33}$$

where z_a initial vertical axle displacement due to loading of tire with respect to the ground axis system.

In the same way, vertical deflection in residual spring is given by

$$\rho_{zr} = (w - z_b)\cos\beta_y + \Delta r \tag{3.34}$$

From literature studies [4], [84], at higher values of slip due to large brake force and at contact axle height conditions, decrease in vertical force due to the displacements of the contact patch is noticed. This is modeled by decreasing the residual spring deflection with the square of the deformations of the contact patch.

$$\rho_{zr} = (w - z_b)\cos\beta_y + \Delta r - q_{Fcx}\rho_x^2 - q_{Fcy}\rho_y^2 \tag{3.35}$$

where the linearized horizontal tire deflections with respect to the wheel axle axis is given as

$$\rho_x = x_{rb} - r_0\theta_{rb} + x_{rc} \tag{3.36a}$$

$$\rho_y = y_{rb} - r_0\gamma_{rb} + y_{rc} \tag{3.36b}$$

$$\tag{3.36c}$$

Vertical Force in Contact Patch

For characterizing vertical force in contact patch, an empirical third-order polynomial, based on vertical deflection in the residual spring is used.

$$F_{cN}^{rad} = \begin{cases} q_{Fzr3}\rho_{zr}^3 + q_{Fzr2}\rho_{zr}^2 + q_{Fzr1}\rho_{zr} & \text{if } \rho_{zr} > 0 \\ 0 & \text{if } \rho_{zr} \leq 0 \end{cases} \tag{3.37}$$

The polynomial coefficients in equation (3.37) are calculated from the sidewall stiffness k_{bz} and the parameters q_{Fz1} and q_{Fz2} which are the linear and quadratic factors in the total vertical load-deflection characteristic are given by:

$$q_{Fzr1} = \frac{k_{bz} A_1}{k_{bz} - A_1} \tag{3.38a}$$

$$q_{Fzr2} = \frac{k_{bz}^3 A_2}{(k_{bz} - A_1)^3} \tag{3.38b}$$

$$q_{Fzr3} = 2\frac{k_{bz}^4 A_2^2}{(k_{bz} - A_1)^5} \tag{3.38c}$$

where:

$$A_1 = \frac{(q_{Fz1} + q_{Fz3}\gamma_e^a)\, F_{z0}}{r_0} \left(1 + \frac{q_{V2}|\Omega| r_0}{V_0}\right) \tag{3.38d}$$

$$A_2 = \frac{q_{Fz2} A_1}{\left(q_{Fz1} + q_{Fz3}\left(\gamma_e^a\right)^2\right) r_0} \tag{3.38e}$$

The constant parameter F_{z0} denotes the nominal vertical load (in N). The factor q_{V2} accounts for the increase in vertical stiffness with speed. The vertical force acting on contact patch in effective road surface plane is give by

$$F_{cN} = \frac{F_{cz}^{rad} + F_{sy}}{\cos\gamma_a^e} \approx \frac{F_{cz}^{rad} + (F_{cy} + F_{y,NL})\sin\gamma_a^e}{\cos\gamma_a^e} \tag{3.39}$$

Contact Patch Area

When the tire is loaded, the deformation of the tire leads to a flattened contact surface between the tire and the ground. This surface area is assumed to have the shape of an ellipse. As the contact patch grows larger with increasing loads, the length of the contact patch is assumed to have a non-linear relationship with the vertical load (or deflection) which can be expressed as:

$$a = r_0 \left(q_{ra2}\frac{F_{cN}}{K_z \cdot r_0} + q_{ra1}\sqrt{\frac{F_{cN}}{K_z \cdot r_0}}\right) \approx r_0 \left(q_{ra2}\frac{\rho_z}{r_0} + q_{ra1}\sqrt{\frac{\rho_z}{r_0}}\right) \tag{3.40a}$$

$$b = wd \left(q_{rb2}\frac{F_{cN}}{K_z \cdot r_0} + q_{rb1}\left(\frac{F_{cN}}{K_z \cdot r_0}\right)\frac{1}{3}\right) \approx wd \left(q_{rb2}\frac{\rho_z}{r_0} + q_{rb1}\left(\frac{\rho_z}{r_0}\right)\frac{1}{3}\right) \tag{3.40b}$$

where a is half of the contact length, wd is is the nominal section width of the tire, q_{ra1}, q_{ra2}, q_{rb1} and q_{rb2} are polynomial fit parameters which are calculated through experiments.

External Forces and Moments on the Belt

The internal contact forces and moments generated in the contact model, as given in equation (3.11) act as external forces on the belt. These forces and moments has to be transformed into the belt axis system. First, the forces in the effective surface plane are obtained by necessary transformation of β_y about y-axis and β_x about x-axis. These force and moments have to be transformed again into belt plane with initial camber γ_a and camber angle induced due to deflection of belt γ_{rb} about x-axis. The external forces and moments on belt in equation (3.8) are given as

$$F_{bx}^{b} = F_{cx} + \beta_y F_{cN} \tag{3.41a}$$

$$F_{by}^{b} = F_{cy} + F_{y,NL} + \left(-\beta_x + \gamma_{rb} + \gamma_a\right) F_{cN} \tag{3.41b}$$

$$F_{bz}^{b} = F_{cN} - F_{cx}\beta_y + \left(F_{y,NL} + F_{cy}\right)\left(\beta_x - \gamma_a\right) \tag{3.41c}$$

$$M_{bx}^{b} = M_{cx} + \beta_y M_{cz} + r_{lb} F_{by}^{b} \tag{3.41d}$$

$$M_{by}^{b} = M_{cy} + \left(-\beta_x + \gamma_a\right) M_{cz} - r_e F_{bx}^{b} + r_{lb} F_{bz}^{b} \beta_y \tag{3.41e}$$

$$M_{bz}^{b} = -\beta_y M_{cz} - M_{cy}\left(\beta_x - \gamma_a\right) + M_{cz} - r_{lb} F_{by}^{b} \beta_y \tag{3.41f}$$

Relaxation Length

As mentioned above, the relaxation behavior of the tire changes due to the loading conditions and operating slip of the tire. The contact patch relaxation length in equation (3.42) decreases with contact patch length a and also decreases with the increase in slippage of tire and it is compensated with an adhesion factor m as given below.

$$\sigma_c = max(a \cdot m, e_{lim}) \tag{3.42a}$$

$$m = max(1 - \theta\zeta_y, 0) \tag{3.42b}$$

The minimum value of the relaxation length is constrained to e_{lim} to ensure the numerical stability of the simulation. θ is the inverse of the sideslip angle at the peak value of the pure lateral force in magic formula characteristic curves. ζ_y is the equivalent transient sideslip angle under combined case

$$\zeta_y = \frac{1}{1+\kappa}\sqrt{\alpha^2 + \kappa^2 \left(\frac{K_{F\kappa 0}}{K_{F\alpha 0}}\right)^2} \tag{3.43}$$

where $K_{F\kappa 0}$ and $K_{F\alpha 0}$ are the longitudinal slip stiffness and lateral cornering stiffness.

Overall Stiffness of Tire

The overall longitudinal, lateral and yaw tire stiffness changes with respect to increase in load and pressure. These effects are modeled using

$$K_x = K_{x0}\left(1 + p_{cfx1}df + p_{cfx2}df^2\right)\left(1 + p_{pcfx3}dp_i\right) \tag{3.44a}$$

$$K_y = K_{y0}\left(1 + p_{cfy1}df + p_{cfy2}df^2\right)\left(1 + p_{pcfy3}dp_i\right) \tag{3.44b}$$

$$K_\psi = K_{\psi 0}\frac{F_{cN}\left(1 + p_{pcmz1}dp_i\right)}{F_{z0}} \tag{3.44c}$$

where K_{x0}, K_{y0} and $K_{\psi 0}$ are the longitudinal, lateral and yaw stiffness of the tire at the nominal vertical load and inflation pressure. The variable df measures the change in vertical load:

$$df = \frac{F_{cN} - F_{z0}}{F_{z0}} \tag{3.45}$$

where F_{z0} is the nominal vertical load.

Residual Stiffness

As mentioned in section 3.1.4, residual springs ensure correct overall stiffness of the tire. The overall stiffness of the tire is modeled using carcass stiffness (sidewall stiffness and residual stiffness) and contact patch stiffness (cornering stiffness and longitudinal slip stiffness).

The residual stiffness are calculated by subtracting sidewall stiffness in equation (3.27) and contact patch stiffness from overall stiffness (3.44)

$$\frac{1}{K_x} = \frac{1}{K_{bx}} + \frac{r_l^2}{K_{b\theta}} + \frac{1}{K_{rx}} + \frac{a}{K_{F\kappa 0}} \tag{3.46a}$$

$$\frac{1}{K_y} = \frac{1}{K_{by}} + \frac{r_l^2}{K_{b\gamma}} + \frac{1}{K_{ry}} + \frac{a}{K_{F\alpha 0}} \tag{3.46b}$$

$$\frac{1}{K_\psi} = \frac{1}{K_{b\psi}} + \frac{1}{K_{r\psi}} + \frac{a}{3K_{m\psi}} \tag{3.46c}$$

where $K_{F\kappa 0}$ and $K_{F\alpha 0}$ are longitudinal slip and cornering stiffness calculated from steady state magic formula. $K_{m\psi}$ is moment stiffness against spin in the contact patch and is given as

$$K_{m\psi} = 2r_0 F_{cN} \left(q_{dz8} + q_{dz9} df\right) \tag{3.47}$$

Effective Rolling Radius

From Figure 3.6, an imaginary point S is defined slightly below the road surface. The distance of the point S to the wheel center is defined as the effective rolling radius r_e. It is in between unloaded radius r and loaded radius r_l. Fundamentally it is used to define the velocity of rolling tire V_r, which is equal to the product of the angular wheel velocity Ω and the effective rolling radius r_e. In order to calculate the velocity of the belt contact point

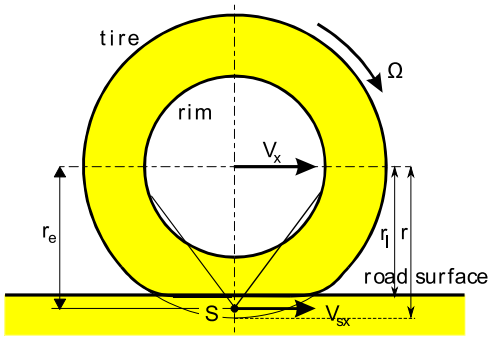

Figure 3.6: Effective rolling radius and loaded radius of the tire [4]

in equation (3.14), the effective rolling radius r_e needs to be obtained, which is calculated

by empirically fitting the experimentally obtained values at various vertical loads. This empirical based model is developed by [2].

$$r_e = R_\Omega - \frac{F_{z0}}{K_z}\left(D_{reff}\arctan\left(B_{reff}\frac{F_{cN}}{F_{z0}}\right) + F_{reff}\frac{F_{cN}}{F_{z0}}\right) \tag{3.48}$$

where B_{reff}, D_{reff} and F_{reff} are model parameters. The total vertical stiffness K_z, which is dependent on the inflation pressure is calculated using the relation:

$$K_z = K_{z0}\left(1 + p_{Fz1}\cdot dp_i\right) \tag{3.49}$$

where p_{Fz1} denotes the linear dependence of the vertical stiffness on inflation pressure. K_{z0} is the nominal vertical stiffness of the tire:

$$K_{z0} = \frac{F_{z0}}{r_0}\sqrt{q_{Fz1}^2 + 4q_{Fz2}} \tag{3.50}$$

Rolling Resistance

Rolling resistance is the opposition experienced by the tire as the tire rolls over a surface. This effect is accounted in equation (3.41). This empirical based model is developed by [2].

$$M_{cy} = -r_e f_r F_{cN}\cdot \mathrm{sgn}\left(\dot{\theta}_b\right) \tag{3.51}$$

where f_r is the rolling resistance coefficient. This coefficient is assumed to vary as a non-linear polynomial function of speed and is expressed as:

$$f_r = \left(q_{sy1} + q_{sy3}\left|\frac{V_x}{V_0}\right| + q_{sy4}\left(\frac{V_x}{V_0}\right)^4\right)\left(\frac{P}{P_0}\right)^{q_{sy8}} \tag{3.52}$$

3.2 Vehicle Modeling

As the tire model used for this study is validated at least up to 75 Hz, appropriate nonlinear vehicle model with the long range of validity has to be selected for fidelity of the vehicle dynamics simulation results. Commercially available vehicle dynamics software CarSim®

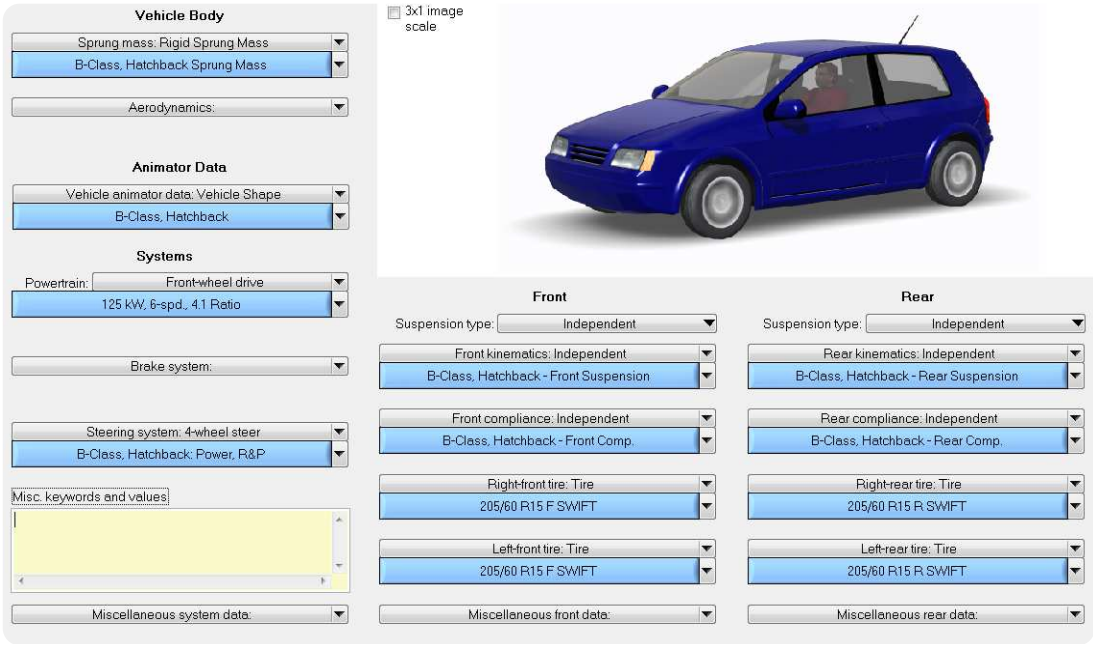

Figure 3.7: Environment in CarSim® with integrated vehicle components

is used for vehicle modeling. The equations of motion in the CarSim® math models are valid for full nonlinear 3 dimensional motions of rigid bodies. These nonlinear dynamics has to considered for vehicle dynamics studies operating under transient conditions. CarSim® requires fairly less parameters and its solvers are computational faster and accurate. This makes it much preferable for vehicle dynamic studies and control systems design. The components that have the greatest effect on handling, braking, and acceleration are suspension, steering kinematics and compliance, CG location, inertia, wheelbase etc., These are assembled from data sets that define the whole vehicle. CarSim® main advantage comes from its solvers (faster than real time) and interfacing with Simulink® for detailed modeling of components or design of controllers. The major kinematics and compliance effects of the suspension and steering system are specified using a data that is obtained from real or simulated kinematics and compliance tests. Details of the linkages and gears in the suspension and steering system are not needed, reducing the amount of information needed to obtain accurate predictions and decrease the computational time significantly. The vehicle mass, inertia and C.G location are obtained from Inertia Test rig. Tire models are based on the

measured data or external models.

As the tire size used for this study is 205/60R15 91V. A B-Class Hatchback is used and Figure 3.7 shows the different components of the vehicle. Aerodynamics effects are neglected and a standard 6 speed automatic transmission model is used in this study. As these effects have a minimum influence on vehicle dynamics pursued in this research (braking, handling, ride), details of these models are not explained. Details of Sprung mass, suspension and steering system are given below.

3.2.1 Dimensions and Inertial Properties of Vehicle

Figure 3.8 shows the vehicle mass, inertia and C.G coordinates. The sprung mass is the portion of the car supported by the suspensions. It is equal to the 90% of curb weight of the vehicle. Wheelbase is the longitudinal distance from the spin axis of the front wheels to that of the rear wheels. The longitudinal position of mass center of sprung mass affects the front-rear weight distribution on the vehicle. With 1.04 m distance from front axle, vehicle has a 60:40 front to rear weight distribution. The height of vehicle sprung mass C.G above the ground effects the roll of the vehicle and changes roll center at front and rear axles. The moment of inertia of the sprung mass about its respective axis constitutes roll, pitch and yaw inertias (I_{xx}, I_{yy} and I_{zz}) of the vehicle. R_x, R_y and R_z radius of gyrations are calculated based on respective moment of inertial values. The product of inertia (I_{xy}, I_{yz} and I_{xz}) are used for a vehicle that is not symmetric about its axes. For most motor vehicles this is not significant, in this case a value of zero is used. Unsprung mass includes the weight of wheels, tires, brakes, and all parts that move vertically with the wheel as the suspension deflects. Figure 3.9 shows the front and rear unsprung mass and track width of front and rear axles. Fraction steered is the portion of the unsprung mass that rotates about the kingpin axis when the wheels are steered.

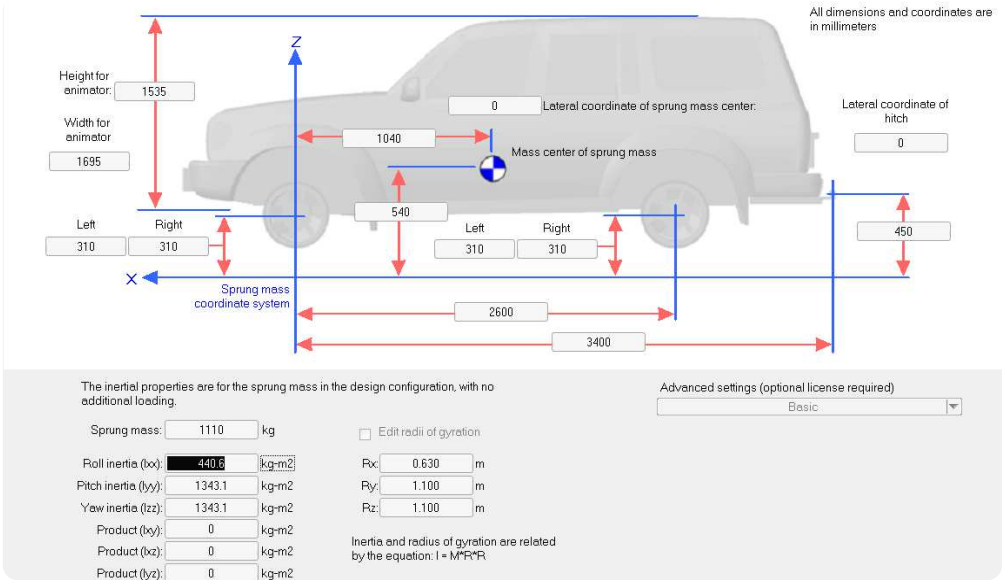

Figure 3.8: B-Class Hatchback sprung mass in CarSim®

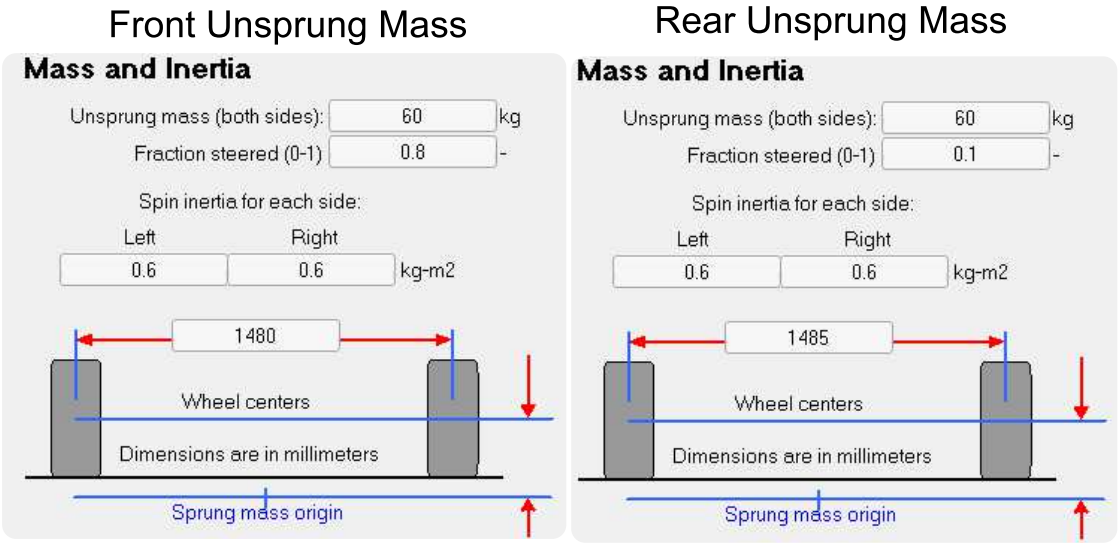

Figure 3.9: B-Class Hatchback hatchback front and rear unsprung mass in CarSim®

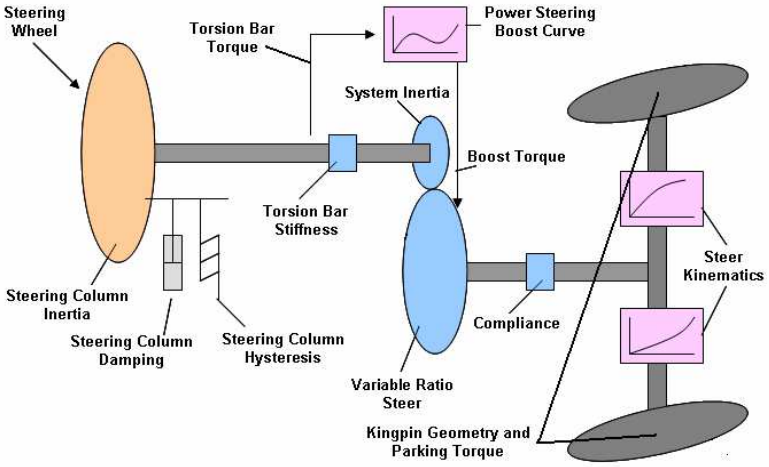

Figure 3.10: Schematic of the Steering system [8]

3.2.2 Steering System

For this study, B-Class Hatchback front wheel power steering system with a steering gear type of rack and pinion is used. Figure 3.11 shows detailed components of the steering system.

Steering Geometry

When the vehicle is steered, the wheel and the steered portion of the suspension rotate about the kingpin axis. The kingpin or steering axis is defined with respect to the wheel center by its inclination in side view (the caster angle) and in front view (the kingpin inclination angle), as shown in Figure 3.11. Vertical load on the tire generates an torque about the kingpin axis, which has to be overcome to steer the vehicle. Caster angle moves the point at which the kingpin axis intersects with the ground ahead of the center of tire contact. Lateral forces at the tire act on this longitudinal moment arm attempting to steer the wheels in their direction of travel, there by reducing slip angle. The combined effects of the offsets and inclination cause the center of the tire contact to move through an arc about the kingpin

axis intersection with the ground, causing the wheel to camber, and move the wheel center vertically with respect to the suspension.

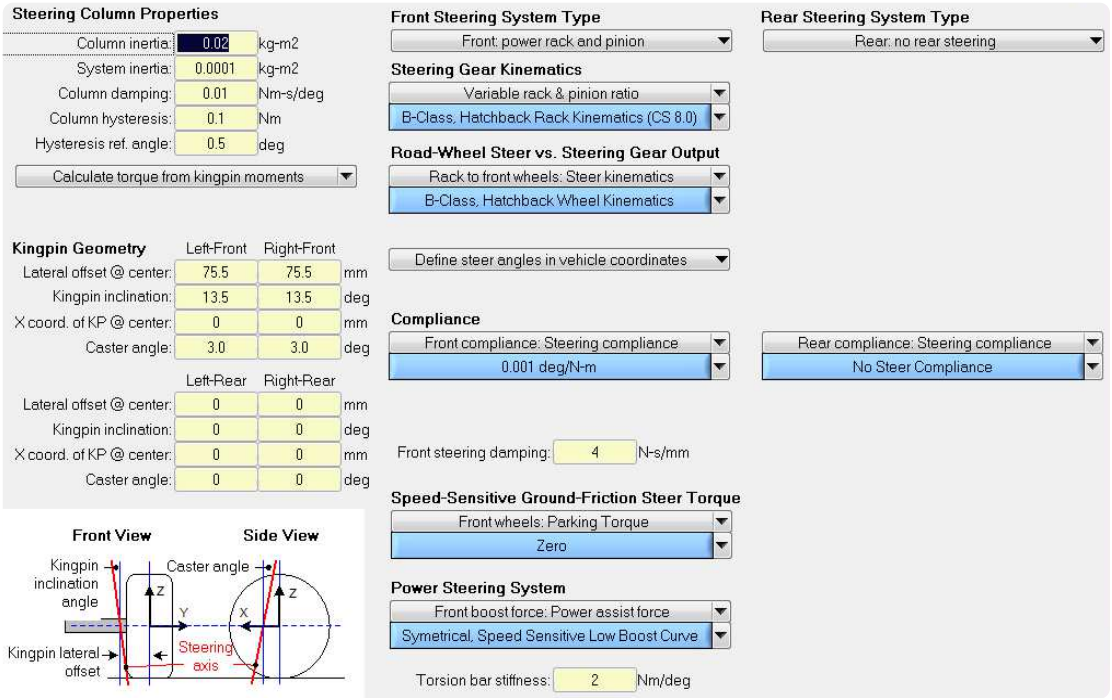

Figure 3.11: B-Class Hatchback steering components in CarSim®

Steering Inertia and Friction

Inertial properties of steering column, steering gear and linkage components (system inertia) are given in Figure 3.11. Damping associated with steering column is also considered. Steering system shows hysteresis behavior, where the torque required to turn the steering wheel to the left and to the right are unequal, due to inherent friction between the column components. This is incorporated by taking one-half the difference in torque when steered to the left and to the right using steering column hysteresis. When the direction of steering is reversed, the friction (hysteresis) torque does not jump instantly from one limit to the other it takes a certain amount of rotation to make this transition, it is incorporated with a time constant of steering column reference hysteresis angle.

Steering Kinematics

Steering kinematics defines the nominal ratio of angles between the steering wheel and the road wheels, here a rack and pinion type steering system is selected. A lookup table is defined for steering gear kinematics describing rack translation in mm per revolution of the pinion gear. Another lookup table is defined to calculate the steer of a road wheel with displacement of rack, plots are shown in Figure 3.12, constituting a steering ratio of 17:1.

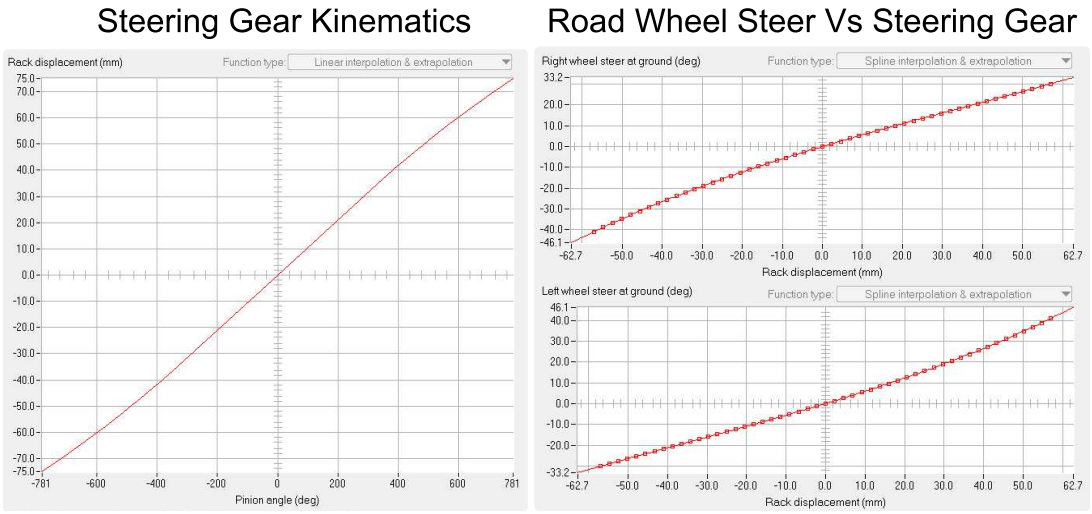

Figure 3.12: B-Class Hatchback steering kinematics in CarSim®

Steering Compliance

The linkage connecting the steering wheel to the road wheels is compliant, as shown in Figure 3.10. Compliance in the steering system is due to the total moment about the kingpin axes of each wheel. When the vehicle turns change in load on left and right tire induces unequal moments about inclined kingpin axis, so a net moment is applied to the steering system, resulting in some compliant steer. Here a constant front compliance of 0.001° per unit kingpin moment $(N - m)$ is assumed, no compliance in rear axle.

Power Steering

In the most common power steering system configuration, a torsion bar is placed between the steering column and steering input gear, as shown in Figure 3.10. Deflection of the torsion bar due to applied torque opens a valve, directing hydraulic pressure to the steering gear in the direction of the deflection. The pressure produces a force or torque to assist the steering. A table is defined for power assist curves as a function of torsion bar torque and vehicle speed as shown in Figure 3.13, with decreasing power steering assistant with increasing velocity.

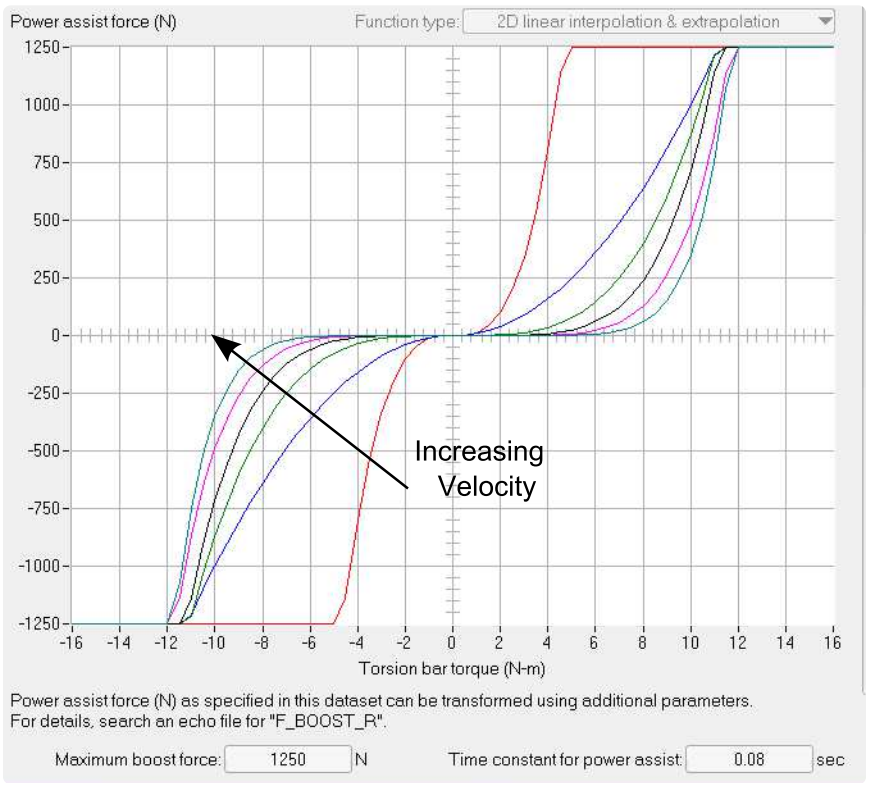

Figure 3.13: B-Class Hatchback power steering boost curves in CarSim®

Preview based Driver Controller

Preview based driver controller is used as a driver model for lane change and constant radius maneuver simulations discussed in Chapter 5. As shown in Figure 3.14, the driver model

applies the desired steering angle for minimizing the vehicle deviations from the desired path by considering preview time and human lag. The desired path is a road previewed by the driver model which is calculated by linear extrapolation using a preview time. The inputs to the driver controller are X and Y coordinates of the front axle of the vehicle, the vehicle-based longitudinal and lateral components of the velocity vector (V_x and V_y), the yaw angle and yaw rate (ψ and $\dot{\psi}$), desired target path and front and rear steer angles induced due to suspension kinematics and compliance (u_{fo} and u_{ro}). The driver controller contains a simple 2 DOF bicycle model. Corrective steering input u_c is computed by optimizing the deviations of the path of the center of the front axle from a target path. Finally, it delays the driver steering control u_c by a constant delay time, to simulate dynamic characteristics of human drivers.

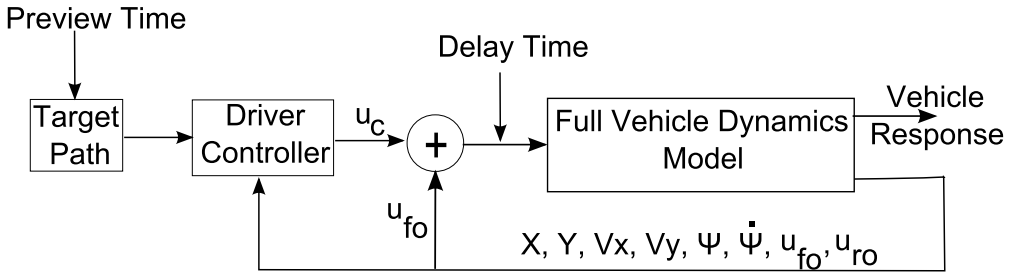

Figure 3.14: Preview based driver controller in CarSim®

3.2.3 Suspension System

Suspension system used in this study is an independent front and rear suspension. The front suspension is front strut type suspension and the rear being 5-Link suspension. The kinematics of the suspension linkages are described by the lateral and longitudinal motions of the wheel as the suspension deflects vertically (jounce). As CarSim® is lookup table based, general definition of these effects using suspension geometry concepts such as roll centers and side view swing arms are not needed. The anti-dive angle describes the suspension reaction creating a vertical force within the suspension when it experiences a longitudinal force. The

vertical reaction resists the tendency of the suspension to lift under forward load transfer in braking. The anti-dive and camber changes due to suspension jounce for a front and rear suspension are also considered.

Suspension Compliance

The compliance properties of an independent suspension are taken into account using springs and dampers curves. Suspension compliance effects are also considered which are induced due to the force in tires and causes a toe change or camber change. The front spring stiffness of 28 KN/m and rear spring stiffness of 35 KN/m are considered. At the end of suspension stroke it encounters bump stops that limits the suspension travel. Here bump stops of -50 mm to 70 mm in front and -40 mm to 40 mm in rear are considered, as shown in Figure 3.15 For characterizing dampers, Force VS Compression rate curves are used. In general, these curves are nonlinear with the largest slope across zero and diminishing at higher velocities. In addition, it is common to have the shock damping force in the compression direction (positive rate) only about half its value in the extension (negative rate) direction. The lower forces in the compression direction prevent sharp bumps from being transmitted to the sprung mass, while allowing for the necessary dissipation of energy when the suspension is extending as shown in Figure 3.16 front damper curve (same for rear damper also).

3.3 Anti-lock Braking System Model

An ABS model consists of two main components: 1. Control algorithm and 2. Pressure model. Both these components are very essential to produce accurate results because having an advanced control algorithm with a simplistic pressure model can lead to un-realistic results. Also, having a detailed pressure model without a robust algorithm can also lead to unfavorable results. Hence, a balance needs to be maintained to ensure confidence in simulation results.

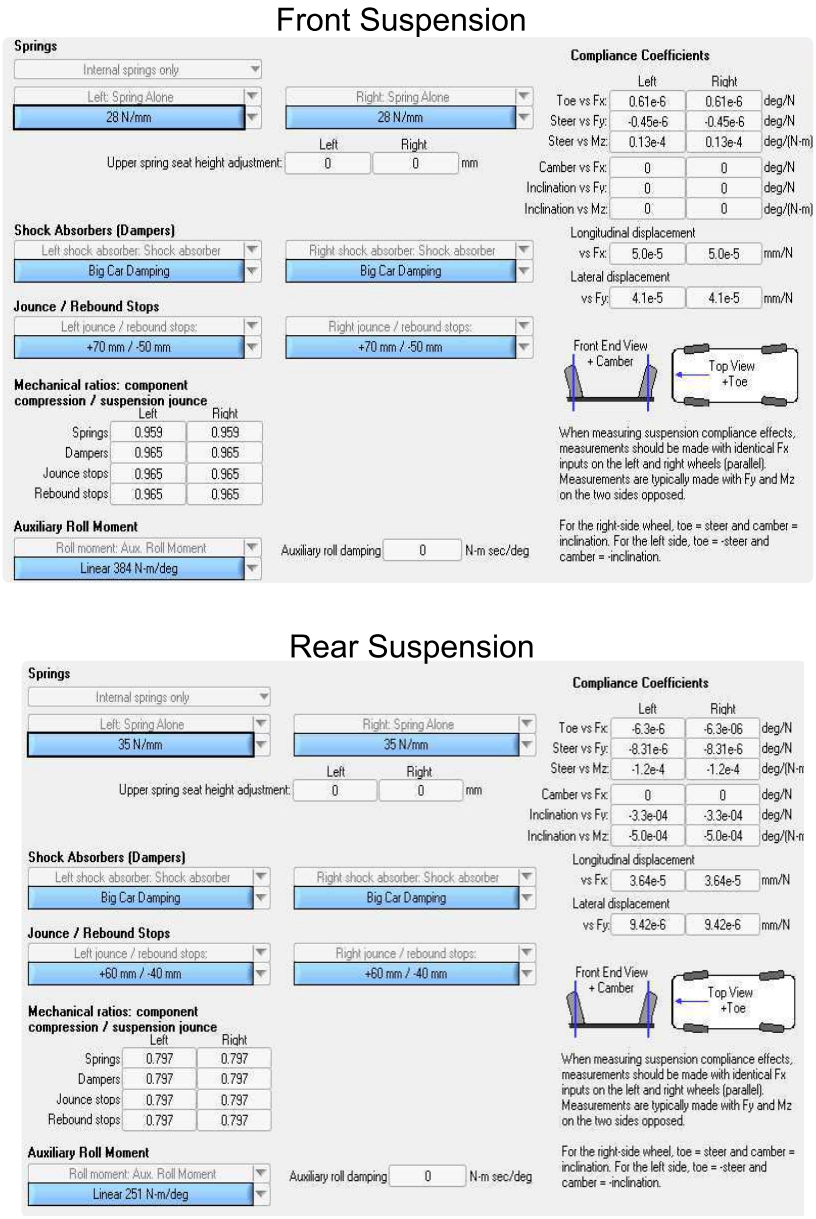

Figure 3.15: B-Class Hatchback suspension compliance in CarSim®

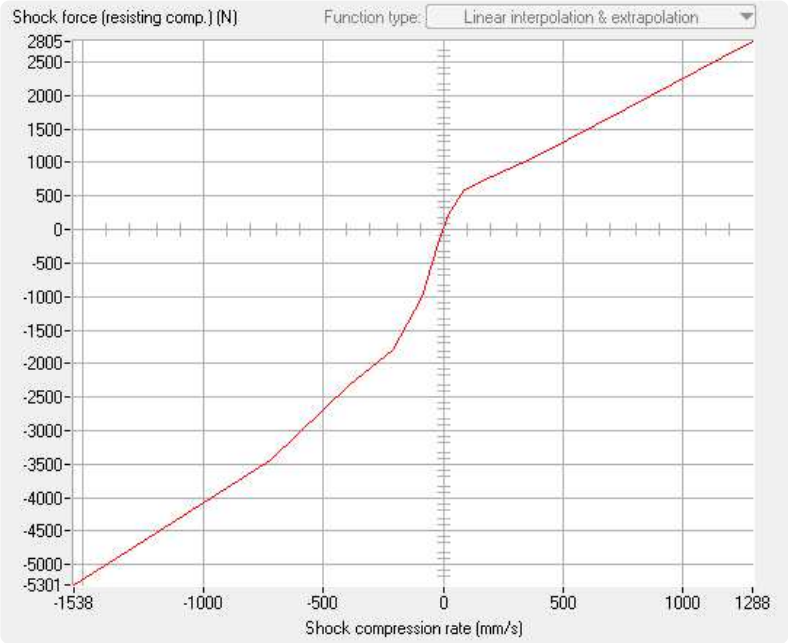

Figure 3.16: B-Class Hatchback suspension damper curve in CarSim®

3.3.1 Inputs and Outputs

Since the ABS unit is only responsible for braking control, the system has a limited set of inputs and outputs:

Inputs : The ABS unit requires longitudinal slip κ and the wheel acceleration ϵ from the tire model.

Outputs : Based on the inputs, the ABS with the included pressure model calculates the braking torque M_{ay} which is again sent to the tire model.

3.3.2 Modeling Assumptions

The hydraulic circuit of a braking system is an extremely complex system. A number of assumptions were made which were aimed towards simplifying the modeling process and on removing factors that had low influence on ABS performance:

- The ABS controller is assumed to know wheel slip and vehicle speed information through measurements.
- Pressure in the master cylinder is assumed to be a constant value.
- Braking torque at the axle is considered to be linearly proportional to the pressure in the brake line.
- Wheel slip and acceleration thresholds do not change during the simulation.
- The delay in the valves is represented as a first order delay.
- Mechanical delay in converting the pressure in the brake line to torque is taken to be a constant value in time.
- The rate of increase and decrease of pressure during different brake states remain constant and cannot be changed during the simulation.
- A minimum speed is required for the operation of the ABS system below which the braking module switches to manual braking.

3.3.3 Brake States

The operating algorithm of an ABS is characterized by the number and the type of brake states utilized by the ABS to achieve optimal control of slip and wheel acceleration. In this ABS control logic designed by Ding et al [132], there are the following primary states for the braking system:

Initialize The ABS begins in this state where the output pressure in the wheel cylinder is set to the master cylinder pressure. This is done to ensure proper build up of pressure before regulation.

Hold Brake Pressure In this state, the ABS directs the wheel cylinder pressure to be maintained in the previous control cycle. This is generally used when the slip and wheel acceleration fall in the desired range.

Increase Brake Pressure In this, the brake pressure in the wheel cylinder is set to increase from its current level up to the master cylinder pressure at a normal rate. The behavior of the wheel cylinder is modeled according to Equation (3.53).

Fast Increase Brake Pressure The wheel cylinder pressure is regulated to increase at a faster rate than the normal rate. This is generally done in cases where a sudden increase in braking force is required (changing surface conditions etc.).

Decrease Brake Pressure This is also known as the pressure release state where the brake pressure in the wheel cylinder is set to decrease from its current to atmospheric pressure. The behavior of the wheel cylinder is modeled according to Equation (3.54).

Step Increase Brake Pressure This is a hybrid-state in which two operations are done in a cycle: 1. Increase 2. Hold. This was introduced to increase the brake pressure and also maintain the wheel acceleration without waiting for the controller to re-calculate until the next cycle. Apart from the regular thresholds in the controller, this stage has a separate wheel acceleration threshold where the pressure is set to hold for a specific amount of time when exceeded.

Step Decrease Brake Pressure The operation of this state is based on the same principle as the step increase in brake pressure with the only difference being in this case the brake pressure is decreased in cycles of decrease and hold (for a specified time).

Exit Braking This state is used when the vehicle is below a minimum speed where the ABS shuts off and switches to manual braking.

3.3.4 ABS Control Cycling

An ABS system deployed in a vehicle is designed to control four wheels with a single controller. In a general scenario, it might be too difficult to calculate control signals all four wheels in a single cycle. This is accomplished by the use of controller flags where one wheel is controlled during a cycle and this is rotated after each cycle. This way, all four wheels are controlled at a reasonable rate. This method is illustrated in Figure 3.17.

3.3.5 State Selection Rules

The selection of brake states are made using a state-flow based approach where the decisions are made based on a set of rules and thresholds. Figure 3.18 shows the chart used in this system for the selection of states. Here, κ denotes the wheel slip and ϵ denotes the peripheral acceleration of the wheel. This was previously designed at the Intelligent Transportation Laboratory with a fixed set of thresholds which are being used.

3.3.6 Pressure Model

In an ABS system, the brake pressure is regulated by means of electromagnetic valves that are installed in the Hydraulic Control Unit (HCU). The pressure can be regulated through three states: 1. Pressure increase; 2. Pressure hold; 3. Pressure release.

In the pressure increase mode, the wheel cylinder pressure P_w is assumed to have an exponential increase and is calculated as:

$$P_w(t) = P_m - \left[(P_m - P_{w0})^{\phi_{inc}} - K_{inc}\phi_{inc}(t - t_0)\right]^{1/\phi_{inc}} \tag{3.53}$$

where P_{w0} is the wheel cylinder pressure at the previous simulation time-step t_0. P_m is the pressure at the master cylinder. K_{inc} and ϕ_{inc} are model parameters for the response characteristics of the brake system.

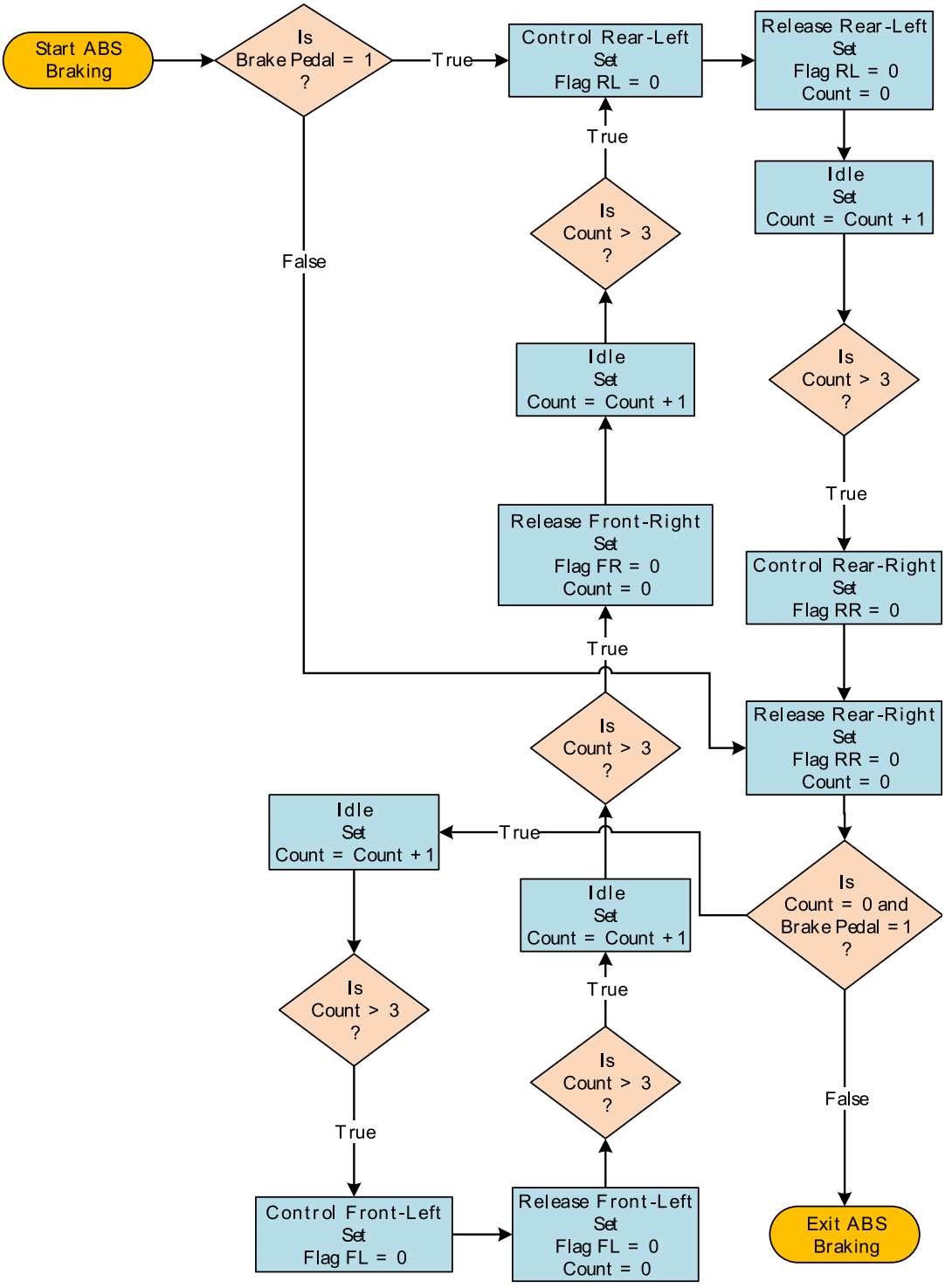

Figure 3.17: ABS control cycling between different tires

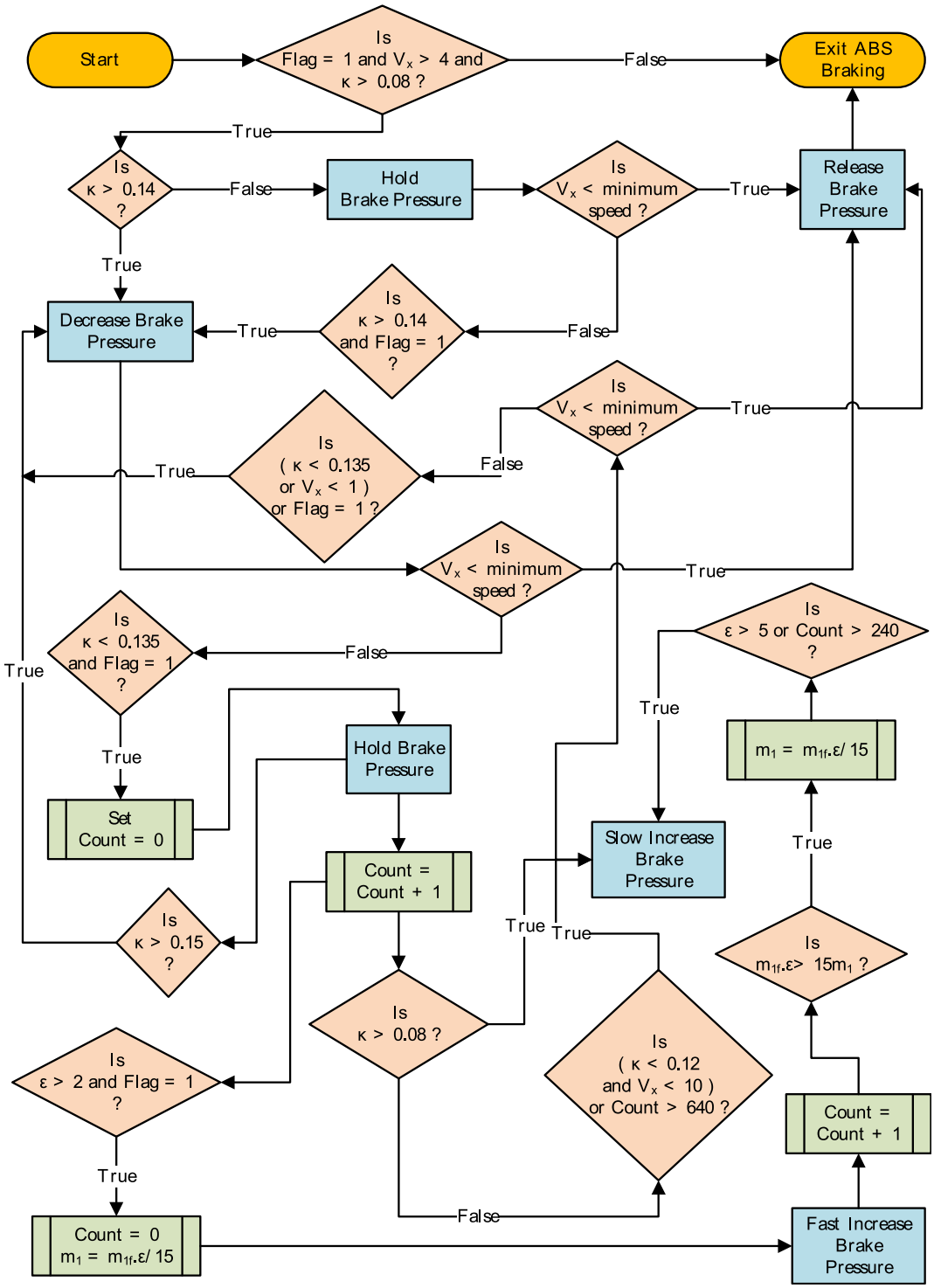

Figure 3.18: Flowchart for the selection of brake states

In the pressure release mode, the pressure in the brake cylinder pressure is governed by the following expression:

$$P_w(t) = \left[(P_{w0} - P_a)^{\phi_{dec}} - K_{dec}\phi_{dec}(t - t_0)\right]^{1/\phi_{inc}} + P_a \tag{3.54}$$

where P_a is the atmospheric pressure. The parameters K_{dec} and ϕ_{dec} are selected based on the desired behavior for pressure decrease. The pressure in the wheel cylinder is retained in its previous value during the hold phase.

The pressure in the wheel cylinder P_w is then converted into brake torque M_{ay} using the relation:

$$M_{ay} = P_w \cdot C_p \tag{3.55}$$

where C_p is the brake torque gain (N.m/Pa) and this value is different for the front wheels and rear wheels . The brake torque is applied to the tire model after a first-order transport delay to account for the dynamics of the valve.

3.4 Conclusion

In this chapter a detailed mathematical modeling of 6 DOF dynamic tire model, enveloping model, contact model and slip model are explained. A commercial based ABS algorithm developed in Matlab/Simulink and a steering model and suspension model from the CarSim® are also explained. These models were then used to develop a simulation platform to perform vehicle dynamic simulation in the subsequent chapters.

Chapter 4

Model Validation

In order to establish the reliability of the tire and vehicle models used for high frequency vehicle dynamic simulations, it is necessary to compare and validate the accuracy of the simulation results with experimental data. This chapter presents the validation of the tire model and vehicle model. The tire model was compared against the experimental data available for tire rolling with fixed axle condition over a oblique cleat at different high velocities and loading conditions. The vehicle model which is used from CarSim®, it is validated against continuous sinusoidal steering input test.

4.1 Tire Model Validation

4.1.1 Tire Modeling in Simulink Environment

Based on the equations discussed in the previous chapter, an appropriate simulation platform was selected for model development. In this study, Matlab-Simulink® was used because of its popularity and widespread adoption as a simulation platform and its block diagram based approach which is easier to understand and interpret. Matlab platform solvers for differential equations are considered to be very efficient and they have the capability to export to C for

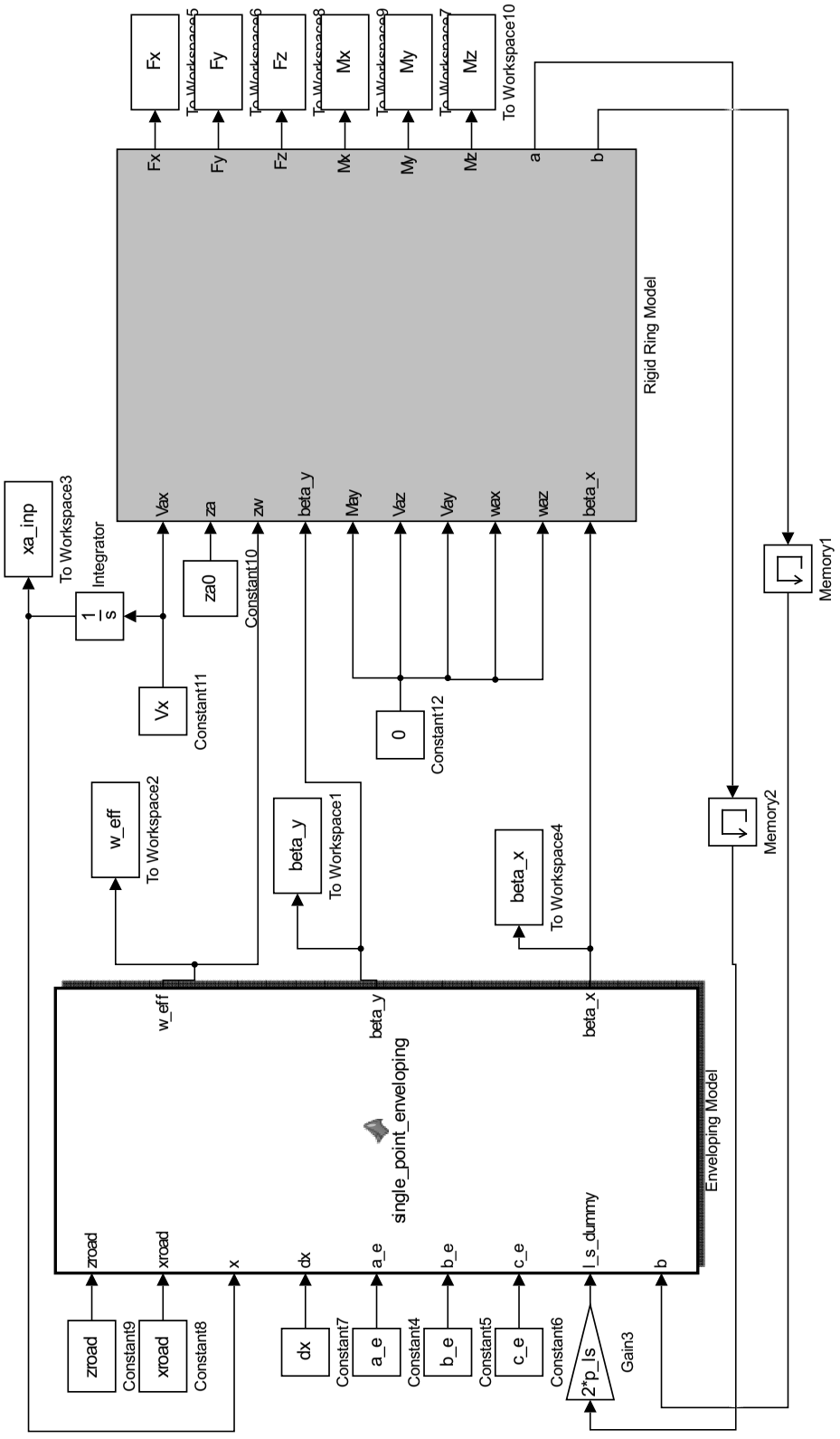

Figure 4.1: Full dynamic tire model in SIMULINK platform

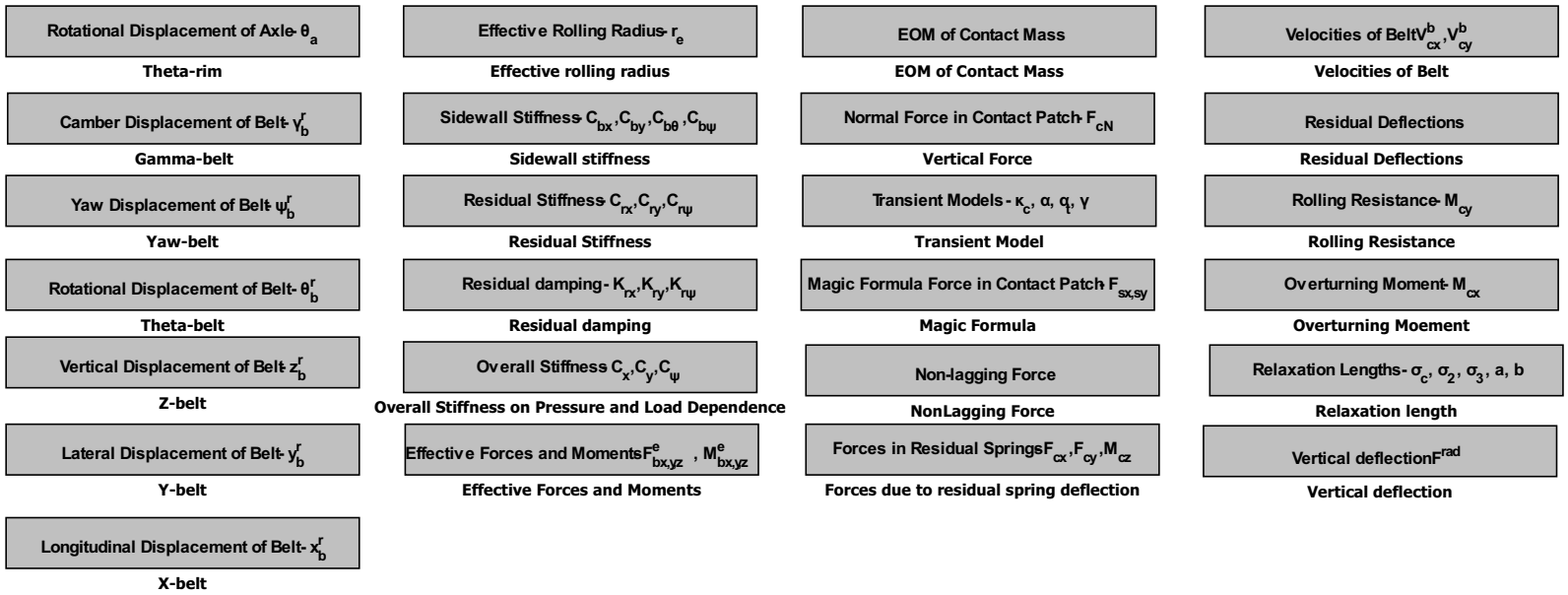

Figure 4.2: Subsystem of rigid ring model in SIMULINK platform

standalone applications and real-time simulations. Also, this platform can be integrated easily with commercial software such as CarSim® for vehicle dynamic simulation.

Figure 4.1 shows the integration of the tandem cam enveloping model and the rigid ring model in Simulink environment. Based on the longitudinal position of axle x, the enveloping model acts below the wheel center with length l_s and width $2b$ at the ground. The enveloping model scans the road profile in longitudinal and lateral directions based on the fixed scan widths at each time interval. The contact point of each cam is found based on maximum vertical height of road profile within the scan interval. Using the criteria given in equation (3.4), the contact point of all cams and the respective vertical deflections are calculated to generate effective height (w), slope (β_y) and camber (β_x) values. Notice, length l_s and width $2b$ of cam model are depend upon contact patch dimensions which change with vertical load. This shift in distance between the cams take into account highly nonlinear enveloping behavior of tire due to changing operating conditions. As shown in Figure 4.1 contact patch dimensions of the previous time step are fedback as inputs to the enveloping model. Figure 4.2 shows various subsystems constituting rigid ring tire model for calculation of deflections of belt, vertical forces in the contact patch, stiffness, Magic formula for contact forces, relaxation lengths, slip velocities, etc. Using all these subsystems, with effective road surface and input conditions of position, orientation of the wheel axle and respective velocities, the force and moment variations at the axle due to the unevenness of the road are computed.

The selection of the solver is extremely important for maintaining the right balance between accuracy of the results and speed of the simulation. In addition to this, the time step should also be selected appropriately. During test runs, it was observed that the iterative calculations in the enveloping model is consuming most of the simulation time. This was due to the fact that a process of scanning of available number of road intervals within scan width is taking place for each cam. So care must be taken for selection of scan width and good road profile resolution. The enveloping model performs scan at every discrete time step of simulation, so care must be taken in selection of time step not to scan redundantly or leave any part of the sharp road profile changes.

The solver used for all simulations were set to ODE4 (Runge-Kutta) discrete time step in view of its low computational load and satisfactory accuracy. During simulations for a fixed axle condition, the discrete time step was chosen to be 0.001 s. The scan width of the enveloping model has been set as $[-a_e/6,\ a_e/6]$ to balance between accuracy and achieving faster results without spending computational effort on a bigger scan interval.

4.1.2 Experimental Procedure

For validation of the developed tire model, the dynamic force response of tire rolling over oblique cleat is measured. The experiments are conducted at Delft University of Technology on a 2.5 m diameter steel drum with attached cleats. The rectangular cleats used for this validation study are shown in Figure 4.3 with dimensions of 50 mm (length) and 10 mm (height) mounted on the drum at angle of 43.5° with respect to the longitudinal velocity of the axle. The axle is constrained to move in vertical direction and the reaction forces and moments and the wheel rotational velocity at the wheel axle are measured. This response is then analyzed in both time and frequency domain and compared with experimental data. A detailed description of the experimental procedure adopted to obtained these datasets are given by TNO [133]. SAE J2730 [134] can be utilized as a standard procedure for performing dynamic cleat testing.

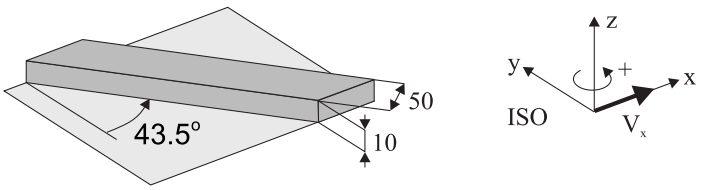

Figure 4.3: Oblique Cleat at 43.5° with 10× 50 mm dimensions

Notation	Meaning
205	Section width in mm
60	Ratio between section height and width in % (aspect ratio)
R	Radial tire
15	Rim diameter in inches
91	Maximum allowable load on the tire - 6030 N (load index)
V	Speed rating - 240 km/h

Table 4.1: Reference tire notation

4.1.3 Reference Tire

In this study, a specific tire was selected as a reference based on the availability of experimental data and the tire parameters. The dimensions of the tire used in this study is denoted as a Goodyear 205/60R15 91V where the numbers are described, and illustrated by Zegelaar [4] in Figure 4.4 and explained in Table 4.1.

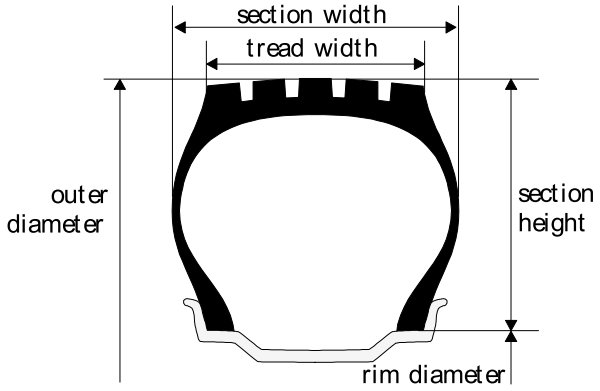

Figure 4.4: Tire dimensions

4.1.4 Validation

The developed tire model is validated for fixed axle condition and at three different load conditions $F_z = 2000$ N, 4000 N, 6000N, and at different velocities $V_x = 25$, 39, 59 Kph. As it is not feasible to present the results of all these 9 conditions, in this section a selection of four test conditions are presented. Figures 4.5 - 4.12 show the results of the experimental cleat tests and their comparison with simulation results in time and frequency domain. Here, the analyzed variables are: the change in longitudinal axle force ΔF_x, change in lateral axle force ΔF_y, change in vertical axle force ΔF_z, the change in rotational velocity $\Delta\Omega$, change in overturning moment axle force ΔM_x, change in self aligning moment ΔM_z, and their respective power spectral densities $S_{F_xF_x}$, $S_{F_yF_y}$, $S_{F_zF_z}$, $S_{\Omega\Omega}$, $S_{M_xM_x}$ and $S_{M_zM_z}$.

The following observations can be made based on the simulation results and their comparison with experimental data:

- For all cases, the simulation results matched quite well with the experimental data, both in time and frequency domains. From frequency plots, clearly all rigid modes of tire given in Figure 2.6 (in-phase and anti- phase rotational mode at 30 Hz and 85 Hz, camber and yaw mode at 45 and 53 Hz and vertical mode at 80 Hz) are excited and the simulation results matched experimental data upto 75 Hz.

- The time and frequency domain response of longitudinal forces ΔF_x, $S_{F_xF_x}$ for all four test cases are almost equivalent to the response of change in rotational velocity $\Delta\Omega$. This is due to the fact that longitudinal slip velocity in contact patch $V_{c,sx}$ as given in equation (3.13), is mainly influenced by the variations in term $r_e\dot{\theta}_b$ which is directly related to the variations in the rotational velocity of the tire. This longitudinal slip generated in the contact patch, results in large (additional) longitudinal forces. This conclusively says that longitudinal force variation in tire is strongly related to the in-phase rotational mode of tire which is shown as first peak in all frequency plots of $S_{F_xF_x}$.

- Comparing the relative magnitude of the longitudinal force variation ΔF_x in all four cases with lateral force variation ΔF_y, former is almost five times the latter. This emphasizes that longitudinal force variation is influenced by the change in effective road slope and road curvature as given in equation (3.13), but lateral force variations is mainly due to change in effective road camber.

- From the time response of ΔF_x, the slight deviations in simulation from experimental data are seen after the tire rolling off the cleat, this again emphasizes the change in the sidewall stiffness with respect to load and velocity, as given in equation (3.27), which is also observed in frequency response plots with slight deviation of first peak (in-phase mode) from experimental data.

- Comparing the simulation at lower load for lower and higher velocity cases, Figures 4.5 - 4.8, shows good correlation with measurements. This indicates the tire model has good level of accuracy at lower loads too.

- From the time domain response of vertical force variations ΔF_z, the relative change in vertical force for most of the case remains almost the same. This is due to the fact that with the inclined cleat angle the effective height becomes longer and smoother, thus causing small variations in ΔF_z with the increase in velocities.

- From the time and frequency domain response of overturning moment ΔM_x, $S_{M_xM_x}$, the response matches almost to lateral force response. This is due to the fact that the lateral forces that act at the contact patch contribute considerably to the overturning moment response of the axle.

- Comparing the time response of self-aligning moment change ΔM_z in Figures 4.5 and 4.7 to those of Figures 4.9 and 4.11, clearly indicates that self-aligning moment accuracy at lower loads in not good. As mentioned in Chapter 3, modeling transient self-aligning moment is complex and using a lead filter with an extra first order equation, as given is equation (3.18), improves accuracy at higher loads only.

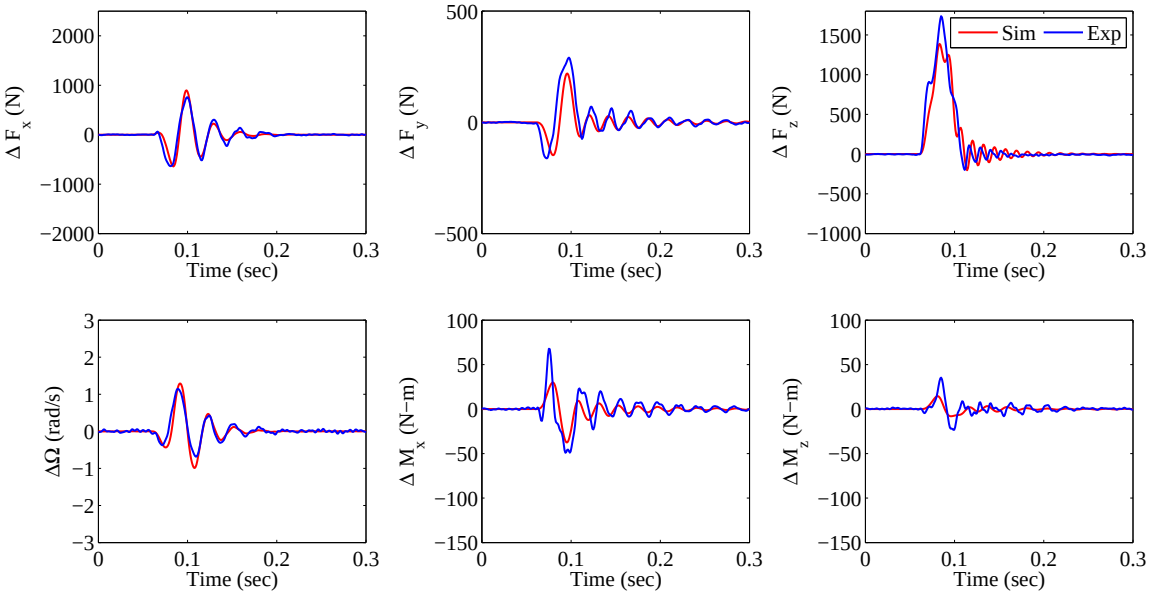

Figure 4.5: Time domain response of tire rolling over oblique cleat 43.5° at 25 kmph and F_z = 2000N

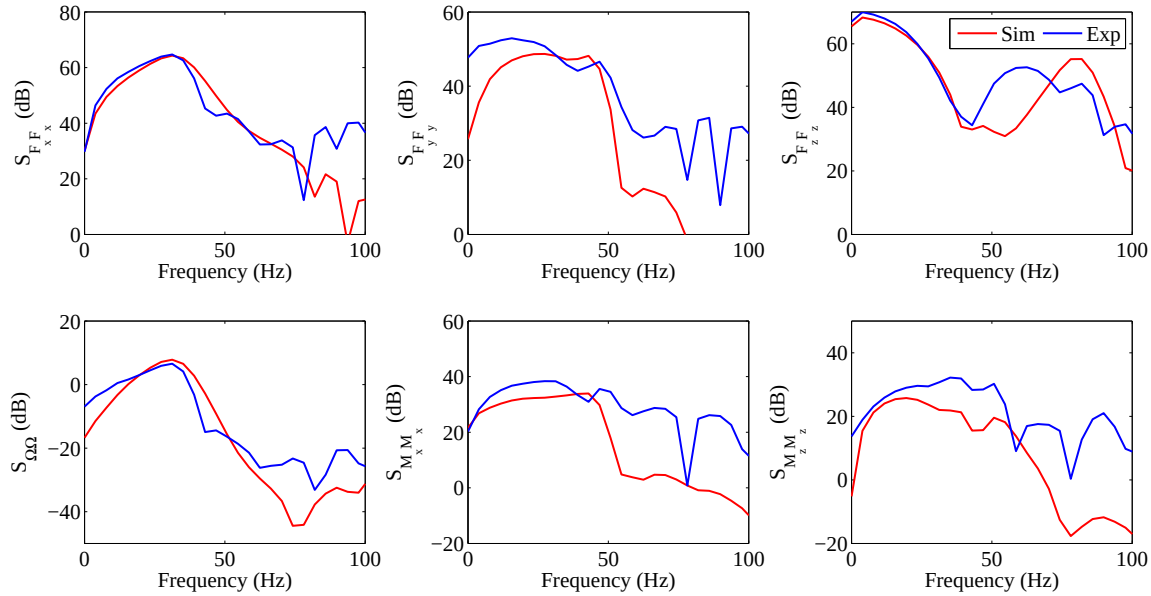

Figure 4.6: Frequency domain response of tire rolling over oblique cleat 43.5° at 25 Kph and F_z = 2000N

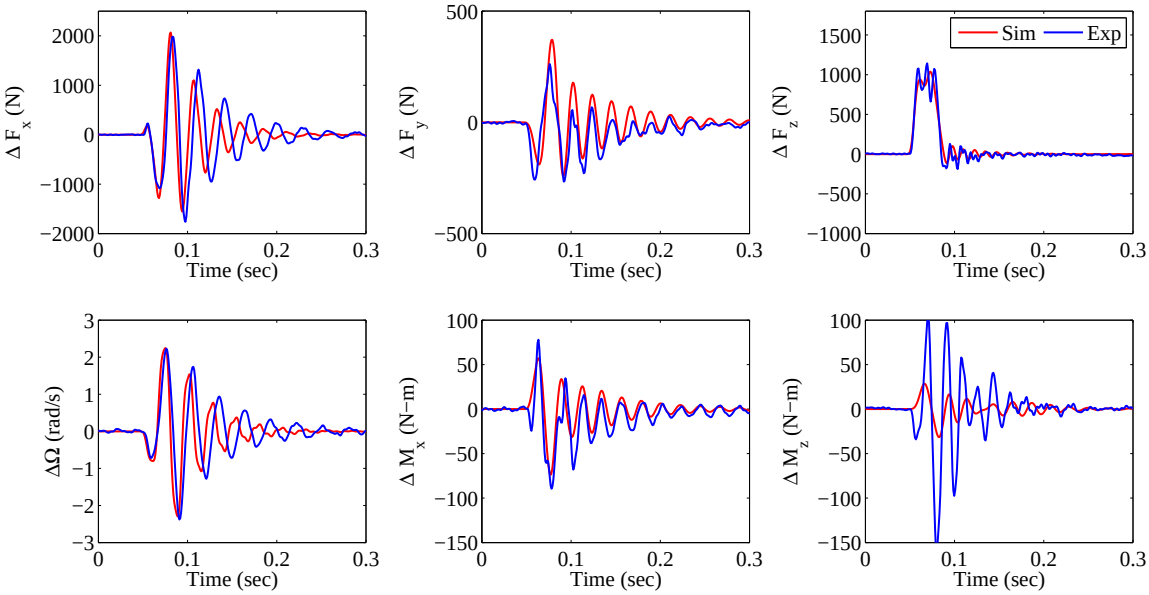

Figure 4.7: Time domain response of tire rolling over oblique cleat 43.5° at 59 Kph and F_z = 2000N

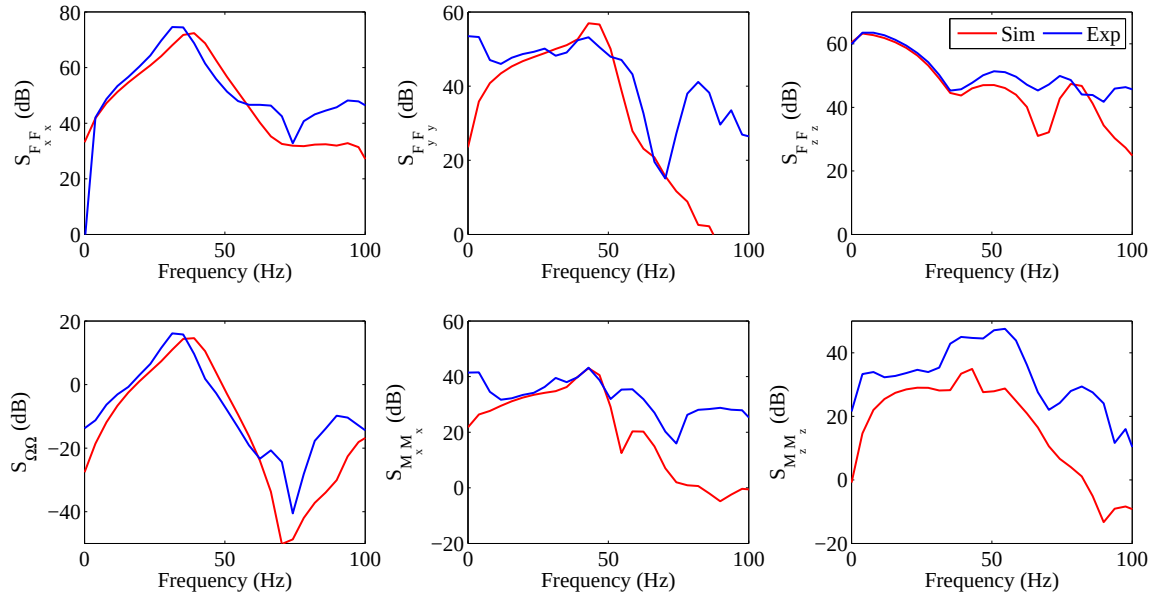

Figure 4.8: Frequency domain response of tire rolling over oblique cleat 43.5° at 59 Kph and F_z = 2000N

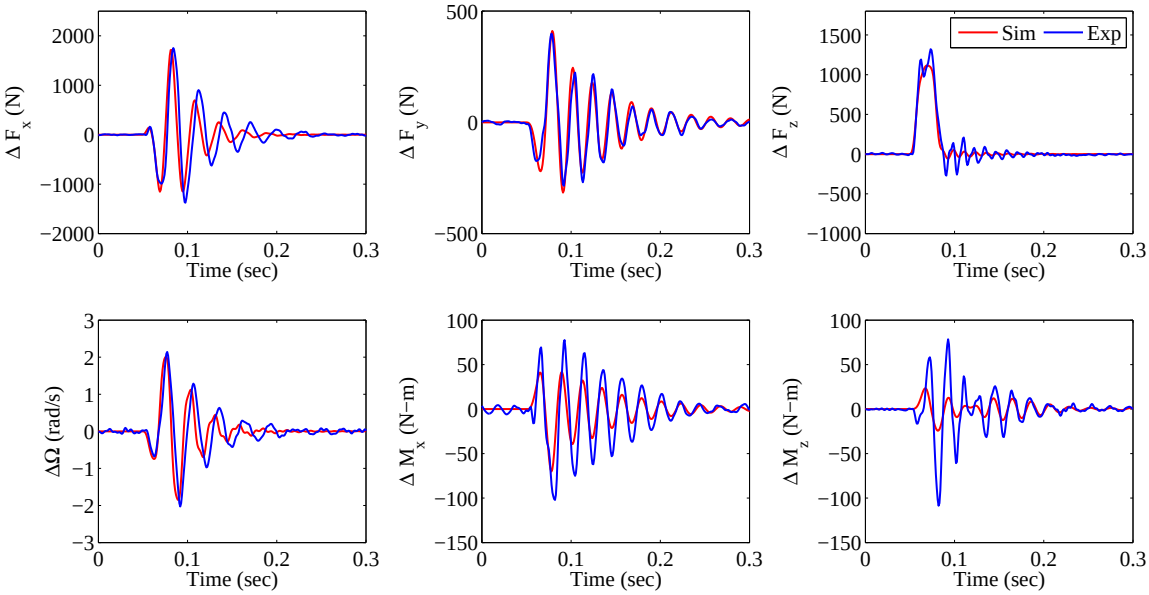

Figure 4.9: Time domain response of tire rolling over oblique cleat 43.5° at 39 Kph and F_z = 4000N

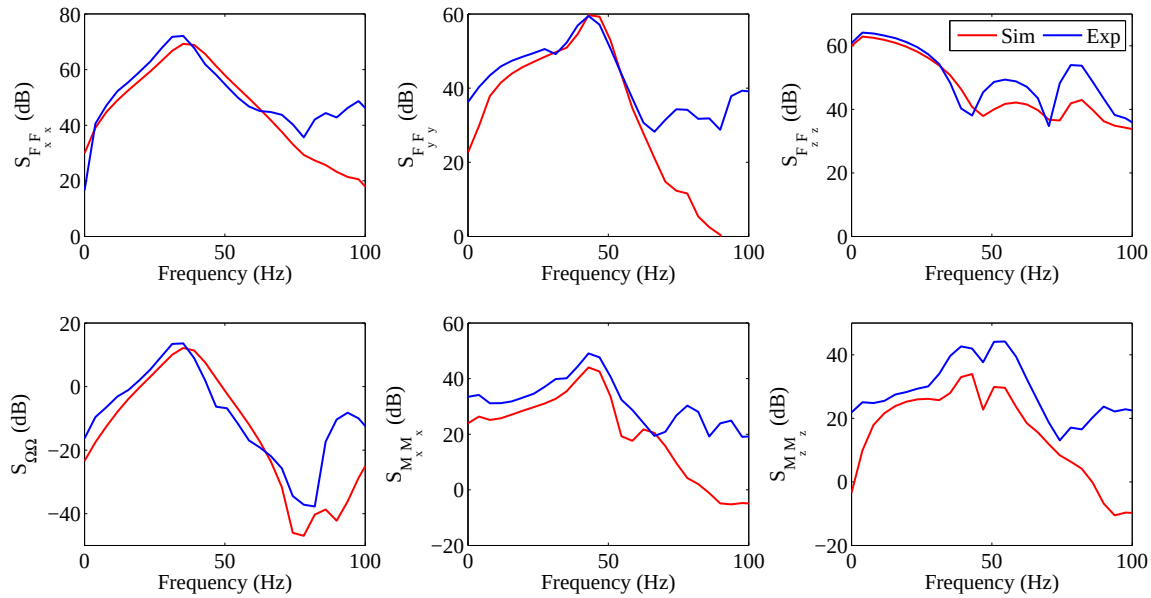

Figure 4.10: Frequency domain response of tire rolling over oblique cleat 43.5° at 39 Kph and F_z = 4000N

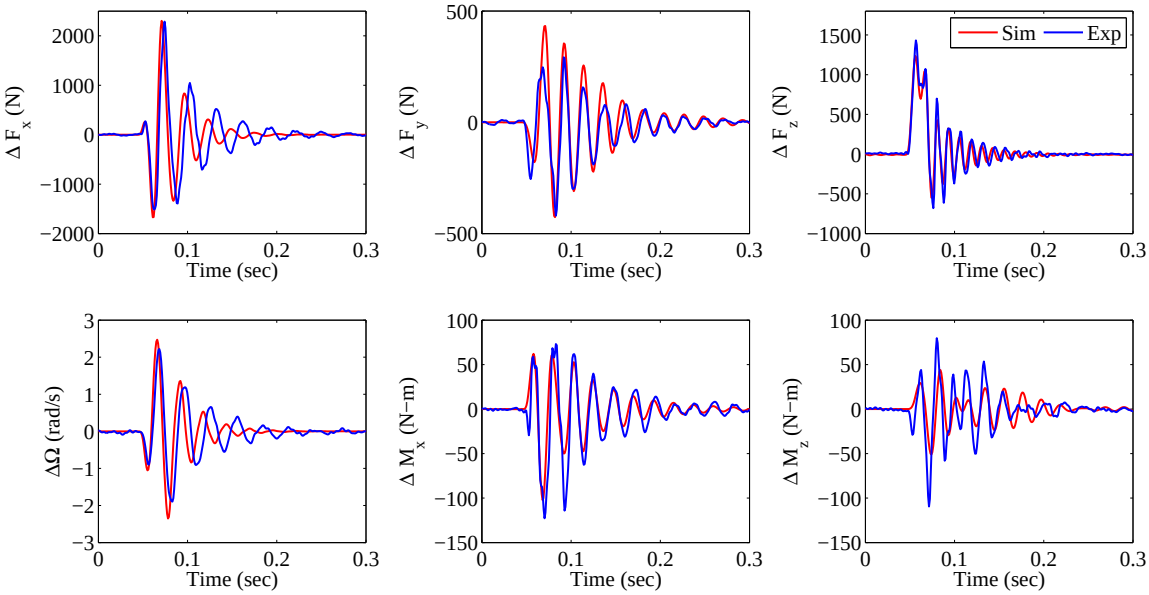

Figure 4.11: Time domain response of tire rolling over oblique cleat 43.5° at 59 Kph and F_z = 6000N

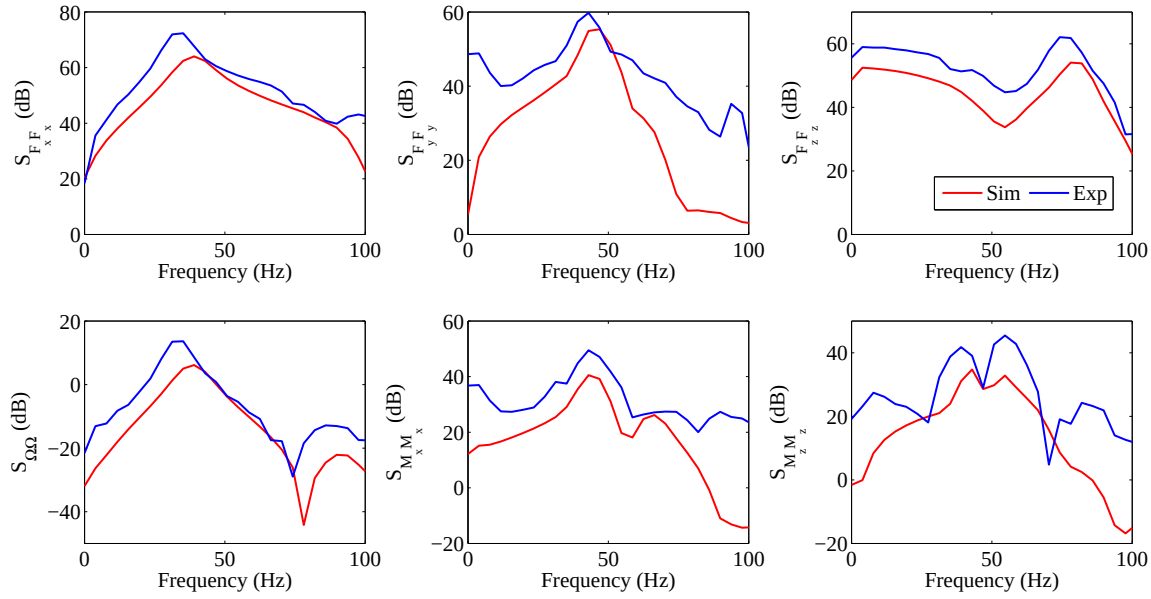

Figure 4.12: Frequency domain response of tire rolling over oblique cleat 43.5° at 59 Kph and F_z = 6000N

4.1.5 Robustness of the Code

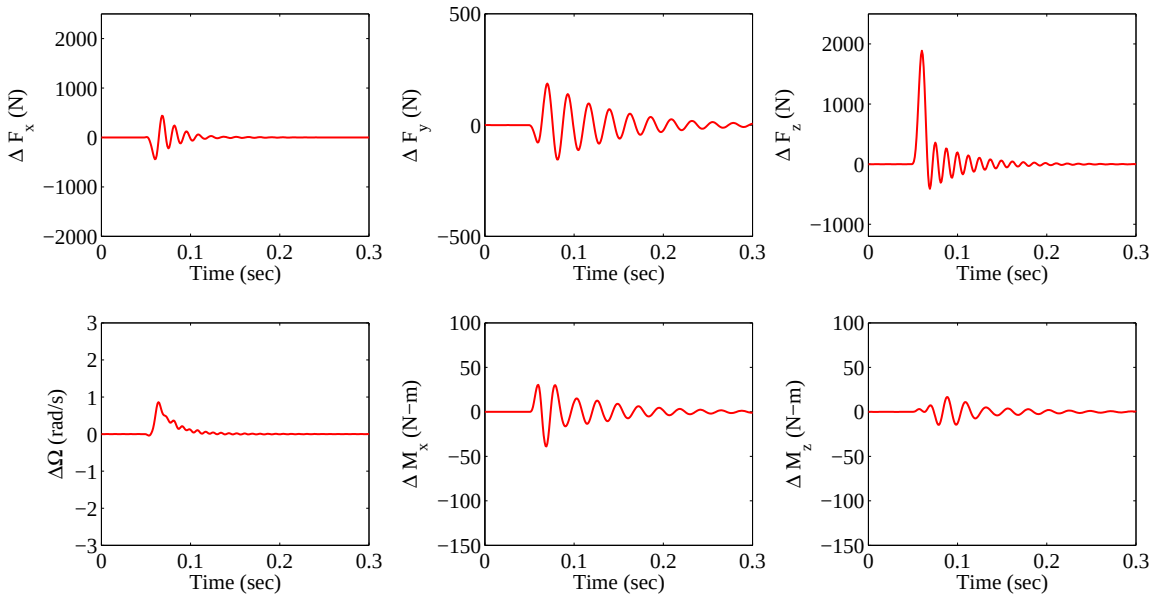

Figure 4.13: Time domain response of tire rolling over oblique cleat 60° at 59 Kph and F_z = 500N

To demonstrate the robustness of the developed tire model, response of dynamic tire model with fixed axle condition rolling at 59 Kph over a oblique cleat of 10 mm at a larger angle of 60° and with load of 500N is simulated. The reason for this case study is that, during the initial debugging of the code, results seemed very sensitive to contact model mass (m_c) and contact rotational inertia (I_c). This caused high oscillations of force response and sometimes causing instabilities in simulation code by driving relaxation length to zero. As shown in Figure 4.2, tire model contains different modular subsystems, integration of multiple subsystems could cause simulation instability. With the proper selection of contact model parameters and setting the correct saturation limits for the contact model variables, the numerically instability of the code was resolved.

Although data for validating these conditions is unavailable, some common trends in the behavior of tire at lower loads can be observed from the previously validated test cases. As

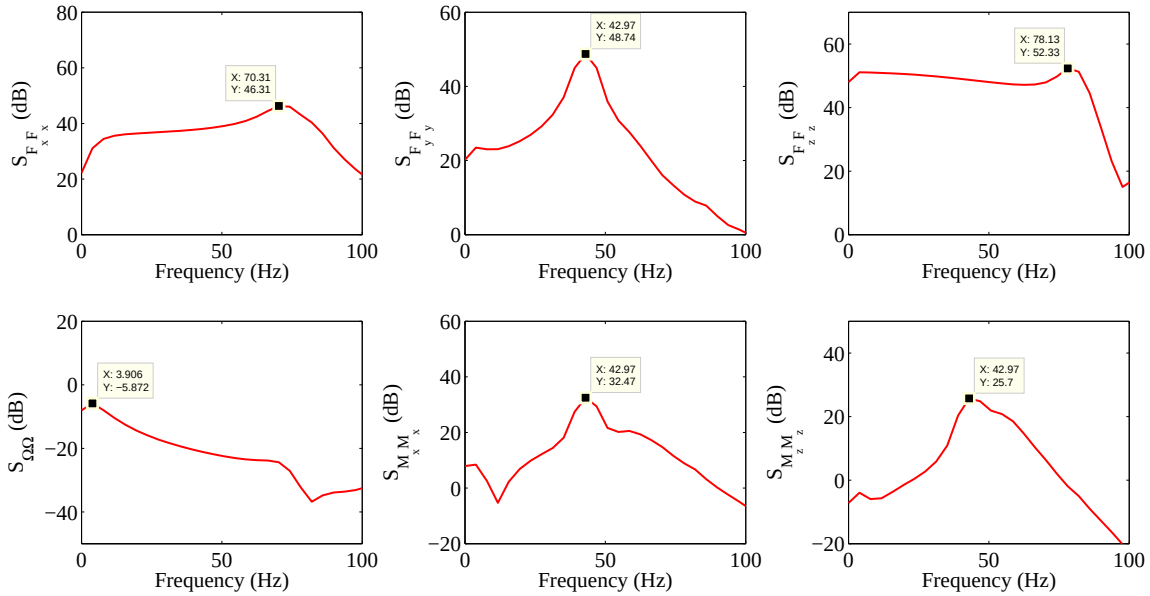

Figure 4.14: Frequency domain response of tire rolling over oblique cleat 60° at 59 Kph and $F_z = 500$N

the tire is rolling at a lower load and at higher velocity, when the tire encounter the cleat the boundary condition at the contact patch of the tire is closely corresponding to free unloaded condition. From Figure 4.14, the rigid modes of vibration of the tire closely correspond to free unloaded modes of tire as given in Figure 2.6. From Figure 4.14, as the load on tire is less, the contact patch stiffness at the ground decreases, causing the in-phase mode barely excited. Also with the increase in cleat angle, the rate of change of slope of road $(\frac{d\beta_y}{dx})$ also decreases, causing less excitation in longitudinal direction.

As the variation of ΔF_x are caused mainly due to the excitation of in-phase mode, thus variations in ΔF_x is relative very small. As the tire is rolling at a lower load and at a higher velocity, the excitation in vertical direction is more which is seen clearly in variation of ΔF_z. It is relatively more when compared with the other forces and moment variations. As the excitation of lateral modes of tire are depend upon oblique cleat angle, the camber mode of the tire is also excited. Due to the lower load acting on the tire, the variation in ΔF_y

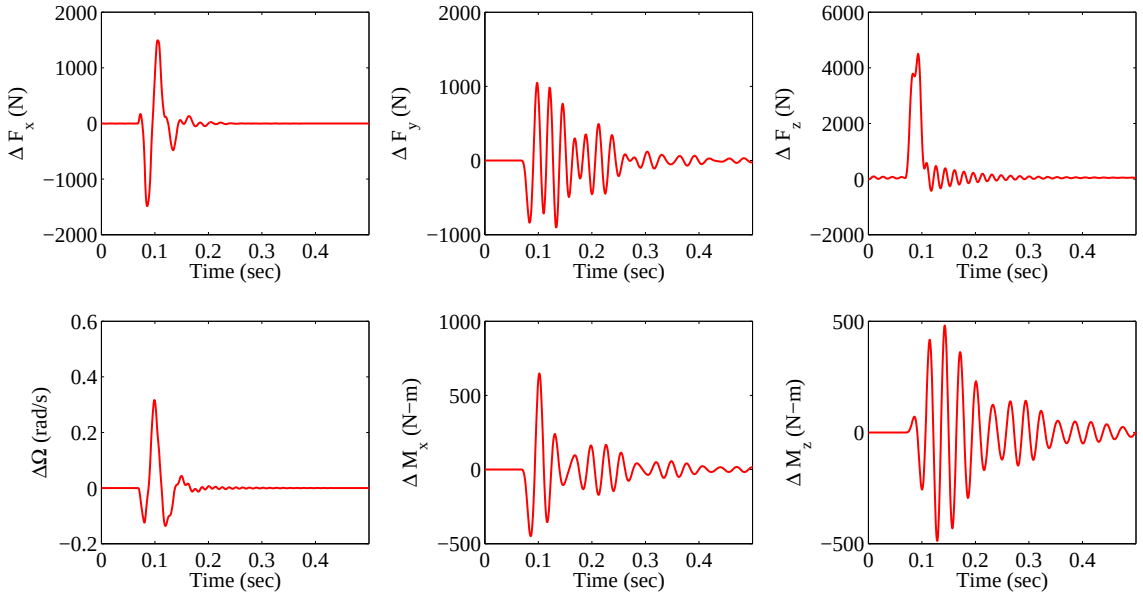

Figure 4.15: Time domain response of truck tire rolling over oblique cleat 43.5° at 59 Kph and $F_z = 30$ KN

and ΔM_x seems to be of less amplitude when compared with the higher loading condition in the previous section. This case study demonstrates the contact model employed is robust enough to represent tire behavior at lower loading conditions also.

4.1.6 Adaptability of the Code

Apart from simulation of developed tire model for passenger tires, with the availability of tire parameters for truck tire of dimension 315/80R22.5, adaptability of tire model for truck size tire was tested. Simulation of truck tire rolling over the 10 mm oblique cleat at 43.5° with fixed axle condition at load of 30000 N was performed. Although data for validating truck tire is unavailable, but some postulations about the modes of vibration of tire like in-phase, anti-phase and vertical modes for truck tires can be made.

As shown in Figure 4.15 same conclusion as in case of passenger tire can be drawn. The

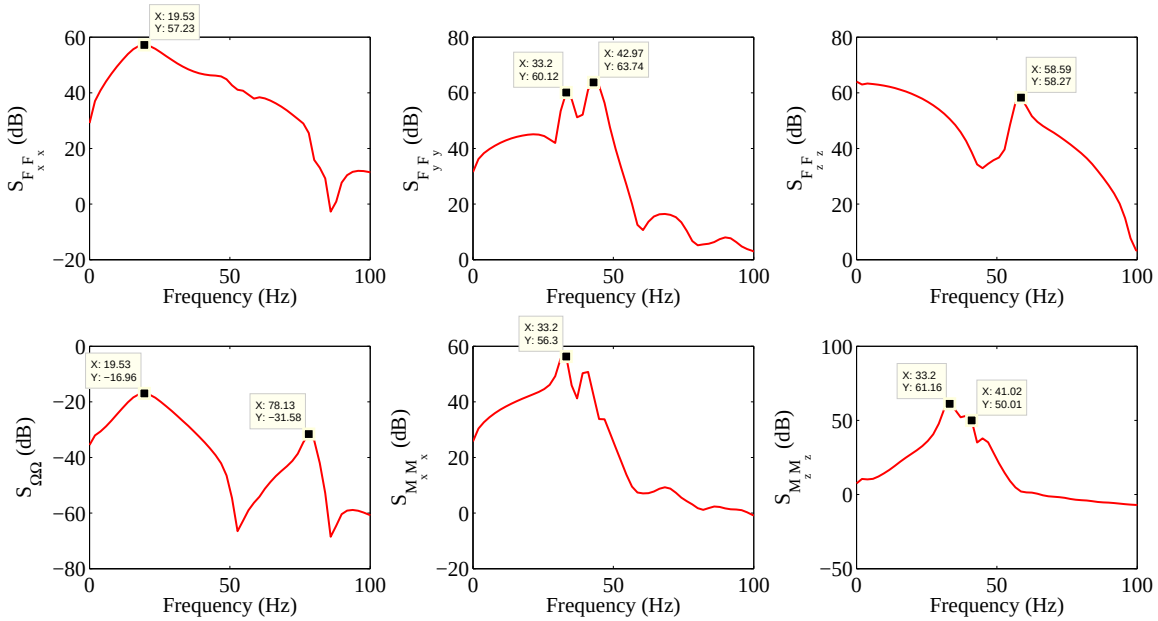

Figure 4.16: Frequency domain response of truck tire rolling over oblique cleat 43.5° at 59 Kph and $F_z = 30$ KN

variation in ΔF_x when tire just encounters the cleat is due to the variation of vertical load but when tire is on cleat and rolling off the cleat, longitudinal response is mainly due to torsional variations $\Delta\omega$ induced due to in-phase mode. The magnitude of variation in ΔF_z is relatively more due to higher vertical stiffness of the truck tire. As shown in Figure 4.16, all the rigid modes of the tire are excited with vertical mode shifted to lower value of 59 Hz. This is due to the fact that although stiffness of tire is increased but the mass of the belt in case of truck tire is almost eight times that of passenger tires.

4.2 Vehicle Model Validation

For the validation of the vehicle model, the measured vehicle response data from a continuous sinusoidal steering test is used (GM Sinusoid). The test is run on a normal flat track at a constant velocity. The steering wheel angle is controlled, with a continuous sinusoidal input

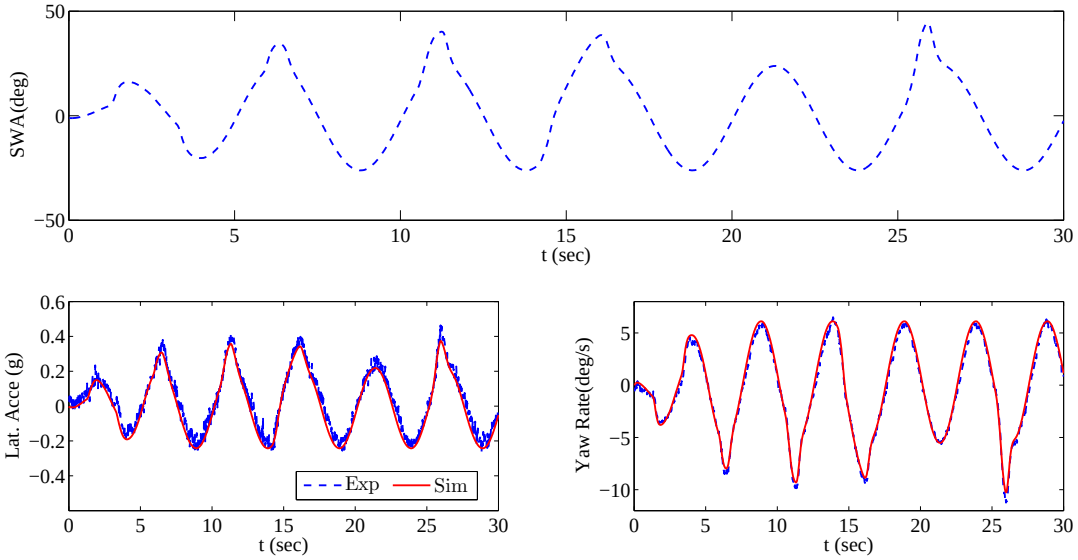

Figure 4.17: Steering angle input, lateral acceleration and yaw rate of the vehicle at 64.37 kph

of 0.2 Hz frequency. This test is specifically used for characterizing on-center handling performance of the vehicle [97] with the lateral acceleration not exceeding 0.4gs. ISO 13674-1 [135] can be utilized as a standard for performing on-center handling tests. The vehicle model is validated for different velocities 64.37, 96.56 and 128.75 kph. The yaw rate and lateral acceleration of the vehicle are compared with the simulated model. From Figures 4.17 - 4.19, the simulated vehicle model response matches quite well with experimental vehicle response at both velocities. It is observed that with the increase in vehicle velocity, the amplitude of the steering wheel angle needed to generate 0.3 - 0.4 g of lateral acceleration is deceasing. It is also observed that, as this test is performed with a driver rather than with a robot, it is very hard to generate consistent steering angle for each cycle. This is more evident for higher velocity tests, the small changes in the steering wheel angle causing sharp spikes in the vehicle response. The vehicle simulation model also includes a road surface model that considers the road profile The road profile used in the simulation model differs from the road surface that the vehicle objective tests were performed. However, since the

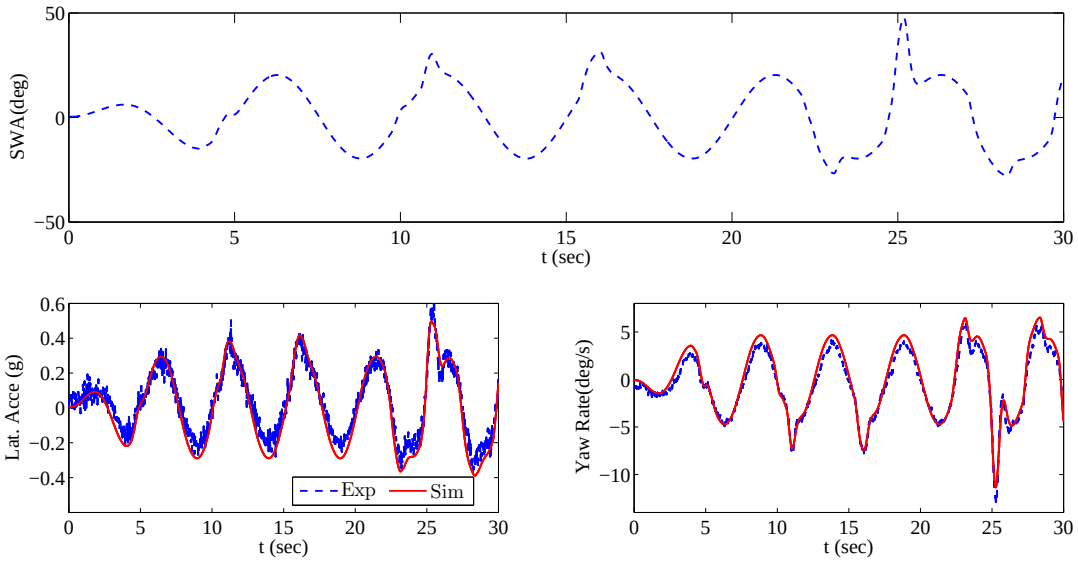

Figure 4.18: Steering angle input, lateral acceleration and yaw rate of the vehicle at 96.56 kph

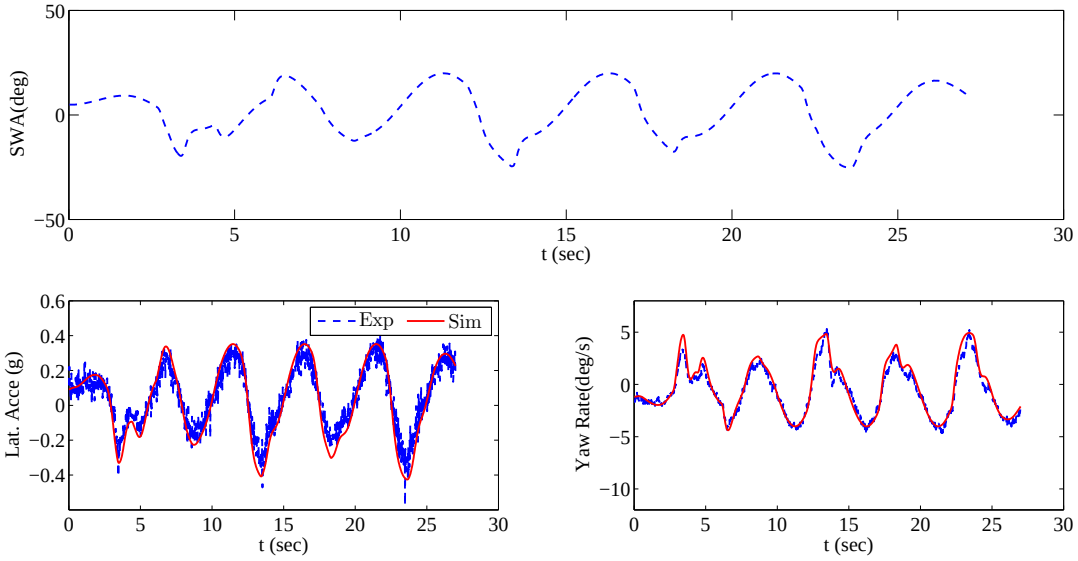

Figure 4.19: Steering angle input, lateral acceleration and yaw rate of the vehicle at 128.75 kph

tests are constrained to lower lateral accelerations, the road profile seems to have minimal effects on the simulated response.

4.3 Conclusion

The accuracy of developed tire and vehicle models are verified against the experimental data. Development of complete dynamic tire model using rigid ring tire model integrated with tandem cam enveloping model in Simulink environment is presented. The developed dynamic tire model was successfully validated against experimental data obtained from fixed axle tests. The simulation results were found to have a satisfactory match with the experimental results and reasons for any discrepancies were discussed. The frequency response (power spectral densities) of the results show that the rigid ring model is able to represent all rigid mode frequencies and is valid upto 75 Hz. Finally, robustness of the developed code was demonstrated at very low loads and higher cleat angles and adaptability of code to 22.5 inch truck tire was also tested and was discussed. The vehicle model developed in CarSim, is also validated using the experimental data from constant sinusoidal steering tests at different velocities.

Chapter 5

Braking and Handling Studies

One of the most important applications of the tire and vehicle models is in the development of safety systems such as Anti-lock Braking System (ABS) and Vehicle Stability Control (VSC) system, which are essential features in all modern automobiles. As the control algorithms for these systems become more advanced, there is a requirement for accurate and computationally efficient tire models to predict the complex interaction of the tire with these systems for the accurate tuning and development of the vehicle. Excitation of tire belt vibrations due to uneven road surfaces, high pressure pulses of ABS cycling and sudden steering inputs has detrimental effects on handling and tractive behavior of the tire [2]. Longitudinal and lateral forces are adversely effected due to dynamic variation of tire properties on uneven roads (friction, stiffness, damping, etc.). To adequately take into account these nonlinearities, tire model for these applications, should be at least valid up to 75 Hz [2].

With the successful validation of the dynamic tire model, as discussed in the previous chapter, in this chapter the tire model and ABS model developed in Matlab/Simulink environment is integrated with Carsim® to develop a simulation tool. This tool is used for performing various vehicle dynamic maneuvers to assess the influence of tire dynamics on braking and handling performance of the vehicle. Finally, a comprehensive tire dependent handling performance metrics which includes the effects of the road undulations are developed to

characterize these effects on the vehicle behavior.

5.1 Integration of CarSim and ABS Modules with Tire Model

As illustrated in Figure 5.1, the enveloping model generates an effective road surface from the measured road profile data. The dynamic contact patch dimensions acts as inputs to the enveloping model. The inputs to the rigid ring model are effective road surface profile (generated due to short wavelength road profiles), deflections at the axle (generated due to net resultant forces from the wheel and vehicle chassis) and high frequency pulsating brake torques from the ABS module. The forces at the axle act as inputs to the vehicle model in CarSim. Using the vehicle longitudinal velocity and rotational wheel velocities as inputs to ABS model, slippage at each of the wheels is computed. Finally, ABS computes braking torque based on slip ratio and wheel rotational acceleration. It should be noted that CarSim uses a fixed axis system at the contact patch and the dynamic tire model uses an axis at the axle under a unloaded condition. Therefore, the necessary transformations have to be accounted for and the input variables units has to be matched with the tire model before the integration can be completed.

5.2 Evaluation of Longitudinal Braking Performance

To assess the braking performance, the dynamic tire model was intergraded with the vehicle model in Carsim. Two case studies were considered. In first case, the effects of short wavelength disturbances on ABS braking performance was studied. Braking maneuvers were performed at 65 km/h on measured bad asphalt road surface with and without an artificially added one centimeter high cleat as shown in Figure 5.2. This would serve as a baseline for comparison of the effects of high frequency belt vibrations, rapid and large changes in tire

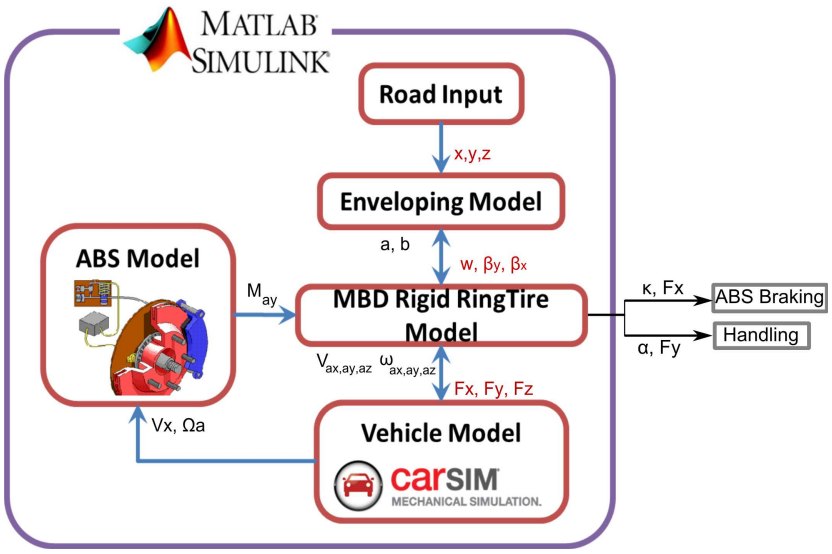

Figure 5.1: Flow chart of inputs and outputs from vehicle, tire and ABS modules

load and slip and the evaluation of response of ABS algorithm to these changes. In the second case, braking maneuvers were performed on split-μ surface at 65 km/h on a flat smooth surface with no undulations to study the effects of high frequency ABS cycling and also adaptability of ABS algorithms to these surface conditions.

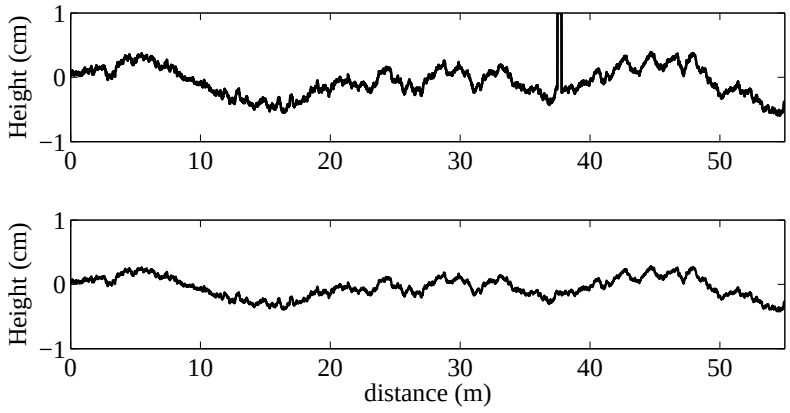

Figure 5.2: Bad asphalt with and without 1 cm cleat

5.2.1 ABS Braking on Bad Asphalt with and without Cleat

The simulation results for ABS performance with and without cleat cases are shown in Figures 5.3- 5.8. In all the cases, braking is applied at the 2 sec of the simulation time and a simulation time step of 0.25 ms is used. The following observations were made based on the simulation results:

- From Figures 5.5 and Figures 5.8, it can be seen that the ABS is able to successfully cycle around the peak area of the force-slip curves for all four tires. The front and rear tires operate close to the maximum tractive force $F_{x,max}$ of 4000 N and 2000 N except when rolling over cleat as illustrated in Figures 5.3 and Figures 5.6, this demonstrates the effectiveness of the ABS algorithm.

- From Figures 5.3 and Figures 5.6, the rate of cycling of brake torque M_{ay} is seen to reflect real-world ABS braking scenario, with an initializing stage of slow buildup of pressure and after reaching the peak value of slip, the other stages of step increase, decrease and hold cycles can be seen. At the end of the simulation, due to lower velocities, wheel tends to slip faster. It is seen after 3.5 seconds of simulation time, ABS responds to this variation and applies braking torque with lower amplitudes and high frequencies.

- The influence of high frequency road input can be seen from Figures 5.6- 5.8, with a sharp spikes in all curves from $t = 2.082$ s to $t = 2.14$ s i.e within a 0.058 s. The wheel slip which is at the peak value of $\kappa = 7\%$ goes towards sliding region of $\kappa = 34\%$ as shown in Figure 5.8. As this is very fast effect, the ABS did not have enough time to decrease the brake torque M_{ay} to bring back the slip to the peak value, when the vehicle was traveling over the cleat.

- Rapid and large variations (3500 N) in longitudinal force F_{xt} is observed in Figure 5.7, for all four tires due to short wavelength road disturbances, leading to variations in

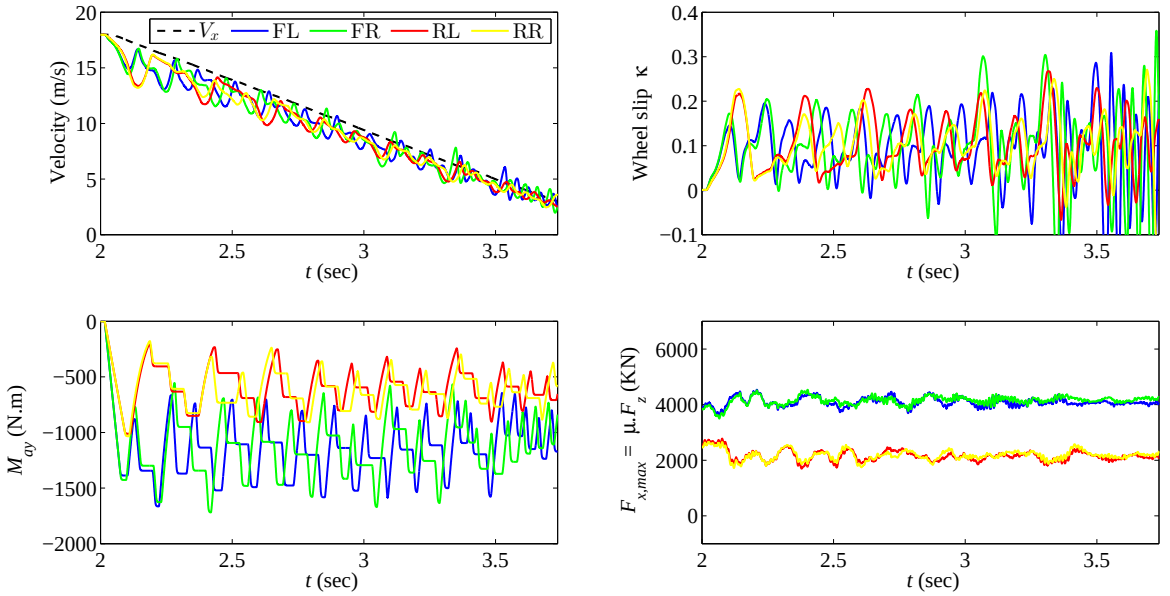

Figure 5.3: ABS braking on bad asphalt without cleat

the angular velocities and thus exciting in-phase rotational mode of the tire. This demonstrates the capabilities of the tire model to account for such effects.

- The variation of vertical load caused the maximum tractive force $F_{x,max}$ available at the tire-road interface to decrease by 4300 N as shown in Figure 5.6, thus directly effecting the longitudinal force F_{xt} generated by the tire at the axle.

- From Figures 5.4 and Figures 5.7, when the ABS is operating at higher stages, spikes in longitudinal forces F_{xt} are seen for front tires. These are also causing more loops in front F_x Vs Slip ratio curves due to the transient dynamics associated with the tire. This proves that rapid pulsing pressure inputs can excite the in-phase mode of tire and cause the variation in wheel angular accelerations, thus eventually inducing longitudinal force F_{xt} variations.

The braking distance with and without the added cleat is shown in Figure 5.9. The presence of 1 cm cleat has increased the braking distance by 1 m which can be very significant under

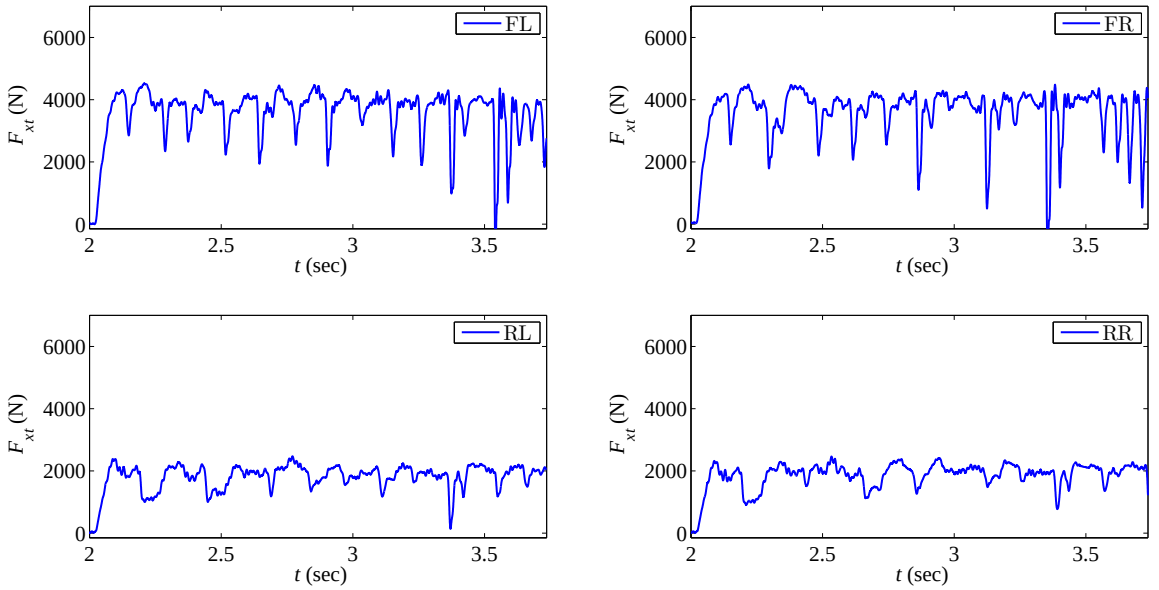

Figure 5.4: Longitudinal force variations on bad asphalt without cleat

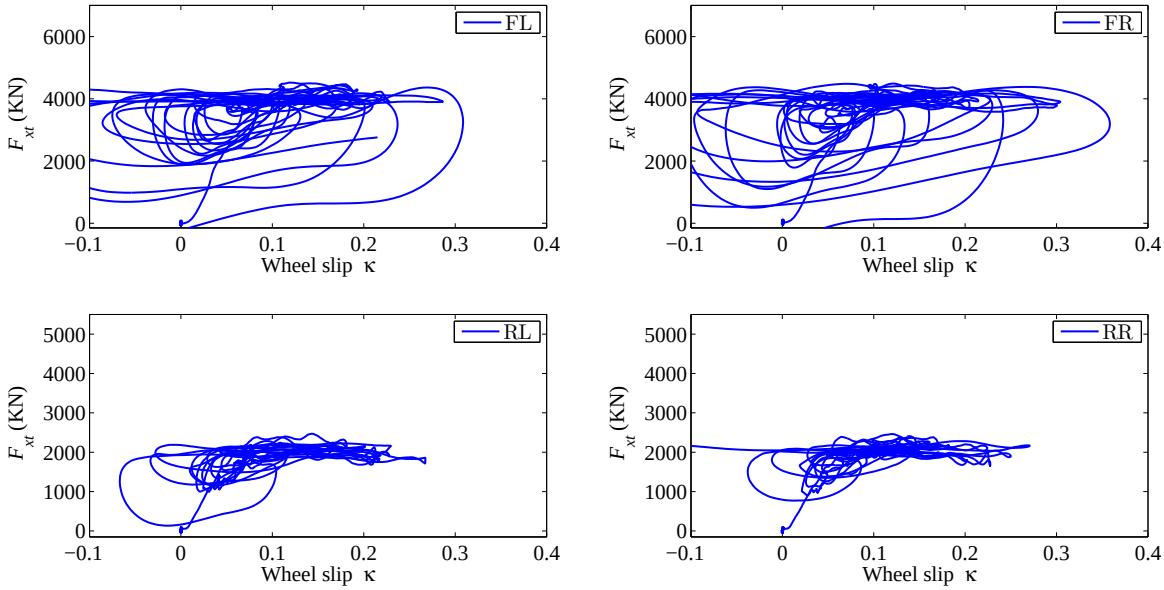

Figure 5.5: ABS operation on bad asphalt without cleat

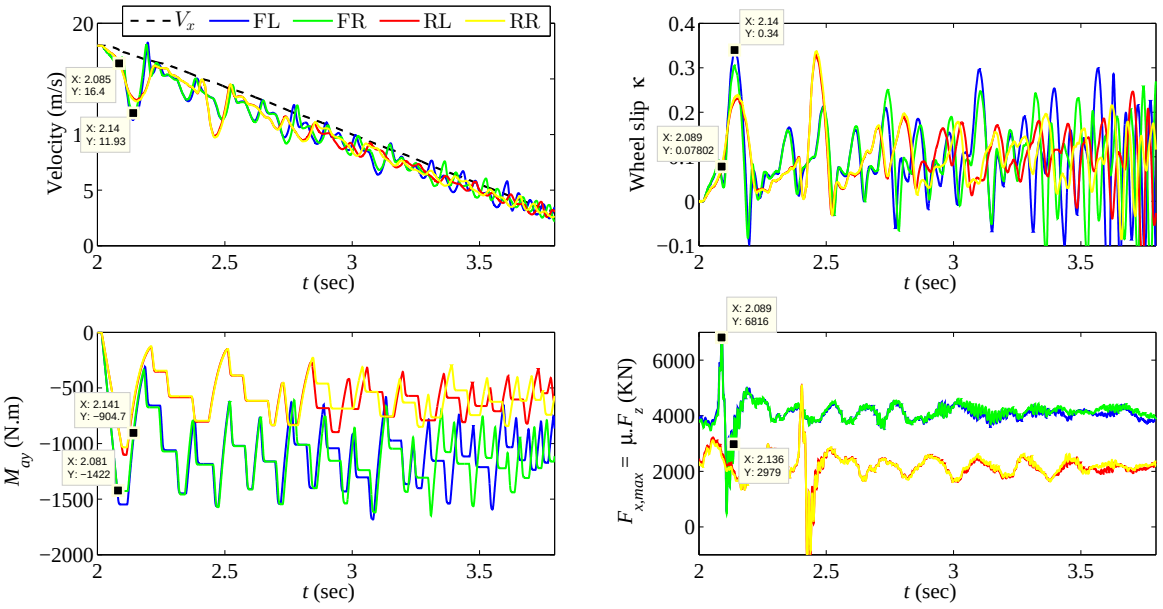

Figure 5.6: ABS braking on bad asphalt with 1 cm cleat

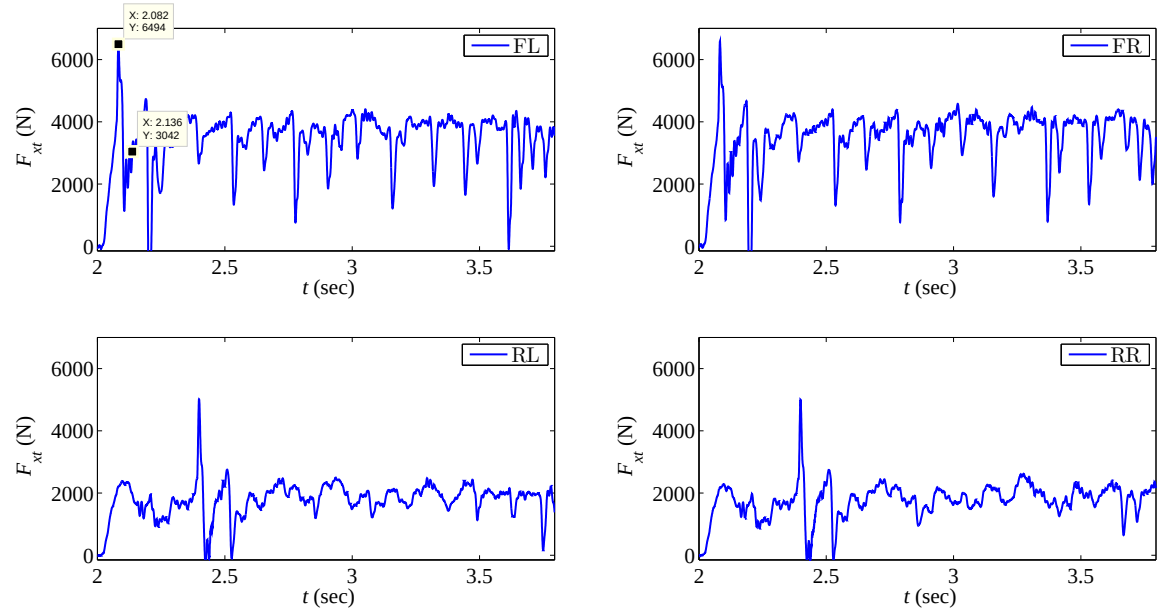

Figure 5.7: Longitudinal force variations on bad asphalt with 1 cm cleat

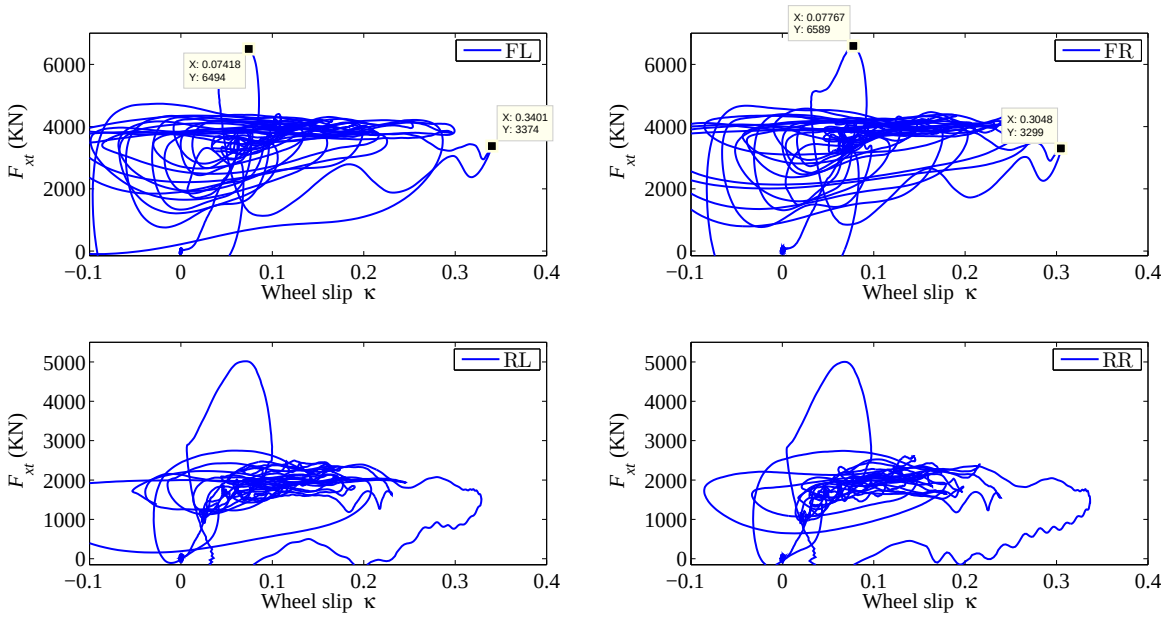

Figure 5.8: ABS operation on bad asphalt with 1 cm cleat

emergency stopping maneuvers. It is observed that the presence of large cleats and potholes have a direct effect on the braking distance of the vehicle. It can be concluded that the vibrations of the tire belt due to short wavelength disturbances have a significant effect on the ABS braking performance of a the vehicle and cannot be neglected. This confirms with the previous studies done by Zegelaar [80] and Pauwelussen [15]. These effects have been clearly demonstrated by the developed a simulation tool using a validated tire model. In such a high frequency scenarios of accident evasive maneuvers, a decrease in braking distance either by improving the tire design or vehicle design can be life saving.

5.2.2 ABS Braking on Split-μ and Normal Surface

The simulation results for ABS braking performance on split-μ surface with 50% less friction on left side of the vehicle are shown in Figures 5.10- 5.12. As seen in Figure 5.10, the available tractive force $F_{x,max}$ on left side tires is 50% less and a the slight increase in tractive force

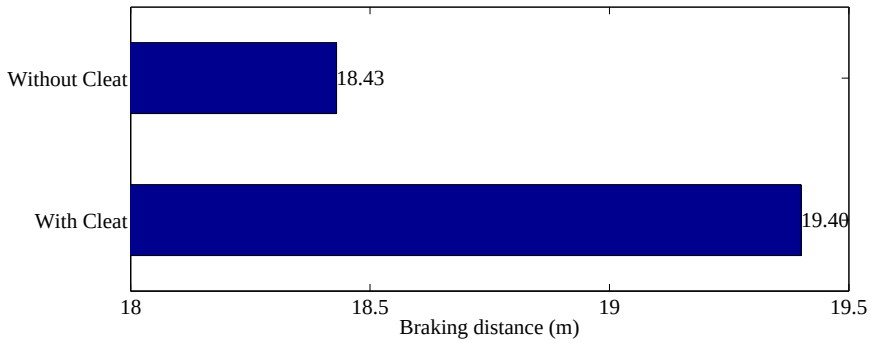

Figure 5.9: Braking distance with and without 1 cm cleat

around $t = 2.5$ sec is noticed due to the weight transfer occurring from the induced roll of the vehicle. From the time history of the braking torque M_{ay} and longitudinal slip κ curves, for left tires the magnitude of maximum braking torque applied by ABS at the end of the full cycle seems to be reducing than the previous cycle but in case of right tires it is increasing at the end of the full cycle. This could be due to the increase in the magnitude of longitudinal slip κ in case of left tires, as the tendency of left tires to lockup is more and the ABS is adapting to these conditions. As mentioned in the previous case and also seen in Figure 5.11, with high pulsing pressure inputs, ABS tends to excite torsional modes of the tire generating high spikes in F_{xt}. This is more for right tires especially for the front right tire. From Figure 5.12, for left tires, the operation region of ABS is distributed from $\kappa =$ 10% - 40%, rather than concentrated at the peak value of friction as it is the case with the right tires. Figure 5.13 illustrates the the vehicle response under braking. It can be clearly seen that longitudinal deceleration (in g's) at vehicle CG (normally equal to peak friction) for split-μ surface is lower than that of the uniform road surface friction. Due to unequal braking forces on left and right sides of the vehicle, these asymmetric forces induce a yaw moment which consequently generates lateral forces, causing lateral acceleration and roll of the vehicle. With the sharp increase in yaw rate, a lateral acceleration of 0.3 g and roll of 1.5° deg are induced at the CG of the vehicle which drives the vehicle off the straight path by almost 2.5 m. Figure 5.14 shows the braking distance on split-μ road surface has increased

by 7.75 m. The primary function and success of ABS is ability to steer the vehicle. Usually, the braking maneuver without the activation of ABS on split-μ surface, drives the vehicle out of control. Although the braking distance has increased, through out the maneuver the vehicle is under the control of driver (stable region).

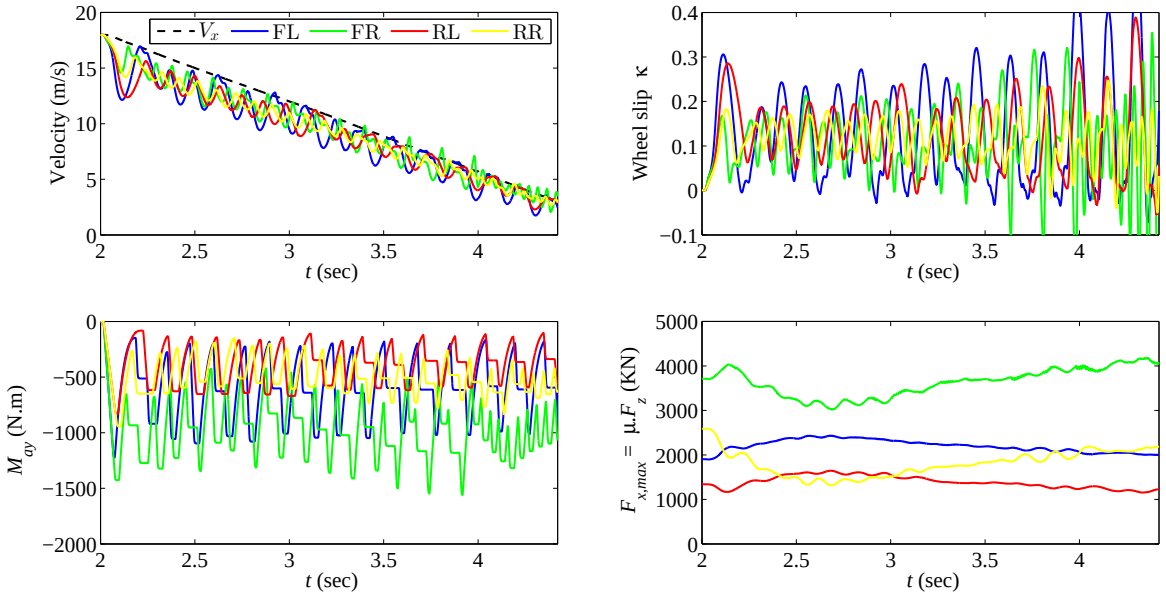

Figure 5.10: ABS braking on split-μ surface

5.3 Evaluation of Limit Handling Performance

In this section, the effects of steering wheel and short wavelength road surface inputs on lateral dynamics of the tire are evaluated. Three cases are considered, in the first case, successive increasing step steering inputs are applied to observe the excitation of lateral mode (camber) of the tire and the variation of lateral forces due to these sudden steering inputs. In the second case, the influence of the road undulations and steering wheel inputs are studied with a step steering input on flat smooth road surface and on a bad asphalt road surface with artificially added cleat. This is shown in Figure 5.2. This serves to study the

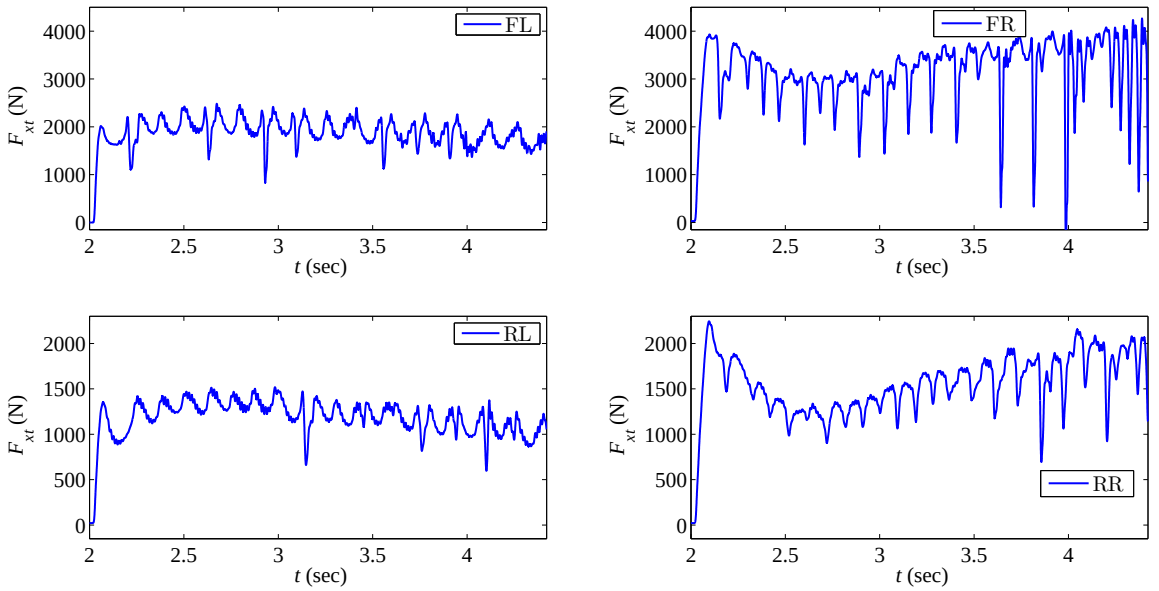

Figure 5.11: Longitudinal force variations on split-μ surface

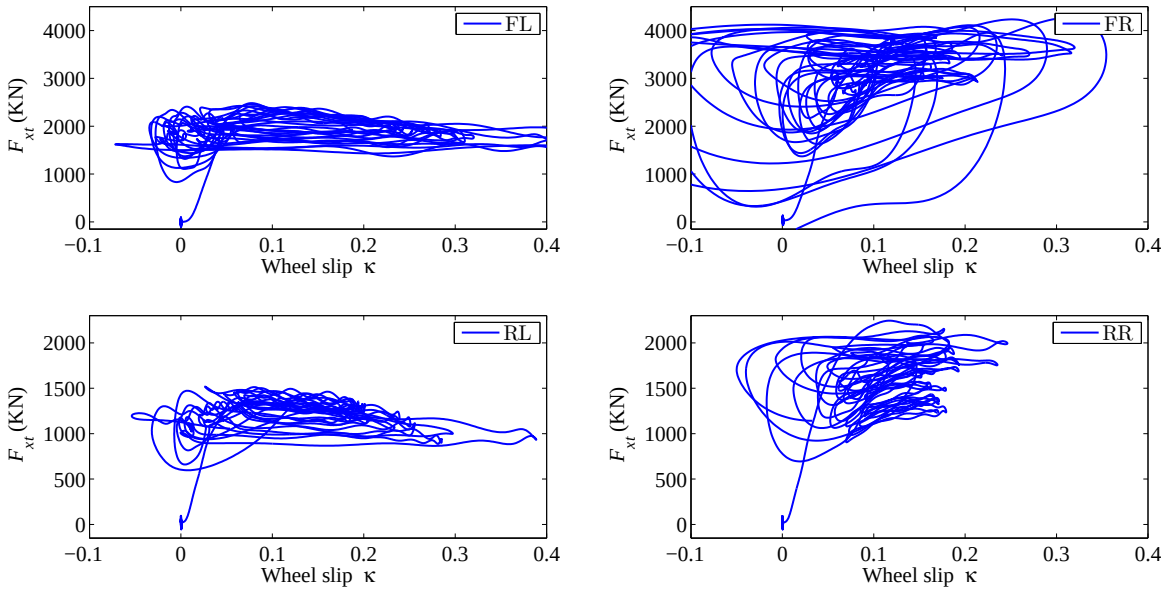

Figure 5.12: ABS operation on split-μ surface

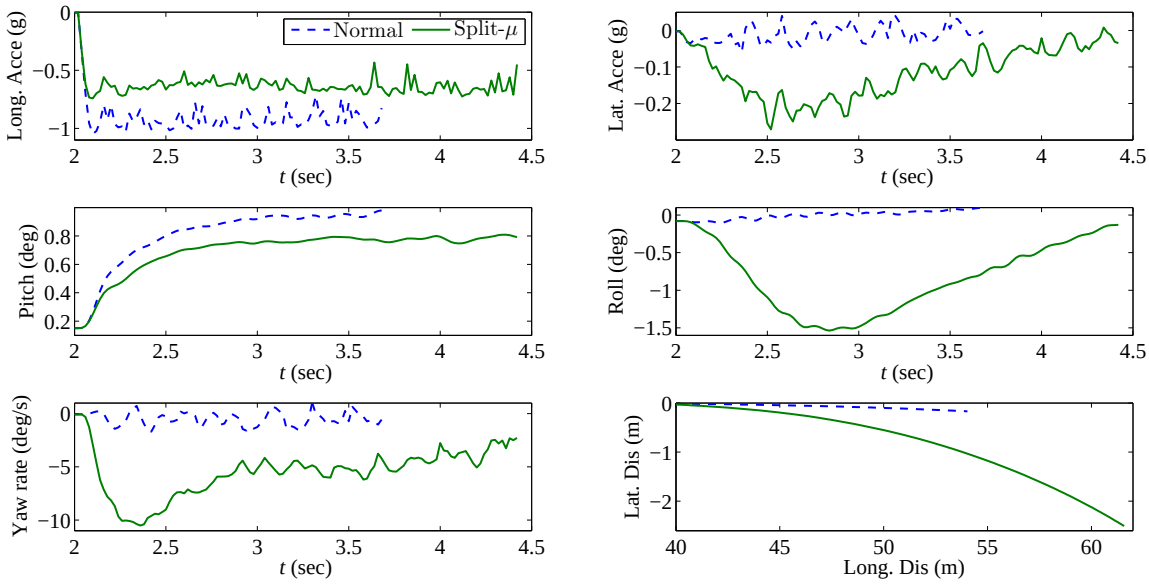

Figure 5.13: Vehicle behavior on split-μ surface

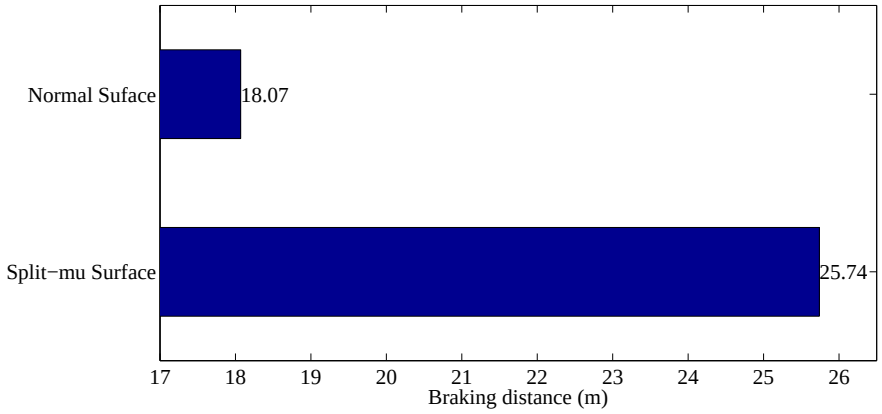

Figure 5.14: Braking distance on normal and split-μ surface

vertical force variations due to short wavelength road inputs and if they cause any increasing influence on the lateral belt vibrations and slip angle variations. In the third case, a tight lane change maneuver was simulated on a flat smooth road surface and on a bad asphalt road surface as shown in Figure 5.2, to evaluate any deviation in vehicle behavior due to steering and road inputs.

5.3.1 Successive - increasing Step Steering

As shown in Figure 5.15, a successive increasing step steering input of 25° is given for each 2 seconds of simulation time at a vehicle velocity of 75 kph. This type of input is used to see how a sudden change in steering input at higher slip angles excites the camber mode of the tire. Figure 5.16 shows the time history of the lateral force and slip angle for all four tires. As the vehicle is a front wheel steering, the camber mode can only be seen in the front tires. From the lateral force VS slip angle curves, the response of the front tires has a cyclic oscillations around the typical steady state curves. With no steering input at the rear tires, its response is a typical steady state behavior with transient relaxation effects. From the time history of the lateral force and slip angle variations for all the four tires, it is observed that, initially at lower slip angles with the step increase in steering input, the force and slip angle response resembles a first order delayed system. Due to the dominance of relaxation effects, the force and slip angles values reach the steady state condition by damping the initial oscillations. However, at the higher slip angles with the increasing steering angle input, relaxation effects of the tire is decreasing and the dominance of the tire inertial belt vibrations are increased. The excitation of tire inertial vibrations is dependent on the vertical load on the tire. It is observed that with the decrease of load on front left tire, saturation of lateral forces occurs at lower slip angles. This causes the influence of tire inertial belt vibrations visible at a simulation time of 4 seconds itself. Figure 5.17 shows the frequency response of forces and moments at the axle. For the front tires, a clear excitation of camber mode of the tire is seen. As road surface inputs are not considered, vertical mode of the tire is not excited. Although, these sudden steering inputs with a magnitude of 25° in 0.01 sec is an extreme steering maneuver, but under the influences of uneven road surfaces the vertical load variation can also excite the lateral dynamics of the tire. This shows the importance of understanding the tire belt vibrations at higher slip angles on uneven road surfaces.

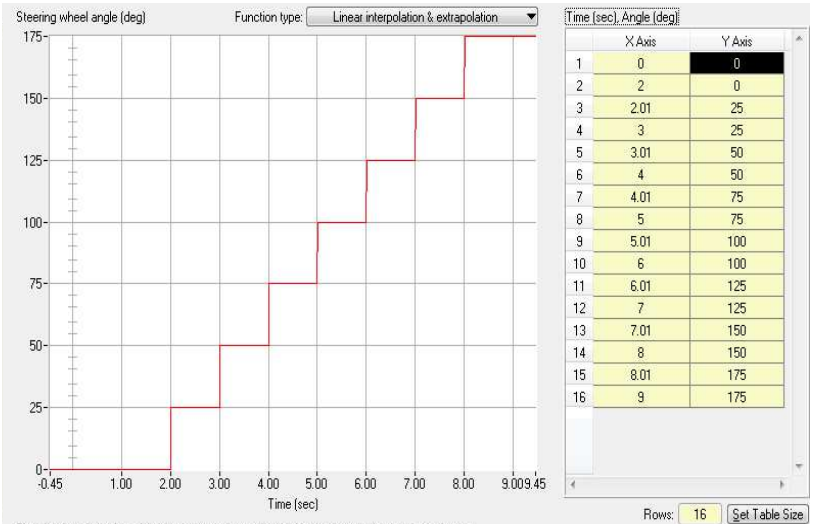

Figure 5.15: Successive increasing step steering wheel input in CarSim

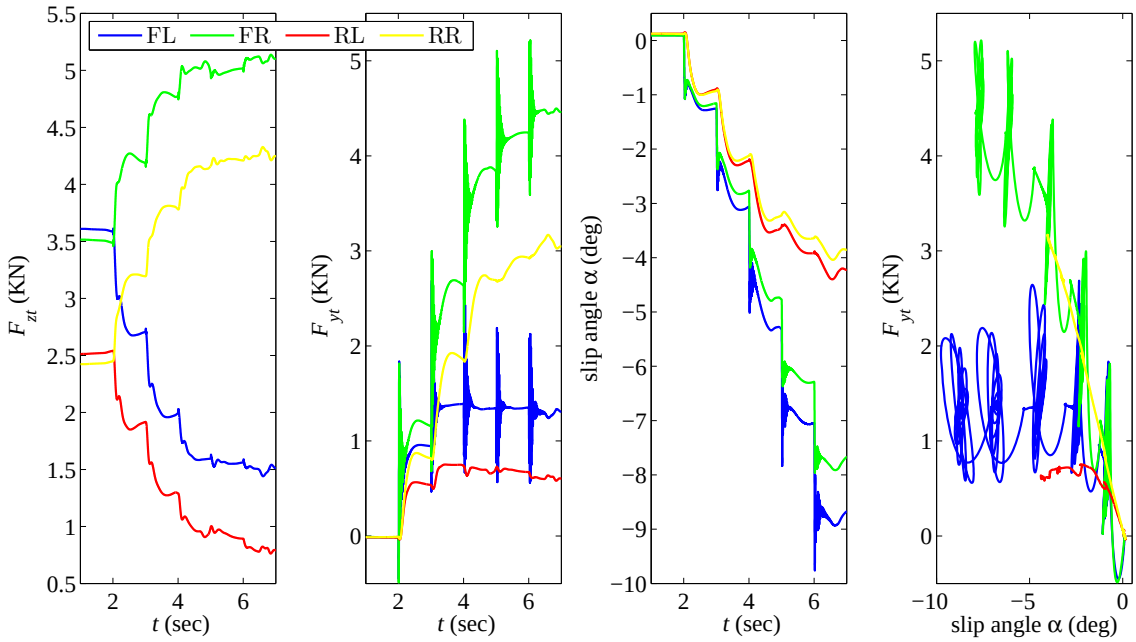

Figure 5.16: Vertical, lateral, slip angle response of four tires with increasing step steering wheel input at $V_x = 75$ kph

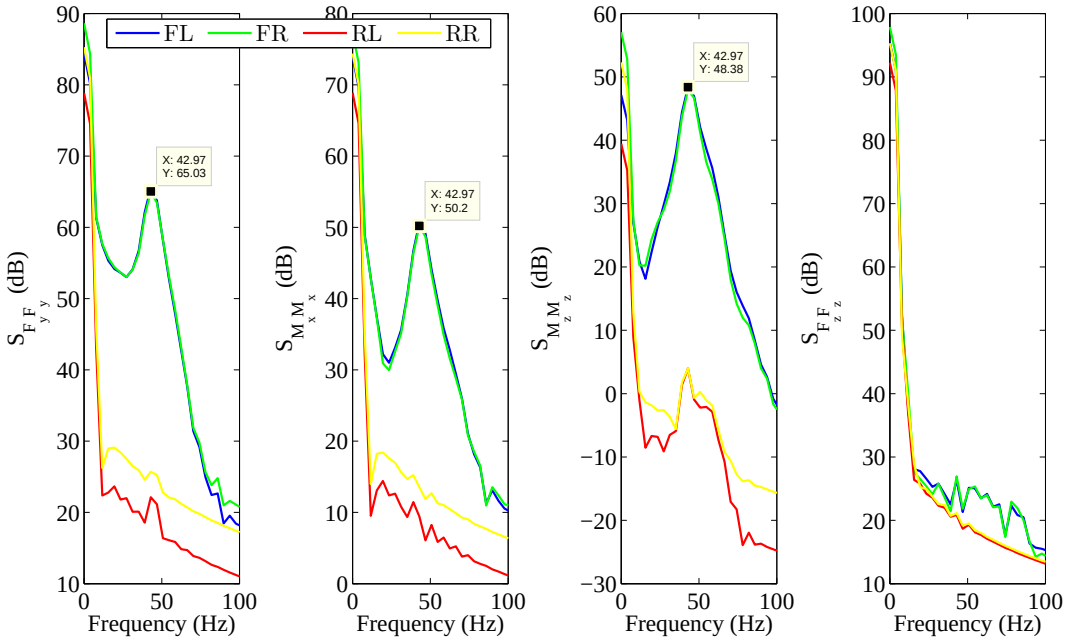

Figure 5.17: Frequency response of lateral, overturning, aligning moments and vertical force for four tires with increasing step steering wheel input at $V_x = 75$ kph

5.3.2 Step Steering on Bad Asphalt with 1 cm Cleat

With the study of the lateral modes of vibrations due to sudden steering inputs, in this section the influence of vertical load variations due to uneven road surface on the lateral forces is studied. For a vehicle maneuver of single or double lane change maneuver on a short wavelength road profile, a study of the interactions of the tire lateral and vertical forces, paves the way for the design of advanced vehicle stability controllers. In this case, a step steering angle as shown in Figure 5.18 is given as input on a flat smooth road (z=0) and on a bad asphalt road surface. On right side wheels a bad asphalt road surface with artificially added cleat is considered. A vehicle velocity of 45 kph is selected.. From Figure 5.19, it can be seen that, after the steering wheel angle reached 180°, small oscillations in the lateral load and slip angle are observed. In this case, the vehicle velocity and the steering wheel input rate is less than the previous case. This causes the relaxation effects of the tire

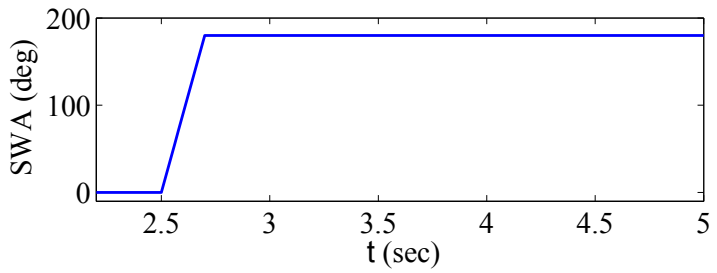

Figure 5.18: Step steering input in CarSim

and the damping in the steering system to have a dominate effect as compared to the tire inertial belt vibrations. From Figure 5.19, the time history of slip angle and lateral forces on a short wavelength road surface seems to differ from the response on smooth road only in between t = 2.8 - 4.8 seconds. At lower slip angles the influence of road undulations are less. At higher slip angles, vertical load variations due to road undulations coupled with lateral oscillations due to steering input, seems to amplify the oscillations in lateral force response. This emphasizes the importance of short wavelength road profile inputs at higher slip angles. More oscillations in time history of slip angle are seen for front and rear left tires due to decreased vertical load on the tire. This causes the saturation of lateral forces at lower slip angles. With the artificially added one centimeter cleat, a slip angle change of 7-10° is observed for front and rear right tires. It is interesting to see small oscillations of frequency 5-8 Hz in time history of lateral and vertical force responses in between t = 3.1 - 3.75 seconds. This is shown in Figures 5.19 and 5.20. These are due to the possible excitation of the roll mode of vehicle due to the addition of cleat on the right side. From Figure 5.21, the frequency response of lateral force on a rough road has a relative increase in the amplitude of camber mode than on a smooth road, in the latter case camber mode is excited only due to steering input. From Figure 5.21, for the rear right tire on a flat smooth road no excitation of camber mode is observed. On an uneven road surface with an artificially added cleat, a peak at 42 Hz with an amplitude higher than the other three tires is observed. This confirm the importance of load variations on possible excitation of camber mode of the tire. A second peak in frequency response of lateral force $S_{F_yF_y}$ on a uneven road is observed,

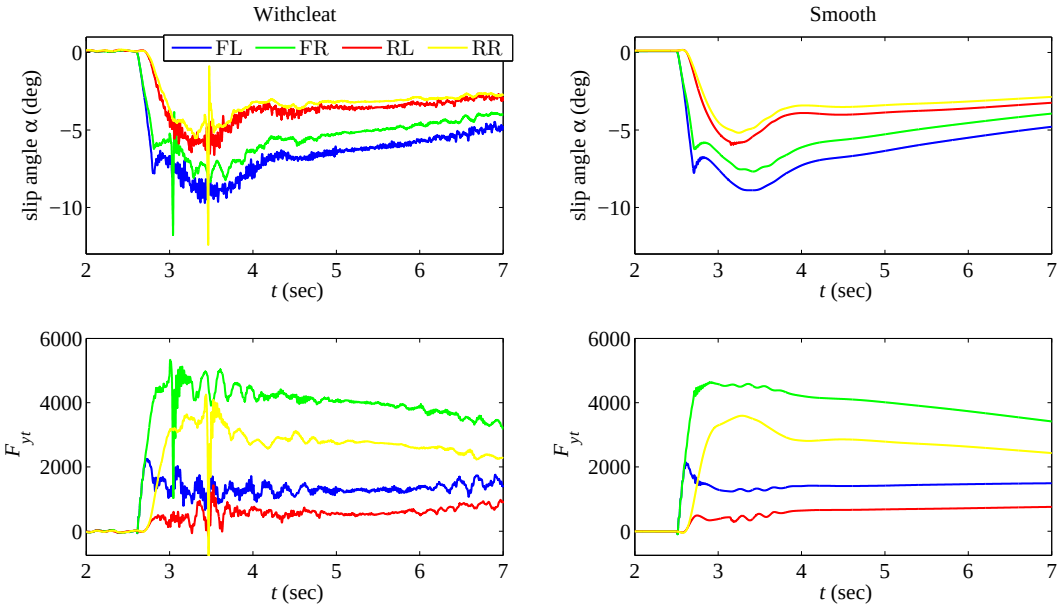

Figure 5.19: Slip angle and lateral forces response on rough road and smooth road at V_x = 45 kph for step steering input

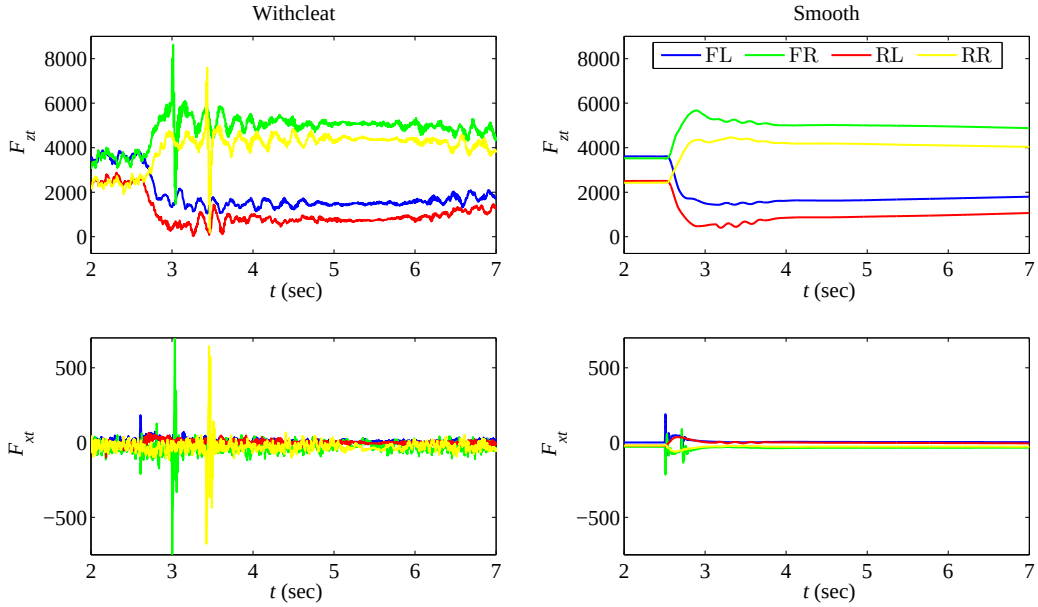

Figure 5.20: Vertical and longitudinal forces response on rough road and smooth road at V_x = 45 kph for step steering input

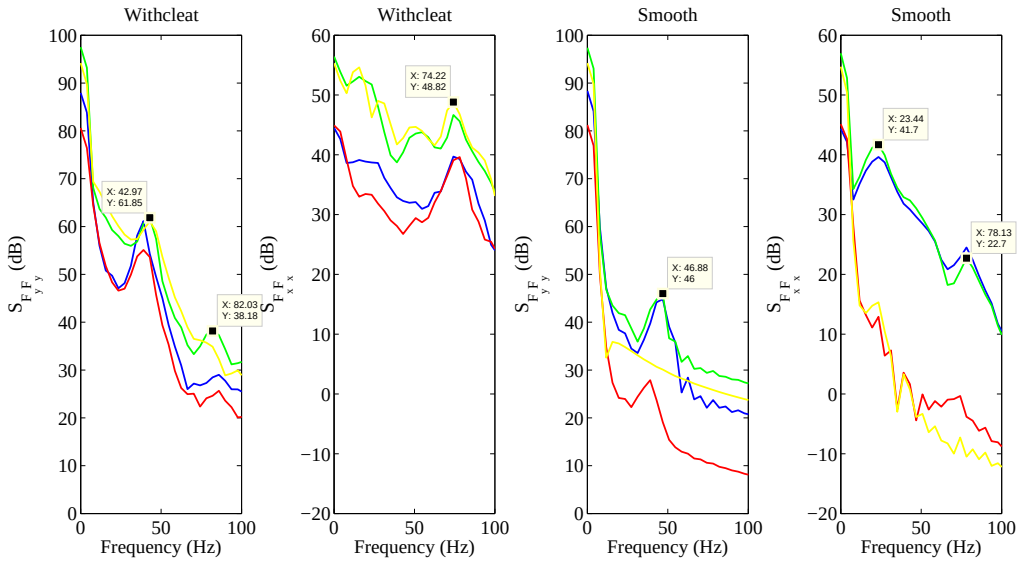

Figure 5.21: Frequency response of lateral and longitudinal forces response on rough road and smooth road at $V_x = 45$ kph for step steering input

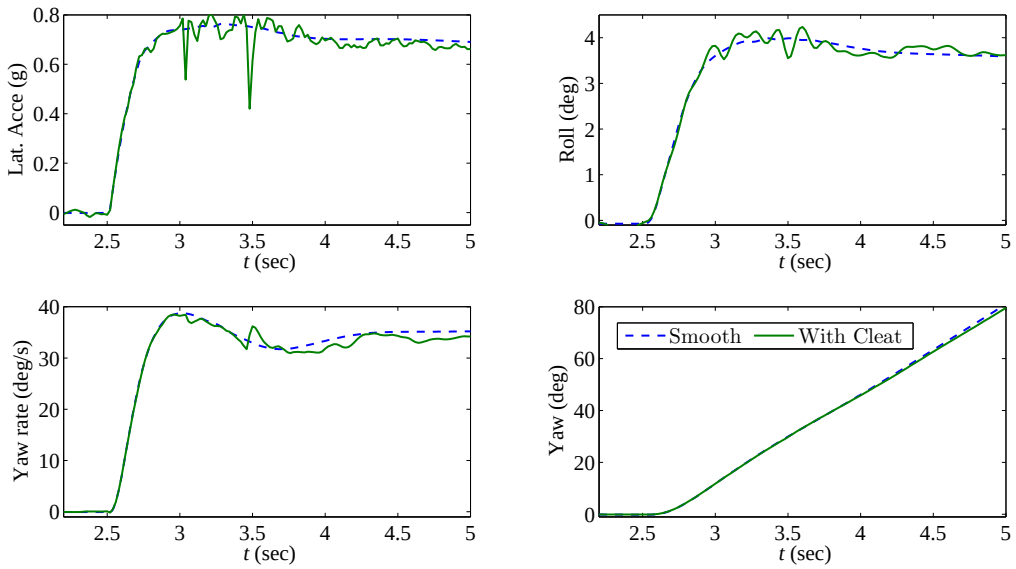

Figure 5.22: Vehicle behavior on smooth and withcleat road

which is the vertical mode of the tire (82 Hz). This emphasizes again the fact that short wavelength road inputs on lateral force variations should not be neglected. For analyzing the interaction of longitudinal and lateral tire modes, frequency response of $S_{F_xF_x}$ on rough and smooth roads is analyzed. It is interesting to see that the in-phase and anti-phase modes are excited on smooth road. Also, this is due to the sudden change in steering wheel input where the tire tends to slip. This is also seen in the time history of longitudinal force response of Figure 5.20. From Figure 5.21, the frequency response of longitudinal forces contain only in-phase and anti-phase modes. This confirms that the lateral oscillations will not corrupt the rotational speed sensor signals [79]. Analysis of the frequency response of lateral and longitudinal forces on a short wavelength road profile indicates that lateral oscillations do not influence longitudinal forces and viceversa. From Figure 5.22, the sharp spike in lateral acceleration signal measured at vehicle CG is observed when the front and rear right tires roll over the cleat. Clearly the excitation of roll mode of the vehicle on uneven road is observed due to cleats being placed only on the right side of the vehicle. When the front tire rolls over the cleat, since the lateral forces generated by the other three tire are not saturated, not much variation in yaw velocity is observed. When the rear tire rolls over the cleat, all the other three tires' lateral force are saturated, so a change in yaw velocity of the vehicle is observed. From this maneuver, the influence and interaction of lateral force with the vertical force variations due to road undulations at higher slip angles is studied. It will be demonstrated in the third case study, that these effects should not be neglected for tight lane change maneuvers especially at higher velocities.

5.3.3 Lane Change on Bad Asphalt without Cleat

A lane change maneuver, at a velocity of 80 kph, is simulated on a flat smooth road and on a bad asphalt road surface. This is shown in Figure 5.2. A preview based closed loop driver controller in CarSim is used with a preview time of 0.5 seconds. Figure 5.23 shows the desired trajectory with a lane shifted by 3.5 m. Maximum limit on applicable steering wheel

angle and steering wheel angle rate are specified. This is shown in Figure 5.23. Figure 5.24

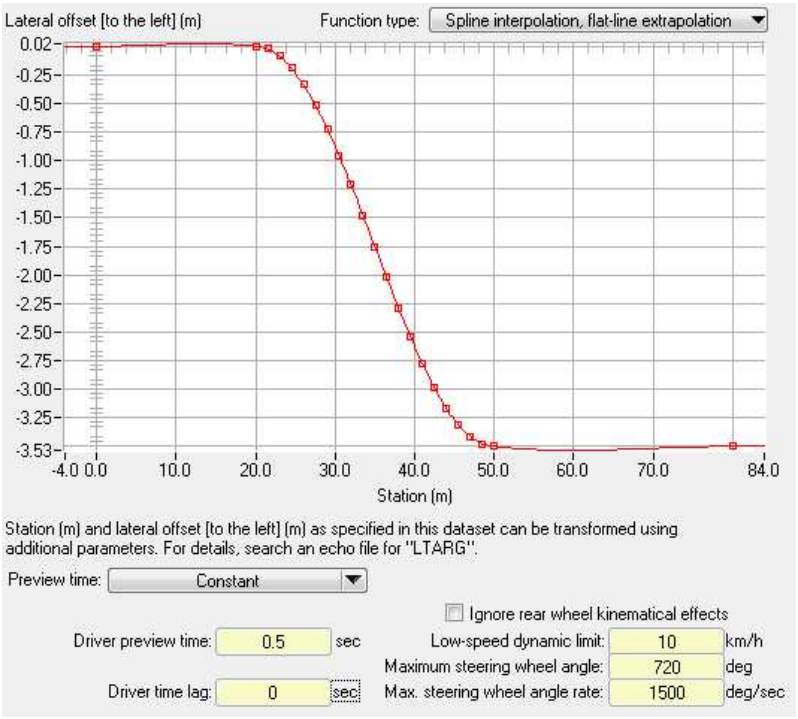

Figure 5.23: Single lane change desired trajectory

shows the time history of lateral force and slip angle variations on the flat smooth and the bad asphalt road surfaces. Although the slip angles in this case are less than the previous case, but more load transfer occur due to the high velocity. As shown in Figure 5.25, this causes saturation of lateral forces at smaller slip angles. When the vehicle is about to change the lane by steering right, load on the right tires decreases causing saturation in slip angle, as shown in the corresponding positive region of lateral forces VS slip angle curve. The same decrease in load on left tires occurs when the vehicle is steered to left to bring the vehicle straight. It is interesting to observe that the oscillations in the time history of slip angle and lateral force on bad asphalt road occurs only when the tire is operating at nonlinear region of lateral forces VS slip angle curve. At the other parts of maneuver, *i.e* when slip angle is not saturated, behavior on smooth and bad asphalt surfaces is nearly same. This is due to the relaxation length of the tire decreasing just before the saturation of slip angle

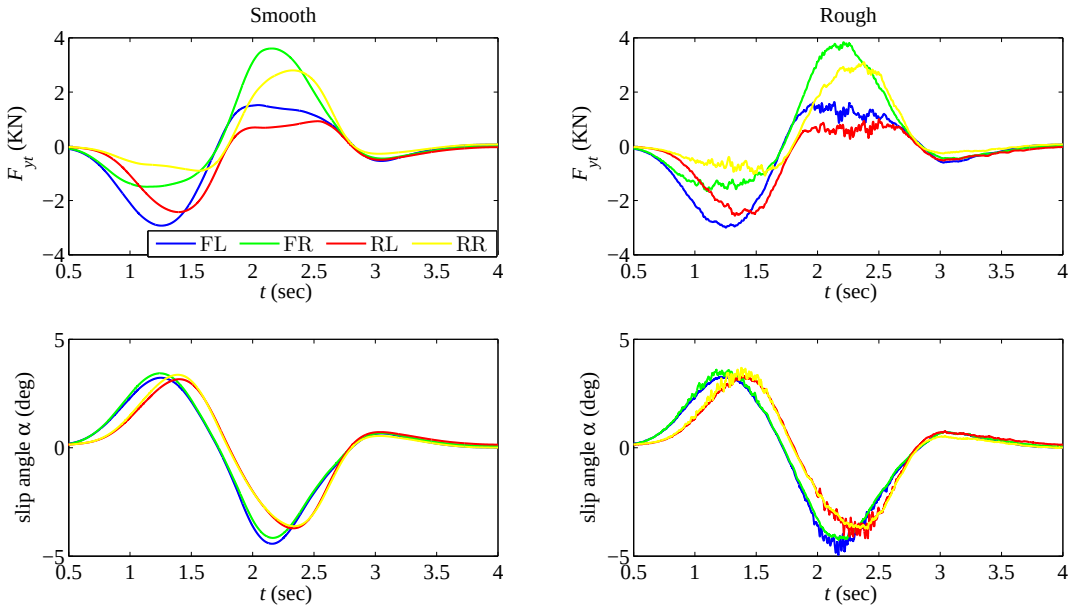

Figure 5.24: Slip angle and lateral forces response for single lane change maneuver on smooth and bad asphalt without cleat

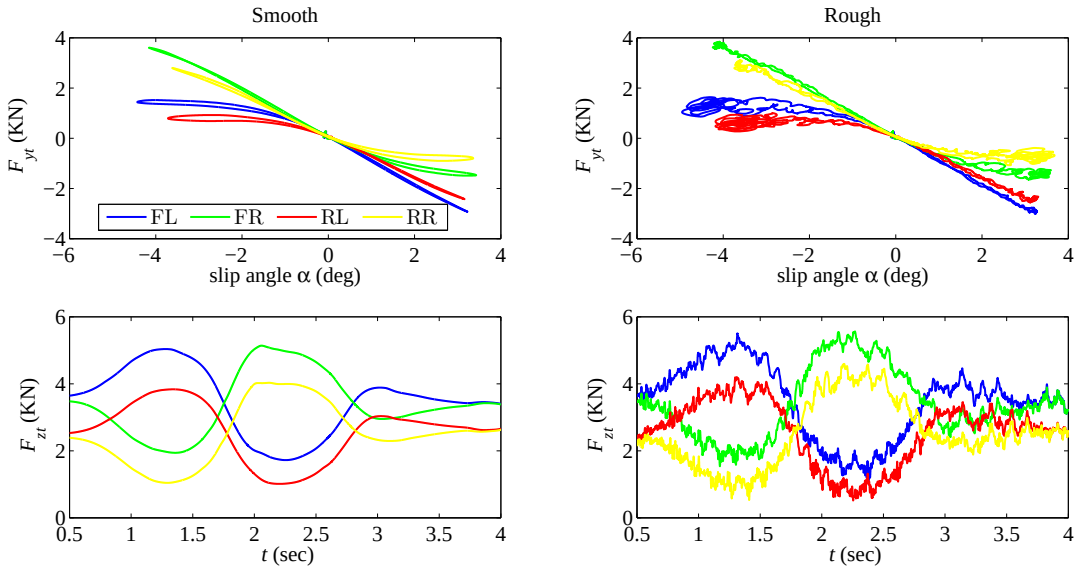

Figure 5.25: Vertical force and lateral force vs slip angle response for single lane change maneuver on smooth and bad asphalt without cleat

of the tire. This causes the excitation of lateral belt vibrations to any changes in road undulations. Figure 5.26 shows the frequency response of lateral and vertical forces on both road surfaces. In case of a flat smooth road surface, no signs of excitation of tire modes are seen but on a bad asphalt road clearly camber and vertical modes of the tire are excited at their respective frequencies. Figure 5.24 also compares the performance of dynamic rigid ring (RR) tire model with the steady state magic formula (MF) tire model. As the transient relaxation effects associated with the steering and tires are neglected, it is observed that the vehicle response with the rigid ring model had a significant delay when compared with the vehicle response using magic formula tire model. The importance of relaxation effects grows at higher slip angles. It is clearly evident from the body roll angle response, which had a strong influence on subjective safety feeling for the driver [136].

It can be concluded that the tire belt vibrations due to short wavelength disturbances have a significant effect on the lateral dynamics of the vehicle just before the saturation of slip angles is reached. This confirms with the previous studies done by Maurice [84] and Pacejka [2]. As the electronic stability controller (ESC) activates only at the physical limits of the vehicle, these effects should be considered in the design of ESC controllers. Figure 5.27 shows the vehicle response during the lane change maneuver. It is observed that the lateral acceleration signal measured at vehicle CG is influenced directly by the excitation of lateral camber mode of the tire. This is seen from lateral acceleration curve with oscillations at higher lateral accelerations. The roll angle of sprung mass of the vehicle on a bad asphalt road surface is increased by 0.5°. The preview based driver controller is applying more steering wheel angle on the bad asphalt road as seen from the steering wheel angle curve. From the time history of yaw rate, on both road profiles the vehicle is stable throughout the maneuver.

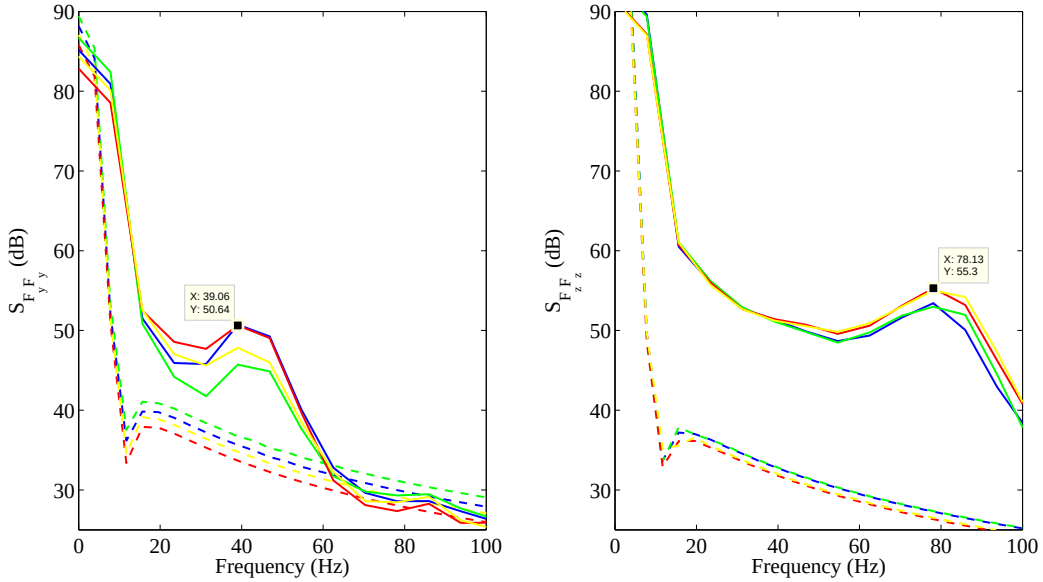

Figure 5.26: Frequency response of lateral and vertical forces response for single lane change maneuver on smooth (dotted lines) and bad asphalt without cleat (solid lines)

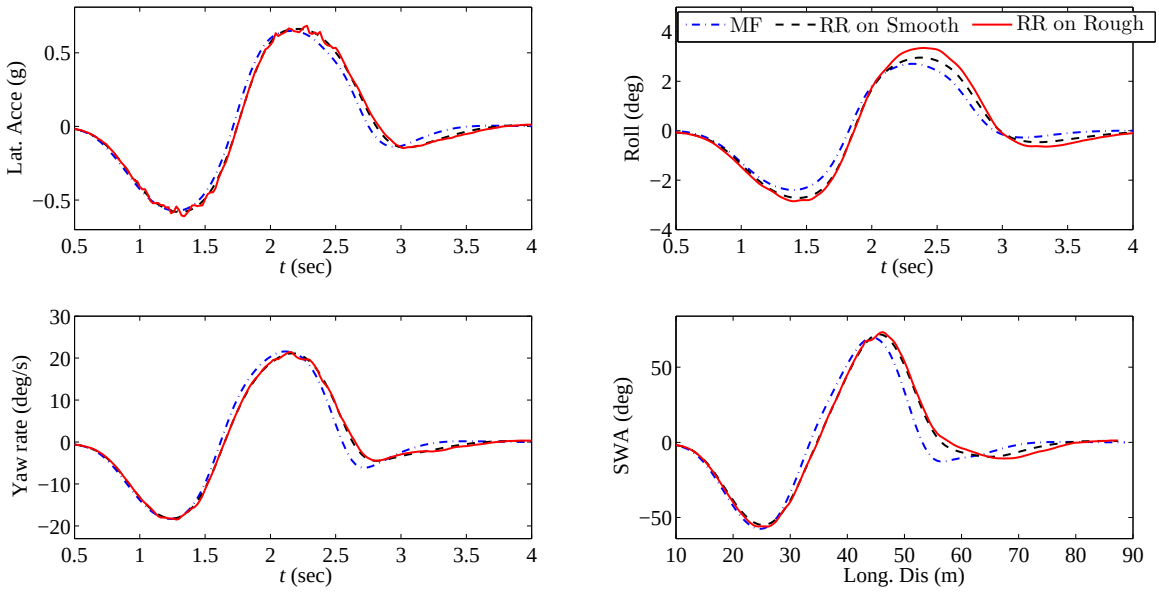

Figure 5.27: Vehicle behavior for single lane change maneuver on smooth and bad asphalt using MF and RR tire models

5.4 Dynamic effects of tire on vehicle handling performance

From the previous simulation case studies, it is know that if the tire is operating under the nonlinear region of side force Vs slip angle curve, then any varying control input or disturbance acting on the tire can excite the belt vibrations. From the point of view of safety, longitudinal deceleration combined with cornering is the most common maneuver during accident avoidance [136]. These maneuvers involves larger longitudinal and lateral forces, and unequal tractive forces on one side of the vehicle. As the tire is operating at the limiting grip, the nonlinear effects of tire has a significant effect on stability of the vehicle. To understand the nonlinear effects excited due to ABS braking, road undulations and steering inputs, two different constant radius maneuvers are performed. The reason for selection of constant radius maneuver is, when the vehicle is undergoing a constant radius turn the tractive power available at the ground is mostly utilized for generating lateral forces. So any disturbance, in longitudinal (braking) or lateral (steering) or vertical (road undulations) direction, can easily excite lateral dynamics of the tire and directly effect the handling performance of the vehicle.

The aim of this study is to understand the effects of inertial vibrations of the tire on vehicle controllability at the limit. This requires to develop objective handling maneuvers, which are significantly influenced by the inertial vibrations of the tire and also develop respective handling metrics to characterize these effects on vehicle behavior. Two test scenarios of ABS braking in turn on a smooth road and accelerating in a turn on uneven and smooth roads are considered. From constant radius ABS braking in a turn simulation, it is observed that after the initiation of ABS, excitations of lateral inertial vibrations of tire and unequal braking forces on one side of the vehicle increased the understeer gradient of vehicle drastically. From a accelerating in constant radius simulation on a smooth and uneven profiles, it is observed that nonlinear effects of the tire inertial vibrations dominated the transient effects on an

uneven road. This caused a clear degradation of handling performance with an increase in roll gradient, steering wheel angle gradient and understeer gradient of the vehicle.

5.4.1 Effects of ABS braking while cornering

In reality, as most vehicles are inherently understeer, usually the tendency of the drivers is to apply brake or release the gas pedal and then control steering slowly around a turn. To study the behavior of the vehicle while braking in a turn, a standard braking in a constant radius turn (100 m) is selected. In this study, vehicle is assumed to be traveling at 80 kph around the steady turn while full braking input is applied at a simulation time of 3 seconds. For not inducing any excessive disturbance in the form of steering inputs, a preview time of 0.5 seconds and driver delay time of 0.1 seconds were used, representing an experienced driver. From Figures 5.28 and 5.29, it is evident that before the activation of ABS at $t = 3$ sec, all the four tires are operating at steady state condition with constant slip angles and constant lateral and vertical forces. After the activation of ABS, load has transferred from rear tires to front tires and ABS controller is operating at peak value of slip ratio by utilizing maximum available tractive at the respective tires. With the huge increase in longitudinal force after the activation of ABS and to generate the required amount of lateral force to steer around the turn, large increase in the front tire slip angles is observed. The events leading to the increase in slip angles can be explained as follows. Due to load transfer in the constant radius turn, available tractive forces at the left and right side of the vehicle are unequal. Therefore, ABS applies unequal braking forces on the left and right side which induces large changes in vehicle yaw rate. This causes the vehicle to severely understeer and thus the increase in the front slip angles. This is clearly seen in the understeer response plot in Figure 5.30. From Figure 5.28, ABS controller is increasing and decreasing the applicable braking torque with a high frequency. As the front tires are operating at the limit due to the application of combined braking and steering inputs, high frequency pressure pulse inputs from ABS are causing disturbance in the yaw motion of the vehicle. These disturbance are

transferred directly to front slip angles, causing similar spikes observed in braking torque inputs. It is also seen from Figure 5.29, that the lateral force response of the front tires is oscillatory, reflecting similar spikes seen in braking torque inputs. From Figure 5.29, excitation of camber mode for front tires is seen. It is clear that, high frequency pressure pulse inputs from ABS has a strong and direct effect on handling performance of the vehicle.

From Figure 5.30, it is seen that before the activation of ABS, all the vehicle variables are

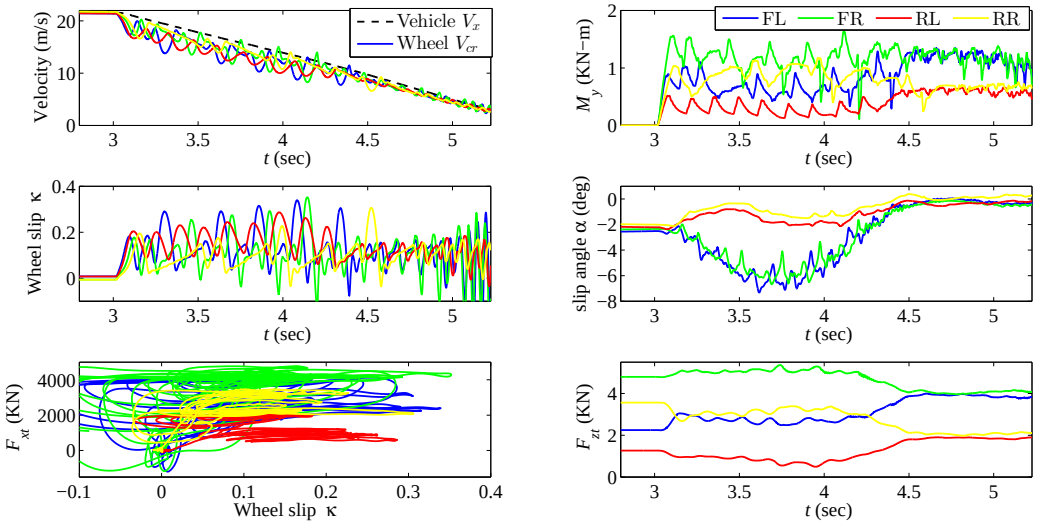

Figure 5.28: Respective forces and slip values for ABS braking in a constant radius turn (100 m) from 80 kph

constant. After ABS activation, understeer coefficient is very high until the vehicle velocity is reduced to zero. To compensate for this, the driver model is increasing the steering wheel angle to keep the vehicle follow the turn, thus pushing the tires towards nonlinear region. It is clear that after activation of ABS, inertial tire belt vibrations result in the degredation of vehicle lateral stability.

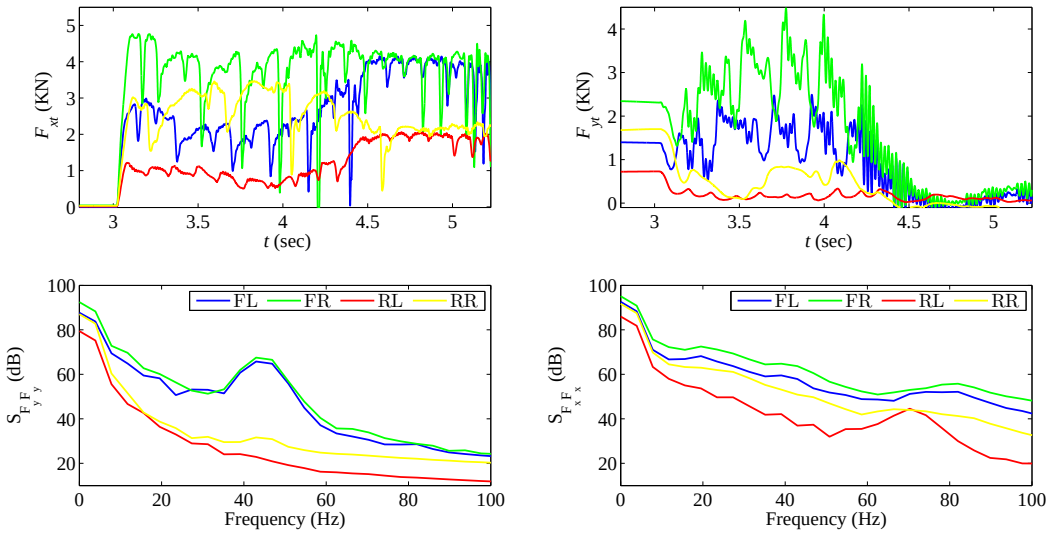

Figure 5.29: Time and frequency response of longitudinal and lateral forces for ABS braking in a constant radius maneuver

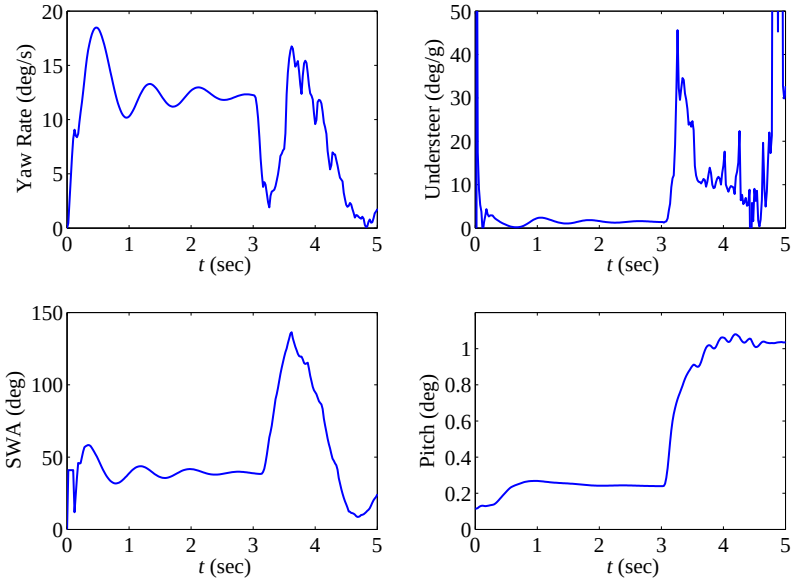

Figure 5.30: Vehicle response during ABS braking in a constant radius maneuver

5.4.2 Effect of road undulations accelerating while cornering

Due to the changes in the peak value of friction, the force and moment characteristics of tires are highly dependent on road surface conditions. Cornering stiffness of tire is a

critical parameter in accessing the handling performance of the vehicle which is dependent on tire construction. From the experimental studies on different rough road surfaces, van der Jagt [137] concluded that high frequency load variations from road undulations can excite higher modes of the tire and these modes can influence tire cornering stiffness. In this case study, effects of road undulations on the handling performance of the vehicle is studied. For this case, linearly accelerating maneuver from 20 - 80 kph in 8 sec is simulated around a constant radius turn of 100 m. The maneuver is simulated on a smooth road with no undulations and on a bad asphalt road surface, as shown in Figure 5.2. A preview time of 0.5 seconds and driver delay time of 0.1 seconds is selected for the driver model.

Figure 5.31 shows the time history of the lateral and vertical force variations on the smooth and bad asphalt road profiles. Figure 5.33 shows the lateral forces vs slip angles curves for both cases. It is evident that vehicle behavior on smooth road is dominated by steady state and transient characteristics of the tire. It is observed that, before $t = 4$ sec, when tire slip angle is in the linear region, behavior on smooth and bad asphalt road is nearly the same. As seen in section 5.3.3, in this linear region, the relaxation effects of the tire and the damping in the steering system dampen the tire inertial belt vibrations. As the vehicle is accelerating in a turn with increasing velocity, tire forces are driven into the nonlinear region, specially for inside front tire, due to the decrease in vertical load and increase in the driving torque. At the higher slip angles with the increasing steering wheel angle, the tire relaxation effects are reduced and the dominance of the tire inertial belt vibrations grows. Therefore, any disturbances in the form of road undulations can excite the lateral inertial belt modes of the tires. After $t = 4$ sec, on bad asphalt road, the oscillations in the lateral force response is increasing and more loops in the force vs slip angle curves are seen. From Figure 5.32, it can be seen that these dynamic effects cause the difference in front slip angles to increase and the vehicle to be more understeer on the rough road. Figure 5.33 shows the frequency response of lateral and vertical forces on both road surfaces. In case of a flat smooth road surface, no signs of excitation of tire modes are seen but on the bad asphalt road, camber and vertical modes of the tire are excited. To study these dynamic

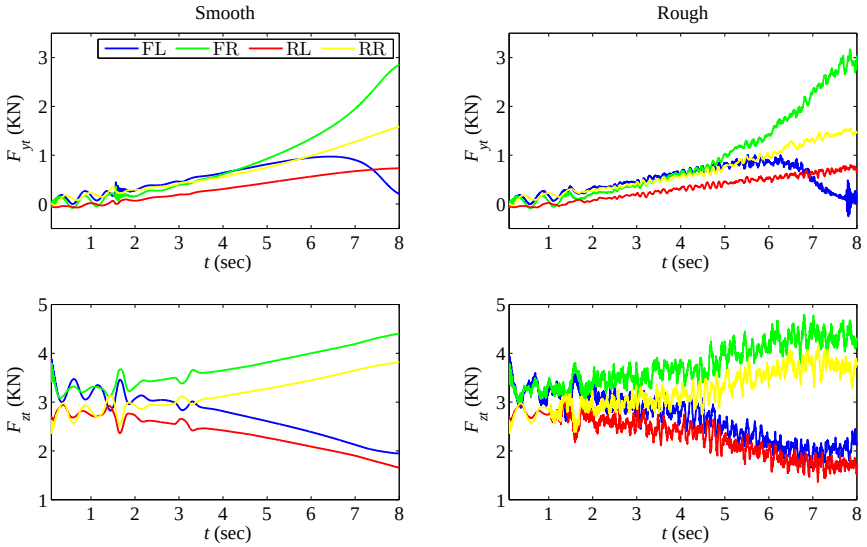

Figure 5.31: Lateral and vertical forces response for accelerating in a constant radius turn on smooth and bad asphalt road profiles

effects on vehicle performance, the following vehicle variable gradients are selected. 1) Roll angle versus lateral acceleration 2) Steering wheel angle versus lateral acceleration and 3) Understeer gradient versus longitudinal distance. From the Figure 5.34, as the vehicle is accelerating around a turn, maximum lateral acceleration of vehicle is reached at 0.4 g. Therefore, the nonlinear dynamics of the vehicle is predominate in between the region of 0.2 - 0.35 g of lateral acceleration. The slope of roll angle, steering wheel angle and understeer coefficient curves are considered in this region. From the Figure 5.34, it is observed that the dominance of dynamic effects of tire after 0.2 g are eventually causing gradient values to increase and deviating the vehicle from the behavior on a smooth road. From the understeer gradient curve in Figure 5.34, the understeer of the vehicle is increasing continuously with the increasing lateral acceleration on rough road and the driver is also increasing the steering angle to compensate for it. The two important criteria for a good handling performance of the vehicle are maximum lateral acceleration and the other is no irregularities or sharp changes in gradient values [136]. It is evident that on the bad asphalt road, the maximum lateral acceleration is decreased and the gradient values also changed drastically. From this

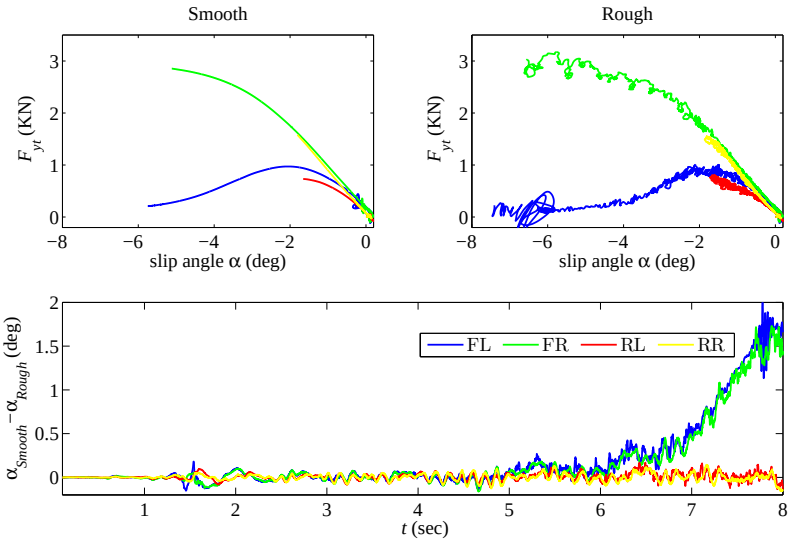

Figure 5.32: Lateral force versus slip angle curves and difference in slip angles on smooth and bad asphalt road profiles for accelerating in a constant radius maneuver

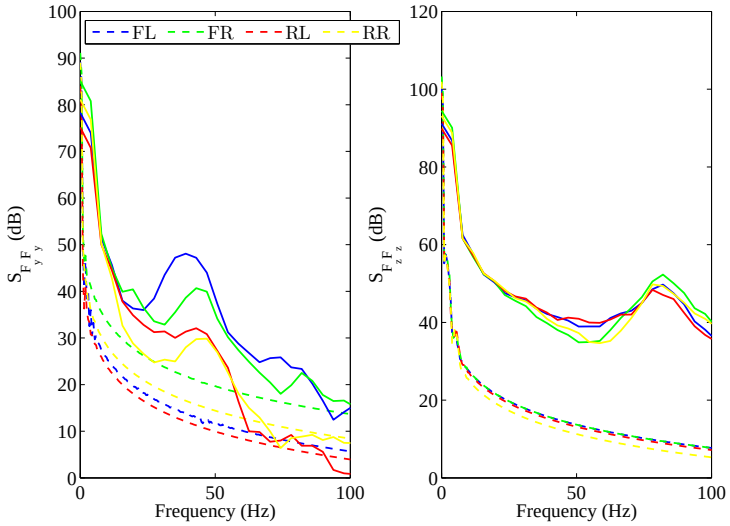

Figure 5.33: Frequency response of lateral and vertical forces response on bad asphalt road (solid lines) and smooth road (dotted lines) for accelerating in a constant radius maneuver

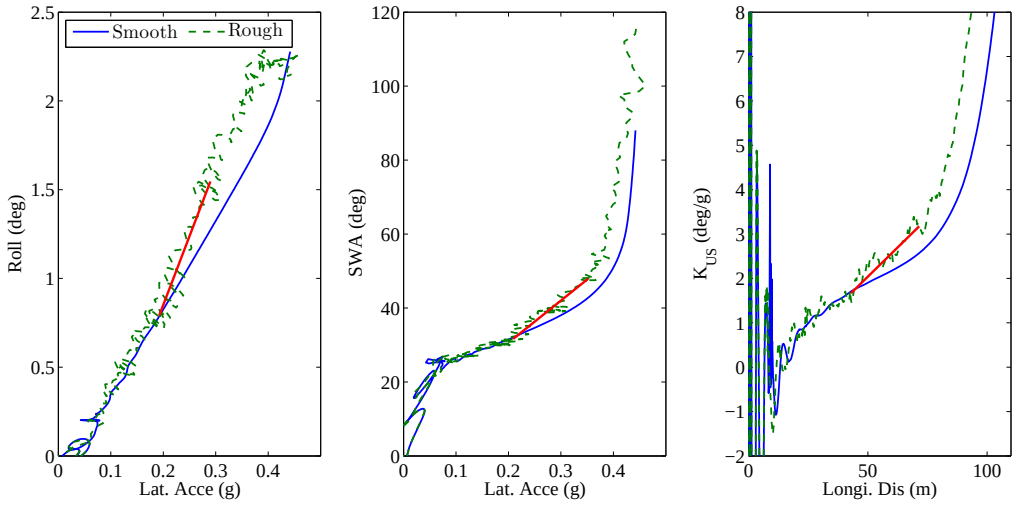

Figure 5.34: Variations in vehicle performance on bad asphalt road and smooth road for accelerating in a constant radius maneuver

case study, it can be concluded that dynamic effects due to road undulations can significantly degrade the handling performance of the vehicle.

5.5 Conclusion

The integration of CarSim with the tire model developed in Matalb/Simulink was presented. Braking and handling performances of the tire-vehicle combination were evaluated. The influence of high frequency ABS pressure pulses and steering wheel angle inputs on tire inertial belt vibrations under short wavelength road profiles were studied. The braking performance on the bad asphalt road surface with and without an artificially added one centimeter cleat were studied. The results showed that the high frequency short wavelength road profile leads to large variations in load and longitudinal slip of the tire, thus reducing the braking performance and causing an increase in braking distance of 1 m. The braking performance on split-μ surface was evaluated to see the effect of ABS cycling on the slippage of the tire and the adaptability of ABS algorithm. Handling performance was evaluated under various

conditions. From the simulation of successive step steering input, the increasing influence of tire belt vibrations at higher slip angles were observed due to sudden steering wheel inputs. From the simulation of step steering input on the bad asphalt road surface with an added cleat and on the flat smooth road surface, it was observed that the lateral performance of the tire at higher slip angles is strongly influenced by the vertical load variations. A single lane change maneuver was simulated on the smooth and bad asphalt road surfaces, demonstrating the strong influence of tire belt vibrations on lateral performance of the vehicle. By comparing the vehicle response using MF and RR tire models, it is shown that MF tire is unable to compensate for transient based relaxation effects of the tire which had a significant influenced at the higher slip angles. Finally, the effects of inertial vibrations of the tire on vehicle controllability at the limit is studied under two operating conditions: ABS braking and accelerating in a turn on a bad asphalt road surface. Simulation results showed that during cornering, if the tire is operating under the nonlinear region of side force versus slip angle curve, disturbance from high frequency ABS pressure pulse inputs or vertical vibrations from uneven road profiles can excited the lateral inertial belt modes of the tire, thus severely degrading the handling performance of the vehicle.

From literature studies [14], [15],[16], [17] and [79], the following have significant effects on the performance of the tire-vehicle system and should be considered in the design of vehicle stability controllers for complex crash avoidance maneuvers:

- The fluctuations in the longitudinal force and wheel angular velocity due to ABS torque inputs
- Short wavelength road profiles
- The lateral force variations due to vertical load or steering oscillations.
- The interaction of lateral and longitudinal force variations under the influence of ABS torque inputs

Chapter 6

Suspension Controller

In this chapter, a novel double damper suspension is introduced to show that a simple design modification of suspension can further improve the performance of the semiactive suspension. A single damper in usual suspension is replaced with two separate dampers in series as shown in Figures 6.3 and 6.4. The added advantage is clearly increase in number of controllable dampers, so during jounce or rebound, the respective damper associated with the sprung mass resort to minimum damping without effecting road holding capability of unsprung mass or unsprung mass resort to minimum damping without effecting vibration isolation of the sprung mass. The goal of this study is two fold, one is to demonstrate the applicability of dynamic tire model in development of suspension controllers and the other is to prove the feasibly of novel double damper based semi-active suspension design. The simulation results demonstrated that the novel semi-active suspension system can emulate as active suspension without bottoming of suspension or deterioration of road holding properties. Thus this approach of ride control based on double damper can significantly improve the ride performance of the vehicle at the reduced power consumption, cost, and complexity with more reliability.

In this chapter, as the study focuses on the control of vertical vibration of the vehicle, influence of lateral dynamics of tire are not considered. A rigid ring tire model with only

longitudinal, vertical and rotational DOFs (In plane) are considered. A Lyapunov based adaptive ride control algorithm using a quarter car vehicle model with single damper and double damper suspension is developed. The advantage of this method is computational simplicity due to effective exploitation of system dynamics. The parameter adaptation laws are derived based on the system dynamics and are selected to be the sprung mass and unsprung mass. For evaluating the ride comfort of human body, RMS acceleration of sprung mass vertical, roll and pitch motions are used as ride performance metrics. An ideal skyhook-groundhook 2 DOF suspension is used as the reference model. From the past studies, skyhook model is considered as optimal control policy for vibration control of 1 DOF mass-spring-damper system with base excitation [138]. A groundhook model is considered as optimal control policy for the control of wheel hopping to increase the road holding capability [139]. As the requirement for the ride controller is to achieve reduced sprung acceleration without deteriorating road holding capacity, a combination of skyhook and groundhook model is used as reference model in this research. The vehicle model consists of a sprung mass with vertical, roll and pitch DOFs, connected with four unsprung masses at four corner of sprung mass through an independent suspensions in both X and Z directions. As mentioned earlier, both the longitudinal and vertical dynamics of the tire plays a crucial role for perceived harshness due to short wavelength road profiles.The vehicle model consists of a sprung mass with vertical, roll and pitch DOFs, connected with four unsprung masses at the four corners of sprung mass through independent suspensions in both X and Z directions. As mentioned earlier, both the longitudinal and vertical dynamics of the tire play a crucial role in perceived harshness due to short wavelength road profiles. This vehicle model with dynamic tire model is used for evaluating the ride performance of no control, fully active control of single damper suspension and semiactive control of double damper suspension. For semi-active control of double damper, first the control forces are computed assuming a fully active system and then by imposing constraints, the system is used in semi-active mode.

6.1 Mathematical Modeling

A vehicle model is considered with variables z_b, θ and ψ representing vertical, roll and pitch motions of the sprung mass. The variables z_1, z_2, z_3, z_4 representing the vertical motion of respective unsprung masses m_1, m_2, m_3, m_4, as shown in Figure 6.1. Figures 6.2 and 6.3 represent the quarter of full vehicle considered in Figure 6.1. As mentioned earlier, the longitudinal force variations at the axle are caused due to uneven profiles, so an independent suspension representing compliance in longitudinal direction X (not shown in Figure 6.1) is also considered. Figures 6.2 and 6.3 represent the active and double damper based semi-active controllers, independently controlling at the four wheels of the full vehicle as shown in Figure 6.1. The vertical stiffness and damping of the suspension are represented by the springs K^z_{fl}, K^z_{fr}, K^z_{rl} and K^z_{rr} and dampers C^z_{fl}, C^z_{fr}, C^z_{rl} and C^z_{rr}. The longitudinal stiffness and damping of the suspension are represented by the springs K^x_{fl}, K^x_{fr}, K^x_{rr} and K^x_{rr} and dampers C^x_{fl}, C^x_{fr}, C^x_{rl} and C^x_{rr}. The inputs to the vehicle model are the reaction forces from the dynamic tire model at the axle and controller forces inputs F_1, F_2, F_3, F_4, F_5, F_6, F_7 and F_8 respectively. The outputs are the axle motions which serve as inputs to the tire model. The distance from the respective front and rear axles to CG are given by constants a and b. t represents the track width of the front or rear axle. The equations of motion of vehicle model is given by

$$
\begin{aligned}
m_b\ddot{z}_b &= C^z_{fl}(\dot{z}_1-\dot{z}_5)+C^z_{fr}(\dot{z}_2-\dot{z}_6)+C^z_{rl}(\dot{z}_3-\dot{z}_7)+C^z_{rr}(\dot{z}_4-\dot{z}_8)\\
&+ K^z_{fl}(z_1-z_5)+K^z_{fr}(z_2-z_6)+K^z_{rl}(z_3-z_7)+K^z_{rr}(z_4-z_8)+F_1+F_3+F_5+F_7-m_bg\\
I_p\ddot{\psi} &= b\left[C^z_{rl}(\dot{z}_3-\dot{z}_7)+C^z_{fr}(\dot{z}_4-\dot{z}_8)+K^z_{rl}(z_3-z_7)+K^z_{rr}(z_4-z_8)+F_3+F_4\right]\\
&- a\left[C^z_{fl}(\dot{z}_1-\dot{z}_5)+C^z_{fr}(\dot{z}_2-\dot{z}_6)+K^z_{fl}(z_1-z_5)+K^z_{fr}(z_2-z_6)+F_1+F_2\right]\\
I_r\ddot{\theta} &= t/2\left[C^z_{fr}(\dot{z}_2-\dot{z}_6)+C^z_{fl}(\dot{z}_1-\dot{z}_5)+K^z_{fr}(z_6-z_2)+K^z_{fl}(z_1-z_5)-F_2+F_1\right]\\
&+ t/2\left[C^z_{rr}(\dot{z}_8-\dot{z}_4)+C^z_{rl}(\dot{z}_3-\dot{z}_7)+K^z_{rl}(z_3-z_7)+K^z_{rr}(z_8-z_4)+F_3-F_4\right] \qquad (6.1)
\end{aligned}
$$

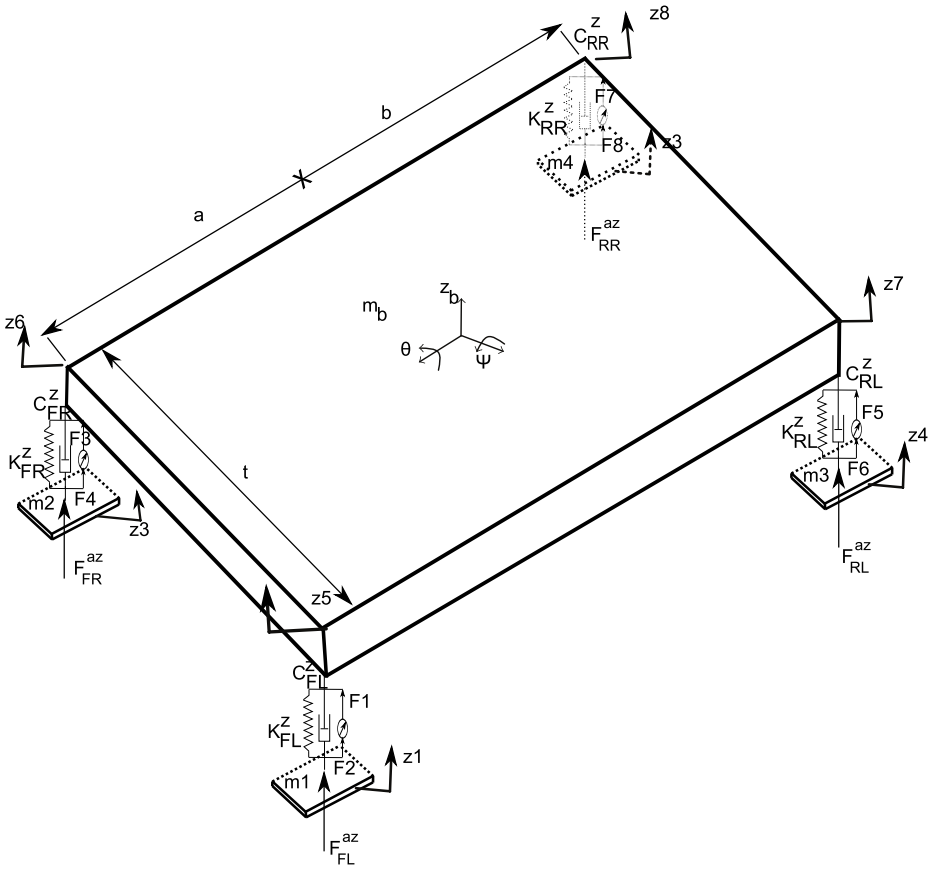

Figure 6.1: Schematic diagram of vehicle model used for ride performance evaluation

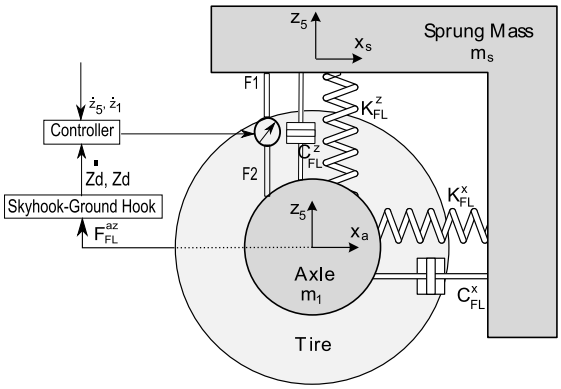

Figure 6.2: Full active controller at front left side of vehicle

$$
\begin{aligned}
m_1\ddot{z}_1 &= C^z_{fl}(\dot{z}_5 - \dot{z}_1) + K^z_{fl}(z_5 - z_1) + F^{az}_{fl} - m_1 * g + F_5 \\
m_2\ddot{z}_2 &= C^z_{fr}(\dot{z}_6 - \dot{z}_2) + K^z_{fr}(z_6 - z_2) + F^{az}_{fr} - m_2 * g + F_6 \\
m_3\ddot{z}_3 &= C^z_{rl}(\dot{z}_7 - \dot{z}_3) + K^z_{rl}(z_7 - z_3) + F^{az}_{rl} - m_3 * g + F_7 \\
m_4\ddot{z}_4 &= C^z_{rr}(\dot{z}_8 - \dot{z}_4) + K^z_{rl}(z_8 - z_4) + F^{az}_{rr} - m_4 * g + F_8
\end{aligned} \tag{6.2}
$$

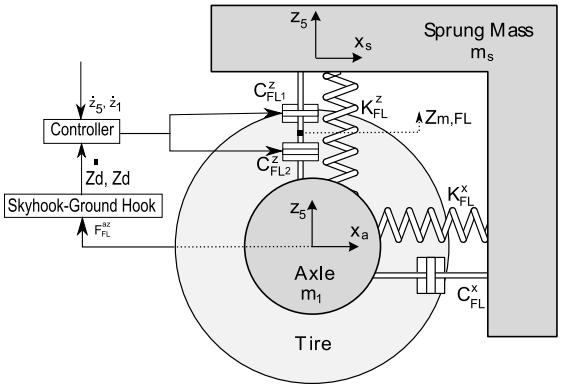

Figure 6.3: Double damper based semi-active controller at front left side of vehicle

For small values of θ and ψ , the displacement equations of four end point with sprung mass are

$$\begin{aligned} z_5 &= z_b + \frac{t}{2}\theta - a\psi \\ z_6 &= z_b - \frac{t}{2}\theta - a\psi \\ z_7 &= z_b + \frac{t}{2}\theta + b\psi \\ z_8 &= z_b - \frac{t}{2}\theta - b\psi \end{aligned} \tag{6.3}$$

As the longitudinal suspension at four wheels of vehicle are independent of each other and are not controlled, only equation of motion for front left longitudinal suspension are given to avoid the repetition of equations.

$$\begin{aligned} m_1\ddot{x}_1 &= C^x_{fl}(\dot{x}_s - \dot{x}_1) + K^x_{fl}(x_s - x_1) \\ \frac{m_b}{4}\ddot{x}_s &= C^x_{fl}(\dot{x}_1 - \dot{x}_s) + K^x_{fl}(x_1 - x_s) \end{aligned} \tag{6.4}$$

6.2 Control Development

The full active and semi-active suspension controllers are developed using a quarter car model. It is implemented as an independent controller at respective corners of the vehicle for minimizing the vertical acceleration at each corner (z_5, z_6, z_7, z_8). In this section, all

the equations are based on quarter car model as shown in Figure 6.4 representing front left corner of the vehicle.

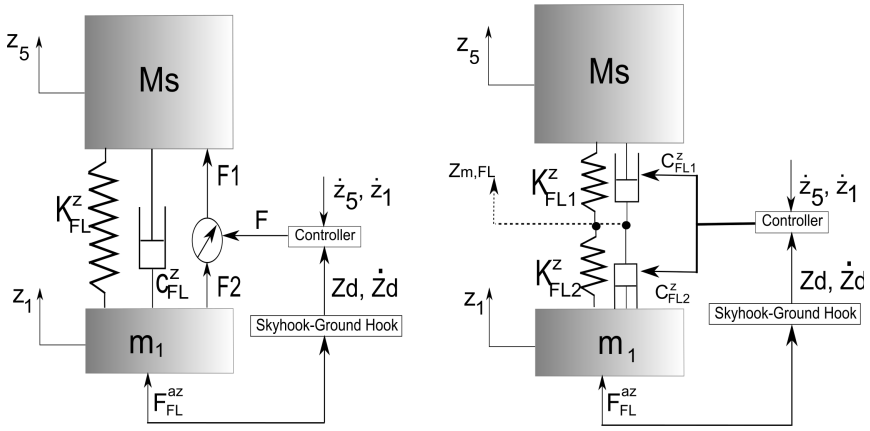

Figure 6.4: Schematic diagram of single and double damper quarter car with active and semi-active controller and reference model

6.2.1 Quarter Car Model with Single Damper

The equations of motion of sprung (z_5) and unsprung masses (z_1) are given in state space form as

$$\dot{Z} + \begin{bmatrix} 0 & -1 & 0 & 0 \\ \frac{K^z_{fl}}{M_s} & \frac{C^z_{fl}}{M_s} & -\frac{K^z_{fl}}{M_s} & -\frac{C^z_{fl}}{M_s} \\ 0 & 0 & 0 & -1 \\ -\frac{K^z_{fl}}{m_1} & -\frac{C^z_{fl}}{m_1} & \frac{K^z_{fl}}{m_1} & \frac{C^z_{fl}}{m_1} \end{bmatrix} Z + \begin{bmatrix} 0 \\ g \\ 0 \\ g - \frac{F^{az}_{fl}}{m_1} \end{bmatrix} = F \tag{6.5}$$

where $Z = [z_5 \ \dot{z}_5 \ z_1 \ \dot{z}_1]^T$, $F = [0 \ F_1 \ 0 \ F_2]^T$ and $M_s = \dfrac{m_b}{4}$.

6.2.2 Quarter Car Model with Double Damper

As shown in Figure 6.4, the equations of motion of double damper constitutes of additional displacement of point in between two dampers (z_m) other than sprung (z_5) and unsprung

mass (z_1).

$$\dot{z}_{m,fl}(C^z_{fl1} + C^z_{fl2}) + z_{m,fl}(K^z_{fl1} + K^z_{fl2}) = C^z_{fl1}\dot{z}_5 + K^z_{fl1}z_5 + C^z_{fl2}\dot{z}_1 + K^z_{fl2}z_1 \tag{6.6}$$

Solving for (z_m) by equating reaction forces in between parallel dampers, the equations of motion are given as

$$\dot{Z} + \begin{bmatrix} 0 & -1 & 0 & 0 \\ \frac{K^z_{fl1}}{M_s} & \frac{C^z_{fl1}}{M_s} & 0 & 0 \\ 0 & 0 & 0 & -1 \\ 0 & 0 & \frac{K^z_{fl2}}{m_1} & \frac{C^z_{fl2}}{m_1} \end{bmatrix} Z + \begin{bmatrix} 0 \\ g - \frac{C^z_{fl1}}{M_s}\dot{z}_m - \frac{K^z_{fl1}}{M_s}z_m \\ 0 \\ g - \frac{C^z_{fl2}}{m_1}\dot{z}_m - \frac{K^z_{fl2}}{m_1}z_m - \frac{F^{az}_{fl}}{m_1} \end{bmatrix} = F \tag{6.7}$$

where C^z_{fl1} and C^z_{fl2} are damping coefficients of two dampers in parallel. K^z_{fl1} and K^z_{fl2} are stiffness of upper part and lower part of suspension spring, here both are assumed equal to $2K^z_{fl1}$ so that equivalent stiffness is same as single damper model.

6.2.3 Skyhook-Groundhook Reference Model

As shown in Figure 6.5, a 2 DOF skyhook and groundhook reference model is used to obtain desired position and velocities for the control algorithm to follow. C_{sky} and C_G are selected appropriately to guarantee less vibration of sprung mass and less hopping of unsprung mass. These values should be selected around actual suspension parameters, so that the desired values are within physical limits. The equation of motion of desired position and velocities are given by

$$\dot{Z}^d + \begin{bmatrix} 0 & -1 & 0 & 0 \\ \frac{K^z_{fl}}{M_s} & \frac{C_{sky}}{M_s} & -\frac{K^z_{fl}}{M_s} & -0 \\ 0 & 0 & 0 & -1 \\ -\frac{K^z_{fl}}{m_1} & 0 & \frac{K^z_{fl}}{m_1} & \frac{C_G}{m_1} \end{bmatrix} Z^d + \begin{bmatrix} 0 \\ g \\ 0 \\ g - \frac{F^{az}_{fl}}{m_1} \end{bmatrix} = F \tag{6.8}$$

From the above equations, the motion of sprung mass is not affected by groundhook damper and unsprung mass is not affected by skyhook damper due to attachment of each damper

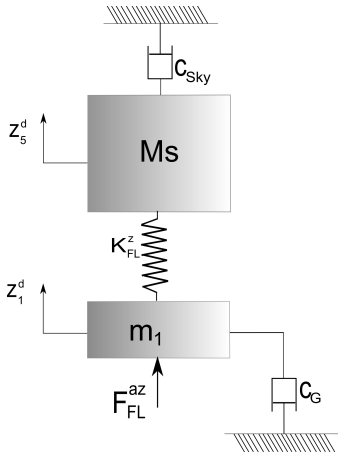

Figure 6.5: Schematic diagram of skyhook-groundhook reference model

to inertial reference frame. This is the main reason for using skyhook-groundhook as an optimal control policy.

6.2.4 Control Algorithm

General Formulation

A new Lyapunov based adaptive control algorithm is developed for ride control. The algorithm consists of a proportional feedback part and a full dynamic feedforword part which estimates unknown model parameters online. The advantage of this method is due to its computational simplicity just like PID, and use of only a velocity sensor for each mass, thus reducing cost and computational power. Due to its simplicity and fast response, it is well suitable for practical implementation on full vehicle model.

The method requires the equations of motion of dynamic system under consideration to be of the form

$$\mathbf{A}\dot{Z} + \mathbf{B}Z + C = F \tag{6.9}$$

Equation 6.5 and 6.7 are represented in above form, where F is the control force output from control algorithm.

To derive the control algorithm and adaption law, a Lyapunov function is considered.

$$V(Z,t) = \frac{1}{2}(\tilde{Z}^T \mathbf{A} \tilde{Z} + \tilde{p}^T \Gamma \tilde{p}) + \int (\tilde{Z}^T \mathbf{B} \tilde{Z}) dt \tag{6.10}$$

where p is an n-dimensional vector containing n unknown model parameters and $\tilde{Z} = Z$ - Z^d is error in states and $\tilde{p} = \hat{p}$ - p is parameter error between estimated $\hat{p}$ and nominal parameters p. From Equation 6.10, Lyapunov function is always positive definite, if the gain matrix is $\mathbf{\Gamma}$ positive definite, here it is selected as positive diagonal matrix If the derivative of $V(x,\ t)$ is negative definite then the system is asymptotically stable. Differentiating $V(x,\ t)$ yields

$$\dot{V}(Z,t) = (\tilde{Z}^T \mathbf{A} \dot{\tilde{Z}} + \tilde{p}^T \Gamma \dot{\tilde{p}}) + (\tilde{Z}^T \mathbf{B} \tilde{Z}) \tag{6.11}$$

The term $\mathbf{A}\dot{\tilde{Z}}$ can be expanded and substituting Equation 6.9 in Equation 6.12, yields the following equation

$$\dot{V}(Z,t) = \tilde{Z}^T[-\mathbf{B}Z^d - C + F - \mathbf{A}\dot{Z}^d] + \tilde{p}^T \Gamma \dot{\tilde{p}}) \tag{6.12}$$

The control law, as mentioned earlier consists of a feedback part and a full dynamics feed-forword part and is defined as

$$F = \hat{A}\dot{Z}^d + \hat{B}Z^d + \hat{C} - K_p \tilde{Z} \tag{6.13}$$

where K_p is a positive definite proportional gain matrix and let $\hat{\mathbf{A}} = \tilde{\mathbf{A}}$ - $\mathbf{A}$, $\hat{\mathbf{B}} = \tilde{\mathbf{B}}$ - $\mathbf{B}$ and $\hat{C} = \tilde{C}$ - C represent error between estimated ($\hat{\mathbf{A}}$, $\hat{\mathbf{B}}$ and $\hat{C}$) and nominal model parameters.

Substituting Equation 6.13 in Equation 6.12 yields

$$\dot{V}(Z,t) = \tilde{Z}^T[\hat{A}\dot{Z}^d + \hat{B}Z^d + \hat{C} - K_p \tilde{Z}] + \tilde{p}^T \Gamma \dot{\tilde{p}}) \tag{6.14}$$

To derive adaption law, let H be defined as

$$H\tilde{p} = \hat{A}\dot{Z}^d + \hat{B}Z^d + \hat{C} \tag{6.15}$$

Substituting Equation 6.15 in Equation 6.14

$$\dot{V}(Z,t) = \tilde{Z}^T[H\tilde{p} - K_p \tilde{Z}] + \tilde{p}^T \Gamma \dot{\tilde{p}} \tag{6.16}$$

The product of $\tilde{Z}^T H\tilde{p}$ is scalar and symmetric, therefore $\tilde{Z}^T H\tilde{p} = \tilde{p}^T H\tilde{x}$ and Equation 6.17 is written as

$$\dot{V}(Z,t) = -\tilde{Z}^T K_p \tilde{Z} + \tilde{p}^T[\Gamma\dot{\tilde{p}} + H^T\tilde{Z}] \tag{6.17}$$

From the above equation, it is clear that, $\dot{V}(Z,t)$ is negative definite if $[\Gamma\dot{\tilde{p}} + H^T\tilde{Z}] = 0$, which is the adaptation law and given as

$$\dot{\hat{p}} = -\Gamma^{-1}H^T\tilde{Z} \tag{6.18}$$

Note $\dot{\hat{p}} = \dot{\tilde{p}}$ because the nominal parameters are always constant. Therefore, the control law in Equation 6.13 and the adaption law in Equation 6.18 are globally asymptotically stable such that

$$\dot{V}(Z,t) = -\tilde{Z}^T K_p \tilde{Z} \leq 0 \tag{6.19}$$

Implementation using Dynamic Models

Next, the parameters to be adapted are selected as sprung mass and unsprung mass, $p = [\frac{1}{M_s}, \frac{1}{m_1}]^T$. The desired displacement and velocities of sprung mass and unsprung mass, are calculated from Equation 6.8. For calculation of control forces in Equation 6.13, the estimated parameters ($\hat{\mathbf{A}}$, $\hat{\mathbf{B}}$ and $\hat{C}$) have to be calculated by solving Equation 6.15 for H and consequently substituting in Equation 6.18 to solve for $\hat{p}$.

Active Control of Single Damper Suspension

For determination of H, dynamic equations of quarter car model for single damper Equation 6.5 are used.

$$\tilde{\mathbf{A}} = 0,\ \tilde{\mathbf{B}} = \begin{bmatrix} 0 & -1 & 0 & 0 \\ K^z_{fl}\tilde{p}_1 & C^z_{fl}\tilde{p}_1 & -K^z_{fl}\tilde{p}_1 & -C^z_{fl}\tilde{p}_1 \\ 0 & 0 & 0 & -1 \\ -K^z_{fl}\tilde{p}_2 & -C^z_{fl}\tilde{p}_2 & K^z_{fl}\tilde{p}_2 & C^z_{fl}\tilde{p}_2 \end{bmatrix}, \tilde{C} = \begin{bmatrix} 0 \\ g \\ 0 \\ g - F^{az}_{fl}\tilde{p}_2 \end{bmatrix} \tag{6.20}$$

where $\tilde{p}_1 = [\frac{1}{\hat{M}_s} - \frac{1}{M_s}]$ and $\tilde{p}_2 = [\frac{1}{\hat{m}_1} - \frac{1}{m_1}]$. Substituting in Equation 6.15 and solving for H

$$H = \begin{bmatrix} 0 & 0 \\ K^z_{fl}(z^d_5 - z^d_1) + C^z_{fl}(\dot{z}^d_5 - \dot{z}^d_1) & 0 \\ 0 & 0 \\ 0 & -K^z_{fl}(z^d_5 - z^d_1) - C^z_{fl}(\dot{z}^d_5 - \dot{z}^d_1) \end{bmatrix} \tag{6.21}$$

Substituting Equation 6.24 in Equation 6.18 to solve for $\hat{p}$ by integration and substituting in Equation 6.13 yields

$$F_1 = \dot{z}^d_5 + K^z_{fl}\hat{p}_1(z^d_5 - z^d_1) + C^z_{fl}\hat{p}_1(\dot{z}^d_5 - \dot{z}^d_1) - K_{p2}(\dot{z}_5 - \dot{z}^d_5) + g \tag{6.22a}$$

$$F_2 = \dot{z}^d_1 - K^z_{fl}\hat{p}_2(z^d_5 - z^d_1) - C^z_{fl}\hat{p}_2(\dot{z}^d_5 - \dot{z}^d_1) - K_{p2}(\dot{z}_1 - \dot{z}^d_1) + g - F^{az}_{fl}\hat{p}_2 \tag{6.22b}$$

where $F = [0\ F_1\ 0\ F_2]^T$.

F_1 and F_2 are the control force outputs from the control algorithm which are applied to fully active suspension actuator as shown in Figure 6.2. From the above equations, the control algorithm uses only the error in velocities of the sprung and unsprung mass. Thus for physical experimentation only velocity sensor for each mass is needed.

semi-active Control of Double Damper Suspension

Solving for H again for double damper case,

$$\tilde{\mathbf{A}} = 0,\ \tilde{\mathbf{B}} = \begin{bmatrix} 0 & -1 & 0 & 0 \\ K^z_{fl1}\tilde{p}_1 & C^z_{fl1}\tilde{p}_1 & -0 & 0 \\ 0 & 0 & 0 & -1 \\ 0 & 0 & K^z_{fl2}\tilde{p}_2 & C^z_{fl2}\tilde{p}_2 \end{bmatrix}, \tilde{C} = \begin{bmatrix} 0 \\ -(C^z_{fl1}\dot{z}_{m,fl} + K^z_{fl1}z_{m,fl})\tilde{p}_1 \\ 0 \\ -(C^z_{fl2}\dot{z}_{m,fl} + K^z_{fl2}z_{m,fl})\tilde{p}_2 + g - F^{az}_{fl}\tilde{p}_2 \end{bmatrix} \tag{6.23}$$

Substituting in Equation 6.15 and following the same procedure used for single damper case yields,

$$H = \begin{bmatrix} 0 & 0 \\ K^z_{fl1}(z^d_5 - z_{m,fl}) + C^z_{fl}(\dot{z}^d_5 - \dot{z}_{m,fl}) & 0 \\ 0 & 0 \\ 0 & -K^z_{fl2}(z_{m,fl} - z^d_1) - C^z_{fl2}(\dot{z}_{m,fl} - \dot{z}^d_1) \end{bmatrix} \tag{6.24}$$

Solving for F_1 and F_2

$$F_1 = \dot{z}^d_5 + (K^z_{fl1} z^d_5 + C^z_{fl1}\dot{z}^d_5 - C^z_{fl1}\dot{z}_{m,fl} - K^z_{fl1} z_{m,fl})\tilde{p}_1 + g - K_{p2}(\dot{z}_5 - \dot{z}^d_5) \tag{6.25a}$$

$$F_2 = \dot{z}^d_1 + (K^z_{fl2} z^d_1 + C^z_{fl2}\dot{z}^d_1 - C^z_{fl2}\dot{z}_{m,fl} - K^z_{fl2} z_{m,fl})\tilde{p}_2 + g + F^{az}_{fl}\hat{p}_2 - K_{p2}(\dot{z}_1 - \dot{z}^d_1) \tag{6.25b}$$

As it being a semi-active suspension, these control forces have to satisfy two criteria, one is the minimum F_{min} and maximum forces F_{max} generated by damper and other is the no energy input, i.e a force in the direction of motion of mass is not applied and the damper can only oppose the motion of the mass.

The control forces are constrained, using simple if logic, in between F_{min} and F_{max} based on physical limitations of the damper.

$$\begin{aligned} F_{1,min} \leq F_i \leq F_{1,max}, \qquad & i = 1, 2 \\ F_{1,min} = C_{fl1,min}(\dot{z}_5 - \dot{z}_{m,fl})\hat{p_1}, \qquad & F_{1,min} = C_{fl1,max}(\dot{z}_5 - \dot{z}_{m,fl})\hat{p_1}) \\ F_{2,min} = C_{fl2,min}(\dot{z}_{m,fl} - \dot{z}_1)\hat{p_2}, \qquad & F_{2,min} = C_{fl2,max}(\dot{z}_{m,fl} - \dot{z}_1)\hat{p_2}) \end{aligned} \tag{6.26}$$

where $C_{fl1,max}$ and $C_{fl1,min}$ are maximum and minimum allowable damping by upper damper. $C_{fl2,max}$ and $C_{fl2,min}$ are maximum and minimum allowable damping by lower damper. Note that the values of C_{fl1} and C_{fl2} in Equation 6.7 have to be non-zero, if not, the open loop system will have poles at the limit of stability and the discretized state space model can go unstable. Therefore, here non-zero positive nominal values are considered. At any time, total maximum and minimum damping available are $C_{fli,max}$ + C_fli and $C_{fli,min}$ + C_fli respectively.

After satisfying constrains in Equation 7.4, for constraining the forces such that no energy is introduced into damper, following clipping method is used, such that if the control force F_1 or F_2 and relative deflection velocity ($\dot{z}_5$ - $\dot{z}_{m,fl}$) or (z_5 - $z_{m,fl}$) are of same sign then the control applies minimum damping force

$$F_1 = \begin{cases} F_1, & \text{if } (\dot{z}_5 - \dot{z}_{m,fl})F_1 \leq 0 \\ F_{1,min}, & \text{if } (\dot{z}_5 - \dot{z}_{m,fl})F_1 > 0 \end{cases}$$
$$F_2 = \begin{cases} F_2, & \text{if } (\dot{z}_1 - \dot{z}_{m,fl})F_2 \leq 0 \\ F_{2,min}, & \text{if } (\dot{z}_1 - \dot{z}_{m,fl})F_2 > 0 \end{cases} \tag{6.27}$$

Control Policy of Skyhook-Groundhook

A 2-state on/off control strategy that switches from high and low damping values is used in order to achieve less sprung mass displacement without deteriorating road holding properties. The control law is based on sprung and unsprung mass velocities and suspension deflection velocity. The damping for both dampers is equal to zero when the sprung or usprung mass velocities and deflection velocity with respect to corresponding masses are in opposite direction [139].

$$C_{sky} = \begin{cases} C_{sky}, & \text{if } (\dot{z}_5 - \dot{z}_1)\dot{z}_5 \geq 0 \\ 0, & \text{if } (\dot{z}_5 - \dot{z}_1)\dot{z}_5 < 0 \end{cases}$$
$$C_G = \begin{cases} C_G, & \text{if } (\dot{z}_1 - \dot{z}_5)\dot{z}_1 \geq 0 \\ 0, & \text{if } (\dot{z}_1 - \dot{z}_5)\dot{z}_1 < 0 \end{cases}$$

6.3 Simulation

The values used for the simulation are $M_s = 300$ Kg, $m_1 = 42.27$ Kg, $K^z_{fl} = 2000$ N/m, $K_1 = K_2 = 2K^z_{fl}$, $C^z_{fl} = 2000$ N/m/s, $C^z_{fl1} = 100$ N/m/s, $C^z_{fl2} = 50$ N/m/s, $C_{fl1,max} = 6500$

N/m/s, $C_{fl2,max}$ = 3500 N/m/s, $C_{fl1,min}$, $C_{fl2,min}$ = 0 N/m/s, C_{sky} = 2000 N/m/s, C_G = 1550 N/m/s. The adaptive gain matrix Γ = diag [8×10^{11} 8×10^{11}] and propositional gain matrix K_p = diag [1 1 1 1]. The initial vertical deflection values (z_5, z_1) are assumed to be equal to initial axle deflection z_a. The initial velocities ($\dot{z}_5$, $\dot{z}_1$) are assumed to be zero.

From the formulations of the control algorithm, the computed control forces are applied to the equations of motion of single and double damper based full vehicle model, given in Equations 6.1 and 6.2. The input road profile used in this study is shown in Figures 6.6 and 6.7. The road profile is of asphalt concrete and it is measured section of smart road at Virginia Tech Transportation Institute with a longitudinal road resolution of 1 cm. Figure 6.6 shows the road profile on left and right sides of the vehicle. An artificially created 1 cm cleat is added to the measured road data at a longitudinal distance of 85 m, to evaluate harshness mitigation of the ride controller. Figure 6.7 represents the elevation power spectral densities of the left and right road profiles sections. ISO 8608 [140] explains the measurement and classifying of road profile data into ISO road classes A through H. With road class A corresponds to a smooth road with a less maximum elevation and H is a very rough road with a high maximum elevation. The elevation PSD values corresponds to the elevation amplitude of the road profile. The road profile considered here comes under smooth road class B as the maximum elevation without the cleat is only 5 mm. The wavelength of road profile is equal to the inverse of the wave number. From Figure 6.7, road profile contains wavelengths from 0.033 m/cycle to 10 m/cycle. The abrupt peak at a wave number of 2 cycle/m is due to the cleat in the road profile. The road profiles considered are short wavelength road profiles, as shown in Figure 6.7 with more frequency content in the power spectral densities in between the wavelengths of 0.1 m/cycle - 0.5 m/cycle (or in between wave numbers of 2 cycle/m - 10 cycle/m). From the previous studies [5], it is observed that the dynamic response of the tire as it deforms around the road profile, can excite both the longitudinal and vertical dynamics of the tire and suspension. Hence for evaluation of ride performance on short wavelength road profiles, the dynamic changes in the contact patch and enveloping of low amplitude sharp elevation changes should be considered. As the developed tire model contains enveloping

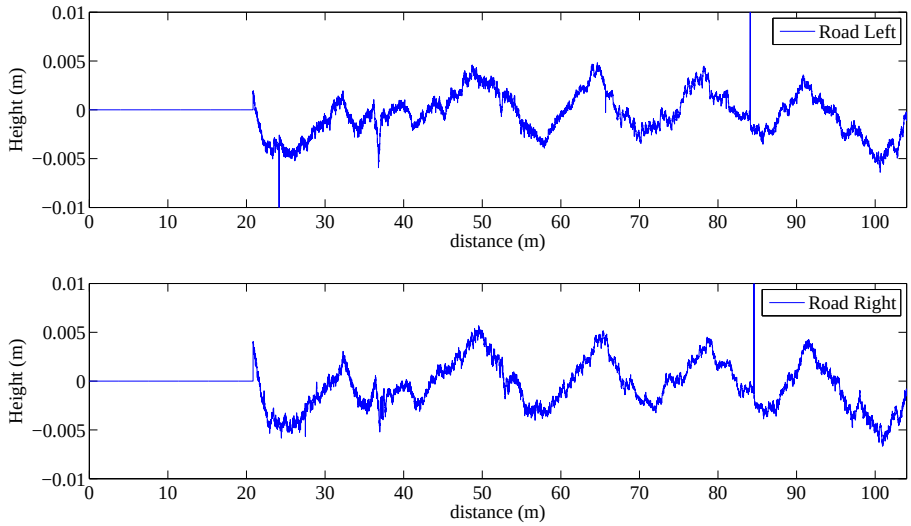

Figure 6.6: Measurement road profile on left and right side of vehicle

model and valid at least up to 75 Hz, it can be used for ride performance evaluations on short wavelength road profiles. The lateral dynamics of tire model are not considered because as shown in Figure 6.7 elevation power spectral densities and corresponding frequency content on left and right road profiles are almost same. So the excitation of high frequency lateral tire mode (camber mode at 47 Hz) is less, when compared with low frequency lateral modes of vehicle (roll mode at 5 - 8 Hz). For characterizing the ride performance, a simple criteria of RMS acceleration of sprung mass vertical, pitch and roll motions at CG are considered. The road holding properties is characterized by maximum axle or unsprung mass displacement z_1. The suspension bottoming is characterized by suspension deflection (z_5 - z_1). The simulations of no control, active controlled single damper and semi-active controlled double damper are performed. The respective RMS accelerations of sprung at different speeds, using input road profile in Figure 6.6, are computed and summarized in Tables 6.1, 6.2 and 6.3. The maximum tire deflection and suspension deflection values are also computed at all four wheels. Tables 6.4 and 6.5 summarizes maximum suspension and axle deflection. For all the three cases, no such abnormal behavior of controlled suspensions from normal suspension is observed. From Tables 6.1, 6.2 and 6.3 the RMS accelerations of active and semi-active

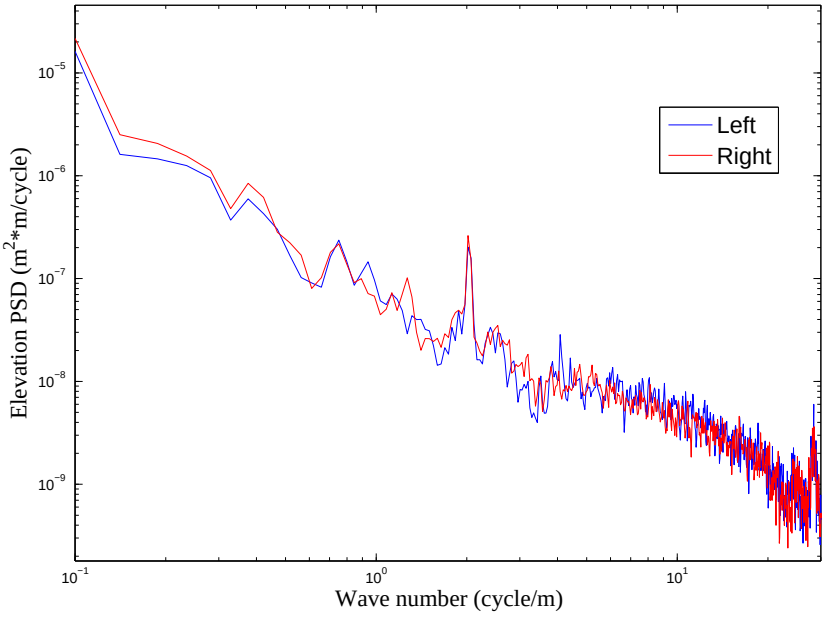

Figure 6.7: Elevation power spectral densities of left and right road profiles

Velocity (kph)	**15**	**30**	**45**	**60**	**75**
Point Contact	0.1816	0.3541	0.4284	0.4743	0.5000
No Control	0.0796	0.1136	0.1411	0.2001	0.2605
Full Active	0.0601	0.0603	0.0888	0.1344	0.1627
semi-active	0.0615	0.0636	0.0911	0.1405	0.1753

Table 6.1: RMS Vertical acceleration of sprung mass (m^2/s) at different velocities (kph)

Velocity (kph)	**15**	**30**	**45**	**60**	**75**
Point Contact	0.1207	0.1858	0.2118	0.2592	0.2870
No Control	0.0554	0.0857	0.1	0.1255	0.1483
Full Active	0.0019	0.0458	0.0602	0.0737	0.0869
semi-active	0.0021	0.0479	0.0607	0.0782	0.0897

Table 6.2: RMS pitch acceleration of sprung mass (rad^2/s) at different velocities (kph)

Velocity (kph)	15	30	45	60	75
Point Contact	0.3265	0.4407	0.5062	0.559	0.5814
No Control	0.1671	0.2555	0.316	0.3302	0.3416
Full Active	0.112	0.0811	0.091	0.0925	0.09
semi-active	0.1206	0.0986	0.1165	0.13	0.1356

Table 6.3: RMS Roll acceleration of sprung mass (rad^2/s) at different velocities (kph)

Velocity (kph)	15	30	45	60	75
Point Contact	4.12	4.34	4.57	4.69	4.69
No Control	2.67	2.71	2.71	2.79	2.77
Full Active	3.01	3.12	3.18	3.5	3.5
semi-active	2.75	2.69	2.69	2.88	2.79

Table 6.4: Maximum suspension deflection (cm) at different velocities (kph)

Velocity (kph)	15	30	45	60	75
Point Contact	5.6	5.55	5.29	5.01	4.95
No Control	2.61	2.51	2.55	2.58	2.6
Full Active	3.03	3.08	3.1	3.14	3.3
Semi Active	2.7	2.51	2.56	2.57	2.57

Table 6.5: Maximum axle deflection (cm) at different velocities (kph)

suspensions are low compared to the no control case. As mentioned earlier, due to the use of the double damper based suspension control, control of damping constants of the two dampers independently, gives the advantage in increasing the performance of the semi-active controller, which is very clearly evident at all speeds. The RMS acceleration values of the fully active case are almost equal to the semi-active case at all the speeds. The roll RMS acceleration for semi-active double damper suspension is a little higher than the active case. This is because the controllers at four wheels are indirectly minimizing roll acceleration of the sprung mass by independently optimizing the RMS accelerations at respective four

wheels. Table 6.4 shows the maximum suspension deflection values and Table 6.5 shows the maximum tire deflection for all the three cases. Although these values are increased in case of active control but are within the acceptable range, with maximum suspension deflection of 3.5 cm and maximum axle deflection of 3.3 cm.

Figures 6.8, 6.9 and 6.10 show the acceleration of the sprung mass at vehicle velocity of 75 kph. The most important outcome is equivalent ride performance in both control cases. Thus semi-active based double damper suspension can emulate as the active suspension. When the front and rear axles of the vehicle rolls over the cleat, oscillations in no control case is observed. This is not observed in both the control cases, controller is effectively dampening these oscillations in vertical, pitch and roll directions. Figures 6.11 and 6.12

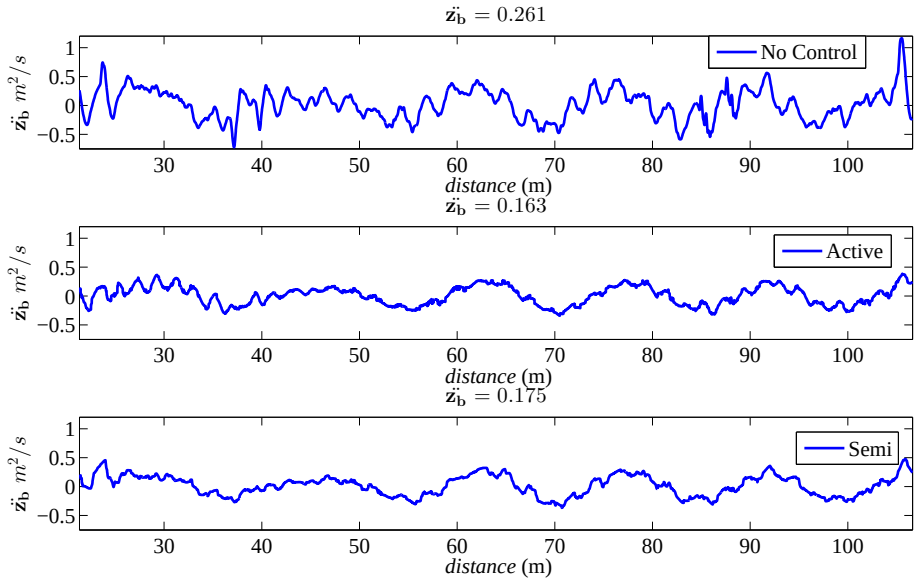

Figure 6.8: Vertical acceleration of sprung mass at 75 kph with no control, active and semi-active control

show the two semi-active damping values for each of the four wheels of the vehicle. All the upper dampers are within the saturation limit of $C_{fl1,max} = 6500$ and lower dampers are within the saturation limit of $C_{fl2,max} = 3500$, as imposed on each damper in Equation 7.4.

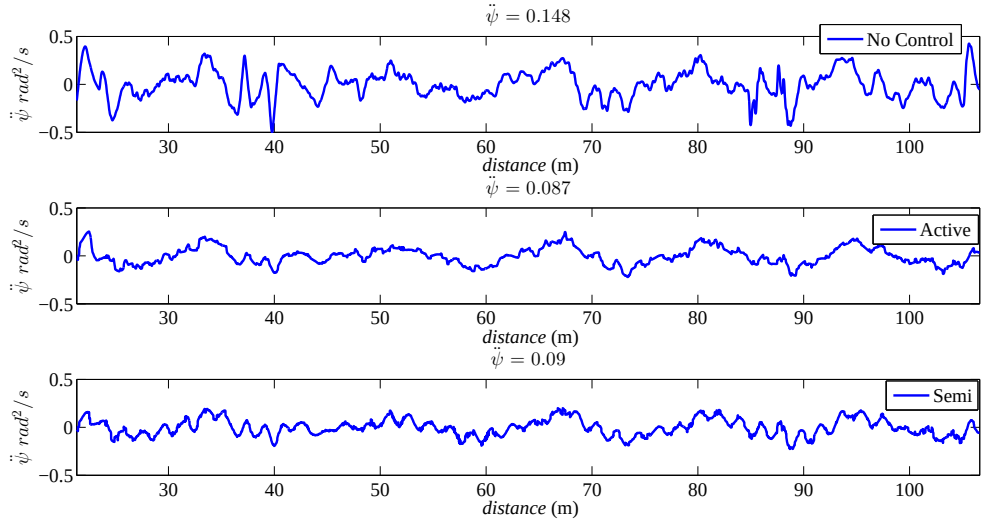

Figure 6.9: Pitch acceleration of sprung mass at 75 kph with no control, active and semi-active control

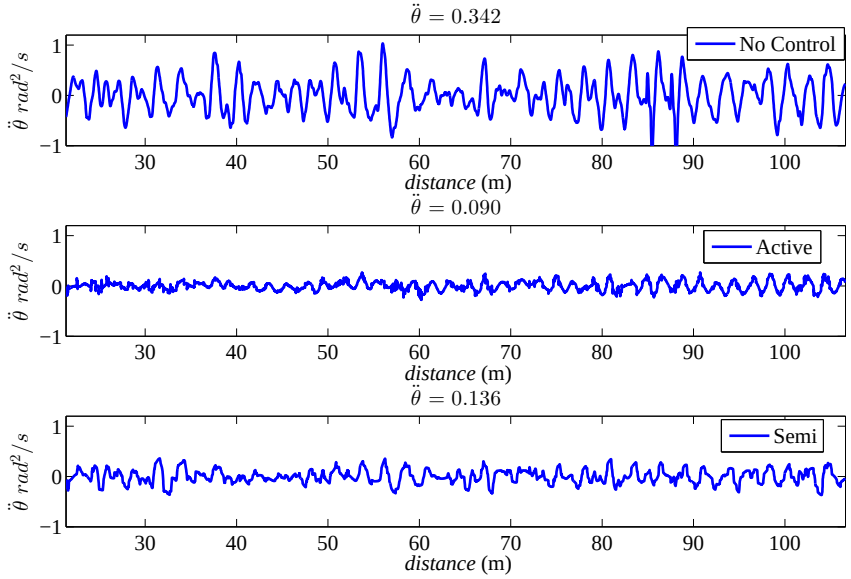

Figure 6.10: Roll acceleration of sprung mass at 75 kph with no control, active and semi-active control

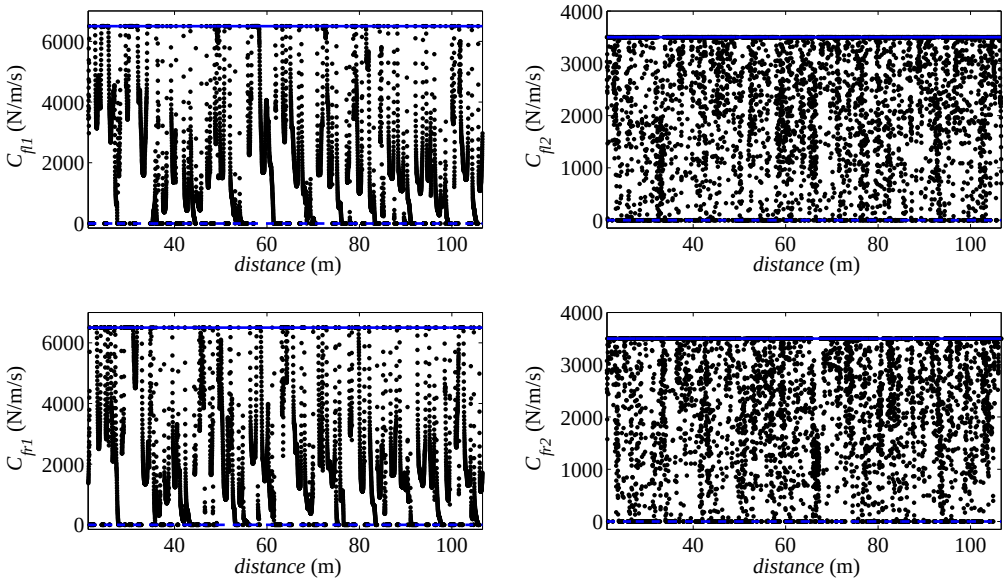

Figure 6.11: Damping coefficients of both front dampers within maximum and minimum limit of the damper at 75 kph

Figures 6.13 and 6.14 show the dissipative constraint on the semi-active dampers based on damper velocity as defined in Equation 6.27. $F_{Up,max}$ and $F_{Up,min}$ correspond to maximum and minimum constrained forces on upper dampers and $F_{Low,max}$ and $F_{Low,min}$ correspond to maximum and minimum constrained forces on lower dampers. One of the important observations is that the lower damper takes more force than the upper damper, which states that the unsprung mass experiences more vertical deflection velocity than sprung mass, thus more vibrations are taken by the lower damper. The saturation limit on upper damper is greater than the lower damper which is also evident from the slope of $F_{Up,max}$ being greater than the $F_{Low,max}$. Apart from the evaluation of ride performance on a normal road surface, effectiveness of the semi-active controller is also evaluated on road profile with 1.5 cm cleats separated at a longitudinal distance of 2.5 m, as shown in Figure 6.15. Figures 6.16 and 6.17 show the vertical and pitch accelerations of the sprung mass. In this case, the roll mode of the vehicle could not be excited due to the equivalent road profile input on left and right tires. Due to the consideration of the enveloping properties of the tires, the

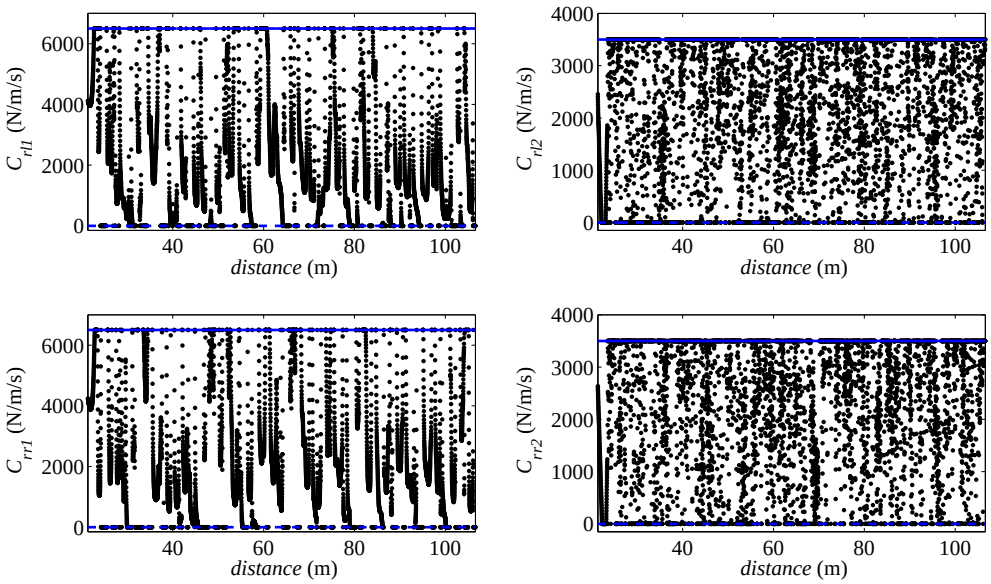

Figure 6.12: Damping coefficients of both rear dampers within maximum and minimum limit of the damper at 75 kph

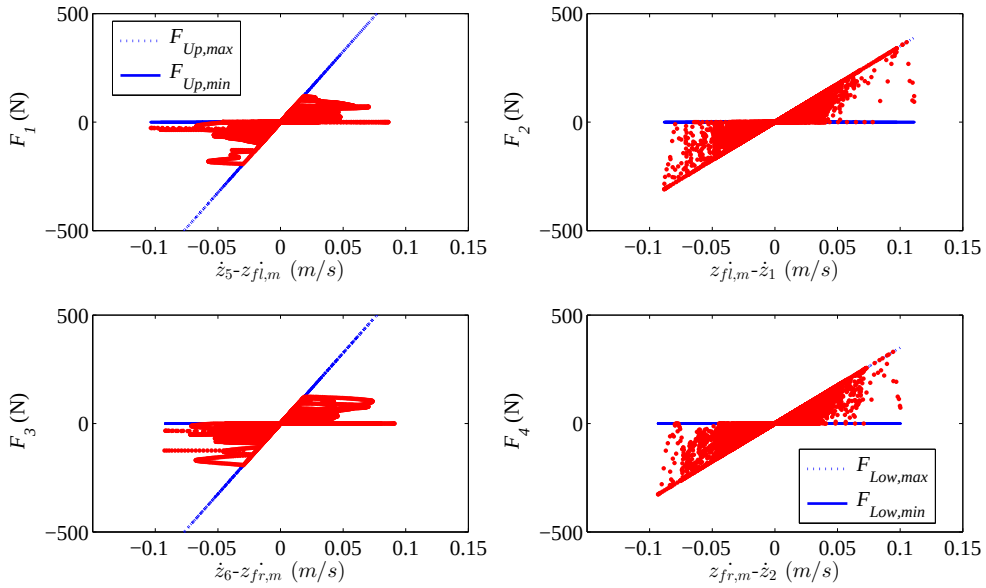

Figure 6.13: Dissipative domain of front semi-active dampers

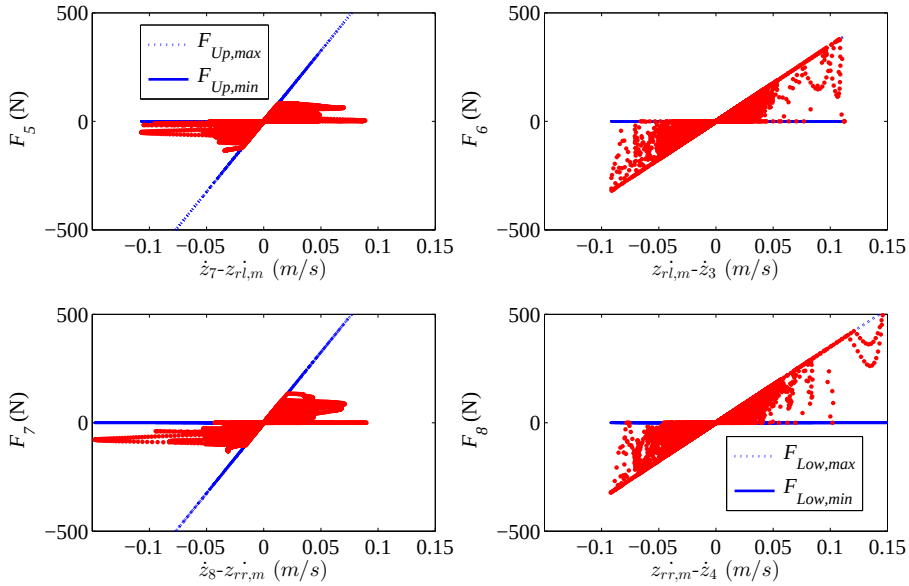

Figure 6.14: Dissipative domain of rear semi-active dampers

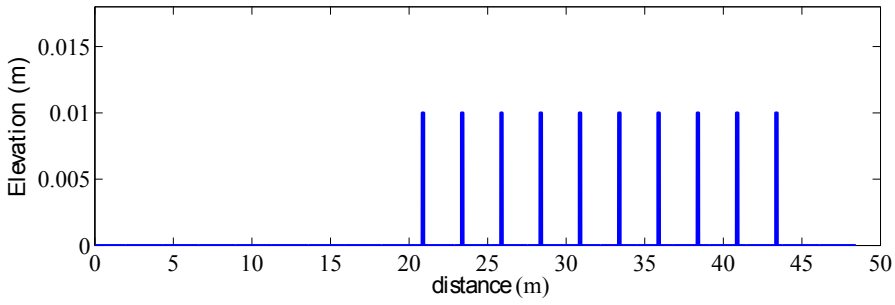

Figure 6.15: Road profile with 1.5 cm cleats at longitudinal distance of 2.5 m

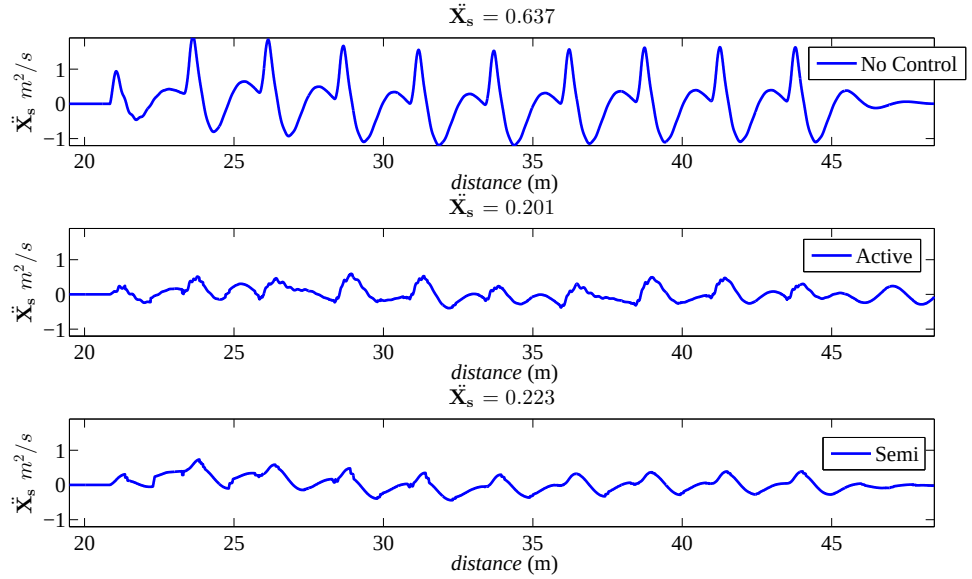

Figure 6.16: Vertical acceleration of sprung mass at 75 kph over road with 1.5 cm cleats

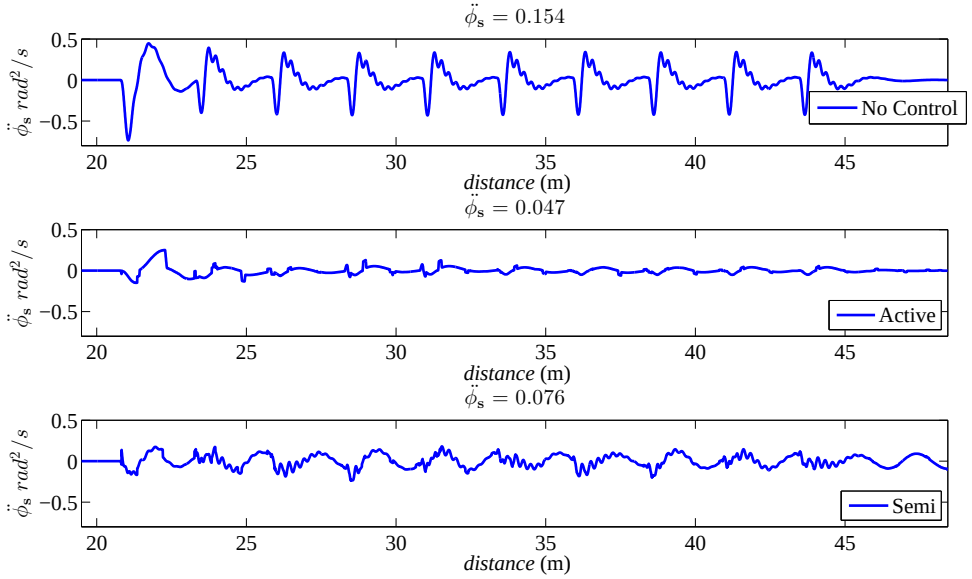

Figure 6.17: Pitch acceleration of sprung mass at 75 kph over road with 1.5 cm cleats

respective accelerations of sprung mass are smoothened around the cleat. From Figure 6.16, the vertical acceleration response of the sprung mass for active and semi-active cases are almost of equivalent response. From Figure 6.17, as the pitch acceleration of sprung mass is controlled indirectly, in case of semi-active control the values are slightly higher than active control case but much improved performance when compared with no control case.

6.4 Conclusion

Integration and application of the dynamic tire model in the development of active suspension controllers is presented. The feasibly of novel double damper based suspension design is demonstrated and its application as semi-active suspension for ride control is discussed. A lyapunov based adaptive controller is developed. The designed controller is used for the full active control of single damper suspension and semi-active control of double damper suspension. The ride performance was evaluated under short wavelength road profiles and road profile with cleats. The simulation results demonstrated that the novel semi-active suspension system can emulate as active suspension without bottoming of suspension or deterioration of road holding properties. Semi-active suspension results are shown to be constrained in saturation and energy limitation of the damper. This approach of ride control based on double damper can be a substituted for full active suspension and shown to significantly improve the ride performance of the vehicle at the reduced power consumption, cost and complexity with more reliability.

Chapter 7

Four Wheel Steering (4 WS) Controller

In this chapter, the potential of a four wheel steering controller in the improvement of lateral transient handling performance near the limits of tire adhesion is explored. When a vehicle is steered, the desired yaw motion to follow a turn is first generated due to the front tires slip angle, while the rear tire slip angles are generated due to the induced yaw motion from front slip angles. The innovative idea of steering the rear wheels simultaneously with the front ones, utilizing the rear tires also in the generation and control of sideslip angle and yaw motion of the vehicle led to the invention of a four wheel steering controller. Four wheel steering controller reduces the delay in generation of cornering forces at the rear tires, thus decreasing the required motion of the vehicle body around the z-axis (yaw motion) and offer better responsiveness during a change in vehicle course [115]. This also causes, the independent control of the vehicle path and sideslip angle.

With the increase in lateral acceleration of the vehicle, vehicle generates different steering responses as the effective cornering stiffness at the front and rear ends of the vehicle are decreased. Steering of rear wheels based on the front steer angle and sideslip angle of the vehicle, offers a quick yaw response at lower lateral acceleration itself. In this study, a

lyapunov based nonlinear 4 WS controller is developed. The controller is integrated with the dynamic tire model (rigid ring) and a simple steady state model (magic formula tire model) and the vehicle response using both models are compared. A simple two degrees of freedom vehicle model is used in the development of the control algorithm. The developed controller and the tire model in Matlab/Simulink is integrated with a nonlinear vehicle model in CarSim. Simulations of double lane change maneuver are performed at different speeds. Simulation results showed that the developed 4 WS control could potentially improve the transient response with reduced yaw rate peaks and increased yaw damping.

7.1 Mathematical Modeling

A 4WS controller is developed based on a 2 DOF bicycle model. The outputs from this model are lateral velocity v and yaw velocity r in response to the applied steering wheel angle δ_f. The equations of motion are given below

$$\begin{bmatrix} m & 0 \\ 0 & I_z \end{bmatrix} \begin{bmatrix} \dot{v} \\ \dot{r} \end{bmatrix} + \begin{bmatrix} \dfrac{C_{\alpha f} + C_{\alpha r}}{u} & mu + \dfrac{aC_{\alpha f} - bC_{\alpha r}}{u} \\ \dfrac{aC_{\alpha f} - bC_{\alpha r}}{u} & \dfrac{a^2 C_{\alpha f} + b^2 C_{\alpha r}}{u} \end{bmatrix} \begin{bmatrix} v \\ r \end{bmatrix} + \begin{bmatrix} -C_{\alpha f}(\delta_f + \delta_{fc}) - C_{\alpha r}\delta_{rc} \\ -aC_{\alpha f}(\delta_f + \delta_{fc}) + bC_{\alpha r}\delta_{rc} \end{bmatrix} = \mathbf{0} \tag{7.1}$$

where $C_{\alpha f}$ and $C_{\alpha r}$ represents effective front and rear cornering stiffnesses, m is the sprung mass of the vehicle, u is the constant longitudinal velocity of the vehicle, a and b represents distance of C.G from front and rear ends, and δ_{fc} and δ_{rc} represent the corrective front and rear steering angles computed using the control law.

The lyapunov method requires the equations of motion of dynamic system under consideration to be of the form

$$\mathbf{A}\dot{Z} + \mathbf{B}Z + C = F \tag{7.2}$$

where

$$\mathbf{A} = \begin{bmatrix} m & 0 \\ 0 & I_z \end{bmatrix},\ \mathbf{B} = \begin{bmatrix} \dfrac{C_{\alpha f} + C_{\alpha r}}{u} & mu + \dfrac{aC_{\alpha f} - bC_{\alpha r}}{u} \\ \dfrac{aC_{\alpha f} - bC_{\alpha r}}{u} & \dfrac{a^2 C_{\alpha f} + b^2 C_{\alpha r}}{u} \end{bmatrix}, C = \begin{bmatrix} -C_{\alpha f}\delta_f \\ -aC_{\alpha f}\delta_f \end{bmatrix}$$

and

$$F = \begin{bmatrix} F_1 \\ F_2 \end{bmatrix} = \begin{bmatrix} C_{\alpha f}\delta_{fc} + C_{\alpha r}\delta_{rc} \\ aC_{\alpha f}\delta_{fc} - bC_{\alpha r}\delta_{rc} \end{bmatrix} \tag{7.3}$$

7.2 Control Development

A Lyapunov based adaptive control law developed in the previous chapter, as explained in section 6.2.4, is utilized for the development of 4WS controller. The parameters to be adapted are selected as front and rear cornering stiffnesses, $p = [C_{\alpha f}, C_{\alpha r}]^T$. The desired lateral velocity v_d is assumed to be the same as actual lateral velocity. The desired yaw rate r_d is derived from the 2 DOF linear model based on the assumption that the vehicle is of understeer type,

$$\begin{aligned} v_d &= v \\ r_d &= \frac{u\delta_f}{L(1 + u^2/u_{char}^2)} \end{aligned} \tag{7.4}$$

where u_{char} represents characteristic speed. It is speed at which steering angle required is twice the ackermann angle. For the calculation of control forces in Equation 6.13, the estimated parameters ($\hat{\mathbf{A}}$, $\hat{\mathbf{B}}$ and $\hat{C}$) have to be calculated by solving Equation 6.15 for H and consequently substituting in Equation 6.18 to solve for $\hat{p}$

For determination of H, dynamic equations of 2 DOF vehicle model in Equation 7.3 are used.

$$\tilde{\mathbf{A}} = 0,\ \tilde{\mathbf{B}} = \frac{1}{u}\begin{bmatrix} \tilde{C}_{\alpha f} + \tilde{C}_{\alpha r} & a\tilde{C}_{\alpha f} - b\tilde{C}_{\alpha r} \\ a\tilde{C}_{\alpha f} - b\tilde{C}_{\alpha r} & a^2\tilde{C}_{\alpha f} + b^2\tilde{C}_{\alpha r} \end{bmatrix}, \tilde{C} = \begin{bmatrix} -\tilde{C}_{\alpha f}\delta_f \\ -a\tilde{C}_{\alpha f}\delta_f \end{bmatrix} \tag{7.5}$$

Solving for H

$$H = \begin{bmatrix} \dfrac{v_d + ar_d}{u} - \delta_f & \dfrac{v_d - br_d}{u} - \delta_r \\ \dfrac{a(v_d + ar_d)}{u} - a\delta_f & \dfrac{-b(v_d - br_d)}{u} + b\delta_r \end{bmatrix} \tag{7.6}$$

Substituting Equation 7.6 in Equation 6.18 to solve for $\hat{p}$ by integration and substituting in

Equation 6.13 yields

$$F_1 = m\dot{v}_d + v_d\frac{\hat{C}_{\alpha_f} + \hat{C}_{\alpha_r}}{u} + r_d(mu\frac{a\hat{C}_{\alpha_f} - b\hat{C}_{\alpha_r}}{u}) - \hat{C}_{\alpha_f}\delta_f - K_{P1}(v - v_d) \tag{7.7a}$$

$$F_2 = I_z\dot{r}_d + v_d\frac{a\hat{C}_{\alpha_f} - b\hat{C}_{\alpha_r}}{u} + r_d\frac{a^2\hat{C}_{\alpha_f} + b^2\hat{C}_{\alpha_r}}{u} - a\hat{C}_{\alpha_f}\delta_f - K_{P2}(r - r_d) \tag{7.7b}$$

The control inputs F_1 and F_2 can be applied as the front and rear wheel steer angles, under the intervention of corrective steer angles supplied by active steering actuators in front and rear.

From the Equation 7.2, the corrective front and rear steering angles can be computed by solving for F_1 and F_2, and given as

$$\delta_{fc} = \frac{F_2 + bF_1}{(a+b)\hat{C}_{\alpha f}} \tag{7.8a}$$

$$\delta_{rc} = \frac{F_2 - aF_1}{(a+b)\hat{C}_{\alpha r}} \tag{7.8b}$$

7.3 Simulation Results

The objective of this study is two folds, one is to accessing the performance of the developed 4WS controller and the other is to see the importance of using a dynamic tire model in vehicle simulation studies. A double lane change maneuver is simulated on a flat smooth road, at two different velocities of 100 kph and 120 kph. A preview based closed loop driver controller in CarSim is used with a preview time of 1 seconds. Figure 7.1 shows the desired trajectory with a lane shifted by 3.5 m. Maximum limit on applicable steering wheel angle and steering wheel angle rate are specified. The characteristic speed u_{char} is assumed to be 37.2 m/s. The adaptive gain matrix Γ = diag [8×10^2 8×10^2] and propositional gain matrix K_p = diag [1000 1000]. The developed controller applied using two different tire models, high frequency rigid ring tire model ($<$ 75 Hz) and a steady state based low frequency magic formula model ($<$ 10 Hz). The following three cases are considered to study controller performance and parallelly to compare the advantages of dynamic tire model over steady state model.

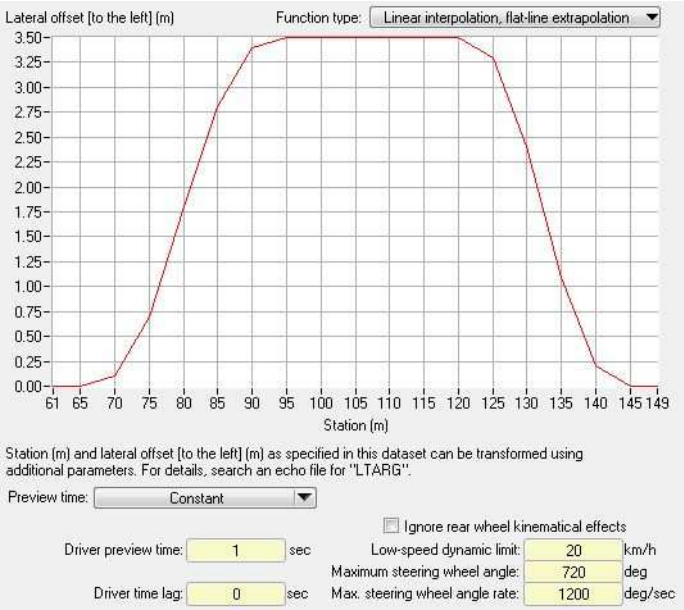

Figure 7.1: Double lane change desired trajectory

1. No control with rigid ring tire model
2. 4 WS control with rigid ring tire model
3. 4 WS control with magic formula tire model

Figures 7.2 and 7.3 shows the time history of lateral acceleration, roll angle, yaw rate and total front right and front left wheels steering input at the road for no control, with 4WS control using rigid ring and magic formula tire models. Comparing the no control case and the 4 WS control case using a rigid ring model, at both the velocities, the performance of the vehicle is improved when compared with no control case. As the rear wheels are steerable, the lag in response of yaw rate and lateral acceleration is minimal for the control case, at both the velocities. Especially, it is observed that at higher velocity of 120 kph, for control case the response curves of yaw rate and lateral acceleration are almost matched, emphasizing the responsiveness of the vehicle. For no control case, a significant delay in generation of lateral forces after the induced yaw moment on the vehicle is observed. Usually, humans are very sensitive to the body roll of the vehicle and it directly effects the confidence with which

a driver negotiates a turn. For the control case, the body roll of the vehicle is also decreased. The important outcome of the controller is significantly decreased peak values of the vehicle yaw rate and also increased yaw damping. From the time history of front steering wheel angles at the road, it is observed that the controller is increasing the steering input with the increasing lateral acceleration and also responding quickly to the changes in the desired path to be followed.

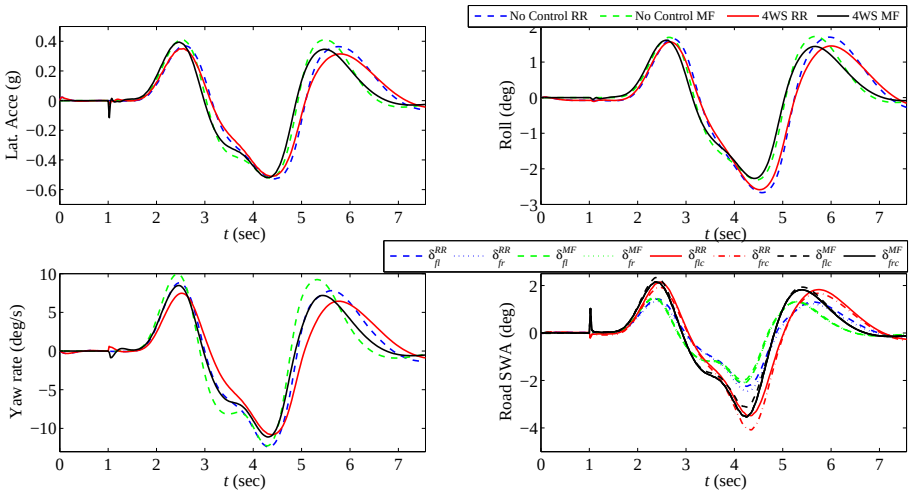

Figure 7.2: Vehicle response for a double lane change maneuver with and without 4 WS controller at 100 kph

As stated in the section , steady state models are valid within the frequency range of less than 10 Hz and are not able to simulate the transient maneuvers as the relaxation behavior of the tire is neglected. As mentioned in the handling simulations of Chapter 5, the relaxation behavior of the tire is dependent upon the vertical load and the slippage of the tire. From Figures 7.1 and 7.2, as the compliance of the tire carcass with respect to the rim is not considered, the vehicle response using steady state model is instantaneous and is it clearly evident as the response curve of steering wheel input matches identically with lateral acceleration and yaw rate of vehicle without any lag. Using a simple steady model also decreases damping of the overall vehicle system, this is evident from the higher peaks in response of

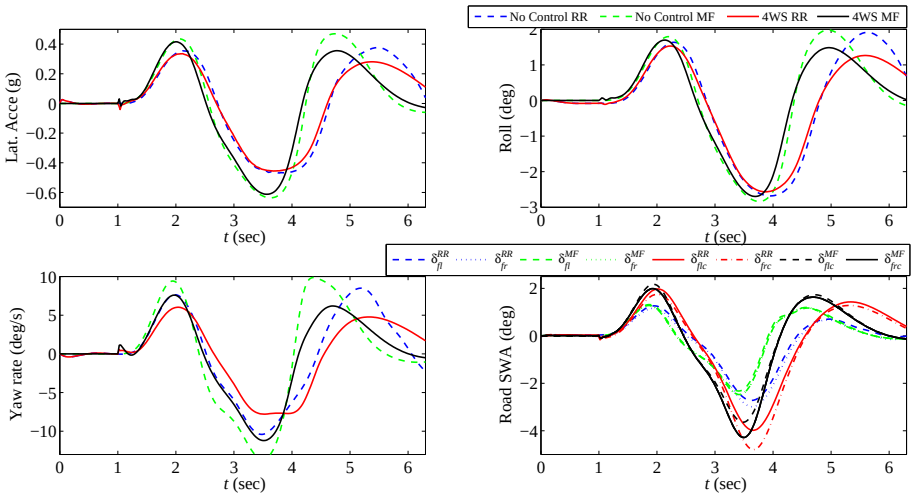

Figure 7.3: Vehicle response for a double lane change maneuver with and without 4 WS controller at 120 kph

lateral acceleration and yaw moment. Figure 7.4 shows the applied rear wheel control input for both the velocity cases. The spike at $t = 1$ sec, is caused due to the activation of 4 WS controller. The controller is not activated until the initial oscillations corresponding to the dynamic tire model are damped. From these simulations, it is observed that simple steady models overestimate the vehicle response and are unable to represent the vehicle response accurately for quick double lane maneuvers.

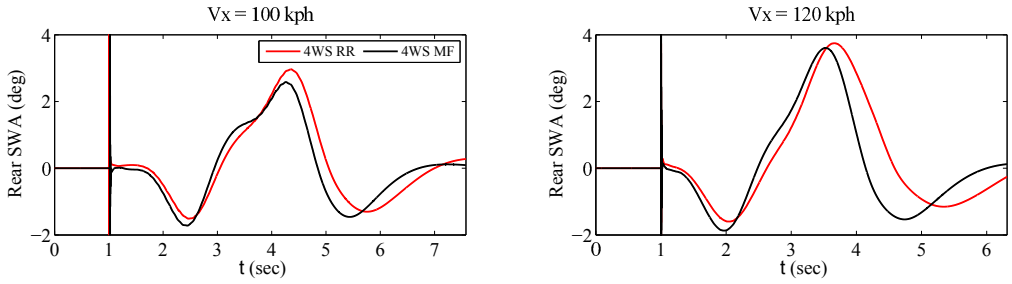

Figure 7.4: Rear steering wheel control input for $V_x = 100$ kph and 120 kph

7.4 Conclusion

A lyapunov based nonlinear 4 WS controller is developed. The developed controller and tire model is integrated with vehicle model in CarSim. A double lane change maneuver is simulated at two different velocities. The potential of 4 WS steering control in the improvement of transient handling performance of the vehicle is explored. From the simulation results, it can be concluded that the developed 4 WS controller have significantly

1. improved transient response
2. improved yaw damping following a transient
3. reduced peak yaw rates
4. reduced lateral acceleration phase lag and
5. reduced body sideslip angles

From the simulation study with dynamic and steady models, it is concluded that dynamic models can predict the vehicle response more accurately by taking into account transient relaxation effects of the tire.

Chapter 8

Enhancements to Dynamic Tire Model

In this chapter, two enhancements for the dynamic model discussed in Chapter 3, are developed. The content of this chapter is as follows. In the Section 8.1, the need to enhance the dynamic longitudinal stiffness variations is discussed, while briefly explaining the factors effecting these stiffness variations. Following this, the proposed model enhancement and improved simulated dynamic response of the tire over the cleat are discussed.

8.1 Dynamic Stiffness Variations

Due to the visco-elastic nature of the tire, the stiffness and the damping of the tire elements are dependent on the loading condition, rolling velocity of the tire, interactions with the road undulations etc,. The rigid ring model effectively models the four main components of the tire: carcass as a rigid belt, the tire sidewalls with pressurised air using nonlinear springs and dampers, the rim, and a contact model. The rigid ring model effectively captures these nonlinear effects by variation of model parameters based on empirical formulations developed

from experiments, eg. relaxation behavior is dependent upon the slippage of the tire, velocity dependent sidewall stiffness, overall stiffness of tire using residual spring elements etc.

The variations of longitudinal and vertical stiffness of the tire plays a significant role in the dynamic behavior of the tire. From the experimental studies [117, 118, 119], e.g., fixed axle cleat tests, it is found that the frequencies of the vertical mode, the in-phase rotational mode and the anti-phase rotational mode decrease with the increasing velocity. The rigid ring model effectively takes this into account by considering sidewall stiffness to be velocity dependent, as given in Equation (3.27). The main objective of the current study is to understand the dynamic stiffness variations of the tire under the influence of uneven road or cleats, especially the variation of in-phase rotational mode frequency and improve the tire model response to various inputs.

8.1.1 Longitudinal Dynamic Stiffness Variations

Figures 8.1 - 8.3 show the ability of the rigid ring model to compensate for dynamic stiffness variations. It is evident that the rigid ring model is able to predict the dynamic stiffness variations due to changes in slip stiffness in the contact patch $K_{F\kappa 0}$, torsional stiffness of sidewall $K_{b\theta 0}$, and inflation pressure changes p. The variations in in-phase and anti-phase rotational modes agreed with the experimental results presented in the literature [120], [15].

From Figure 8.4, it is observed that the rigid ring model is unable to compensate for the changing dynamic stiffness due to the load conditions on the tire. Usually, the increase in vertical load on the tire increases the area of contact patch, especially contact length as given in Table 8.1. With the change in the boundary condition in the contact patch, rotational resistance from the contact patch while the tire is traversing on the cleat also changes. The length of the cleat used for this study is 5 cm, as shown in Figure 4.3. For vertical loads higher than 3000 N, the length of contact patch is greater than the length of the cleat. This causes multiple contact patches while the tire is traversing the cleat. Due

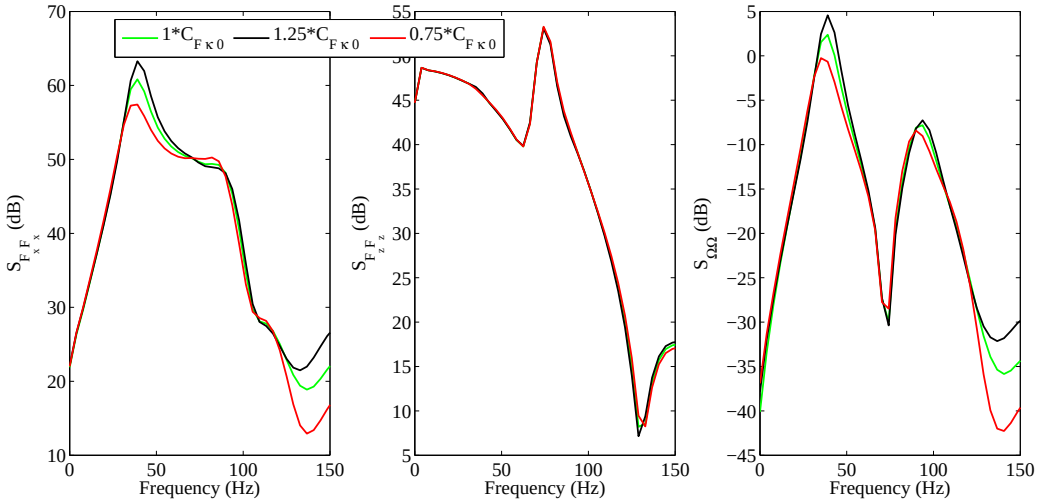

Figure 8.1: Simulated dynamic stiffness variations due to slip stiffness in the contact patch using rigid ring model

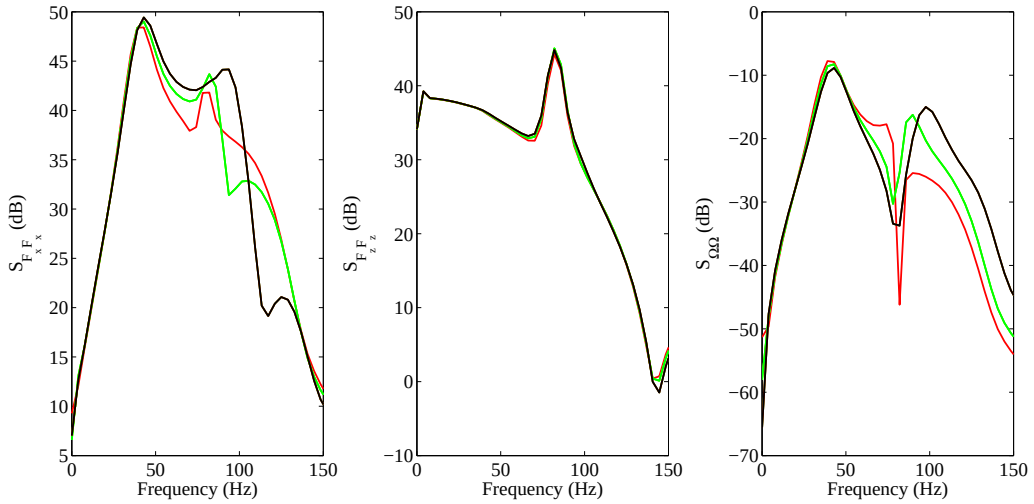

Figure 8.2: Simulated dynamic stiffness variations due to rotational stiffness using rigid ring model

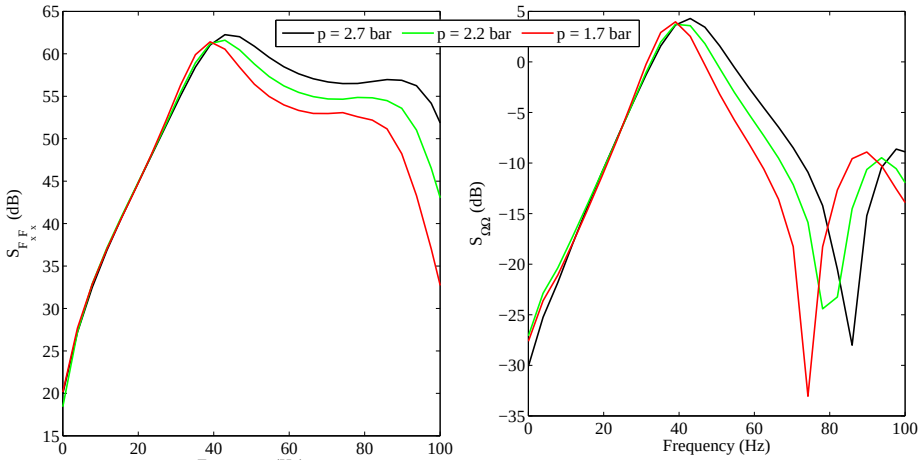

Figure 8.3: Simulated dynamic stiffness variations due to inflation pressure using rigid ring model

to this the rotational resistance acting on tire also changes, thus generating an varied input excitation. Due to the large variation in the applied longitudinal force in a short time span, this causes a shift in the rotational modes of the tire. Table 8.2 shows the experimentally determined in-phase and vertical mode frequencies for a tire rolling over a cleat with a fixed axle condition. It is observed that with the increase in the vertical load, the in-phase mode frequencies are excited in the range of 31.25 - 35.16 Hz and the variation of vertical mode frequency is not seen. These stiffness variations are also evident from the tire validation studies presented in Chapter 4. From Figures 4.5 - 4.12, a slight decrease in accuracy of simulated time response after the tire rolled off the cleat, is observed. This was caused due to the variation of longitudinal stiffness with the input frequency. As the rigid ring model is a single point contact model integrated with multiple cam based enveloping model which uses a finite contact length these variations in stiffness of the tire, especially longitudinal stiffness is not represented by this model.

Usually these frequency dependent longitudinal stiffness variations are modelled with the addition of Maxwell elements. As shown in Figure 8.5, the stiffness of spring C_{dyn} dynamically changes with the applied frequency. In this research, these nonlinear dynamic longitudinal

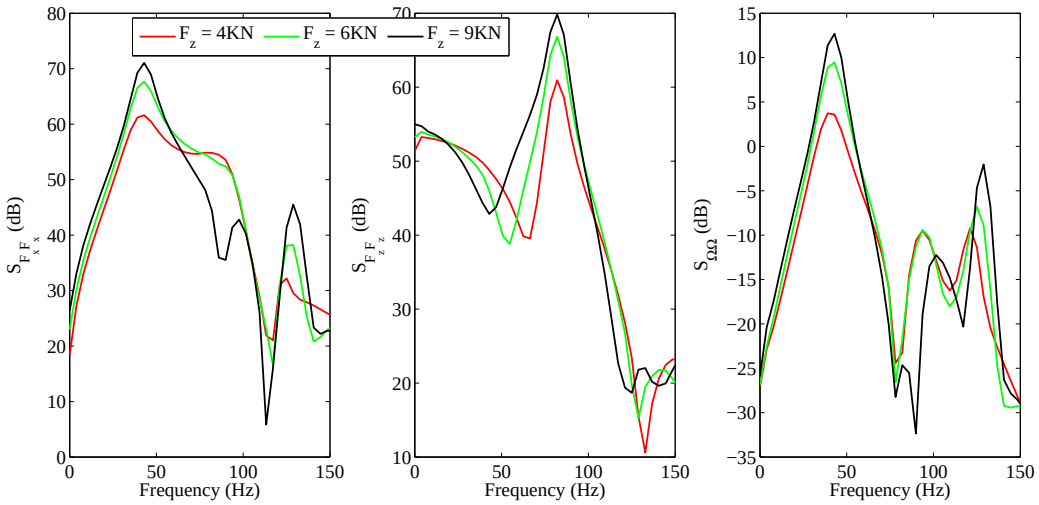

Figure 8.4: Simulated dynamic stiffness variations due to load variations using rigid ring model

Load (N)	**Contact Length (cm)**	**Contact Width (cm)**
2000	4.5	6.11
4000	6.67	7.09
6000	8.41	7.55
9000	10.61	7.84

Table 8.1: Variations of contact patch dimensions with vertical load

	Vx = 25 kph		**Vx = 39 kph**		**Vx = 59 kph**	
Load (N)	***In-phase***	***Vertical***	***In-phase***	***Vertical***	***In-phase***	***Vertical***
2000	35.16	82.03	35.16	82.03	35.16	78.13
4000	31.25 - 35.16	78.13	31.25 - 35.16	78.13	31.25 - 35.16	78.13
6000	31.25 - 35.16	78.13	31.25 - 35.16	78.13	31.25 - 35.16	78.13

Table 8.2: Variations of in-phase and vertical mode frequencies (Hz) with respect to vertical load at different velocities from fixed axle cleat tests

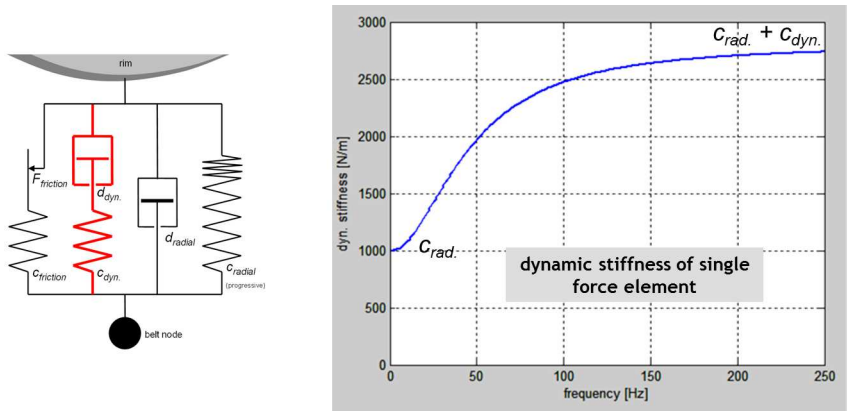

Figure 8.5: Frequency dependent nonlinear dynamic stiffness [9]

stiffness variations are taken into account by considering the sidewall stiffness parameters to be dependent upon variations of vertical force acting in the contact patch. To accomplish this, an empirical based quadratic function is developed to describe the variations in dynamic stiffness due to changing contact lengths while rolling over the cleat.

From the above discussion, it is evident that longitudinal stiffness variations on uneven load profiles is load dependent. To obtain this influence, some parameters of the model have to be made load dependent. Looking at the tire parameters, sidewall stiffness have one of the largest influences on the tire natural frequencies. As this phenomenon of variation of contact length while rolling over a cleat causing this natural frequency change, a function dependent on vertical load in the contact patch is considered. It is assumed that the longitudinal stiffness changes quadratically (nonlinear) with the increase in vertical load. This function is defined taking into account the maximum allowable load on the 205/60R15 tire, e.g., 10000 N.

It is observed that longitudinal stiffness is influenced mostly by f_{long}variable, and multiplying it with a load dependent factor can enable to shift the peaks to shift similar to the ones shown in Figure 8.1. Through manual optimization, the corresponding multiplication factors were found for 2000, 4000, and 6000 N load cases. We considered function dependence on vertical load in the contact patch, so any large increase of vertical load decreases the longitudinal

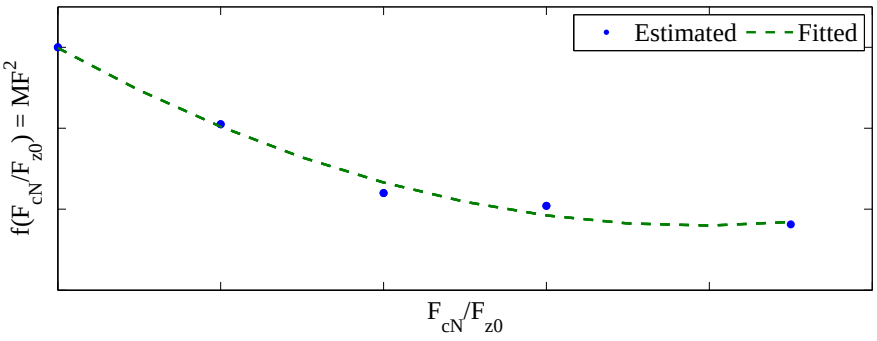

Figure 8.6: Comparison of enhanced and initial rigid ring models time domain response for rolling over cleat at 39 kph and Fz = 4000N

stiffness mimicking an added resistance in rolling direction. From Equation (3.27) and (3.26), it is known that

$$k_{bx0} = 4\pi^2 \cdot m_b \cdot f_{long}^2 \tag{8.1a}$$

$$k_{bx} = k_{bx0}\,(1 + 0.65 \cdot dp_i)\left(1 - q_{bVx}\sqrt{Q_V}\right) \tag{8.1b}$$

After substituting, f_{long} with a multiplication factor in above Equation, yields

$$k_{bx} = MF^2 \cdot k_{bx0}\,(1 + 0.65 \cdot dp_i)\left(1 - q_{bVx}\sqrt{Q_V}\right) \tag{8.2a}$$

$$MF^2 = f(\frac{F_{cN}}{F_{z0}}) \tag{8.2b}$$

$$k_{bx} = f(\frac{F_{cN}}{F_{z0}}) \cdot k_{bx0}\,(1 + 0.65 \cdot dp_i)\left(1 - q_{bVx}\sqrt{Q_V}\right) \tag{8.3}$$

where the MF is a multiplication factor, now this factor should change according to the variations of vertical load F_{cN} given in Equation (3.37), thus mimicking the variation of stiffness due to loading conditions. Figure 8.6 shows the fitted quadratic function to the estimated multiplication factors from the optimization. The values of the axes in Figure 8.6 and the fitted quadratic function are hidden due to confidentiality of the work.

Figures 8.7 - 8.10 show the time domain and frequency domain response using enhanced rigid ring model. It is evident that the, accuracy of simulated results improved at all part of the time response and also matched the corresponding excited in-plane mode frequency.

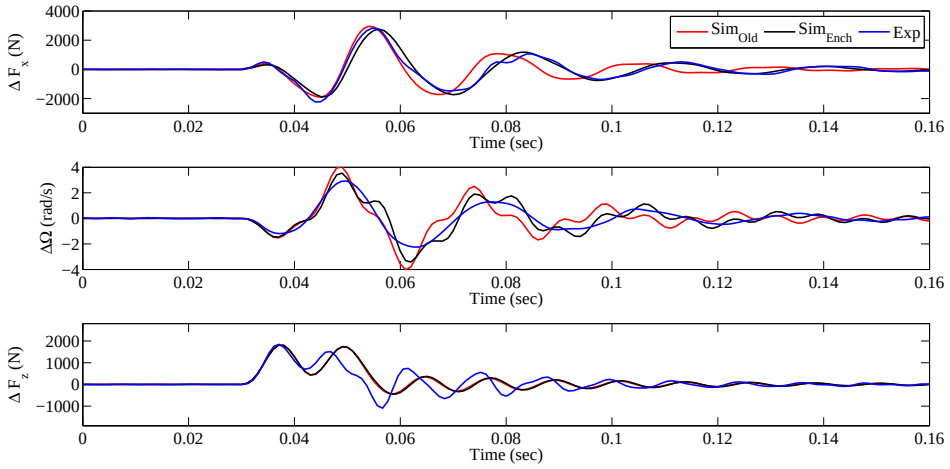

Figure 8.7: Cleat time domain response of enhanced and initial rigid ring models at 39 kph and Fz = 4000N

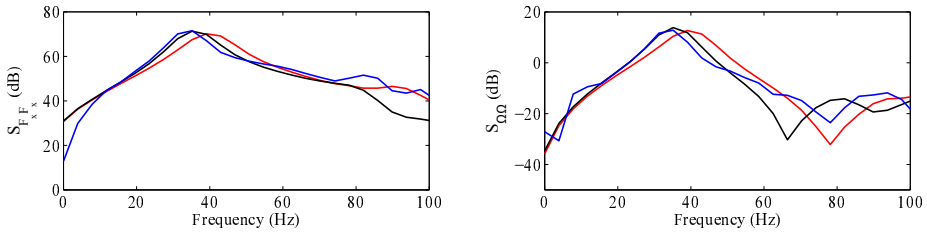

Figure 8.8: Cleat frequency domain response of enhanced and initial rigid ring models at 39 Kph and Fz = 4000N

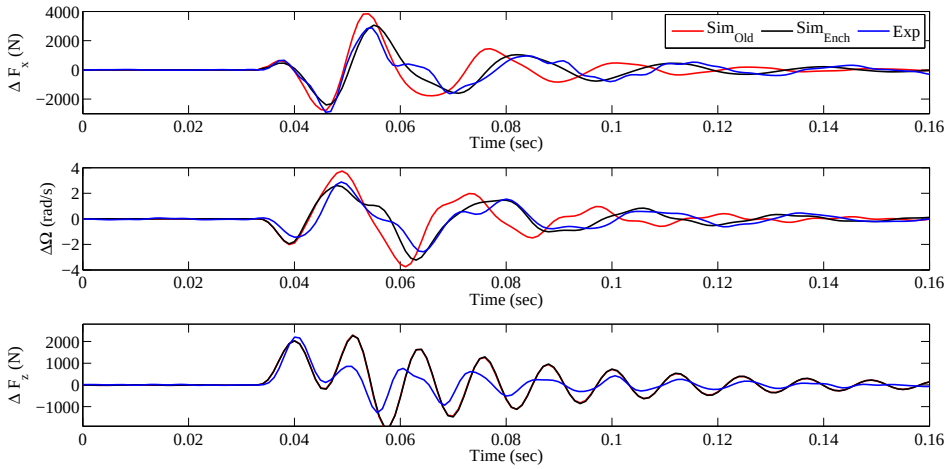

Figure 8.9: Cleat time domain response of enhanced and initial rigid ring models at 59 kph and Fz = 6000N

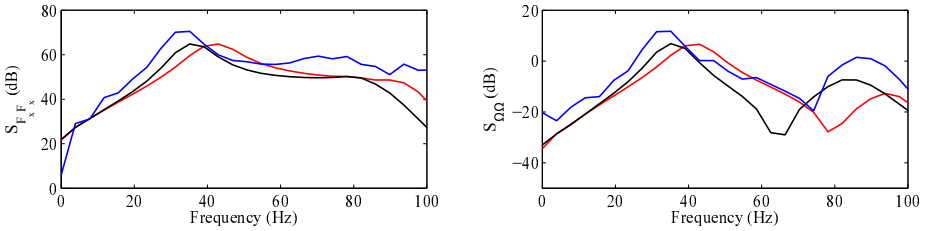

Figure 8.10: Cleat frequency domain response of enhanced and initial rigid ring models at 59 Kph and Fz = 6000N

8.2 Thermal Modeling

From previous studies, it is common knowledge that tire performance is heavily affected by the temperature level of the tire components [122, 123]. The standard tire models like Magic Formula used for vehicle dynamics simulations do not take into account the variation of the model parameters as functions of the estimated temperature of the tire components. In the literature, most of the tire temperature modeling is limited to indoor testing where the tire measurement input conditions do not correspond to the actual road surface conditions. Under heavy ABS braking due to the continuous operation of tire at or close to the peak value of road friction potential, the temperature of tire surface grows exponentially [90]. There is a need for such evaluation tools incorporating the influence of tire surface temperature. In this regard, an addition was made to the tire testing trailer currently owned by CenTiRe and was used to measure the tire temperature during braking.

8.2.1 Testing Apparatus

A few braking experiments were conducted at Virginia Tech Transportation Institute (VTTI) Smart Road Facility. For experimental studies, the testing trailer at CenTire fitted with a fifth wheel is used. A designed fixture maintains a constant vertical load on the tire by varying the stiffness of air spring, as shown in Figures 8.11, 8.12. The tire is mounted on a wheel force transducer (Kistler RoaDyn P530). The wheel force transducer is capable of measuring three orthogonal forces (F_x, F_y, F_z) and torques (M_x, M_y, M_z) that the wheel experiences. The tire is mounted on to force transducer using a wheel adapter to match the bolt pattern of the rim and force transducer. The tire used for testing is instrumented with an accelerometer on the inner liner and a Infrared (IR) temperature sensor is also attached to the rim, as shown in Figure 8.14. This makes the tire rather than being a passive object, intelligent enough to pass the data for advanced chassis design or to model the contact mechanics of the tire-road interactions. The same tire size used for validation studies in

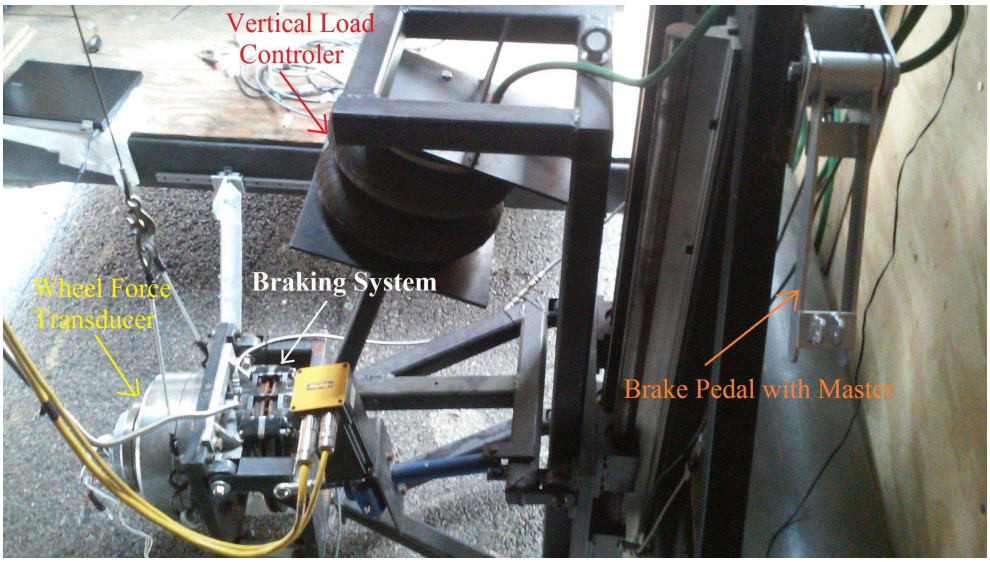

Figure 8.11: Braking system, wheel force transducer and vertical load controller

Chapter 4 is used, which is Goodyear 205/60R15 91V. A braking system is designed for the application of braking input. It contains an 11 inch diameter brake disc and it is mounted on the shaft of wheel force transducer using an adapter. A bracket is designed to hold the brake caliper and FEA analysis of the bracket is performed to take into account stresses and vibrations induced during braking. The caliper is connected to a master cylinder using a liquid hose. The pressure in the master cylinder is varied by compressing the brake pedal which eventually presses the calipers onto the brake disc. A tachometer is also mounted to the end of force transducer shaft, to measure the angular velocity of the wheel. Figure 8.11, 8.12 show the inside of the trailer with braking system, wheel force transducer and vertical load controller. This system can be used effectively for performing the braking tests at different vertical loads. At present, the braking actuation is performed manually by pressing the brake pedal but in future a controllable linear actuator will be used.

For measuring the temperature while braking, three IR sensors are used, one inside the tire rim as shown in Figure 8.14 and other two IR sensors are be mounted at the entry and exit of the tire contact patch. For mounting an IR sensor on the rim surface, a 3D printed mount matching the curvature of the rim is designed. The IR sensor is screwed to this mount and

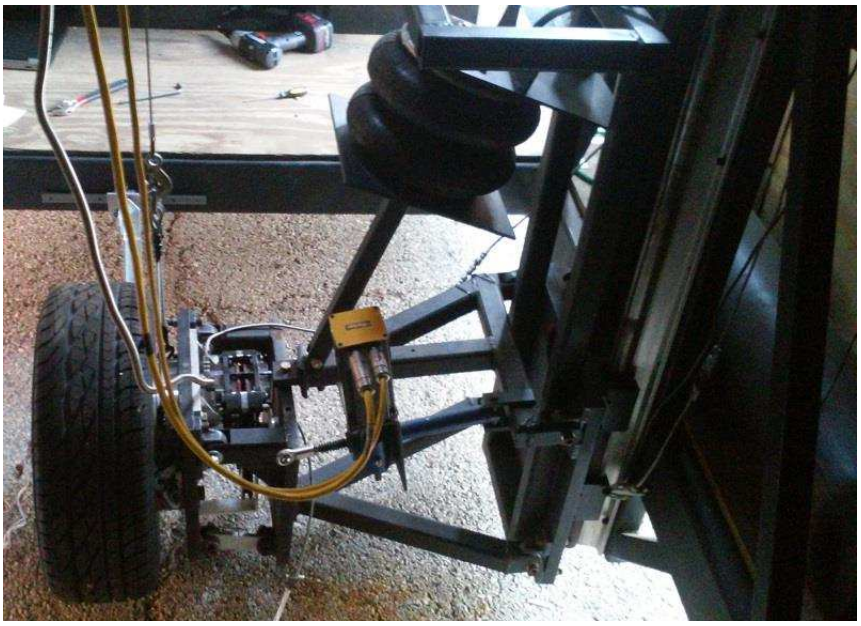

Figure 8.12: Testing system fitted with tire

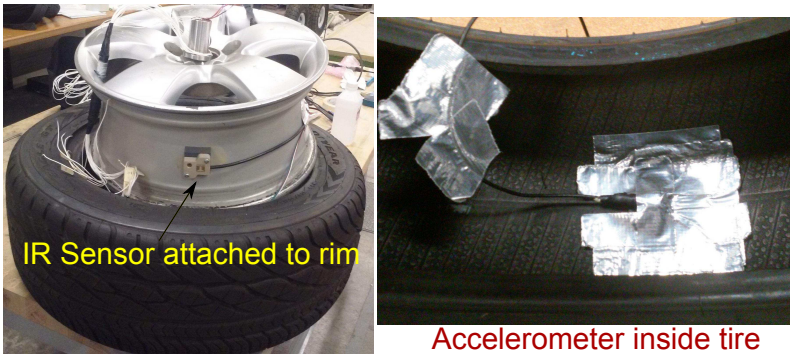

Figure 8.13: Intelligent tire with accelerometer and IR sensors

Figure 8.14: Wheel force transducer with braking system and rotational speed sensor mounted on to the shaft

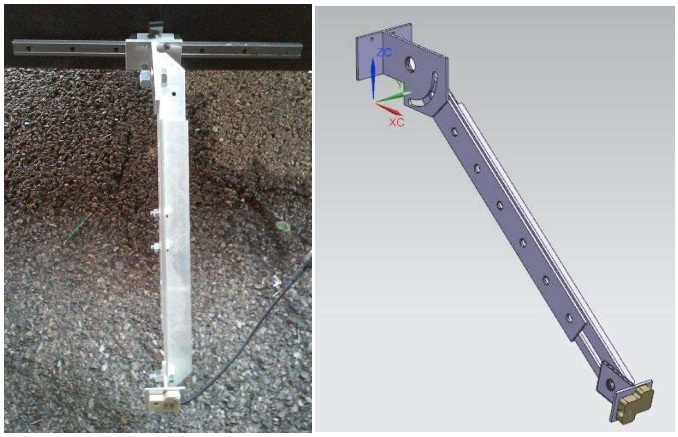

Figure 8.15: Adjustable fixture for measuring the temperature at the tread of the rolling tire

finally glued it onto the rim surface. A fixture is design to mount the IR sensors outside the tire as shown in Figure 8.15, by adjusting the fixture arms it can be adapted for larger and small diameter tires. Using, the measurements from IR sensors the heat conducted from the tire tread component can be measured. Schematic of test apparatus with the mounted tire is shown in Figure 8.16.

Figure 8.16: IR sensors at the entry and exit of the contact patch of the tire

8.2.2 Experimental studies

The physical testing at VTTI smart road facility was performed on May 6th and the ambient temperature is around 25°C. The IR sensor attached to the rim worked before mounting the tire at the shop, but after mounting the IR sensor stopped working due to the complex wiring network inside the tire. After the start of the test, the design fixture holding the IR sensor at the exit of contact patch is hit by a sudden bump in the road, which unmounted and damaged the fixture. So for all braking testing, only the temperature data at the entry of the contact patch is measured.

Experiments are conducted at two different vertical loads of $F_z = 3000$ N and 5000 N, and the braking is applied while is trailer is towed at speed of 15.65 m/s (35 mph). The force and moments at the axle, angular velocity and temperature at the entry of the tire tread surface are measured. Using the longitudinal force data, the magic formula tire model is enhanced with temperature dependent functions, as given below.

$$D_x = D_{x0}\left(1 + p_{Dxt1}dT + p_{Dxt2}dT^2\right) \tag{8.4a}$$

$$K_{x\kappa} = K_{x\kappa 0}\left(1 + p_{Kxt1}dT\right) \tag{8.4b}$$

$$E_x = E_{x0}\left(1 + p_{Ext1}dT\right) \tag{8.4c}$$

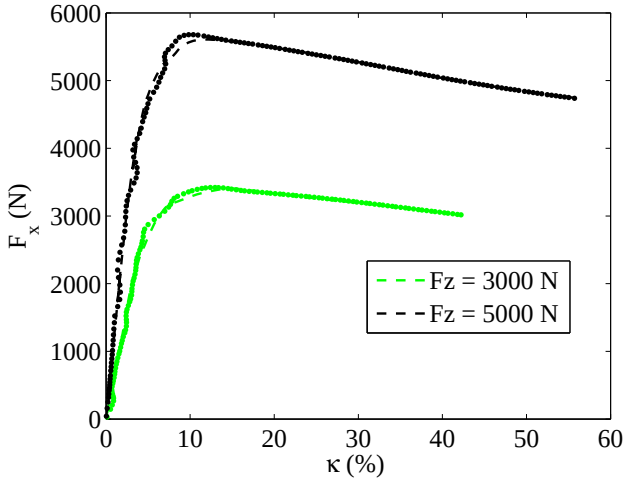

Figure 8.17: MF with temperature dependent longitudinal fitting curves at various vertical loads

where D_{x0}, $K_{x\kappa 0}$ and E_{x0} are peak value of friction, longitudinal slip stiffness, and variation curvature with respective load at nominal conditions. From literature it is found that, these parameters of magic formula tire model are influenced more due to the rise in tread temperature of the tire [122, 123].

$$dT = \frac{(T - T_0)}{T_0} \tag{8.5}$$

where T is rise in temperature at the tread of the tire, T_0 is nominal values which is fixed before performing the parameter identification as 35°C.

The wheel force data from the transducer is processed using a signal processing unit supplied by Kistler. The obtained data is in the form of voltage and it is converted into force and moment data. The wheel force data is further processed using a fifth order butterworth filter with a cutoff frequency of 2 Hz. By fitting the enhanced magic formula model using the longitudinal force data, temperature dependent functions coefficients are estimated. Figure 8.17 shows the fitted curves and Table8.3 gives the estimated parameters.

Figure 8.20 shows the temperature of tire tread under braking at different vertical loads.

Parameter	Value
p_{Dxt1}	-0.09107
p_{Dxt2}	0.012707
p_{Kxt1}	0.36727
p_{Ext1}	-0.039816

Table 8.3: Temperature dependent function coefficients

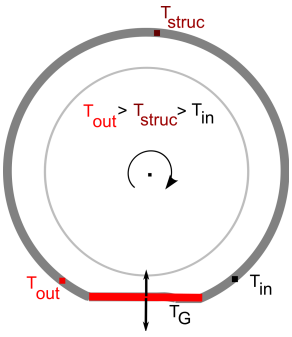

Figure 8.18: Temperatures at various sections of tire tread

It is observed that the temperature rise is less than 4 °C. As it is being the temperature at the entry of the contact patch T_{in}, the heat generated due to slippage has enough time to flow to the environment. So it is unable to estimate heat transfer coefficients due to the lack of enough temperature data. Using the existing data, an exponential function is fitted, assuming that temperature rise is exponential with respect to the slippage of the tire. Figure 8.20 shows the fitted exponential curves.

The simulation of ABS braking studies on a smooth and bad asphalt road (as were done in Chapter 5), are performed again with temperature effects included. The objective of this case study is to see if any possible deviations in predicted braking distance as compared to the results shown in Chapter 5 are observed with the inclusion of temperature effects. An exponential functions is used as the thermal model to predict the rise in temperature. The magic formula coefficients are adjusted to compensate for this rise in temperature, as given in Equation (8.4).

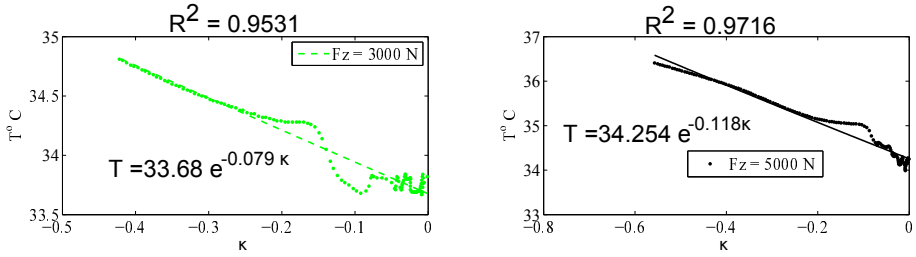

Figure 8.19: Exponentially fitted curves to the temperature data at the entry of the contact patch

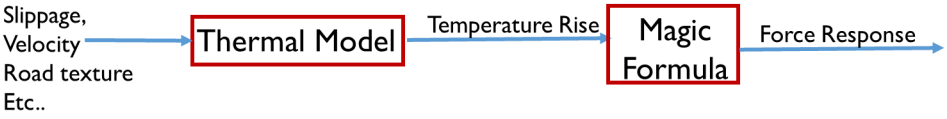

Figure 8.20: Flow chart of the thermal tire model with different modules

From Figure 8.21, it is observed that the braking distance is only increased slightly for simulations on bad asphalt and smooth road profiles with the temperature effects included. It is could due to the fact that as the temperature data used is at the entry of contact patch and moreover the thermal model used is a low fidelity exponential function rather than a physical based heat transfer model. So a more realistic temperature data from the Flat Trac testing is used, which is supplied by a third party supplier. In this case, as the temperature of tire tread is measured at the exit of contact patch, the temperature rise is more than 45 °C as shown in Figure 8.23. Again using the longitudinal force data, magic formula temperature dependent functions are determined. Figure 8.22 shows the fitted curves and Table 8.4 gives the estimated parameters.

The temperature rise at the contact patch of the tire for a braking maneuver on a dry surface is dependent upon the tread rubber material properties and type of road texture and, this rise in temperature has a direct influence on frictional characteristics at the tire-road interface. The primary heat generation and transfer mechanisms associated are: heat conducted to road surface T_G and tire structure T_{struc} due to slippage in the contact patch and the other

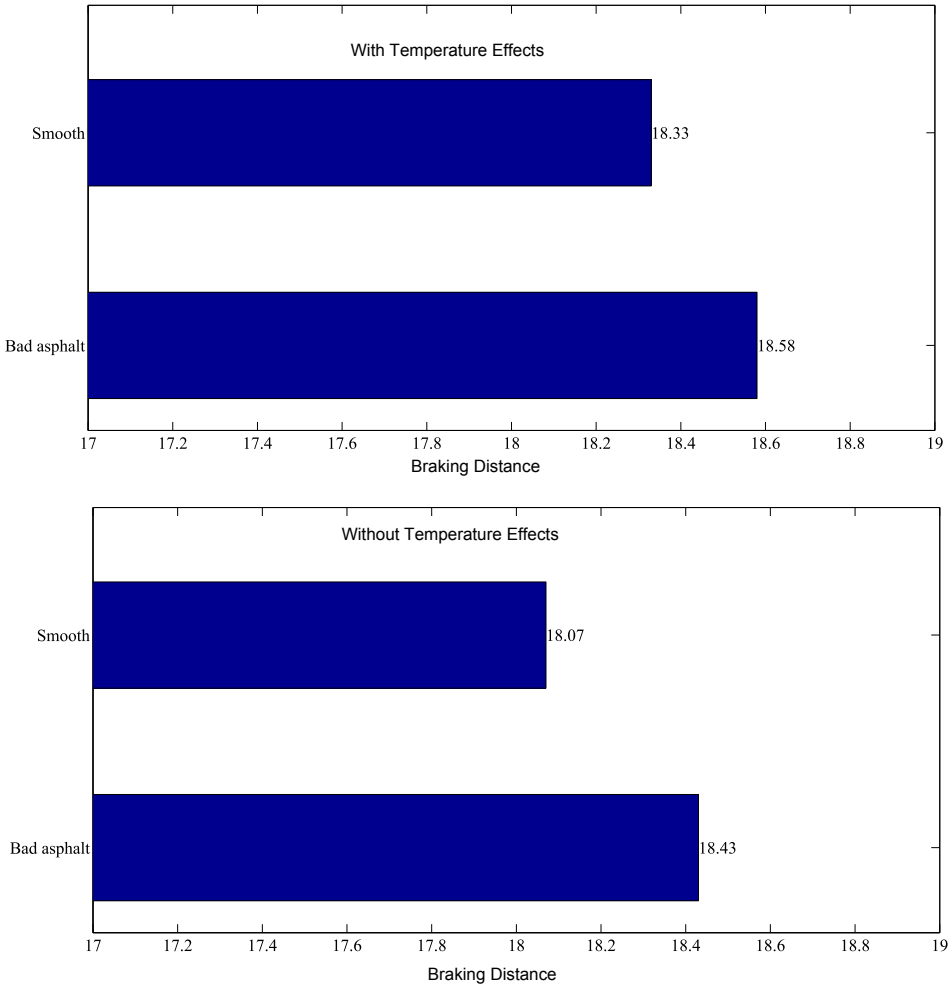

Figure 8.21: Simulated braking distance with exponential based thermal model

Parameter	Value
p_{Dxt1}	-0.10307
p_{Dxt2}	0.062204
p_{Kxt1}	0.89313
p_{Ext1}	-0.65555

Table 8.4: Temperature dependent function coefficients using Flat Trac data

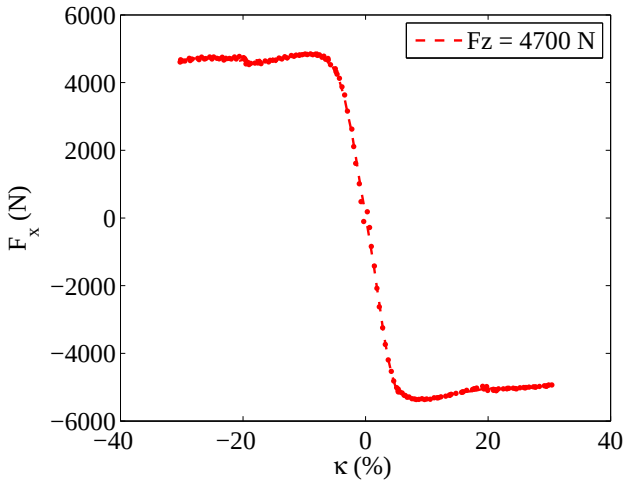

Figure 8.22: MF with temperature dependent longitudinal fitting curves using Flat Trac data

is the heat convected, which flows into the air around the tire, as shown in Figure 8.18. The heat is also generated in the tire structure due to compression of air molecules inside the tire, although this heat flows steadily into the tire tread regions but comparing the small duration of applied braking input, this heat flux can be neglected.

8.2.3 Thermal Modeling

The thermal model is developed by considering the heat generated due to the slippage of tire and the heat which flows to environment due to convection.

The heat flux generated due to the slippage of tire, is assumed to be an exponential function and is given as

$$q''_{cond} = Be^{(A\kappa)} \tag{8.6}$$

where B and A can be assumed to be dependent upon the surface texture, tire tread compound and vertical load on the tire.

After the tread elements exit the contact patch, the generated heat is convected to the

environment. To model this effect, the equation based on convective heat transfer is given as

$$q''_{conv} = hA_t \left(T_{strc} - T_{amb}\right) \tag{8.7}$$

where h is the convective heat transfer coefficient, A_t is the area of tire tread other than the area in contact with the road and T_{amb} is ambient temperature.

The temperature rise is obtained by using the heat transfer balance between Equations (8.6) and (8.7),

$$\frac{dT}{dt} = q''_{cond} - q''_{conv} \tag{8.8}$$

Substituting the equations

$$\frac{dT}{dt} = Be^{(A\kappa)} - hA_t \left(T_{strc} - T_{amb}\right) \tag{8.9}$$

The variable T in above equation is assumed to be T_{out}, as shown in Figure 8.18. As the above equation contains two variables, for simplicity it is assumed that $T_{strc} \approx T$. The temperature rise in Equation 8.10 is a function of time, hence the slip ratio variable is converted into a function of time. For the Flat Trac testing using the rate of slip ratio sweep κ is equal to c t. Substituting the equation is given as

$$\frac{dT}{dt} = Be^{(Act)} - hA_t \left(T_{strc} - T_{amb}\right) \tag{8.10}$$

The slip ratio sweep associated with testing is 10 % per second, therefore $c = 0.1$. The differential equation is solved using Mathimatica software and the solution is given as

$$T(t) = \frac{B}{Ac + hA_t} \left(e^{Act} - e^{-A_t ht}\right) + T_{amb} \tag{8.11}$$

The equation is used for fitting the temperature data from Flat Trac testing, the fitting results are shown in Figure 8.23 With the estimation of heat transfer model parameters, the heat transfer model given in Equation (8.10) and magic formula with temperature effects are integrated with the dynamic tire model. The simulation of ABS braking is performed on a smooth road. With the addition of temperature module to the existing dynamic tire model, numerical errors as stated in Chapter 4, were encountered for ABS simulation on bad

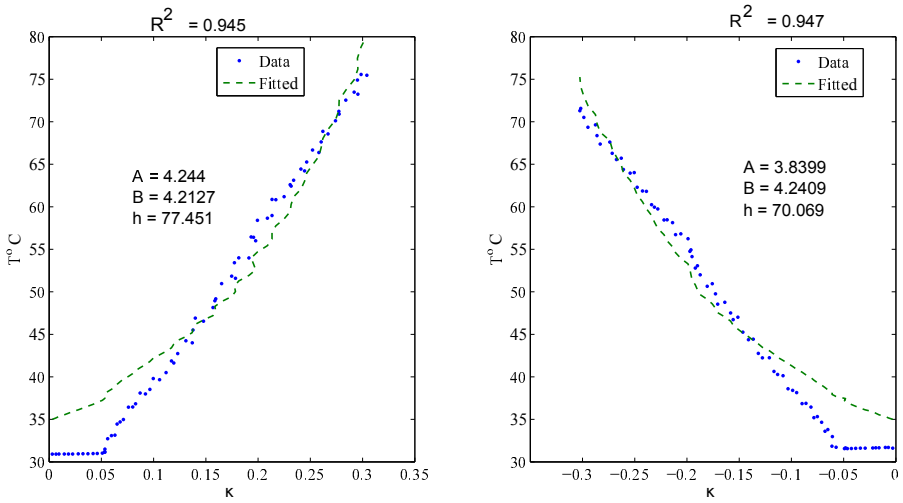

Figure 8.23: Estimation of thermal model parameters using temperature data from the Flat Trac

asphalt road profile, so the ABS braking simulation is performed on smooth road profile only. Figure 8.24 compares the braking distance with and without the temperature effects. The braking distance has increased by 1 meter. Figure 8.25, shows the estimated temperature rise at all the four tires. It is observed that the predicted temperature rise for rear tire seems to be constant after simulation time $t = 2.7$ sec. The reason could be due to the fact that the data from Flat Trac machine is obtained at a vertical load of 4700 N, which closely corresponds to the load on front tire but the load on rear tire is around 2000 N, as shown in Figure 5.5. So the obtained heat transfer parameters A, B and h could be sensitive to the loading condition which are causing these deviations. It is also seen from Equation (8.10), with the decrease in vertical load on the tire, the amount of area of the tire A_t which convects heat also increases. In future, a more comprehensive temperature data is needed to study the variations of these heat transfer parameters.

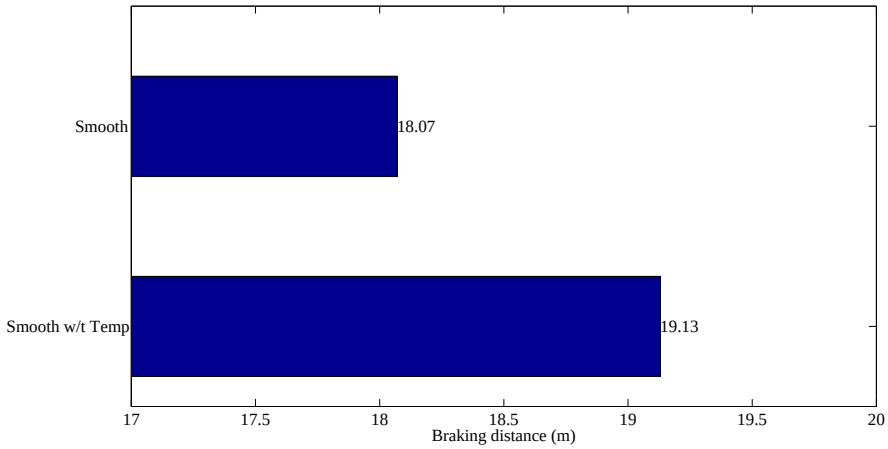

Figure 8.24: Simulated braking distance using heat transfer based thermal model

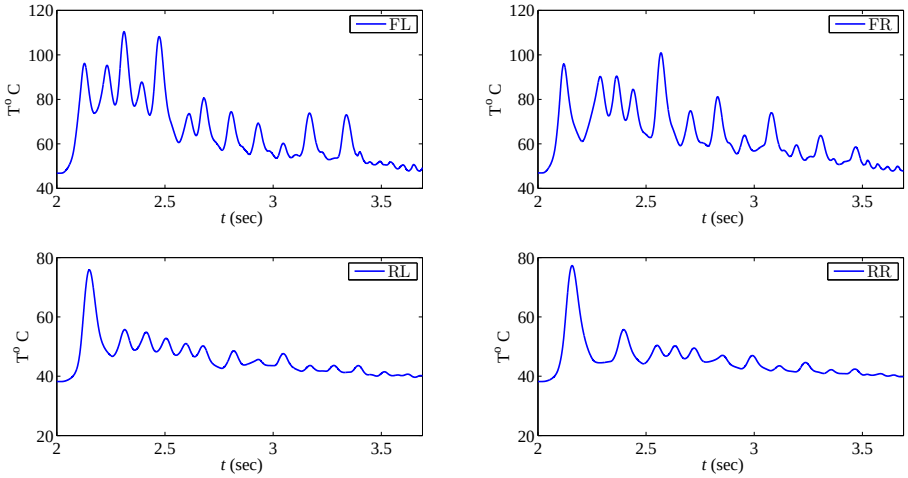

Figure 8.25: Simulated temperature rise in the contact patch of four tires during ABS braking maneuver

8.3 Conclusion

It is shown that rigid ring based dynamic tire model is unable to compensate for dynamic stiffness variations of a tire rolling over a cleat. A slight decrease in accuracy of simulated longitudinal force response after the tire rolled off the cleat and a shift in longitudinal

frequency peak, is observed. It is shown that it is due to the generation of multiple contact patches of the tire while traversing the cleat. As it is the important boundary condition acting on the tire, and influences the dynamic longitudinal stiffness of the tire. These dynamic stiffness variations are taken into account by considering the sidewall stiffness parameter to be dependent on vertical load acting in the contact patch. An empirical based dependent function is developed and the simulated time and frequency response of the tire while rolling over a cleat has improved. Initial braking experiments with the intelligent tire fitted with braking system and force transducer are performed. Three IR sensors, one inside the tire and two at the entry and exit of the tire contact patch are mounted using an adjustable fixture. Unfortunately, only the temperature data at the entry of the contact patch are recorded during the course of the tests. ABS braking maneuvers are simulated on smooth and bad asphalt using the fitted MF formula and exponential thermal models shown no variation in braking distance. So, a heat transfer based model is developed using realistic data from Flat Trac testing. The heat transfer model effectively takes into account convective and conductive heat generated due to slippage. The simulation of ABS braking maneuver shown to increase the braking distance by one meter with the developed thermal model. Future testing and more temperature data can be utilized to enhance the thermal model with some of the model parameters dependent upon vertical load or road texture or tire tread compound.

Chapter 9

Conclusion and Future Work

9.1 Conclusion

The main goal for this research is the enhancement and application of the rigid ring tire model for evaluating the dynamic effects of tire on the vehicle braking, handling and ride performance. As stated in Chapter 1, the objective set forward are

1. To develop, implement and validate a rigid ring tire model and a simulation tool to assist both tire designers and the automotive industry in analyzing the effects of tire belt vibrations, road disturbances, and high frequency brake and steering torque variations on the handling, braking, and ride performances of the vehicle.

2. To further enhance the tire model by considering dynamic stiffness changes and temperature dependent friction properties.

3. To develop, and implement novel control algorithms for braking, stability, and ride performance improvements of the vehicle.

To achieve these objectives, firstly a comprehensive literature review of all the available tire models is performed. After carefully evaluating the advantages and drawbacks of var-

ious models described in the literature, a 6 DOF the rigid ring based model developed by Schmeitz [5] is used. The point contact rigid ring model is integrated with elliptical cam model to effectively capture the enveloping behavior of the tire rolling over uneven road undulations. The modeling elements of rigid ring, enveloping model and vehicle in CarSim environment are explained in detailed. The tire model is validated using fixed axle high-speed oblique cleat experimental data and the tire model is proven to be valid up to 75 Hz frequency. The vehicle model developed in Carsim® is also validated using continuous sinusoidal steering tests. With the integration of the vehicle model in CarSim® with the tire and ABS models in Matalb/Simulink, various high frequency vehicle dynamics maneuvers are performed, as given below

1. ABS braking on bad asphalt road profile with and without cleat and
2. ABS braking on split-μ and smooth surface
3. Successive - increasing step steering on a smooth surface
4. Step steering on bad asphalt with cleat and without cleat
5. Lane change on bad asphalt on bad asphalt and smooth roads
6. ABS braking in turn on a smooth road
7. Accelerating in a turn on bad asphalt and smooth roads

These manoeuvres help comprehend the dynamic inertial effects of tire under common extreme maneuvers like handling while braking with ABS, handling on rough road, transient steering, and power on or accelerating in a turn. These maneuvers could also be used in evaluation and design of ESC/ABS controller performance. The following main conclusions were drawn with regard to the dynamic effects of tire on vehicle performance.

- It is observed that the short wavelength road disturbances excite the torsional modes of the tire. The presence of large cleats and potholes have a direct effect on the braking distance of the vehicle.

- Rapid pressure pulse inputs from ABS controller can also excite the torsional modes of the tire. This causes ABS controller to be counterproductive, as the induced vibrations causes slippage of tire at the end of each cycle and the ABS compensates for it in the next cycle.

- It is observed that, initially at lower slip angles the effects of fast transient steering inputs and road undulations on excitation of lateral mode of the tire is negligible. At higher slip angles, due to decrease in relaxation length of the tire and vertical load on the inside tires. The lateral belt vibrations are excited due to any changes in road undulations or steering inputs.

- It is observed that using dynamic models can predict the vehicle response more accurately for fast lane change maneuvers by effectively taking into account transient relaxation effects of the tire than steady state based tire models.

- For the maneuvers involving longitudinal acceleration/deceleration combined with cornering, disturbance from high frequency ABS pressure pulse inputs can excited the lateral inertial belt modes of the tire.

- Application of longitudinal braking or driving forces while in a turn, has a severe effect on the handling performance of the vehicle.

The dynamic tire model is also integrated in the development of active controllers: active/semi-active suspension controller and 4 WS steering controller. In this study, a novel double damper suspension is introduced. Due to its potential to increase the band width of the control system with the addition of two controllable dampers, the novel double damper semi-active suspension system can emulate closely as active suspension. Parallely, it is

demonstrated that for the perceived harshness rating of a suspension in response to short wavelength road profiles, the vibration transmissibility of tire and the enveloping behavior of the tire as it deforms around the road undulations are important. From simulation studies, it is shown that the longitudinal and vertical (non-linear) dynamics of the tire plays a crucial role in the secondary ride performance of the vehicle. The possibility to improve the lateral transient handling performance near the limits of tire adhesion is explored with the development of 4 WS controller. It is demonstrated that with the steering of the rear tires simultaneously with front tires, the yaw response of the vehicle is improved. Finally, two enhancements to the rigid ring model are introduced. It is demonstrated that present rigid ring model is unable to capture the dynamic longitudinal stiffness variations while rolling over the cleat. These dynamic stiffness variations are taken into account by considering the sidewall stiffness parameter to be dependent on vertical load acting in the contact patch. An empirical function is developed and the simulated time and frequency response of the tire while rolling over a cleat has improved. A heat transfer based thermal model and magic formula with temperature dependent functions are developed using the data from Flat Trac testing. The braking distance increased slightly for a simulated ABS braking maneuvers with the included temperature effects.

9.2 Future Work

The following recommendations are given for future work pertaining to this study:

- Utilizing the updated testing trailer at CenTire for the development of heat transfer based thermal model by determination of conductive and convective heat transfer coefficient using the temperature from all the three IR sensors.
- Implementation of a GUI for the simulation tool that would require minimal user intervention for conducting simulations.

- Integration of the developed simulation tool with the Hardware in the Loop (HiL) testing rig. To tune the wheel acceleration thresholds of the ABS controller for minimal excitation of torsional modes of the tire.

- As the rigid ring is validated up to 75 Hz and also due to the availability of model parameters, with the help of testing trailer fitted intelligent tire, the parameters estimated from the accelerometer signals like length of contact patch, velocity of the contact patch can be validated with the developed tire model. This requires a ADAMS model of the testing rig integrated with the developed tire model.

- Adding a tire wear sub module to dynamic tire model, to take into account force and moment variation

- Development of integrated chassis controller and evaluating its performance using dynamic tire model.

Bibliography

[1] S. Taheri, "Tire mechanics." Lecture Notes Virginia Tech, Spring 2013.

[2] H. B. Pacejka, *Tire and Vehicle Dynamics*. Butterworth-Heinemann, 3 ed., 2012.

[3] W. Hirschberg, G. Rill, and H. Weinfurter, "Tire model tmeasy," *Vehicle System Dynamics*, vol. 45, no. suppl1, pp. 101 – 19, 2007//.

[4] P. Zegelaar, *The dynamic response of tyres to brake torque variations and road unevennesses*. PhD thesis, TU Delft, 1998.

[5] A. Schmeitz, *A Semi-Empirical Three-Dimensional Model of the Pneumatic Tyre Rolling over Arbitrarily Uneven Road Surfaces*. PhD thesis, Delft University of Technology, 2004.

[6] A. T. Van Zanten, *Road and Off-Road Vehicle System Dynamics Handbook - Control of Horizontal Vehicle Motion*. CRC Press, 1 ed., 2014.

[7] D. Ammon, *Road and Off-Road Vehicle System Dynamics Handbook - Detailed Modeling, Simulation, and Analysis of Vehicle Dynamics*. CRC Press, 1 ed., 2014.

[8] *CarSim Steering Systems*. Mechanical Simulation - VehicleSim Browser Reference Manual, 2008.

[9] M. Gipser, "FTire, a new fast tire model for ride comfort simulations," *International ADAMS User's Conference Berlin*, 1999.

[10] J. Weber, *Automotive Development Processes*. Springer Berlin Heidelberg, 1 ed., 2009.

[11] D. Ammon, "Vehicle dynamics analysis tasks and related tyre simulation challenges," *Vehicle System Dynamics*, vol. 43, no. suppl, pp. 30 – 47, 2005.

[12] D. Chen, D. Crolla, C. Alstead, and J. Whitehead, "Comprehensive study of subjective and objective vehicle handling behaviour," *Vehicle System Dynamics*, vol. 25, no. Suppl, pp. 66 – 86, 1996.

[13] A. T. Van Zanten, R. Erhardt, and G. Pfaff, "Vdc, the vehicle dynamics control system of bosch," *SAE Technical Papers*, 1995.

[14] J. Maurice, "The influence of belt dynamics on cornering and braking properties of tyres," *Vehicle System Dynamics*, no. November 2012, pp. 37–41, 1998.

[15] J. Pauwelussen, L. Gootjes, C. Schröder, K.-U. Köhne, S. Jansen, and a. Schmeitz, "Full vehicle ABS braking using the SWIFT rigid ring tyre model," *Control Engineering Practice*, vol. 11, pp. 199–207, Feb. 2003.

[16] S. T. Jansen, P. Zegelaar, and H. B. Pacejka, "The Influence of In-Plane Tyre Dynamics on ABS Braking of a Quarter Vehicle Model," *Vehicle System Dynamics*, vol. 32, pp. 249–261, Aug. 1999.

[17] T. Day and S. Roberts, "A Simulation Model for Vehicle Braking Systems Fitted with ABS," in *SAE World Congress and Exhibition*, SAE, 2002.

[18] P. Haney, *The Racing and High-Performance Tire: Using Tires to Tune for Grip and Balance*. Society of Automotive Engineers, 1 ed., 2003.

[19] H. B. Pacejka and E. Bakker, "The Magic Formula Tire Model," *Vehicle System Dynamics*, vol. 21, pp. 1–18, Jan. 1992.

[20] W. Hirschberg, G. Rill, and H. Weinfurter, "User-appropriate tyre-modelling for vehicle dynamics in standard and limit situations," *Vehicle System Dynamics*, vol. 38, no. 2, pp. 103 – 25, 2002/08/.

[21] H. Dugoff, P. Fancher, and L. Segel, "An analysis of tire traction properties and their influence on vehicle dynamic performance," *SAE Technical Paper*, 1970.

[22] J. Bernard, L. Segel, and R. Wild, "Tire shear force generation during combined steering and braking maneuvers," *SAE Technical Paper*, 1977.

[23] C. Canudas de Wit, H. Olsson, K. Astrom, and P. Lischinsky, "A new model for control of systems with friction," *IEEE Transactions on Automatic Control*, vol. 40, no. 3, pp. 419 – 25, 1995.

[24] C. Canudas-de Wit, P. Tsiotras, E. Velenis, M. Basset, and G. Gissinger, "Dynamic friction models for road/tire longitudinal interaction," *Vehicle System Dynamics*, vol. 39, no. 3, pp. 189 – 226, 2003.

[25] C. Canudas de Wit and P. Tsiotras, "Dynamic tire friction models for vehicle traction control," vol. vol.4, (Piscataway, NJ, USA), pp. 3746 – 51, 1999//.

[26] P. Dahl, "Solid friction damping of mechanical vibrations," *AIAA Journal*, vol. 14, no. 12, p. 16751682, 1976.

[27] E. Bakker, H. B. Pacejka, and L. Lidner, "A new tire model with an application in vehicle dynamics studies," (400 Commonwealth Drive, Warrendale, PA 15096-0001, United States), 1989.

[28] J. Bernard and C. Clover, "Tire modeling for low-speed and high-speed calculations," (Detroit, MI, United states), 1995.

[29] H. Pacejka, *The Wheel Shimmy Phenomenon*. PhD thesis, TU Delft, 1966.

[30] G. Gim and N. Kang, "Requirements of a tire model for practical cornering simulations of vehicles," (Detroit, MI, United states), 1996.

[31] F. Braghin and E. Sabbioni, "A Dynamic Tire Model for ABS Maneuver Simulations," *Tire Science and Technology*, vol. 38, pp. 137–154, June 2010.

[32] P. Lugner and M. Plochl, "Tyre model performance test: first experiences and results," *Vehicle System Dynamics*, vol. 43, no. suppl, pp. 48 – 62, 2005//.

[33] R. W. Scavuzzo, T. R. Richards, and L. T. Charek, "Tire Vibration Modes and Effects on Vehicle Ride Quality," *Tire Science and Technology*, vol. 21, pp. 23–39, Jan. 1993.

[34] A. van Zanten, A., Ruf, W., Lutz, "Measurement and Simulation of Transient Tire Forces," *SAE Technical Paper*, 1989.

[35] Zanten, A., Erhardt, R., Lutz, A., "Measurement and Simulation of Transients in Longitudinal and Lateral Tire Forces," *SAE Technical Paper*, 1990.

[36] Y. Chang, M. E. Gindy, and D. a. Streit, "Literature survey of transient dynamic response tyre models," *International Journal of Vehicle Design*, vol. 34, no. 4, p. 354, 2004.

[37] S. K. Clark, "The rolling tire under load," (Chicago, IL, United states), 1965.

[38] F. Bhn, "Models for the radial tire for high frequency rolling contact," (Kingston, Canada), 1989.

[39] H. B. Pacejka, *Mechanics of Pneumatic Tires*. U.S. Government Printing Office, 1981.

[40] J. Padovan, "On viscoelasticity and standing waves in tires.," *Tire Science and Technology*, vol. 4, no. 4, pp. 233 – 246, 1976.

[41] G. Potts, C. Bell, L. Charek, and T. Roy, "Tire vibrations.," *Tire Science and Technology*, vol. 5, no. 4, pp. 202 – 225, 1977.

[42] K. Yamagishi and J. Jenkins, "Circumferential contact problem for the belted radial tire.," *Journal of Applied Mechanics, Transactions ASME*, vol. 47, no. 3, pp. 513 – 518, 1980.

[43] K. Yamagishi and J. Jenkins, "Singular perturbation solutions of the circumferential contact problem for the belted radial truck and bus tire.," *Journal of Applied Mechanics, Transactions ASME*, vol. 47, no. 3, pp. 519 – 524, 1980.

[44] A. Umsrithong and C. Sandu, "Parameter identification and experimental validation of a discrete mass tire model for uneven rigid terrain," vol. 6, (Chicago, IL, United states), pp. 499 – 510, 2012.

[45] B. J. Chan and C. Sandu, "Development of a 3-d quasi-steady-state tyre model for on-road and off-road vehicle dynamics simulations: Part ii-off-road rigid wheel model," *International Journal of Vehicle Systems Modelling and Testing*, vol. 9, no. 2, pp. 107 – 136, 2014.

[46] C. Sandu, E. Pinto, S. Naranjo, P. Jayakumar, A. Andonian, D. Hubbell, and B. Ross, "Off-road soft soil tire model development and proposed experimental testing," (Blacksburg, VA, United states), pp. 110 – 124, 2011.

[47] S. Taheri, C. Sandu, S. Taheri, E. Pinto, and D. Gorsich, "A technical survey on terramechanics models for tire-terrain interaction used in modeling and simulation of wheeled vehicles," *Journal of Terramechanics*, vol. 57, pp. 1 – 22, 2015.

[48] S. Gong, *A Study of in-plane Dynamics of Tires*. PhD thesis, Delft University of Technology, 1993.

[49] P. Zegelaar and H. Pacejka, "The in-plane dynamics of tyres on uneven roads," *Vehicle System Dynamics*, no. November 2012, pp. 37–41, 1996.

[50] J. Maurice, M. Berzeri, and H. Pacejka, "Pragmatic tyre model for short wavelength side slip variations," *Vehicle system dynamics*, no. November 2012, pp. 37–41, 1999.

[51] D. Allison and R. Sharp, "On the low frequency in-plane forced vibrations of pneumatic tyre/wheel/suspension assemblies," *Vehicle System Dynamics*, vol. 27, pp. 151–162, Jan. 1997.

[52] D. Belluzzo, F. Mancosu, R. Sangalli, F. Cheli, and S. Bruni, "New Predictive Model for the Study of Vertical Forces (up to 250 Hz) Induced on the Tire Hub by Road Irregularities," *Tire Science and Technology*, vol. 30, pp. 2–18, Jan. 2002.

[53] a. J. C. Schmeitz, I. J. M. Besselink, and S. T. H. Jansen, "Tno Mf-Swift," *Vehicle System Dynamics*, vol. 45, pp. 121–137, Jan. 2007.

[54] K. Guo, "Dynamic tire model used in advanced chassis control," in *2011 International Conference on Electric Information and Control Engineering*, pp. 4957–4961, IEEE, Apr. 2011.

[55] F. Mancosu, C. Savi, P. Brivio, G. Travaglio, and I. Ramirez, "New dynamic tyre model in multi-body environment," (Detroit, MI, United states), 2001.

[56] M. Gipser, "Dns-tire, a dynamic nonlinear spatial tire model in vehicle dynamic," (Torino, Italy), 1987.

[57] M. Gipser, "FTire: a physically based application-oriented tyre model for use with detailed MBS and finite-element suspension models," *Vehicle System Dynamics*, vol. 43, pp. 76–91, Jan. 2005.

[58] H. R. Dorfi, R. L. Wheeler, and B. B. Keum, "Vibration modes of radial tires: Application to non-rolling and rolling events," (Traverse City, MI, United states), 2005.

[59] H. Dorfi, "A study of the in-plane force transmission of tires," *Tire Science and Technology*, vol. 32, no. 4, pp. 186 – 213, 2004.

[60] K. Guo, "Tire roller contact model for simulation of vehicle vibration input," *SAE Technical Paper*, 1993.

[61] S. A. Lippmann and J. D. Nanny, "A Quantitative Analysis of the Enveloping Forces of Passenger Tires," *SAE Technical Paper*, 1967.

[62] P. Bandel and C. Monguzzi, "Simulation Model of the Dynamic Behavior of a Tire Running Over an Obstacle," *Tire Science and Technology*, vol. 16, pp. 62–77, Apr. 1988.

[63] a.J.C. Schmeitz, S. Jansen, H. Pacejka, J. Davis, N. Kota, C. Liang, and G. Lodewijks, "Application of a semi-empirical dynamic tyre model for rolling over arbitrary road profiles," *International Journal of Vehicle Design*, vol. 36, no. 2/3, p. 194, 2004.

[64] J. A. II, M. El-Gindy, and K. Koudela, "Development of a Rigid Ring Quarter-Vehicle Model With an Advanced Road Profile Algorithm for Durability and Ride Comfort Predictions," in *International Design Engineering Technical Conferences & Computers and Information in Engineering Conference*, pp. 1–8, 2008.

[65] SAE J2246, "Anti-Lock Brake System Review," *SAE Standard*, 1992.

[66] R. R. Guntur and H. Ouwerkerk, "Adaptive brake control system," *Proceedings of the Institution of Mechanical Engineers 1847-1982 (vols 1-196)*, vol. 186, no. 1972, pp. 855–880, 1972.

[67] H. Ouwerkerk and R. R. Guntur, "Skid Prediction," *Vehicle System Dynamics*, vol. 1, no. 2, pp. 67–88, 1972.

[68] S. Taheri, "A Feasibility Study of the Use of a New Nonlinear Control Law for Automobile Anti-Lock Braking Systems," *Transportation Systems*, 1990.

[69] S. Taheri and E. H. Law, "Investigation of a combined slip control braking and closed loop four wheel steering system for an automobile during combined hard braking and severe steering," in *American Control Conference,*, Proceedings of the American Control Conference, pp. 1862–1867, Publ by American Automatic Control Council, 1990.

[70] S. Drakunov, U. Ozguner, P. Dix, and B. Ashrafi, "ABS control using optimum search via sliding modes," *IEEE Transactions on Control Systems Technology*, vol. 3, pp. 79–85, Mar. 1995.

[71] G. Mauer, "A fuzzy logic controller for an ABS braking system," *IEEE Transactions on Fuzzy Systems*, vol. 3, no. 4, pp. 381–388, 1995.

[72] J. Yu, "A robust adaptive wheel-slip controller for antilock brake system," in *Proceedings of the 36th IEEE Conference on Decision and Control*, vol. 3, pp. 2545–2546, IEEE, 1997.

[73] S. Taheri and E. Law, "Slip control braking of an automobile during combined braking and steering manoeuvres," *ASME Advanced Automotive Technologies*, vol. 40, pp. 209–227, 2005.

[74] K. B. Singh and S. Taheri, "An Intelligent Tire Based Tire-Road Friction Estimation Technique and Adaptive Wheel Slip Controller for Antilock Brake System," *Journal of Dynamic Systems, Measurement, and Control*, vol. 135, p. 031002, Feb. 2013.

[75] A. a. Aly, "An Antilock-Braking Systems (ABS) Control: A Technical Review," *Intelligent Control and Automation*, vol. 02, no. 03, pp. 186–195, 2011.

[76] Robert Bosch GmbH, "Automotive handbook," 2004.

[77] Kiril Z. Rangelov, *Simulink Models of a Quarter-Vehicle with an Anti-lock Braking System*. Masters thesis, Eindhoven University of Technology, 2004.

[78] M. Watanabe and N. Noguchi, "A new algorithm for abs to compensate for road-disturbance," (Detroit, MI, United states), 1990.

[79] A. van, Zanten, R. Erhardt, and A. Lutz, "Measurement and simulation of transients in longitudinal and lateral tire forces," No. 815, (Detroit, MI, United states), 1990.

[80] P. Zegelaar and H. Pacejka, "Dynamic tyre responses to brake torque variations," *Vehicle System Dynamics*, no. November 2012, pp. 37–41, 1997.

[81] W. Zhang, N. Ding, M. Chen, G. Yu, and X. Xu, "Development of a Low-cost Hardware-in-the-loop Simulation System as a Test Bench for Anti-lock Braking System," *Chinese Journal of Mechanical Engineering*, vol. 24, 2011.

[82] P. Bosch, D. Ammon, and F. Klempau, "Tyre models - desire and reality in respect of vehicle development," *Darmstdter Reifenkolloquium*, October 2002.

[83] N. W. Frey, *Development Of A Rigid Ring Tire Model And Comparison Among Various Tire Models For Ride Comfort Simulations*. Masters thesis, Clemson University, 2009.

[84] J. Maurice, *Short Wavelength and Dynamic Tyre Behaviour under Lateral and Combined Slip Conditions*. PhD thesis, Delft University of Technology, 2000.

[85] T. Wei and H. Dorfi, "Tire transient lateral force generation: Characterization and contribution to vehicle handling performance," *Tire Science and Technology*, 2013.

[86] A. Van Zanten, W. Ruf, and A. Lutz, "Measurement and simulation of transient tire forces," (Detroit, MI, United states), 1989.

[87] M. Jaiswal, G. Mavros, H. Rahnejat, and P. King, "Influence of tyre transience on anti-lock braking," *Proceedings of the Institution of Mechanical Engineers, Part K: Journal of Multi-body Dynamics*, vol. 224, no. 1, pp. 1 – 17, 2010.

[88] M. Y. . S. H. Yamashita, H., "Longitudinal tire dynamics model for transient braking analysis: Ancf-lugre tire model," *Journal of Computational and Nonlinear Dynamics*.

[89] J. Adcox, B. Ayalew, and T. Rhyne, "Interaction of Anti-Lock Braking Systems with Tire Torsional Dynamics," in *Tire Science and Technology*, no. September 2011, pp. 1–18, 2011.

[90] B. Persson, "Rubber friction and tire dynamics," *Journal of Physics Condensed Matter*, vol. 23, no. 1, 2011.

[91] T. Takahashi and H. B. Pacejka, "Cornering on uneven roads," *Vehicle System Dynamics*, vol. 17, no. sup1, pp. 469–480, 1988.

[92] van der Hofstad, "Study on improving the MFSwift tyre model," Master's thesis, TU Delft, 2009.

[93] G. Gim, *Vehicle dynamic simulation with a comprehensive model for pneumatic tires*. PhD thesis, The University of Arizona, 1988.

[94] S. Lee, *Development of new dynamic tire model for improved vehicle dynamics simulation*. PhD thesis, Ohio State University, 1994.

[95] S. Taheri, C. Sandu, S. Taheri, E. Pinto, and D. Gorsich, "A technical survey on terramechanics models for tire-terrain interaction used in modeling and simulation of wheeled vehicles," *Journal of Terramechanics*, vol. 57, pp. 1 – 22, 2015.

[96] G. Gim, *Road and Off-Road Vehicle System Dynamics Handbook - Control of Horizontal Vehicle Motion*. CRC Press, 1 ed., 2014.

[97] K. D. Norman, "Objective evaluation of on-center handling performance," *SAE Technical Papers*, 1984.

[98] T. Mimuro, M. Ohsaki, H. Yasunaga, and K. Satoh, "Four parameter evaluation method of lateral transient response," (Dearborn, MI, United states), 1990.

[99] D. Crolla, D. Chen, J. Whitehead, and C. Alstead, "Vehicle handling assessment using a combined subjective-objective approach," (Detroit, MI, United states), 1998.

[100] ISO 4138:1996, "Passenger cars - Steady-state circular driving behaviorOpen-loop test procedure," 1996.

[101] ISO 7401:2003, "Road vehicles - Lateral transient response test methodsOpen-loop test methods," 2003.

[102] ISO 8725:1998, "Road vehicles - Transient open-loop response test method with one period of sinusoidal input," 1998.

[103] ISO 7975:1996, "Passenger cars - Braking in a turnOpen-loop test procedure," 1996.

[104] ISO 38881, "Passenger cars - Test track for a severe lane-change manoeuvrePart 1: Double lane-change," 1999.

[105] J.-J. Slotine and W. Li, "On the adaptive control of robot manipulators," *International Journal of Robotics Research*, vol. 6, no. 3, pp. 49 – 59, Fall 1987.

[106] S. Taheri, *An investigation of design of slip control braking systems integrated with four wheel steering*. PhD thesis, Clemson University, Greenville, 1987.

[107] Y. Liu, H. Matsuhisa, and H. Utsuno, "Semi-active vibration isolation system with variable stiffness and damping control," *Journal of Sound and Vibration*, vol. 313, no. 1-2, pp. 16 – 28, 2008/06/03.

[108] J. C. Whitehead, "Four wheel steering: Maneuverability and high speed stabilization," (Detroit, MI, United states), 1988.

[109] A. G. Nalecz and A. C. Bindemann, "Handling properties of four wheel steering vehicles," (400 Commonwealth Drive, Warrendale, PA 15096-0001, United States), 1989.

[110] M. Nagai and M. Ohki, "Theoretical study on active four-wheel-steering system by virtual vehicle model following control," *International Journal of Vehicle Design*, vol. 10, no. 1, pp. 16 – 33, 1989.

[111] M. Nagai, E. Ueda, and A. Moran, "Nonlinear design approach to four-wheel-steering systems using neural networks," vol. 24, (Netherlands), pp. 329 – 42, 1995.

[112] P. Ro and H. Kim, "Four wheel steering system for vehicle handling improvement: a robust model reverence control using the sliding mode," *Proceedings of the Institution of Mechanical Engineers, Part D: Journal of Automobile Engineering*, vol. 210, no. 4, pp. 335 – 346, 1996.

[113] T. Takiguchi, N. Yasuda, S. Furutani, H. Kanazawa, and H. Inoue, "Improvement of vehicle dynamics by vehicle-speed-sensing four-wheel steering system," *SAE Technical Papers*, 1986.

[114] Y. Shibahata, N. Irie, H. Itoh, and K. Nakamura, "The development of an experimental four-wheel-steering vehicle," *SAE Technical Papers*, 1986.

[115] H. e. a. Takeda, "A review of four-wheel steering studies from the viewpoint of vehicle dynamics and control," *Vehicle System Dynamics*, vol. 18, no. 1-3, pp. 151–186, 1989.

[116] T. R. Richards, L. T. Charek, and R. W. Scavuzzo, "The effects of spindle and patch boundary conditions on tire vibration modes," *SAE Technical Papers*, 1986.

[117] S. Bruni, F. Cheli, and F. Resta, "On the identification in time domain of the parameters of a tyre model for the study of in-plane dynamics," vol. 27, (Berlin, Ger), 1997. In plane tire dynamics;.

[118] Y. Kobiki, A. Kinoshita, and H. Yamada, "Analysis of interior booming noise caused by tyre and powertrain-suspension system vibration," *International Journal of Vehicle Design*, vol. 11, no. 3, pp. 303 – 313, 1990.

[119] T. Ushijima and M. Takayama, "Modal analysis of tire and system simulation," (Detroit, MI, United states), 1988.

[120] H. R. Dorfi, "Tire cleat impact and force transmission: Modeling based on ftire and correlation to experimental data," *SAE Technical Papers*, 2004.

[121] C. Wei and O. A. Olatunbosun, "Transient dynamic behaviour of finite element tire traversing obstacles with different heights," *Journal of Terramechanics*, vol. 56, pp. 1 – 16, 2014.

[122] A. Sorniotti, "Tire thermal model for enhanced vehicle dynamics simulation," *SAE Technical Papers*, 2009.

[123] M. Masahiko, "Development of Tire Side Force Model Based on Magic Formula with the Influence of Tire Surface Temperature," *Research and Development Review of Toyota CRDL*, vol. 38, Oct. 2003.

[124] P. Fvrier and G. Fandard, "Thermal and mechanical tyre force and moment modelling," *TV Sd Automotive Gmbh Congress*, Dec. 2006.

[125] G. Smith, "Advanced tire cae," *Tire Technology International-The Annual Review of Tire Materials and Tire Manufacturing Technology*, vol. 1, pp. 48–50, 2014.

[126] F. Farroni, *Development of a grip and thermodynamics sensitive tyre/road interaction forces characterization procedure employed in high-performance vehicles simulation.* PhD thesis, University of Naples, 2014.

[127] TNO Automotive, "MF-Tyre & MF-Swift 6.1.2 Equation Manual," 2010.

[128] A. Schmeitz and W. Versteden, "Structure and Parameterization of MF-Swift, a Magic Formula-based Rigid Ring Tire Model," *Tire Science and Technology*, pp. 142–164, 2009.

[129] S. Sivaramakrishnan, "Discrete Tire Modeling for Anti-lock Braking System Simulations," Master's thesis, Virginia Polytechnic Institute and State University, 2013.

[130] A. Higuchi, *Transient Response of Tyres at Large Wheel Slip and Camber.* PhD thesis, Delft University of Technology, 1997.

[131] E. Vinesse, "Tyre vibration testing from modal analysis to dispersion relations," *Proceedings of ISATA*, 1988.

[132] N. Ding, W. Wang, G. Yu, W. Zhang, X. Xu, D. Nenggen, W. Weida, Y. Guizhen, and Z. Wei, "Research and Validation of the Adaptive Control Strategy for ABS Based on Experimental Knowledge," *Automotive Engineering*, vol. 31, no. 1, 2009.

[133] TNO Automotive, "Measurement requirements and TYDEX file generation for MF-Tyre/MF-Swift 6.1," 2008.

[134] SAE J2730, "Dynamic Cleat Test with Perpendicular and Inclined Cleats," *SAE Standard*, 2006.

[135] ISO 13674-1, "Test method for the quantification of on-centre handling," 2010.

[136] J. C. Dixon, *Tires, suspension, and handling.* Society of Automotive Engineers, 2 ed., 1996.

[137] P. v. d. Jagt, *The road to virtual vehicle prototyping.* PhD thesis, TU Eindhoven, 2000.

[138] D. Karnopp, M. Crosby, and R. Harwood, "Vibration control using semi-active force generators," vol. 96 Ser B, no. 2, pp. 619 – 626, 1974.

[139] M. Savaresi, C. Poussot-Vassal, C. Spelta, O. Sename, and L. Dugard, *Semi-Active suspension control design for vehicles.* Butterworth-Heinemann, 1 ed., 2010.

[140] ISO 8608-1995, "Mechanical vibration - Road surface profiles - Reporting of measured data," 1995.